EFFECTS OF WATER VAPOR ON THE HIGH TEMPERATURE OXIDATION OF ALUMINA-FORMING COATINGS AND NI BASE SUPERALLOYS

by

Monica C. Maris-Sida

BS, Technical University of Timisoara, Romania, 1992

MS, University of Pittsburgh, 1999

Submitted to the Graduate Faculty of

School of Engineering in partial fulfillment

of the requirements for the degree of

Doctor of Philosophy

University of Pittsburgh

2004

UNIVERSITY OF PITTSBURGH

SCHOOL OF ENGINEERING

This dissertation was presented

by

Monica C. Maris-Sida

It was defended on

October 5th, 2004

and approved by

Dr. J. Yang, Professor, Materials Science and Engineering

Dr. G.E. Klinzing, Professor, Chemical and Petroleum Engineering Department, Office of the Provost

Dr. J.M. Rakowski, Research Associate, Product Development, Allegheny Ludlum

Dr. G.H. Meier, Professor, Department of Materials Science and Engineering
Dissertation Co-Director

Dr. F.S. Pettit, Professor, Department of Materials Science and Engineering
Dissertation Co-Director

EFFECTS OF WATER VAPOR ON THE HIGH TEMPERATURE OXIDATION OF ALUMINA-FORMING COATINGS AND NI BASE SUPERALLOYS

Monica C. Maris-Sida, PhD

University of Pittsburgh, 2004

Oxidation studies were performed at 1100°C, 900°C and 700°C in dry air and air containing fixed partial pressures of water vapor on specimens of Ni base superalloys and coatings on these alloys that form α-alumina scales under oxidizing conditions. The materials studied included René N5, PWA1484, CMSX4, diffusion aluminide coatings (with or without Pt addition) on René N5, Thermal Barrier Coatings on René N5, and a Ni-8wt%Cr-6wt%Al model. All of these alloys and metallic coatings are normally α-alumina-formers under oxidization conditions. The observed important effects of water vapor include:

• Increased severity of cracking and spalling of α-alumina scales in wet environments especially for those systems with alumina only moderately adherent in dry air;

• Water vapor affects the nucleation and growth of α-alumina scales – the growth rate of α-alumina is increased in water vapor conditions;

• Thicker oxides form during oxidation in wet air than dry air. The transient oxidation phenomenon is affected by the presence of water vapor due to more rapid growth of NiO during the transient period. The selective oxidation of aluminum is inhibited in water vapor conditions; even more adverse effects of water vapor are observed as the oxidation temperature is lowered.

• Spinel phase forms on top of the alumina scales during long term oxidation. Current results indicate that nickel diffusion at alumina grain boundaries significantly contributes to the

formation of new spinel phase at the oxide/gas interface and water vapor is found to enhance this process.

Mechanisms for these observations are proposed.

TABLE OF CONTENTS

LIST OF TABLES

LIST OF FIGURES

ACKNOWLEDGEMENT

First, I would like to extend my thanks to Prof. Frederick Pettit and Prof. Gerald Meier for their patience and guidance through my work. They unconditionally shared their knowledge and support, providing me with lots of insights and best ideas for the research. I will always remember my colleagues from the High Temperature Group with whom I made some great friendships to last a lifetime.

I would like to acknowledge the financial support through which this work has been possible by the Office of Naval Research under contract # N00014-03-0030.

Finally, I would like to thank my husband with whom I gracefully go through all joys and sorrows of life and my parents who unselfishly crossed an ocean to give me and their granddaughter the best of everything. Thank you from all my heart!

1.0 INTRODUCTION

The long-term viability of machine components operating at high temperatures in an oxidizing environment often relies on the integrity of a thin, protective layer of oxide, typically alumina, chromia or silica. In general, alumina (e.g. α-Al_2O_3) formers have better high temperature resistance than their chromia-forming counterparts. This is partly due to the inherently slower transport of reactive species through alumina. Moreover, the volatility of chromia in air at temperatures above 1000°C limits its high temperature use. Improvements in the oxidation resistance of components have been made by the development of single crystals with low sulfur concentration; single crystals show improved mechanical properties, but not much improvement in the oxidation resistance unless they have low sulfur concentration. Furthermore, protective coatings such as MCrAlY that form alumina scales and thermal barrier coatings that prolong the life of the component are being used. Alloy elements usually added to improve mechanical properties include Ta, W and Mo (solid-solution hardening) and Al, Ti and Ta (formation of a γ' precipitate in a γ matrix).

Degradation by oxidation is one of the main failure modes of hot parts in gas turbines, so that understanding the mechanisms of the formation of a protective oxide layer and the processes that affect its mechanical integrity, particularly during temperature changes, are major challenges to the oxidation community. This is most difficult since the oxidation process is sensitive to the temperature, alloy composition, gas flow pattern and velocity and thermal fluctuations of the environment, which are usually not well defined. The alloys are composed of a number of

elements, each of which affects the oxidation behavior, and other factors such as component geometry and service stress complicate the problem.

Water vapor in the oxidizing atmosphere has been described as increasing the oxidation rate of metals and alloys at high temperature. Water vapor, present in virtually every atmosphere in which high-temperature materials are exposed, may significantly affect the oxidation behavior of these metals and alloys. Most technical steels oxidize faster in air or combustion gases containing water vapor than in correspondingly dry gases [1]. Although it is well documented that water vapor affects the high temperature oxidation process, the mechanism has not been described in detail. The existing data in the literature show that water in the gaseous state can have a variety of effects on the oxidation of alloys. The presence of water vapor during oxidation has been shown to cause cracking and spalling of the oxides [2,3], changes in transport processes in oxides [4,5] and modification of selective oxidation processes[6].

In order to improve the lives of superalloys and coatings now used in gas turbines, it is required that the effects of water vapor be clearly understood.

2.0 BACKGROUND

2.1 FUNDAMENTALS OF OXIDATION

One of the characteristics of the oxidation reaction, which serves to define what is meant by the oxidation of a metal, is that the reaction is heterogeneous and does not proceed exclusively in the interior of one phase. Heterogeneous reactions occur between two immiscible phases and usually result in the formation of a new phase; namely, reaction occurs between the oxidants in the gas phase and a solid phase, metal or alloy, with the formation of an oxide phase.

When the oxide scales are continuous, the reactants – metal and oxygen – are separated and the reaction may only proceed through a solid-state diffusion of the atoms or ions and electrons through the scales. Diffusional transport of atoms or ions and transport of electrical charges take place because of the presence of imperfections or defects in solid materials. Generally, diffusional transport processes govern the overall oxidation process and may also play an important role in many of the changes that take place during scale growth.

High temperature oxidation resistance requires the formation of a continuous, adherent and thermodynamically stable oxide.

Assuming a simple divalent oxide "MO", the oxidation process takes place in two steps and the two cases are written below:

at metal-oxide interface: $M \rightarrow M^{2+} + 2e$

at oxide-gas interface: $M^{2+} + 1/2O_2 + 2e = MO$

or

at oxide-gas interface: $1/2O_2 + 2e \rightarrow O^{2-}$

at oxide-metal interface: $M + O^{2-} = MO + 2e$

As the oxide forms at the gas surface or at the metal-oxide interface, further reaction can be limited by the diffusion of the species across the oxide, in which case, the rate of the oxidation reaction can be expressed as:

$$x\,dx = k'\,dt \qquad (1)$$

k′ is the parabolic rate constant; x is the scale thickness. Figure 1 shows the values of rate constants for a number of oxide systems [7].

If pure nickel, for example, is oxidized in air at about 1000°C, the rate is inversely proportional to the instantaneous thickness of the oxide layer, which in turn is proportional to the displacement Δx_{metal} of the metal surface. The parabolic rate law is:

$$d\Delta x_{metal}/\,dt = k_c^{o}/\,\Delta x_{metal} \qquad (2)$$

where k_c^{o} is the "corrosion constant".

If the parabolic law is obeyed, the corrosion constant may be calculated:

$$k_c^{o} = (\Delta x_{metal})^2/\,2t \qquad (3)$$

from which the displacement of the metallic surface is readily obtained.

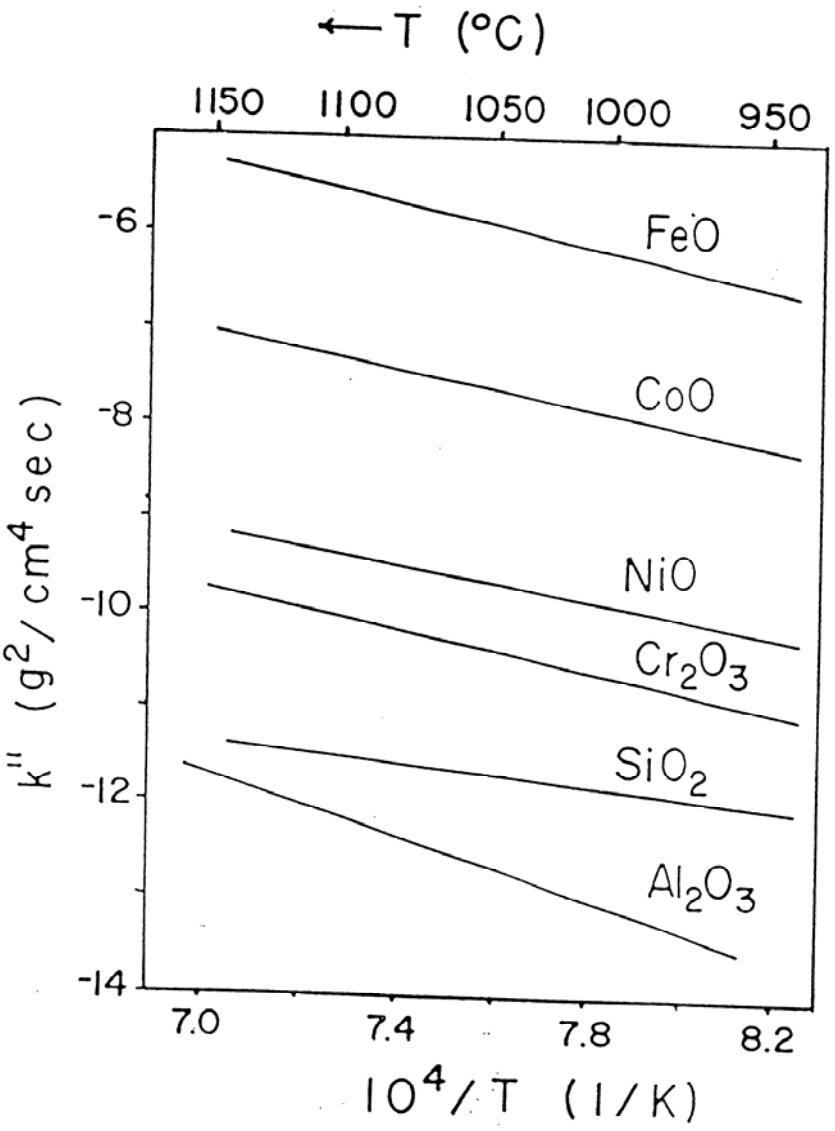

Figure 1 Rate constants for the growth of selected oxides (Ref. 7)

For a continuous and adherent scale of sufficient thickness, the rate-controlling factor is the migration of ions or electrons; the rate of oxidation of a pure metal is often parabolic with time.

It can be shown that the cation vacancy concentration in a metal deficit oxide MO will vary with the oxygen partial pressures:

$$1/2O_2 = O_o + 2h^{\bullet} + V_M^{''} \quad (4)$$

From which:

$$C_{VM''} = K'P_{O2}^{1/6} \quad (5)$$

More generally (for neutral, singly charged or doubly charged vacancies):

$$C_{VM} = K'P_{O2}^{1/n} \quad (6)$$

The parabolic rate constant can be shown to vary with oxygen partial pressure across the oxide scale as:

$$k' \alpha \ [(P_{O2}^{''})^{1/n} - (P_{O2}^{'})^{1/n}] \quad (7)$$

where P_{O2}'' and P_{O2}' are the oxygen pressures at the oxide/gas and metal/oxide interfaces, respectively. The oxygen partial pressure at the scale/metal interface can be taken as negligible, so that:

$$k' \alpha (P_{O2}'')^{1/n} \quad (8)$$

For a p-type oxide, the parabolic rate constant is dependent on the partial pressure of oxygen in the gas phase. For an n-type oxide with non-metal deficit or metal excess, a similar calculation results in a negative exponent for the dependence on oxygen partial pressures [8] and k' is insensitive to the oxygen pressure in the gas phase.

2.2 OXIDATION OF ALLOYS

Materials used for high temperature applications are usually alumina or chromia formers. Due to mechanical property requirements, only small additions of Al or Cr (or both) are made and the alloys are Ni, Co or Fe-base. Once protective layers of alumina or chromia scales are formed, even though the concentrations of Al and Cr are low, the oxidation rate decreases by some orders of magnitude.

The major part of the oxide scales on unalloyed Fe, Co and Ni substrates is formed by outward metal diffusion via metal vacancies [9]. Self diffusion of metal ions in FeO, CoO and NiO is several orders of magnitude higher than for Cr in Cr_2O_3 or Al in Al_2O_3 and, at rather low concentrations of the alloying element, the oxide scales consist, therefore, of an outer layer of FeO, CoO or NiO. These oxide scales are single phase but might consist of two well defined

layers parallel to the oxide/alloy interface – the outer layer with coarse columnar grains and the inner layer with fine, equiaxed grains. The interface between the two layers approximately reflects the initial surface [10]. Such duplex oxide morphologies are apparent during oxidation of unalloyed base metals at low temperatures, especially for some slower growing scales such as for the oxidation of Ni [11].

For the alumina formers, the oxidation kinetics are determined by either the inward transport of oxygen, the outward transport of aluminum, or both of these types of diffusion. Transport can take place through the lattice or through short-circuit paths such as grain boundaries or dislocations. If the oxide layer has interconnected pores or contains large numbers of microcracks, oxygen molecules may also permeate through these discontinuities.

It has been stated that if the cation outward transport predominates, via short-circuit paths or lattice diffusion, the reaction always occurs at the oxide/gas interface.

On the other hand, if the oxidation primarily occurs by inward transport of oxygen, the following possibilities exist: (1) transport through pores or microcracks; (2) transport through grain boundaries and dislocations; (3) transport by lattice diffusion. Rapid transport through pores or microcracks results in all the reaction taking place at the oxide/substrate interface. The growth of an oxide scale on a metal substrate can be discussed in conformity to Wagner's theory. After formation of a thin but continuous protective oxide layer, the further oxidation and scale growth take place by slow diffusion of oxygen and metal ions accompanied by chemical reactions at the gas/oxide and oxide/metal interfaces. If the oxygen transport is dominating, the oxide layer grows inwardly; when cation transport is predominant, an outward growth of the oxide layer occurs. When diffusion of both species is similar, there is a dual layer forming [12].

Generally speaking, aluminum transport in the alumina scale is more rapid than the diffusion of oxygen at any temperature [13], so that aluminum diffusion should be rate controlling.

The fact that the presence of grain boundaries and line defects in alumina might increase the outward growth of the scale as these features represent short-circuit diffusion paths for cations should be taken into account. At the same time, though, grain boundaries, pores and microchannels may facilitate the inward transport of oxygen. It is now generally accepted that most of the growth of alumina takes place by inward diffusion of oxygen along grain boundaries.

Before the thin protective oxide layer forms, initially all elements that have an affinity for oxygen undergo oxidation and all these oxides are called transient oxides. As oxidation proceeds further, the most stable oxide develops into a continuous layer at the metal surface, under all the transient oxides.

Transport processes responsible for alumina scale growth have not yet been completely elucidated.

2.3 SUPERALLOYS

Superalloys are a class of high temperature materials proven to have great capabilities to maintain good room and high temperature mechanical properties as well as structural stability at elevated temperatures (e.g. <1050°C). These materials are widely used in aircraft, marine and industrial gas turbines as well as rocket engines, nuclear reactors, steam power plants, just to mention a few from the broad palette of high-temperature applications.

There are three main groups of superalloys: nickel base, cobalt base and iron base. Single crystal nickel-base superalloys can be utilized to $0.8T_m$ (melting point) and for times up to

around 100,000 hours at somewhat lower temperatures. Ni-base alloys are the most widely used for the hottest parts in high-temperature applications and the alloys' physical metallurgy is the most complex and sophisticated of all superalloys. The high tolerance of nickel for alloying, the tendency of forming adherent and exceptionally oxidation-resistant alumina scales at high temperatures, development of chromia-rich scales (with chromium addition) for lower temperature use make Ni-base superalloys the most appealing material for high temperature industrial applications.

The composition of many types of nickel base alloys is comprised of at least 12 or 13 basic elemental components to which an addition of about 10 more 'trace' elements such as manganese, silicon, phosphorus, sulfur, oxygen and nitrogen should be carefully controlled. However, most of the polycrystalline nickel base alloys contain 10-18% chromium, about 6% aluminum, optional additions of cobalt, tantalum, molybdenum and tungsten and small amounts of boron and carbon.

The major phases present in the structure of a nickel base superalloy are:

- gamma matrix (γ - FCC austenite)

The continuous matrix is an FCC Ni-base austenitic phase, usually containing a high percentage of solid-solution elements such as Co, Mo, Cr, Ta, W, Ti, and Al providing strengthening to the nickel matrix.

- gamma prime (γ')

γ' is the major precipitate phase; it invariably precipitates coherently with the austenite. Typically, in a Ni-base superalloy, γ' is $(Ni, Co)_3(Al, Ti)$ with nickel and aluminum dominating. γ' is a unique intermetallic phase; as the temperature increases, the strength of γ' increases.

Unlike the strengthening that is developed by high hardness carbides, the inherent ductility of γ' helps prevent cracking.

- carbides

There is 0.05 to 0.2% carbon present in superalloys and it often reacts with refractory elements to form primary stable carbides. Carbides appear to prefer grain boundaries of Ni-base superalloys, at high temperatures. It is widely accepted today that carbides exert a significant and beneficial effect on rupture strength at high temperatures, albeit previous investigators noted detrimental effects on ductility from grain boundary carbide morphologies.

- borides

Boron is present at levels of 50 – 500 ppm. It is located at grain boundaries and it is considered an essential addition by providing enhancement of the grain boundary cohesion hence reducing the grain boundary tearing under creep rupture loading.

- topologically close packed (TCP) phases

The TCP phases, σ, μ and Laves, commonly formed in Ni-base alloys, are undesirably hard phases having a detrimental effect on the properties of the alloy. Their platelike morphology is a source for crack initiation and crack propagation leading to brittle failure at relatively low temperatures. Also, they contain a high refractory metal concentration taken from the γ matrix, thus weakening the superalloy.

Great improvements in the performance of gas turbines have come from the development of directional solidification and the production of single crystal turbine blades. Single crystals of Ni-base superalloys, based on the constituent γ/γ', are widely used for hot-section turbine parts. Generally, the γ' phase occupies a volume fraction between 40% and 70% and it is regularly distributed in cuboidal particles in the γ matrix after the heat treatment [(14)]. Under extreme

temperatures and loading conditions, the γ' precipitates have been observed to undergo a process of anisotropic coalescence resulting in morphologies consisting of needles aligned with the load axis or plates perpendicular to it [15].

The fact that single crystal materials have no grain boundaries allows the removal of grain boundary strengtheners, such as borides and carbides, which along with elements like Zr and Hf tend to lower the solidus of the alloy, in many cases preventing the complete dissolution of γ' during solution heat treatments.

During cooling, some elements tend to accumulate in the dendrite core, while other elements concentrate in the interdendritic regions. For example, Re and W have been reported to join the dendrite core, whereas Al, Ti and Ta tend to segregate in the interdendritic region [16]. The refractory metal concentrations have continued to rise in superalloys from the first to the present third generation. Particularly, W, Re and Ta levels have been reported to increase steadily in the three generations of single crystal nickel base superalloys. The refractory elements confer increased creep resistance and strength due to solid solution strengthening, strengthening of γ' and slower diffusion rates.

Most high temperature alloys achieve some degree of oxidation resistance by growing a protective external oxide. These scales form on the surface of the materials provided that the alloy aluminum content is sufficiently high to ensure selective oxidation of this element. The alumina scale separates the alloy from the corrosive environment thereby preventing the formation of rapidly growing oxides (e.g. nickel, cobalt or iron) and consequently the corrosive degradation of the metallic component. At temperatures in the range of 1000°C to 1300°C, α-Al_2O_3 is one of the most protective types of scale because it is slow growing, dense, relatively inert and has low volatility (unlike Cr_2O_3). Added to these qualities, the scale also must be

adherent in order to achieve extended oxidation resistance lifetimes. Usually, for good scale adhesion, a reactive element (Zr, Y or Hf) is added to the alloy.

2.4 COATINGS

Superalloys are used in many industrial applications, one of the largest uses for these materials is in the combustion chamber and turbine section of gas turbine engines. Temperatures of operation for these components (disks, blades and vanes) vary from 700°C to 1100°C, affecting them primarily by oxidation, hot corrosion, high mechanical stress and mechanical and thermal fatigue. Therefore, the demanding operating conditions for gas turbine engines have led to the development of coatings designed to protect turbine components from environmental attack, which is a life-limiting factor along with creep and fatigue. Protective coatings are frequently applied on superalloys to make them more resistant to oxidation and corrosion attack.

The coatings fall into two categories: diffusion coatings and overlay coatings. The most widely used diffusion coatings are the aluminide coatings, while typical overlay coatings are physically vapor deposited (PVD) coatings and nowadays, more widely used, low-pressure or argon-shroud plasma spraying (PS). Both types of these coatings are subject to a number of forms of degradation when exposed at various temperatures. In practical high temperature applications (e.g. turbine blades), the coatings undergo isothermal and cyclic oxidation and interdiffusion with the substrate. At lower temperatures, the coatings are subject to degradation by hot corrosion, often in the form of surface deposits such as sulfates.

Aluminide coatings have been for years the most important among various kinds of high temperature coatings. Aluminide coatings are the most widely used protection system for

superalloys. Conventional processing routes for aluminide coatings include pack cementation, 'above the pack' and chemical vapor deposition (CVD) technologies. Local deposition of the aluminizing compound, usually in the form of a liquid mixture, can be used as an alternative process. 'Slurry' aluminizing can have advantages in simplicity and economy of the process in many cases.

Aluminum is diffused into the alloy surface converting it to an intermetallic compound containing approximately 50 at% Al. On oxidation, this intermetallic compound forms a layer of alumina, which serves as the main barrier against further reaction with environmental species. Cyclic conditions could induce cracking and spalling of the protective alumina layer, so that the underlying aluminide is again exposed and a new protective scale is rebuilt. The aluminide coatings prevent the underlying alloy from direct exposure to the oxidizing conditions, hence increasing the life of the components.

Platinum-modified aluminide coatings have been shown to possess better oxidation and corrosion properties at high temperatures compared to their 'straight aluminide' peers. Platinum aluminide coatings are being used for the protection of nickel base superalloys in gas turbine engines from the aggressive conditions in which modern industrial turbines operate. At high temperatures, in the coatings, high Al concentration promotes an oxide scale of complete and adherent alumina on the surface. Platinum additions, which were initially intended to prevent aluminum diffusion from the coating into the substrate, also proved to improve the hot corrosion resistance and scale adherence.

Platinum aluminide coatings are produced by electroplating a layer of Pt (5 – 7 μm thick) on the substrate, which is then given a diffusion heat treatment in a protective atmosphere. The interdiffusion between the platinum layer and the substrate results in a diffusion layer on the

surface. Subsequently, the diffusion-treated parts are aluminized by using the pack cementation technique or chemical vapor deposition (CVD).

Two types of platinum aluminide coatings have been developed. One is produced with a high temperature and low activity of Al and the other uses a low temperature and high Al activity. The two types of coatings that result from these two kinds of processes are known as the inward and outward types, depending on the direction of diffusion of Al and Ni in the aluminide coating once Al diffuses through the Pt-enriched region.

Second generation single crystal turbine blade materials generally contain concentrations of refractory elements (Ta, W, Re) to provide adequate mechanical properties at high temperatures. However, concentrations of Al and Cr, which enhance the oxidation resistance, are reduced to balance for the higher content of refractory elements. Some investigations [17-22] have studied the interdiffusion behavior after exposure to high temperatures for long times; this causes the degradation of coatings and changes of the diffusion region at the coating/substrate interface which could reduce the oxidation resistance. Some studies [17-19] have reported that Pt, during inward diffusion, excludes the refractory elements, a phenomenon believed to be linked to the formation of an intermetallic compound known as a TCP (topologically close-packed) phase.

The presence of platinum in the aluminide coatings improves the oxidation performance of these diffusion aluminide coatings. Recent studies [23] show that the presence of Pt has helped the retention of the alumina scale even under cyclic heating and cooling. Based on the results in this study, there is the requirement of a minimum content of Pt corresponding to a certain thickness of the initial Pt layer.

2.5 THERMAL BARRIER COATINGS

To achieve higher operating temperatures, gas turbine components are coated with a system consisting of a ceramic external layer composed of zirconium oxide. The system is called a thermal barrier coating. To avoid phase transitions, the zirconia layer is doped with 8 to 10 wt% yttrium oxide. The ceramic layer has a low thermal conductivity and due to its structure, a thermal expansion coefficient compatible for use on metals. Zirconia has a high ionic conductivity, facilitating oxygen diffusion through it, so that the latter reaches the metallic substrate and develops an oxide scale.

For high temperature resistance and corrosion resistance, the substrates are usually coated with a protective layer of metal (often aluminides or platinum-modified aluminides) before the ceramic outer layer is applied. This protective layer is called a 'bond coat' and it provides protection against corrosion.

Basically, thermal barrier coatings are a system that lowers the metal surface temperature. TBCs give the potential to drop metal surface temperatures by up to 150°C in conjunction with component cooling. This temperature reduction of the surface temperature of a gas turbine component has the effect of reducing oxidation rates by one order of magnitude and would be furthermore beneficial by reducing the component's tendency to creep.

Low thermal conductivity and good phase stability makes yttrium-stabilized zirconia the most successful ceramic layer in combination with a metallic bond coat layer. Both layers can be applied by thermal spraying (plasma spraying) or by electron beam physical vapor deposition (EBPVD).

During plasma spraying, the melting of fine ceramic powder particles, acceleration and final impact on the substrate lead to a lamellar structure. Between the individual lamellae, there

is an extended network of microcracks responsible for strain tolerance. Each lamella consists of small parallel columns, an order of magnitude smaller than columns from EBPVD. Plasma-sprayed TBCs have been used since the early 1950s, but only in the last decade have TBCs been used on highly stressed turbine components in commercial gas turbine engines.

The atomic deposition during EBPVD leads to a columnar structure. Grain boundaries between individual columns are weak, but provide a good strain tolerance of the brittle ceramics. Processing TBCs by EBPVD, a strain-tolerant microstructure can be produced – expressly because of this type of microstructure, thermal barrier coatings have been a success in highly stressed turbine components operating without (or with very little) spalling.

EBPVD TBCs have nevertheless a significantly higher thermal conductivity compared to plasma-sprayed TBCs (1.8 W/mK compared to 0.8 W/mK) [24,25]. EBPVD TBCs provide good thermal shock resistance and erosion resistance – microstructures that would match the thermal conductivity of the plasma-sprayed coatings are desirable.

The increased reliability of TBCs has come from improvements in the processes used for deposition, largely because of improvements in coating texture. However, one of the difficulties in choosing a combination of substrate/bond coat/TBC for improved reliability is that the mechanisms by which TBCs spall have not yet been fully identified.

2.6 CHARACTERISTICS OF ALUMINA

The main metastable aluminum oxides that form during the transient stages of oxidation are γ-Al_2O_3, θ-Al_2O_3 and δ-Al_2O_3. These phases, called transition aluminas, transform after further high-temperature exposure to the α phase (α-Al_2O_3), also known as corundum.

The stable α-Al_2O_3 structure consists of closed packed planes of large oxygen ions forming an approximate hexagonal close packed anion lattice, whereas the aluminum cations are located in octahedrally coordinated interstitial sites in the anion sublattice [26]. Only two thirds of the octahedral sites are filled with cations so as to maintain charge neutrality. Figure 2 shows the basal plane of the unit cell of alpha-alumina containing 10 ions ($6O^{2-}$ and $4Al^{3+}$) per unit cell. The lattice parameters a_o and c_o are about 0.475 and 1.299 nanometers, respectively [27].

For materials used at high temperatures, diffusivity plays probably the most important role. The kinetics of diffusion depends on the mobility of the diffusing species. Diffusion data in α-Al_2O_3 shows that both aluminum and oxygen are mobile in the oxide and they diffuse at similar rates [28].

The oxide scale grows according to Wagner's parabolic law. After further exposure, the growth rate slows down, possibly because of the reduction of grain boundaries that act as diffusion paths. The grain boundaries seem to have a significant role for oxygen diffusion[29]. However, other studies emphasize the role of aluminum diffusion. Although the bulk diffusivity of Al is about three times larger than that of O, it is very important to mention that the effective grain boundary diffusivity of oxygen exceeds by far all other diffusivities for a wide range of grain sizes.

The alumina scale has a dual morphology: usually, the outer region of the layer consists of small and equiaxed oxide grains, whereas in the inner zone, the grains become columnar-shaped and coarser [30,31].

Also, the scale morphology changes with temperature: the oxide/gas interface grown at about 900°C shows long oxide whiskers extending from the specimen's surface (i.e. metastable θ-Al_2O_3). Conversely, an almost completely flat interface develops at 1200°C (i.e. α-Al_2O_3) [32].

From this study, it could be concluded that the scale growth mechanism changes with temperature. If the prevalent mechanism is cation diffusion, the result is an outwards scale

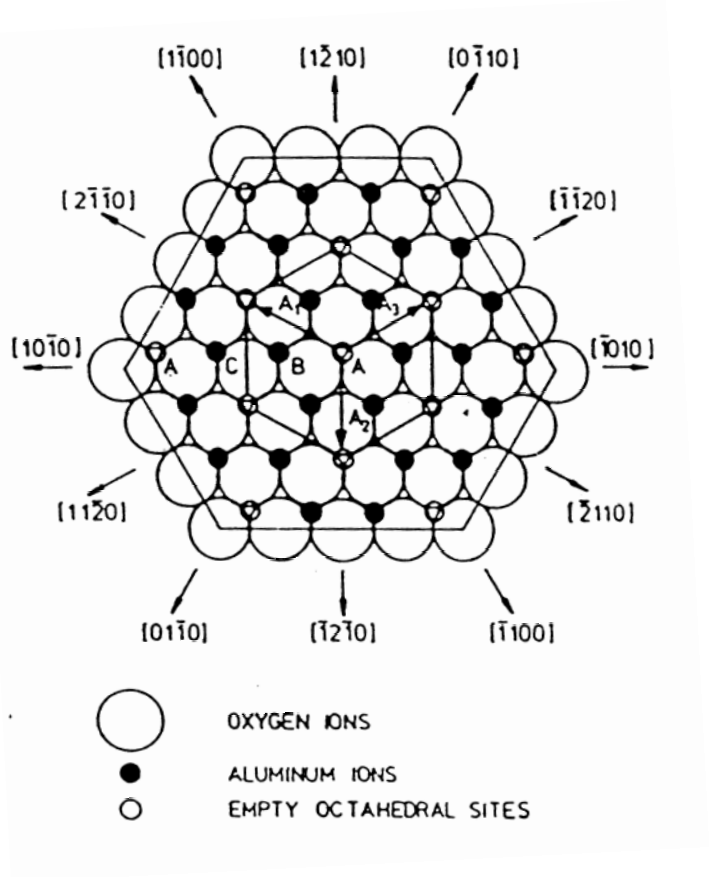

Figure 2 Packing of Al and O ions in the basal plane of alpha-alumina. (The upper layer of O ions is not shown. Basal hexagonal cell vectors and directions are indicated. Ref. (27))

growth; when the growth mechanism is controlled by oxygen diffusion, the result is an inward growing scale.

Since a number of high-temperature alloys depend on slow growth of alumina scales for oxidation protection, these scales must exhibit very good adherence to the substrate. This fact appears to be crucial for long-term cyclic oxidation resistance.

Generally, the thermal expansion difference between the metal and the oxide is large enough to result in residual compressive stresses of the order of about 5 GPa [33] at room temperature. This brings an interfacial shear stress resulting in buckling which may progress in spallation at the scale/metal interface.

Degradation due to cracking and spalling is displayed by weight changes over time of exposure. On such plots, a fairly adherent scale exhibits a parabolic growth and a shallow slope (minimal weight gain), whereas a non-adherent scale results in an approximately linear weight loss behavior. Kinetic data are obtained from the parabolic rate equation:

$$(\Delta W/A)^2 = k_p t \qquad (9)$$

where $\Delta W/A$ represents weight change per unit surface area, t is time and k_p is the rate constant.

Scale growth kinetics are diffusion controlled and the parabolic rate constant can be predicted from Wagner's scaling theory [12] on the assumption that the electron transport number is unity, as

$$k_p = k \int D_M \, d\ln P_{O2} \,, \qquad (10)$$

integrated over limits P_{O2}' and P_{O2}", where k is a constant and D_M is the self-diffusion coefficient for the mobile species predominantly responsible for mass transport through the growing scale. The limit values, P_{O2}' and P_{O2}", apply to the metal/oxide and oxide/gas interfaces, respectively.

$$D_M = D^o_M[M] \tag{11}$$

where [M] is the concentration of mobile defects and D^o_M represents their self-diffusion coefficient assumed to be independent of composition.

It is important to note that when comparing isothermal scale growth to cyclic oxidation, the amount of metal consumed by the latter is considerably larger than that due to an isothermal exposure. The high rate of re-oxidation after spalling appears to be the cause for the increased metal consumption rate in cyclic exposures.

Cyclic oxidation is one of the fundamental methods used to assess high temperature resistance of materials. Achieving good adhesion of alumina scales to the surface of alloys has been traditionally done by simple additions of small ($\leq$ 0.1%) amounts of reactive elements such as Hf, Y, Zr or other group III and IV elements, including the lanthanide and actinide series [35]. Yttrium has been the most widely used additive and often proven the most effective. Hafnium and zirconium seem to be quite effective in M-Cr-Al or Ni-Al systems, but not as effective in more complex superalloys.

It is unanimously agreed that the amount and uniformity of the reactive element dopant is critical for scale adhesion. At levels around 0.1wt%, good adhesion is obtained and the growth rate is maintained slow.

A newer procedure, reduction of the sulfur impurity level to less than 1 ppm, has given very good results [34]. The mechanism is based on sulfur segregation to the oxide/metal interface and subsequent degradation of interfacial adhesion (by interfacial voids – by segregating at the open surface of cavities and lowering their surface energy – or decreasing the chemical bond strength). When reactive elements are added, they react with sulfur, preventing its diffusion and segregation. Low-sulfur single crystal superalloys have become a subject of interest lately.

2.7 EFFECTS OF WATER VAPOR

Changes in the reaction kinetics and the composition of oxide scales in the presence of water vapor have been linked to:

- an enhancement of the phase-boundary reaction at the gas/oxide interface
- transport of oxygen across voids at the metal/oxide interface
- changes in the concentration of point defects in the compound forming the oxide scale followed by changes in the transport properties of the scale

It is known that, in most cases, oxidation in water vapor atmospheres has different kinetics than those observed with oxygen. This is generally true although the oxygen thermodynamic activity is the same.

It is difficult to isolate the effects of water vapor since many variables, such as grain size and porosity could affect the mechanical properties of the oxide scales.

Water vapor is present in virtually all environments where alloys and coatings are used at high temperatures. In gas turbines, water vapor is present in the air used for combustion and it is formed during the combustion process. In the case of oxidation of alloys and coatings at high

temperatures, the exact effects due to water vapor depend upon the particular oxide that is formed during the oxidation process and the exposure conditions such as temperature and water vapor pressure.

The interaction of water vapor with thin alumina films is of technical importance in areas such as corrosion, heterogeneous catalysis and microelectronics. The alumina surface may be altered by interaction with H_2O and it is important to understand what effects such as amount of water vapor or water vapor partial pressure have on the alumina surface properties when exposing in water vapor conditions.

At the same time, issues such as diffusion of substrate species into the oxide and the formation of interfacial phases are of practical as well as scientific interest in the above mentioned areas.

2.7.1 Oxidation Mechanism. Oxidation Kinetics

Rahmel and Tobolski [4] have suggested that the presence of water vapor may change the structure of the oxide scales and their performance at elevated temperatures. This work showed the effect of water vapor on the oxidation of unalloyed Fe in H_2/H_2O and O_2/H_2O mixtures at high temperatures by enhancing the scale growth by a factor of about 1.6 at 950°C [4].
It has been found that oxidation of iron in H_2/H_2O is faster than in CO/CO_2 atmospheres. Studies in the 1960s [35] reported oxygen transfer in H_2/H_2O mixtures about 100 times faster than in CO/CO_2 mixtures.

It appears to be generally agreed that surface-controlled oxidation of iron [36,37] is appreciably faster in H_2/H_2O than in CO/CO_2, but there is no generalization on this matter

concerning oxidation of metals. It is necessary to know the composition and the defect structure and to perform experiments to determine the rates at which local equilibrium is established.

Increased dissociation of molecular oxygen ($O_2 \longrightarrow 2O$) and complete dissociation of molecular water ($H_2O \longrightarrow 2H + O$) on surfaces of metal oxides facilitate an increased transport of both O and O^{2-} in the oxides due to an increased concentration gradient of O and O^{2-} over the oxides [38].

Gulbransen and Copan [39] demonstrated in experiments carried out with pure Fe at 450°C for 48 hours that water vapor could have a profound effect on nucleation, lateral growth and morphology of oxide films. Their work concluded that water vapor facilitates nucleation, promotes surface diffusion and expands reaction sites.

Roosendaal et al [40] found for the passivation of Fe by oxidation in water vapor environments that, in contrast with the oxidation in O_2, the oxide formed in water vapor contains Fe^{3+} and that the Fe^{3+}/Fe^{2+} ratio, combined with the H/O ratio, supports the assumption that H is present as OH-groups in the oxide layer.

Intrusion of water vapor to the metal/oxide interface is caused by deterioration of the mechanical properties of certain protective oxide scales accompanying the generation of cracks, either due to dissolution of hydrogen into the oxide scale or due to an initially brittle scale. Jianian et al [41] investigated the mechanism of breakaway oxidation in Fe-Cr alloys at 900°C in wet oxygen and suggested that microchannels or microcracks in the initially formed Cr_2O_3 scale enabled water vapor to pass through the scale, resulting in the formation of nodule-like oxides, with the subsequent development of an external scale consisting of iron oxides (Fe_2O_3, Fe_3O_4) and an inner scale consisting of an Fe-Cr spinel oxide.

Fritscher and Lee [42] suggested that the oxidation kinetics of Incoloy 800 (Fe - 30Ni – 20Cr – max 1%Si) is governed mainly by cation diffusion through p-type chromia layers when the oxidation takes place in air. However, in air containing water vapor, chromia becomes n-type and an inner layer of silica becomes rate determining. The silica layer, in contact with the metal matrix or the chromia scales or with other silica scales, dictates the oxygen activity within the matrix in accordance with their respective dissociation pressures.

Foley [43] reported that, for the oxidation of Fe – 41Ni alloy in controlled O_2/N_2 and water vapor atmospheres, the gross effect of H_2O in the oxidizing atmosphere is to increase the oxidation rate. The effect of water vapor is observed at 600°C and 700°C and it is more evident at 900°C and 1000°C. The rates are increased approximately threefold over the water vapor partial pressures range studied (3, 50, $250x10^{-5}$ atm).

The study on the high temperature oxidation of Fe-Cr in 'wet oxygen' [41, 44] showed that a primary reason for the effect of water vapor is that a protective, continuous chromia scale fails to be maintained after initial oxidation stages, and instead, the oxide scales consist mainly of porous iron oxides. This study further reveals that the higher the amount of water vapor or the oxidation temperature, the shorter the duration of the initial stage of oxidation.

Taniguchi et al [45] indicated oxidation kinetics approximately following linear rate laws for isothermal exposures at 1200K of TiAl coupons in water vapor conditions, quite different from the oxidation in O_2 where near parabolic kinetics were observed. They concluded that the oxidation of TiAl specimens was much enhanced by the addition of H_2O to O_2 at 1100K and 1200K; however, the addition of water vapor did not change the type of the oxide formed, but did change the nature of its grains (directionally grown grains versus fine ones). There is a much larger solubility of hydrogen or its isotopes in TiO_2 than in Al_2O_3 [46-49]; therefore, the oxidation

rate enhanced by the addition of water vapor is linked to the enhanced diffusion through titanium oxide, although the direct mechanism for this is not known yet.

Zeller et al [50] reported that the presence of water vapor in the atmosphere during the oxidation of TiAl led to a significant acceleration in the oxidation kinetics as well as to a change in the crystal morphology and microstructure of the oxide scales formed during exposures at 700°C and 750°C.

Henry et al [51] suggested that the growth of the internal subscale of chromia grown on Cr, more rapid in H_2O than in O_2, was due to the transport of oxygen-containing species, slow diffusing oxide ions in O_2 (r_{O2-} = 140pm) and probably very mobile hydroxide ions in H_2O (r_{OH-} = 95pm). The study found that a subscale is always present when oxidizing in H_2O, even for low oxidation durations, due to the rapid transport of OH^- ions through the scale.

On the other hand, Passier et al [52], for the thermal oxidation of niobium at 800°C – 1000°C by water vapor found that water vapor reacts as a molecule and not through its equilibrium oxygen. Due to the slow kinetics observed, solid-state transport of OH species need not be taken into account, as was the case of rapid oxidation of titanium in water vapor [53]. The study concluded that the reaction of Nb with water vapor, between 800°C and 1000°C, is very slow compared to that in oxygen.

2.7.2 Influence on Hydrogen-Defects Concentration

Studies have demonstrated that water vapor interacts with metal oxides to form hydrogen defects [54]; dissolved protons are the main hydrogen defects at high temperatures. They associate with oxygen ions on oxygen sites to form hydroxyl ions. The formation of such hydrogen defects may be written in terms of Kroger-Vink notation as follows:

$$H_2O(g) + 2O^x_o = 2HO^{\bullet}_o + 2e' + 1/2O_2(g) \quad (12)$$

As seen from this equation, the concentration of dissolved protons is dependent on both the activities of water vapor and oxygen. Relatively large concentrations of hydrogen may be dissolved in oxides doped with lower valent cations and with oxygen vacancies as the predominant native point defect. In this case, the interaction of water vapor may be written as follows:

$$H_2O(g) + V_O^{\bullet\bullet} = HO^{\bullet}_o + h^{\bullet} + 1/2H_2(g) \quad (13)$$

From this equation, upon reaction with water vapor, it can be seen that the oxygen vacancies are gradually filled and at the same time protons dissolve in the oxide.
In the literature, this type of defect ($OH^{\bullet}_o$) is often called an interstitial proton.

Studies on the electrical conductivity of α-Al_2O_3 with Mg as the impurity have shown that hydrogen defects introduced by water vapor can affect the properties of alumina [54,55]. Fujii and Meussner [56] found linear oxidation rates for Fe – 15Cr alloys exposed in Ar – 10% H_2O at 1100°C. The oxide scales formed were layered and consisted of FeO and spinel with voids at the interface. They suggested that the high linear rates were caused by hydrogen from water vapor dissociation acting as a carrier to move oxygen across the voids in the oxide scale.

Other investigators reported that isothermal oxidation rates increased with the addition of water vapor to the exposure conditions. It was suggested that this effect might be connected to the incorporation of hydrogen or hydroxide ions into the oxide lattice. From here, subsequent

alterations of defect structures might result in an increase of the oxidation rate and an enhancement of the solid-state reactions between several oxides in the scale hence forming a less protective oxide layer.

As part of the research on oxide proton conductors for high temperature use, Fukatsu et al [57] found that hydrogen can be incorporated into an alumina-rich magnesium aluminate spinel reversibly from the surrounding atmosphere containing water vapor. The dissolved hydrogen exists as a proton located between the oxide ions by forming a hydrogen bond.

The following reaction is most probable as the hydrogen incorporation reaction:

$$H_2O\ (gas) + V_o^{\cdot\cdot}\ (crystal) = 2H_i^{\bullet}\ (crystal) + O_o^{x}\ (crystal) \qquad (14)$$

When the dissolution is determined according to the above reaction,

$$[\ H_i^{\bullet}\ ]\ \alpha\ [\ V_o^{\cdot\cdot}\ ]^{1/2}\ P_{H2O}^{1/2} \qquad (15)$$

is deduced from the mass action law and dilute solution approximation.

By changing the hydrogen concentration in a metal substrate, the rate of metal-ion transport in the oxide may be altered and by adding Pt or rare earth metals to the substrate and/or oxide, the rate of oxygen-ion transport in the oxides may also be altered [58]. Therefore, the oxide growth and the protective abilities of the oxides may be influenced by hydrogen-defect concentration or even by amounts of Pt or other elements in the substrate or oxide. The group of Swedish researchers[58] concluded that an increased metal transport in the oxide and a reduction

in oxygen transport to the inner part of the oxide could be linked to the presence of hydrogen in a FeCrAlY alloy oxidized at 900° - 1000°C.

2.7.3 Volatility Effect

The protective properties of chromium oxide scales in atmospheres containing water vapor may be reduced or lost by evaporation of volatile oxyhydroxides if chromia is in direct contact with the gas. Two volatile species of chromium have been identified: $CrO_2(OH)$ and $CrO_2(OH)_2$ [59,60]. Due to volatility effects, chromia-forming alloys are not widely used at temperatures higher than 900°C.

At least four aluminum hydroxyl species have been reported in the literature: $Al(OH)_3$, AlO_2H, AlOH and HAlO [61]. From these, $Al(OH)_3$ is the most stable [61]. However, at temperatures around 1100°C, water vapor would not cause significant volatilization of alumina.

Studies of silica behavior in the presence of water vapor suggest that the vapor species may be $Si(OH)_4$, $SiO(OH)_2$ and $Si_2O(OH)_6$[61,62]. Based on this work and results of Jacobson [63], it is believed that, in the paralinear oxidation/volatilization of SiC in an environment containing 50% H_2O / 50% oxygen at 1atm total pressure and temperatures between 1200°C and 1400°C, the silica scale volatilizes as an $Si(OH)_4(g)$ species. It has been demonstrated that oxidation of silicon in wet oxygen increases with increasing water vapor content. This increase is the result of the modifying effect of (OH) in silica and the breakup of the network structure is believed to facilitate a faster transport through the oxide. The hydrated oxide is volatile and evaporates fast enough so that the silicon surfaces are free from oxides at high pressures of water vapor.

2.7.4 Promotion of Solid-State Reactions

There appear to have been no detailed studies on the effect of the presence of water vapor on alumina-formers. However, Kvernes et al [6] did not observe any effect of water vapor on the isothermal oxidation of a Fe – 13Cr – 4Al alloy at a range of temperatures of 680, 820 and 920°C. It has been noted that by increasing the aluminum content, aluminum is oxidized more selectively. The optimal concentration of Al necessary to form a single-layered, protective alumina scale depends on the temperature; particularly for this alloy, the higher the temperature, the higher the Al concentration was necessary.

Studies of the transient oxidation of Fe-Cr steels [64] at 600 – 700°C showed some effect of water vapor for 9%Cr, but no effect for $\geq$ 12%Cr, so that water vapor seemed to affect the initial stages of oxidation.

2.7.5 Change in the Plasticity of Oxide Scales

Water vapor can affect the plasticity of oxide scales. Some studies showed that decreasing of oxide plasticity by exposure in water vapor atmospheres results in an increase of the spalling rate [2]; other investigators propose the reverse scenario in which improved adherence is obtained by exposing under conditions including water vapor [65].

Tuck et al [66] are supporters of the latter and their studies focused on the oxidation of iron at 950°C; they found that there was an acceleration of the thickening of the oxide scale by introduction of water vapor to the oxidizing atmosphere. A conclusion was that water vapor (i.e. hydrogen) prevents the loss of contact between the scale and the substrate and this is possible by the increased plasticity of the oxide in wet conditions. The water vapor or hydrogen increases the

number of dislocations and/or their sources and sinks, or the mobility of already existing dislocations.

Rahmel and Tobolski [4] suggested that oxygen is rapidly transported inwards through unstable pores. These pores could act as both sources and sinks for dislocations and hence would enable the scale to creep. There must be an equal number of iron and oxygen lattice vacancies in or near the dislocations in order to maintain electrical neutrality. The addition of hydrogen ions in the form of hydroxyl (OH^-) would lead to additional Fe vacancies (one for each two H^+). It is possible that additional distortion around the dislocation would make it more mobile.

Rounded and spalled edges were observed on Fe specimens cycled in wet air, suggesting a lowering of the oxide plasticity in wet air. The degradation manifested first at the specimen edges where plastic deformation and accommodation of the surface oxide are required during thermal cycling in order to avoid spallation. This was observed in comparison to dry air exposure where the oxide was sufficiently plastic to deform at the edges and maintain adherence to the substrate during cycling.

Another result from this study [4] was the rapid weight loss of oxide that was initiated much earlier in air containing water vapor.

2.7.6 Selective Oxidation

Wagner's theory for the transition from internal to external oxidation in alloys assumes that this transition is caused by the blocking of the diffusion processes upon the formation of a critical volume fraction of the internal oxide in the matrix[12]. When the mole fraction of the less noble component in a binary alloy is increased to exceed a critical amount, the alloy no longer oxidizes internally but rather forms a compact, protective layer of the oxide of the less noble element on

the outer surface of the alloy. A change from the relatively fast oxygen uptake during internal oxidation (determined by the diffusion of oxygen in the matrix) to the very slow oxidation rate for the growth of a compact oxide layer (determined by the diffusion of the less noble element ions or oxide ions through its oxide) occurs upon exceeding this critical composition.

The presence of water vapor affects the selective oxidation. Kvernes et al [6] reported a decrease in the duration of the initial oxidation stage with water content in the ambient gas and an increase in the subsequent reaction rate under the same conditions for the high temperature oxidation of Fe-13Cr-xAl alloys. Though thicker scales formed, they were also less protective, including spinel in the inner part of the scale.

Buscail [67] has found that water vapor decreases the isothermal oxidation rate of Fe-Cr-Al at 1000°C. Although the effect was not large, the study proposed that the initial transient oxidation processes are affected by the wet conditions and that water vapor might have significant effects on the cyclic oxidation of certain alloys.

2.7.7 Reaction of H_2O with Cr

Studies involving the initial oxidation of Cr at 730K in gas mixtures containing water vapor shed some light on the dissociation of water and its reaction with chromium in such gas mixtures. Investigators considered that the dissociation reaction of water with many metals could form stable bulk products [68]:

$$H_2O \longrightarrow \textit{dissociation products} \longrightarrow Me_xO_y;\ Me_n(OH)_m;\ Me_rH_s \qquad (16)$$

In this study, percentages of $(CrOH^+ + Cr_2OH^+)/(CrO^+ + Cr_2O^+ + CrOH^+ + Cr_2OH^+)$, where O in all species comes from water, were used to evaluate the water dissociation. Further in this study, it was observed that at low temperatures (300 – 450K), the high OH percentage indicates a dominating partial dissociation:

$$H_2O = OH + H \qquad (17)$$

At higher temperatures (730K), the lower OH indicates a dominating complete dissociation:

$$H_2O = O + 2H \qquad (18)$$

Oxygen is reactive in the water dissociation:

$$H_2O + 1/2O_2 = 2OH \qquad (19)$$

at room temperature and this reaction is known to be metal-specific [68]. Such a process seems to operate in the reaction system shown above. At a higher temperature, the reaction of oxygen with hydrogen as shown below

$$yH_2O + xFe = Fe_xO_y + 2yH \quad (20)$$

$$2H + 1/2O_2 = H_2O \quad (21)$$

may promote the sequence from the partial dissociation of water vapor to a complete dissociation:

$$H_2O = HO + H = O + 2H. \quad (22)$$

2.7.8 Influence on Strain Rate

Kotchick's [69] work on the environmental effects on the strain-rate sensitivity of strengths of sapphire and silicon carbide-on-carbon filaments with pristine and damaged surfaces shows an increase in average fracture stress with increasing strain rate for the filaments tested in water. Previous studies [70,71] of the strength of sapphire have documented the susceptibility of the aluminum oxide to stress corrosion in environments containing moisture.

2.7.9 Cyclic Oxidation

In the case of isothermal exposures, the rate of oxidation determines the rate of material consumption. In general, the oxidation rate and the rate of material consumption are controlled by solid-state diffusion through the scale and they both show parabolic kinetics in which the instantaneous rate is inversely proportional to the existing scale thickness.

However, in actual applications, many components experience cyclic oxidation processes involving start-up period and shutdown periods. Most often encountered, the cracking and spalling of portions of the oxide scales occurs upon cooling and results in loss of the protective diffusion barrier provided by a fully intact scale. Upon subsequent reheating, the component will experience accelerated oxidation in the spalled areas because of the inverse growth rate dependence upon thickness.

Cyclic oxidation testing has therefore been an important tool of material characterization and performance for high temperature materials. It is used to assess high temperature environmental resistance of materials. During heating and subsequent cooling, the thermal expansion mismatch between metal and oxide results in thermal strains, a major cause of degradation of the protective oxide layer.

Ideally, cyclic tests should have a uniform heating rate, cycle duration and cooling rate. Another important parameter in cyclic oxidation tests is the frequency of the cycles or the length of time at temperature during each cycle. The effect of the cycle frequency in oxidation testing is highly dependent on the scale adhesion to the substrate, the total test time and the test temperature. The collected data is usually the specimens' mass-change versus time.

Smialek [30] reported some effects of water vapor on the spallation of oxide scales on Ni-Al. This work along with another study[3] demonstrated that the degradation of the oxide scale increased by a factor of 3 to 4 when the specimens that were subjected to cyclic oxidation were more frequently weighed.

3.0 RESEARCH OBJECTIVES

High temperature alloys and coatings that are used in gas turbines for air and marine applications develop oxidation resistance by formation of protective alumina or chromia during exposure to oxidizing conditions. As mentioned previously in the background section, water vapor has a deleterious effect on the oxidation of superalloys and coatings on superalloys, including thermal barrier coatings.

There are a number of publications in the literature discussing effects that can arise during the oxidation of alloys in the presence of water vapor; nevertheless, in order to understand the effects of water vapor on the oxidation of alloys, it is necessary to investigate different alloy systems and to develop a point of view that would allow establishing basic principles concerning this matter.

According to data in the literature, the following appear to be critical effects of water vapor during oxidation of alumina-forming alloys on:

- cracking and spalling of the alumina scale
- the growth rate of alumina scales
- the selective oxidation of aluminum
- spinel formation and on thermal barrier coatings failures
- regarding certain experimental variables:
    - water vapor pressure
    - specimen thickness

- temperature
- specimen cooling rate

However, the mechanisms and details of the processes that lead to the above-mentioned effects need to be closely investigated. Greater amounts of transient oxides formed on alloys exposed to wet conditions is an effect that has to be understood. By elucidating the mechanism by which water vapor causes an increased transient oxidation rate, this effect could be prevented or inhibited by appropriate factors. Furthermore, investigation of the factors that increase the severity of cracking and spalling of α-alumina scales from alloys and coatings appears to be of importance in order to be able to improve the performances of such systems. The interplay of these two processes, transient oxidation and scale spalling, determine the degradation rates for turbine airfoil alloys and coatings in water vapor conditions. Also, spinel formation affecting TBCs' life expectancy has to be investigated in more detail to better understand the mechanism by which water vapor affects the thermal barrier coating performance. Therefore, this study has concentrated on investigating alloy and coating systems behavior at high temperature oxidation in water vapor conditions, emphasizing the critical factors mentioned.

The specimens used in this study range from Ni base superalloys (PWA 1484, CMSX4, René N5) and aluminide/platinum-modified aluminide diffusion coatings on Ni base alloy substrates to state-of-the-art TBCs (EBPVD 8wt%YSZ) using the same Ni base superalloy substrate.

The specimens were subjected to cyclic oxidation test conditions at temperatures from 700°C to 1100°C in flowing gas mixtures of dry air and air containing defined partial pressures of water vapor. The fracture surfaces and cross sections were examined using optical and scanning electron microscopy (SEM) and X-ray diffraction techniques.

Specimens were examined after short time exposures in order to be able to investigate and eventually determine the initial stages of water vapor effects on oxidation. Comparisons of as-processed and exposed specimens were made to provide information on the microstructural changes, especially at critical interfaces.

Shorter time isothermal exposures in dry air as well as in wet air at appropriate temperatures were executed in order to determine a change in the rate of oxidation due to the presence of water vapor.

Different temperatures, water vapor partial pressures, specimen thickness were used to attempt to understand effects under various test conditions. Comparison of oxidation behavior under dry and wet conditions, under isothermal and cyclic exposures contributed to the better understanding of water vapor effects on high temperature oxidation.

Based on initial results from oxidation behavior, the critical factors that have an impact on the effects of water vapor and affect the performance of the specimens were determined.

During growth of oxide scales and cooling from temperature, alumina scales crack and spall due to residual stresses. The thickness of the specimens can affect the magnitude of these stresses. Coupons of 0.4 (thin) and 2mm (thick) were cyclically oxidized at 1100°C to compare oxidation behavior in dry and wet air.

More basic systems were brought into the research in order to further examine the effects of water vapor on the oxidation at high temperatures with a goal to simplify the interpretation of the oxidation mechanisms. Systems like Ni-Cr-Al (with a sufficient concentration of Al for the alloy to be an alumina former) were examined.

With regard to effects of water vapor on the performance of EBPVD-YSZ TBCs at 1100°C, experiments were directed at examining the process by which water vapor accelerates the formation of spinel phases in TBCs.

In summary, the purpose of this study was to investigate the effect of oxidation in the presence of water vapor of Ni base superalloy and coating systems and to perform an in-depth study in order to understand the mechanisms involved.

4.0 EXPERIMENTAL APPROACH

The specimens used in this work are single crystal Ni base superalloys, namely PWA 1484, PWA 1480, CMSX4 and René N5, single crystal Ni base alloys coated with aluminide/platinum-modified aluminide and thermal barrier coatings with compositions given in Table 1.

Table 1 – Composition (wt%) of the alloys

	Ni	Al	Cr	Ta	Co	Mo	W	Re	Ti	Hf	Y	C/B
René N5 regS (3-5ppm)/ lowS (<1ppm)	bal	6.2	7.0	6.5	7.5	1.5	5.0	3.0	-	0.15	0.01	0.05/0.004
PWA1484 regS (5-8ppm)/ lowS (1-2ppm)	bal	5.6	5.0	8.7 (9.0)	10.0	2.0	6.0	3.0	-	0.1	-	
CMSX4	bal	5.6	6.5	6.5	9.0	0.6	6.0	3.0	1.0	0.1	-	
PWA 1480	bal	5.0	10	12	5	-	4	-	1.5	-	-	
Diffusion Aluminide on René N5												
PtAl on René N5												
EBPVD 8wt% YSZ TBC on René N5												

Normal casting procedures for René N5 give sulfur concentrations between 3 – 5ppm. Special procedures to remove sulfur give concentrations less than 1ppm. Regular sulfur contents for PWA 1484 are in the range of 5 – 8ppm and low sulfur contents in PWA 1484 are between 1 – 2ppm. Regular sulfur content and low sulfur content specimens of René N5 and PWA 1484 were used in this work.

Some of the specimens were coupons with surface areas of 1 to 2 cm^2 and 0.3-0.4 to 2 mm thicknesses and the TBCs were circular discs 25.4 mm in diameter and 3.2 mm in thickness. A hole for the hangdown wire was made using a drill with a 1.2mm diameter.

The polished samples were prepared by grinding, followed by fine-polishing with a diamond paste and alumina suspension. The surface finish was 600 grit SiC abrasive paper for some specimens, while the majority of specimens were polished down to 0.05μm alumina suspension.

The aluminide coatings were obtained by using a high temperature low activity chemical vapor deposition (CVD) process and the top coat for the TBC discs was a typical yttria stabilized zirconia (YSZ) deposited by an electron beam physical vapor deposition (EBPVD) process on Pt-modified diffusion aluminide bond coats. A thermally grown oxide (TGO) develops along the YSZ/bond coat interface during deposition. The TGO becomes thicker during oxidation at high temperatures.

The specimens were subjected to thermal cyclic tests at high temperatures (700°C – 1130°C) in an apparatus that enables the specimens to be cycled in and out of the hot zone, Figure 3. The basic structure of the furnace is a thick walled silica horizontal tube. The cycles consisted of 45 minutes at temperature and 15 minutes in the cold zone (approximately 100ºC) of the apparatus. Tests were performed in both dry air and air saturated with water at 33.1ºC, 46.1ºC and 88.1ºC, yielding a water partial pressure of 0.05, 0.1 and 0.5 atm, respectively. The fraction of H_2O was controlled by passing air through a water bath heated to a specific temperature so that the partial pressure of the water vapor could be adjusted. The temperature of the water tank was carefully monitored at the desired temperature to ensure a stable water vapor pressure. Two bubbling systems in series were used. The gas flow in the furnace was 0.1cm/s. The specimens were periodically removed from the apparatus and weight measurements were performed along with visual examination.

Top view images of the oxidized specimens were observed and polished cross-sections of the specimens were prepared in order to investigate the oxide morphology and the oxide growth behavior on the specimens.

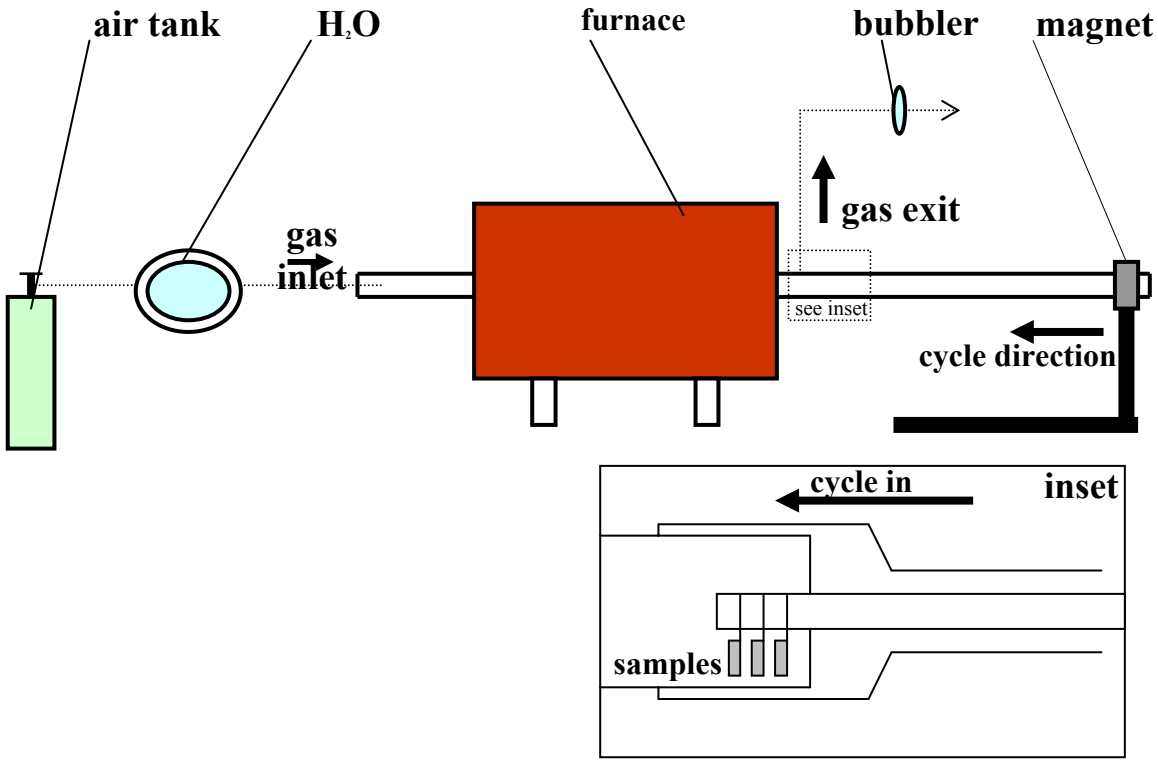

Figure 3 Experimental apparatus used for cyclic oxidation tests

Thermogravimetric analysis (TGA) is the primary analytical technique to examine the kinetics of oxidation, i.e. the weight change due to exposure to an oxidizing atmosphere. The schematic configuration of the electrobalance is shown in Figure 4. A Cahn D200 microbalance with direct digital output to a computer was employed. The balance is connected via a ball and socket joint to a vertical quartz reaction tube. Specimens were hung to the balance arm with a platinum wire. The resulting data was analyzed for weight gain versus time, data that was also plotted as weight change versus the square root of time with the slope being the parabolic rate constant.

Optical microscopy and scanning electron microscopy (SEM) with energy dispersive X-ray analysis (EDS) were used for the characterization of the microstructures and the chemical composition. The backscattered electron mode in the SEM was employed for compositional contrast imaging.

The oxide phases were determined by X-ray diffraction (XRD) techniques at room temperature. A potential of 40kV and a current of 30mA were used to produce Cu Kα radiation. Data was analyzed using the Philips XRD Organizer software. Standard θ/2θ diffraction geometry was used to analyze layers with sufficient thickness. For very thin layers, a fixed incidence angle diffracting mode, referred to as “glancing angle X-ray diffraction” was used. This allowed diffraction information to be obtained from thin oxide films without (much) interference from the substrate.

Stresses that persist in the absence of any external forces are called “residual stresses”. Residual stresses at room temperature result from thermal stresses and growth stresses. The residual stress in alumina scales formed on specimens of Ni base superalloys was measured at room temperature using the tilting and rocking techniques. X-ray diffraction techniques can be

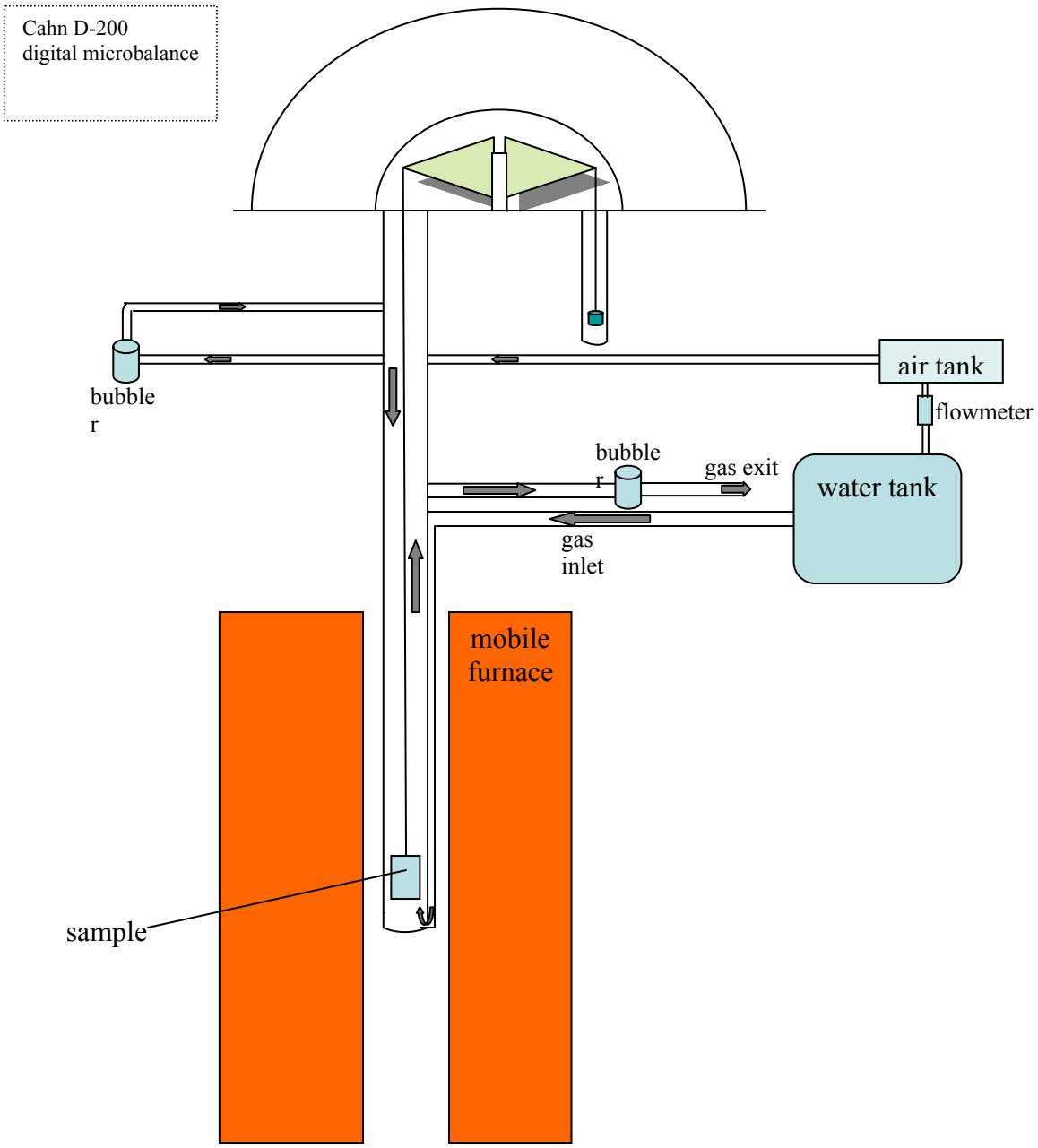

Figure 4 Cahn D-200 microbalance with digital recording - schematic diagram showing the TGA apparatus for isothermal oxidation of specimens in flowing gases with defined and controlled amounts of water vapor in air at a total pressure of 1atm. Arrows show directions of gas flow. The airflow in the upper region of the reaction tube is to prevent water vapor condensation in the balance area.

used to determine residual stresses in oxide scales and substrates and these can be done at room temperature or at the oxidation temperature (in situ). The "$\sin^2\psi$" method is commonly used to measure residual stresses. In a polycrystalline material with grains of sizes very small compared to the irradiated volume, a number of grains diffract X-rays at a given ψ-tilt. The lattice spacing determined from the angular position of the maximum diffracted intensities will be an average value for all these grains. Measurements are made at multiple ψ tilts and the stresses are then calculated from the slope of the d_{hkl} spacing versus $\sin^2\psi$ plot – this is the procedure known as the "$\sin^2\psi$" technique.

The experimental procedure used to taper-polish sections of oxide on exposed specimens consisted of polishing the specimens to a 1μm finish using diamond lapping, usually at a small angle (1° or 2°) to the major surface to expose 300 – 350μm widths of sections of the scale and, in this way, to form tapered sections of the scale. A tripod polisher equipped with a micrometer base and non-rotating micrometer precision locking feet was used.

5.0 RESULTS AND DISCUSSIONS

5.1 MICROSTRUCTURAL CHARACTERIZATION OF SUPERALLOYS AND ALUMINIDE COATINGS ON SUPERALLOYS PRIOR TO EXPOSURE

PWA 1484, CMSX4 and RenéN5 are all single crystal γ/γ' superalloys. All these single crystal alloys contain a fine dispersion of γ' particles in a γ matrix.

Single crystal Ni base superalloys typically show a dendritic solidification structure in which both the dendritic areas and the interdendritic areas consist of cubic γ' (Ni_3Al) precipitates uniformly distributed in a single crystal γ phase nickel matrix, Figure 5. In certain areas, the γ' precipitates in the interdendritic areas are larger than in the dendritic areas. Some (γ + γ') eutectic precipitates could also be present as isolated white zones at the interdendritic areas. The γ' and γ phases are heavily substituted with alloying elements.

The compositions of these superalloys are presented in Table 1 on page 41. All of the alloys have compositions such that an alumina scale is formed during oxidation at 1100ºC after a period of some transient oxidation.

An isothermal Ni-Cr-Al diagram shows the compositional limits for three oxidation mechanisms of these alloys (Ni-Cr-Al) at 1100°C, Figure 6.

For the aluminide coated René N5 processed by CVD (Chemical Vapor Deposition (low activity process)), the outward diffusion of nickel is favored for subsequent reaction with aluminum. Precipitates in the form of intermetallics and carbides (MC, M_6C, $M_{23}C_6$) form in an

interdiffusion zone, Figure 7. Precipitates have formed in the first place because of the low solubility of substrate elements in NiAl. A surface micrograph of the as-processed aluminide coatings on superalloys, Figure 8, shows the ridges that develop at the grain boundaries. After

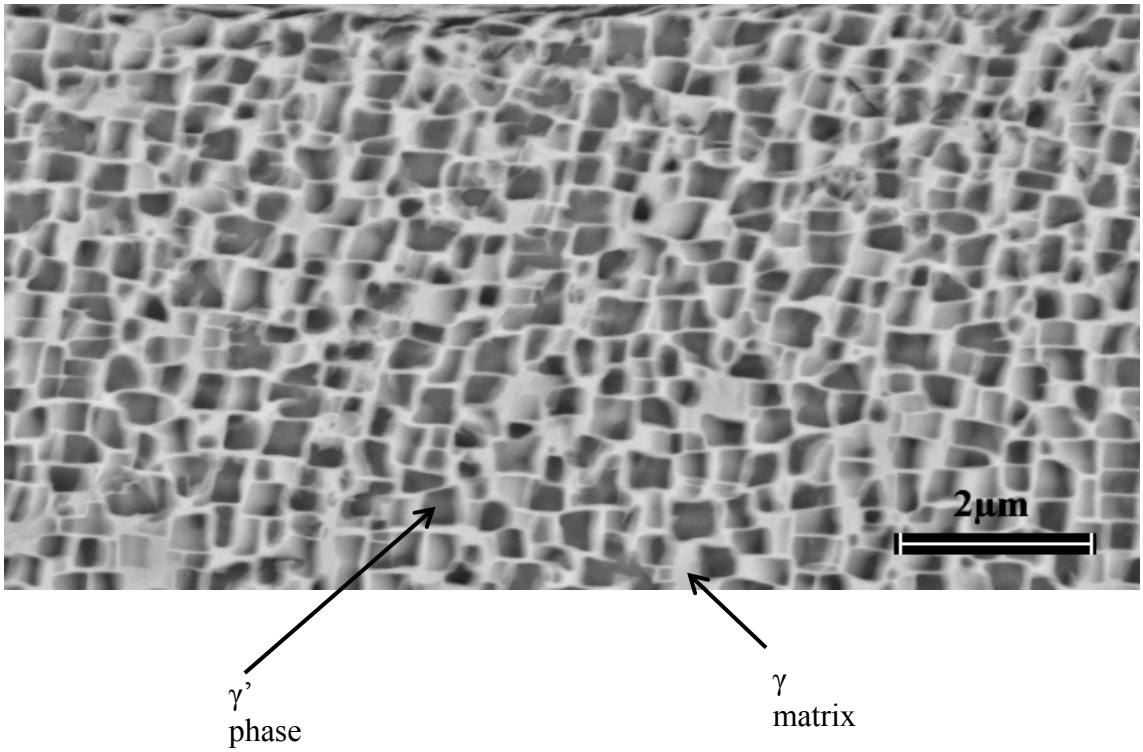

Figure 5 Single crystal Ni base superalloy – typical structure. BSE image in SEM with γ phase appearing bright and γ' phase in a darker cubic morphology

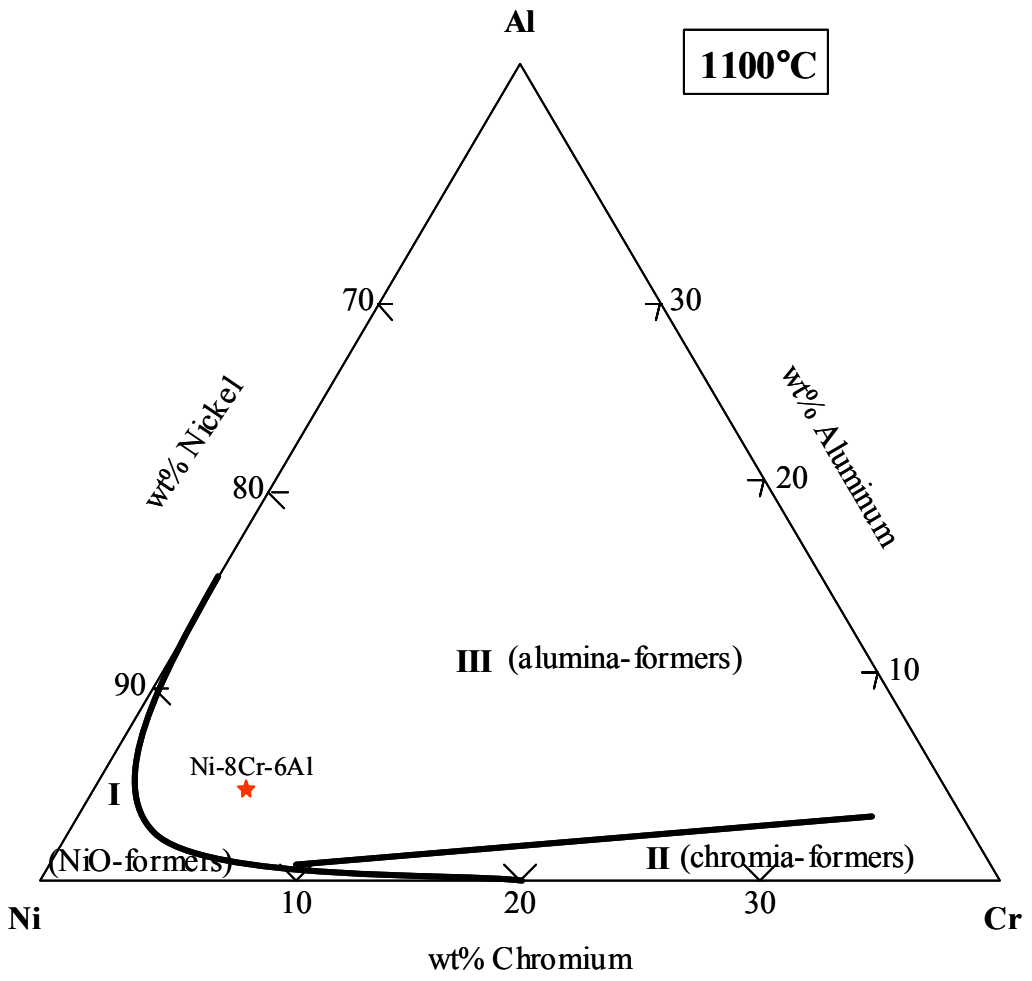

Figure 6 Isothermal diagram showing the compositional limits for the three oxidation mechanisms of Ni-Cr-Al alloys in 0.1atm of oxygen at 1100°C: I – NiO-formers; II – chromia-formers; III – alumina-formers (*After C.S.Giggins, F.S.Pettit – J. Electrochem. Soc., 118, 1782 (1971))

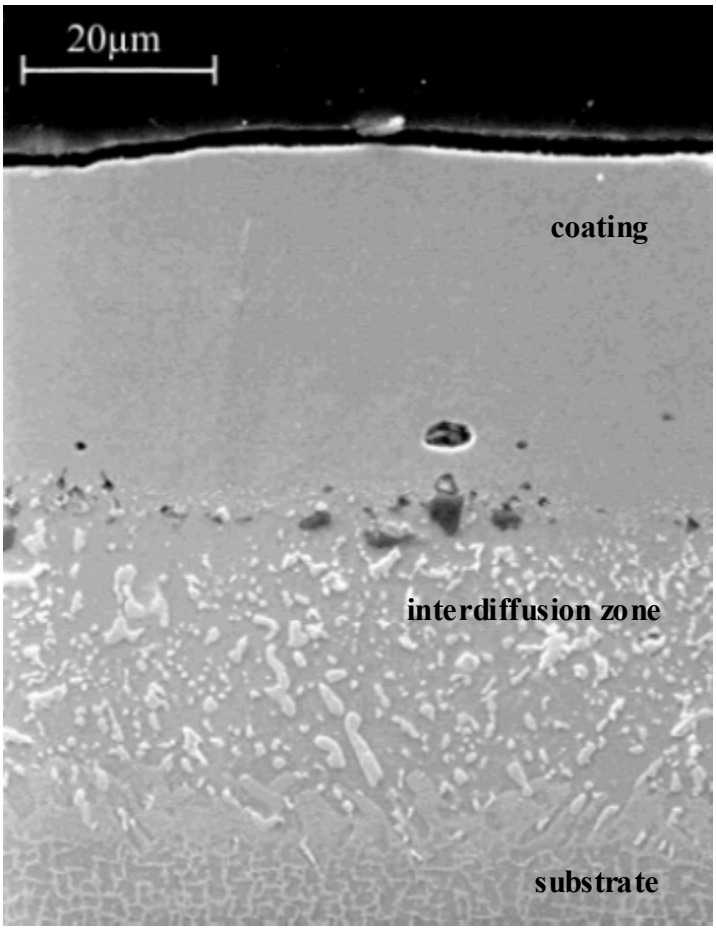

Figure 7 Typical cross-section of an aluminide coating on a superalloy René N5 substrate

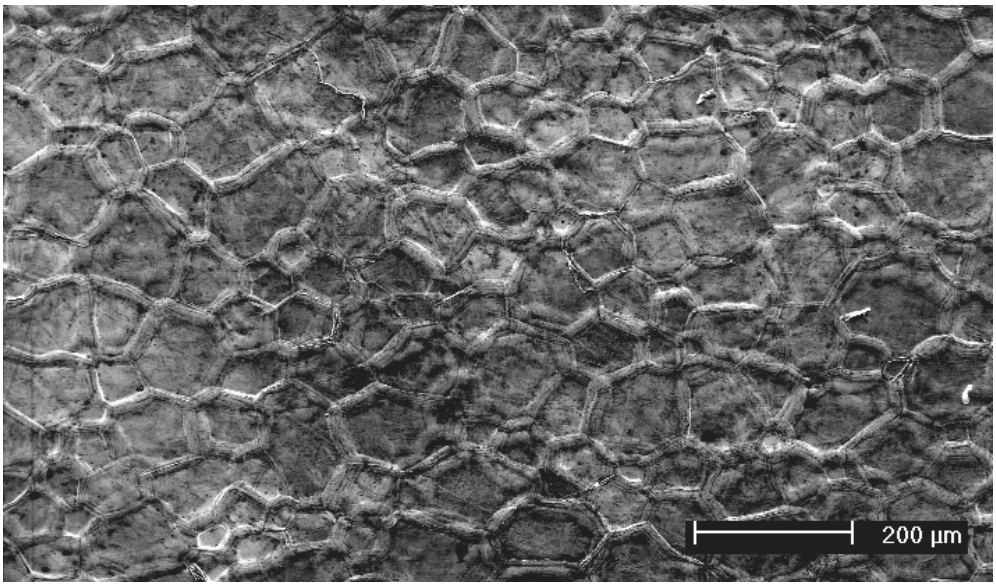

(a)

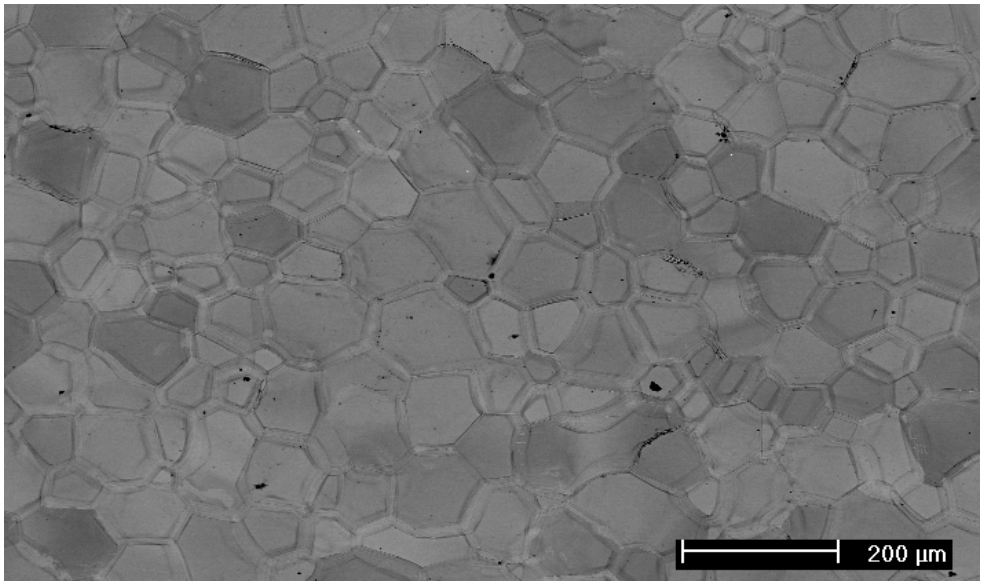

(b)

Figure 8 Top view images for as-processed Pt-modified aluminide coatings (a) SE mode; (b) BSE mode in the scanning electron microscope

cyclic exposure, cracks were observed on these grain boundary ridges, Figure 9. These cracks have been reported to be due to out-of-plane tensile stresses generated at the peaks of the ridges[72].

5.1.1 Effects of Water Vapor on Cracking and Spalling of α-Al_2O_3 Scales and on the Growth Rate of Alumina Scales

5.1.1.1 Cracking and Spalling of α-Al2O3 Scales during Superalloys Oxidation α-Al_2O_3 is one of the most protective oxide layers that form upon oxidation on high temperature alloys because it is chemically inert, dense and slowly growing due to its low defect concentration. Slow scale growth rates and thin scales are common attributes of alumina scales; however, the adhesion of alumina scales can be variable. In most cases, its adherence to the metallic substrate is poor and, especially during thermocycling, cracking and spalling occur, leading to rapid oxidation subsequently.

The delamination of Al_2O_3 scales is attributed to growth stresses [73] by lateral oxide growth [74], to thermal stresses and to void formation at the scale/alloy interface [75] promoted by segregation of impurities (e.g. sulfur) to the metallic surface of the cavities[76].

For the present work, weight change versus time measurements – in which the data were normalized per unit area - are presented in Figure 10 for René N5 and low sulfur content René N5 specimens exposed at 1100°C in gases with different amounts of water vapor. It can be seen that the weight losses are smaller for the low sulfur content N5 specimens compared to the regular sulfur content N5 specimens. The plots also suggest that the amount of degradation of N5

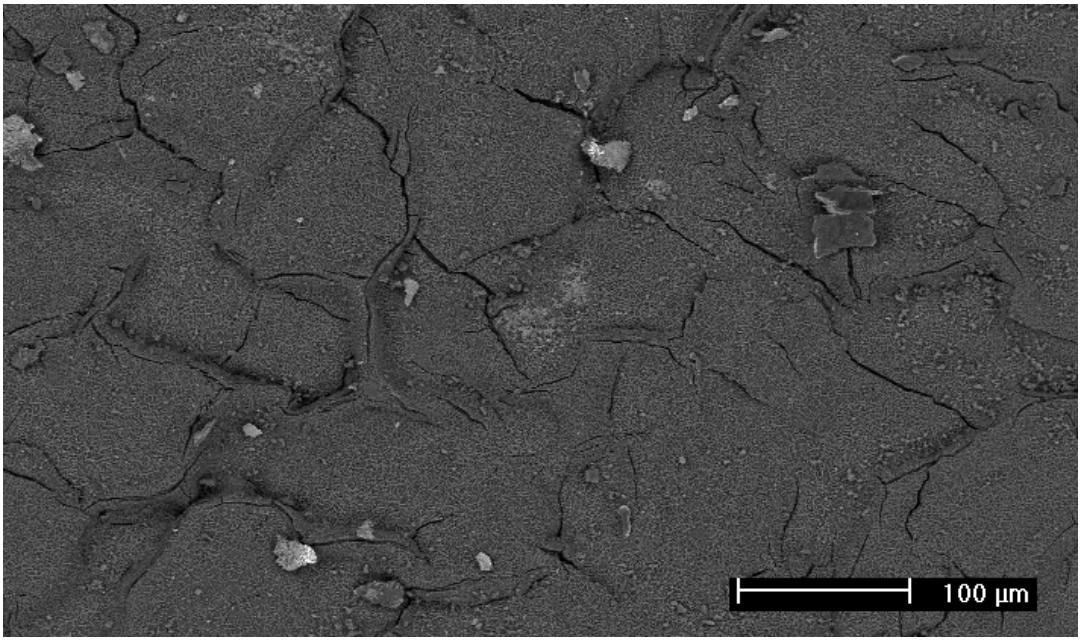

Figure 9 Cracks developed at ridges on a specimen of Pt-modified aluminide coating on René N5 after cyclic exposure of 1500 hours at 1100°C

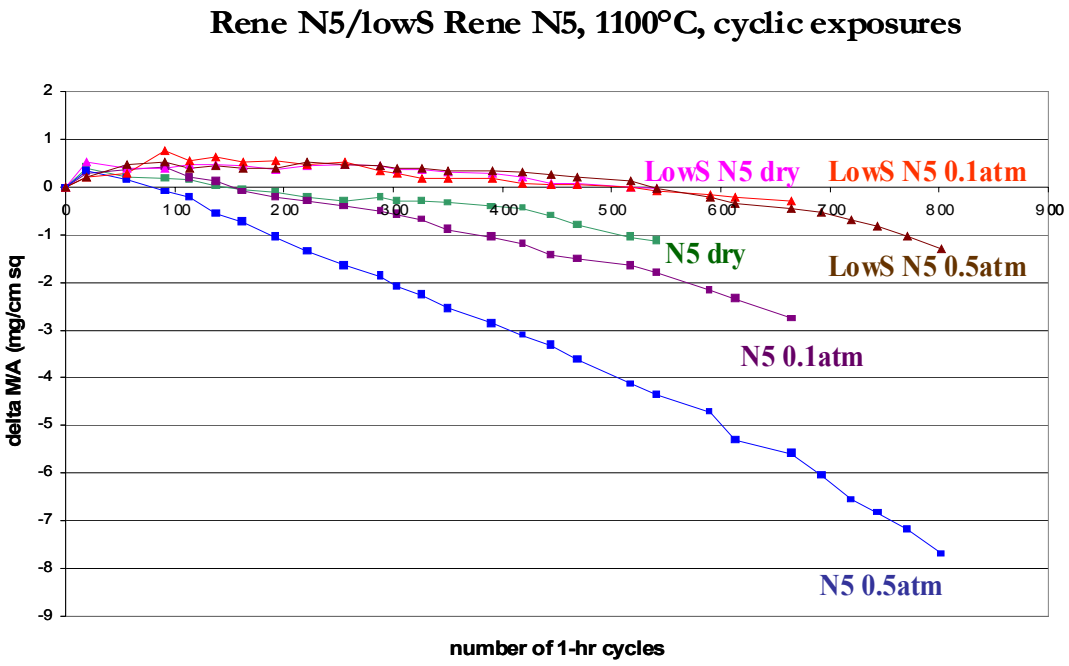

Figure 10 Weight change versus time measurements for René N5 specimens - low S (< 1ppm) and regular S (3-5ppm) - cyclically oxidized in dry and wet air at two water vapor pressures (0.1atm and 0.5atm)

specimens increases as the partial pressure of water vapor in the gas increases. Surface micrographs of specimens exposed in this test are presented in Figure 11. It can be seen that more spalling of oxide is evident for regular sulfur content N5 compared to low sulfur content N5 and the amount of spalled oxides increases as the water vapor pressure in the gas is increased, whereas the water vapor pressure had no significant effect on degradation of low sulfur content N5.

Scanning electron micrographs showing cross-sectional views of the exposed specimens are consistent with the previous results. An external scale containing NiO with practically no continuous α-Al_2O_3 is evident on the N5 specimen exposed for 802 cycles at 1100°C in a gas mixture with 0.5 atm of water vapor, Figure 12a, whereas the low sulfur content N5 exposed to similar conditions, Figure 12b, exhibits a scale of continuous α-Al_2O_3 with an overlayer of transient oxides. The transient oxides, in the case of nickel base superalloys such as René N5, are generally NiO, Cr_2O_3 and Ta_2O_5, but the oxides of some other elements in the alloy can be present as well. With the exception of the reactive elements (i.e., Y, Hf), α-Al_2O_3 is the most thermodynamically stable oxide. Aluminum is selectively oxidized and the transient oxides develop before the α-Al_2O_3 is formed as a continuous layer over the alloy.

In a cyclic test, if the scale does not spall, the α-Al_2O_3 layer becomes continuous for sufficiently long exposure times and the oxidation rate is controlled by diffusion through the α-Al_2O_3 scale. The transient oxides can react with the α-Al_2O_3 to form spinels (e.g. $NiAl_2O_4$, $NiCr_2O_4$). A schematic description of such scales is shown in Figure 13. When the scales spall during cyclic oxidation, the oxides scales that develop subsequently exhibit much more transient oxide because the alloy has been depleted of aluminum, Figure 12a, and the α-Al_2O_3 layer

requires long exposure times to develop continuity. For short cycles, the α-Al_2O_3 layer may not develop continuity and the weight losses are large, Figure 10.

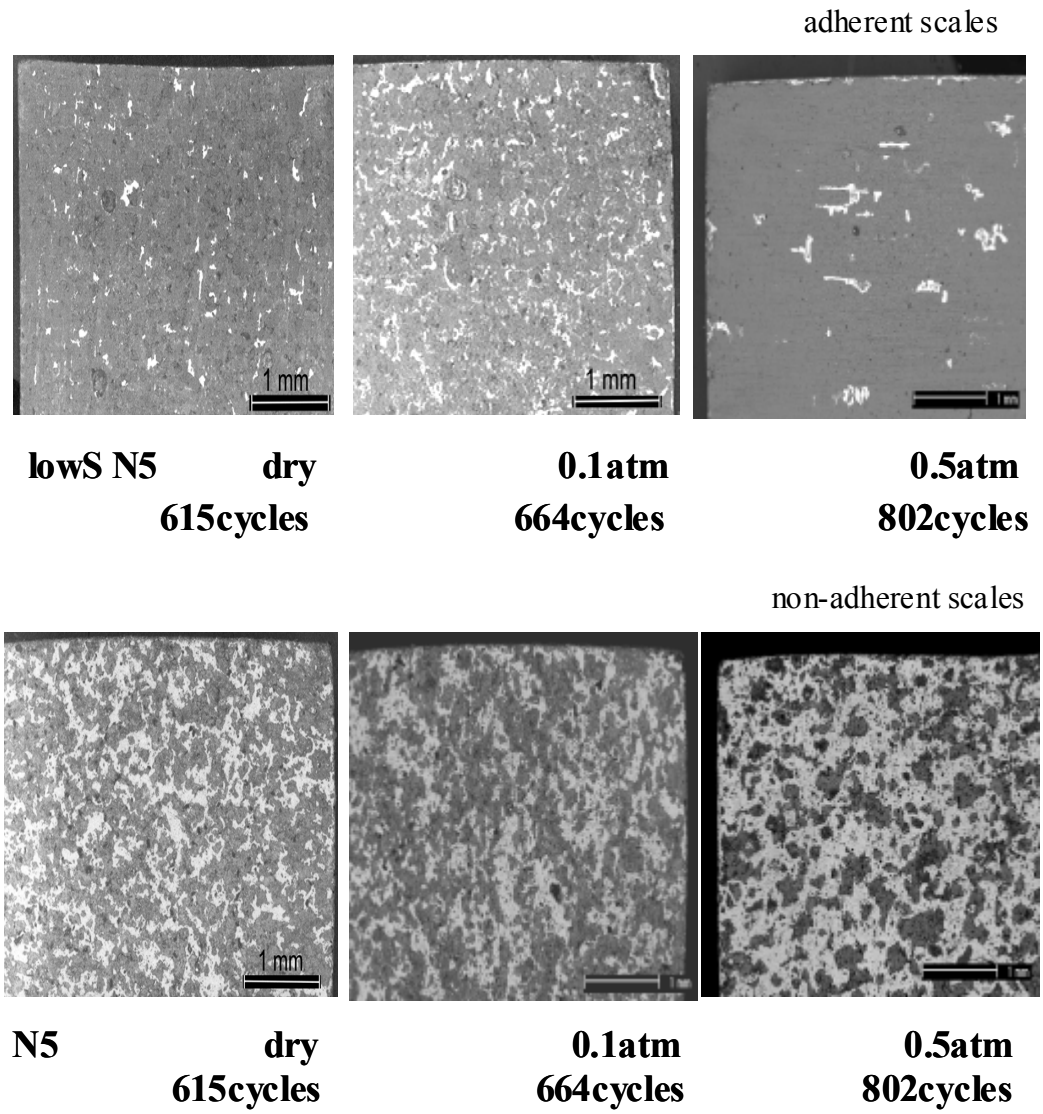

Figure 11 Cyclic exposures @ 1100°C of René N5 and low sulfur content René N5; all surfaces: light coloration-spalled regions, darker coloration-mixed oxides and a-Al_2O_3

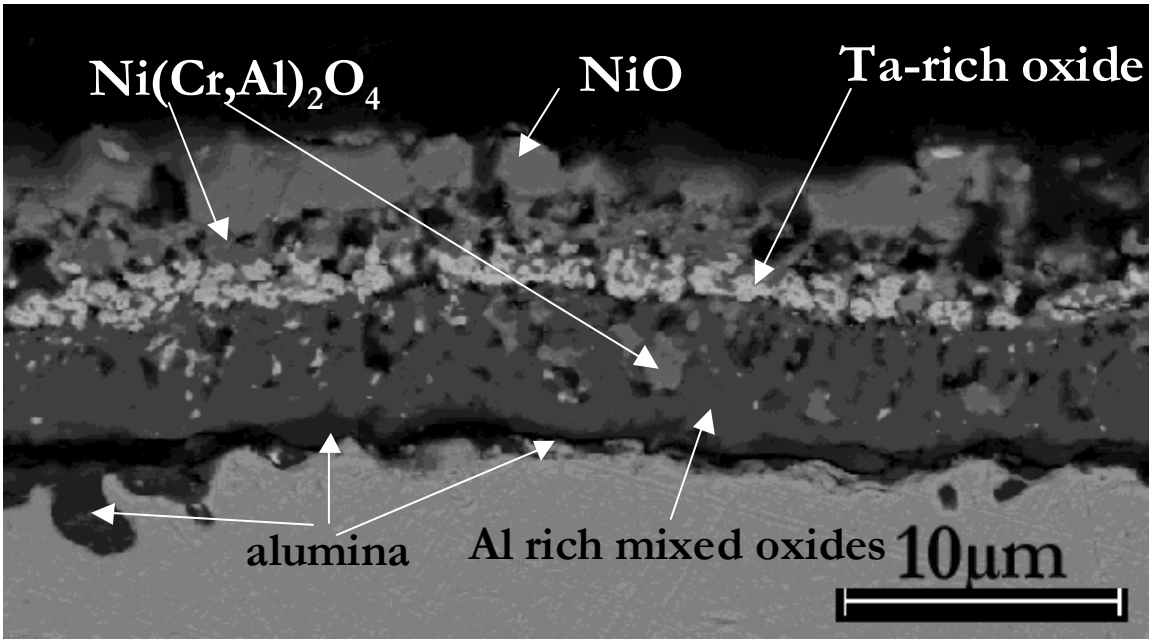

(a)

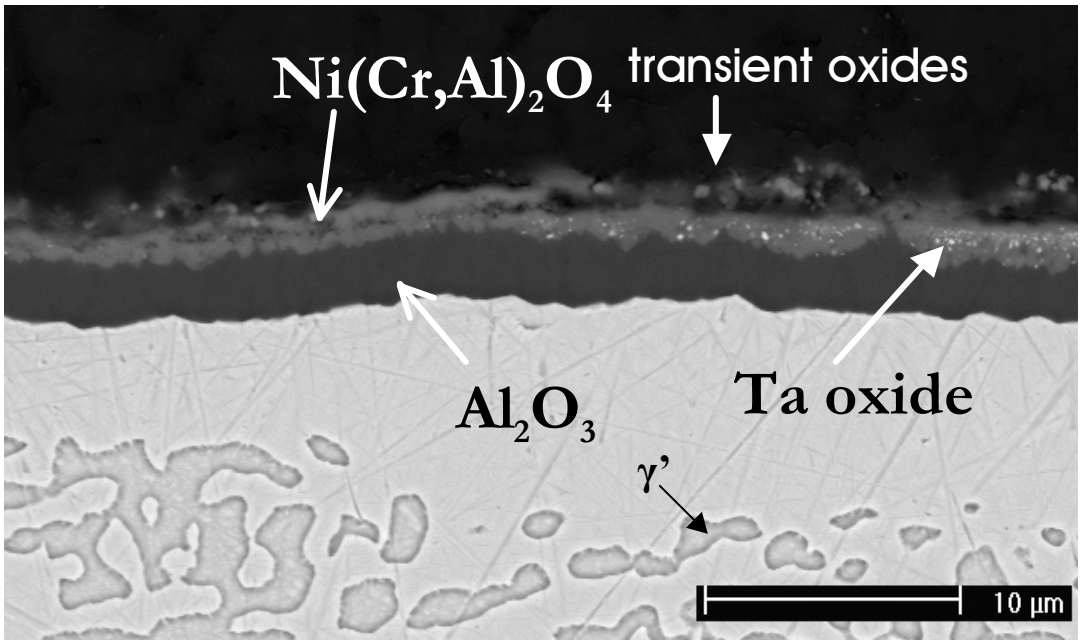

(b)

Figure 12 (a) René N5 with regular S content oxidized for 802 cycles @ 1100°C in air with 0.5atm water vapor. The original a-Al_2O_3 has spalled. (b) René N5 with low S content exposed for 802 cycles @ 1100°C in wet air (0.5atm water vapor). The original a-Al_2O_3 has not spalled.

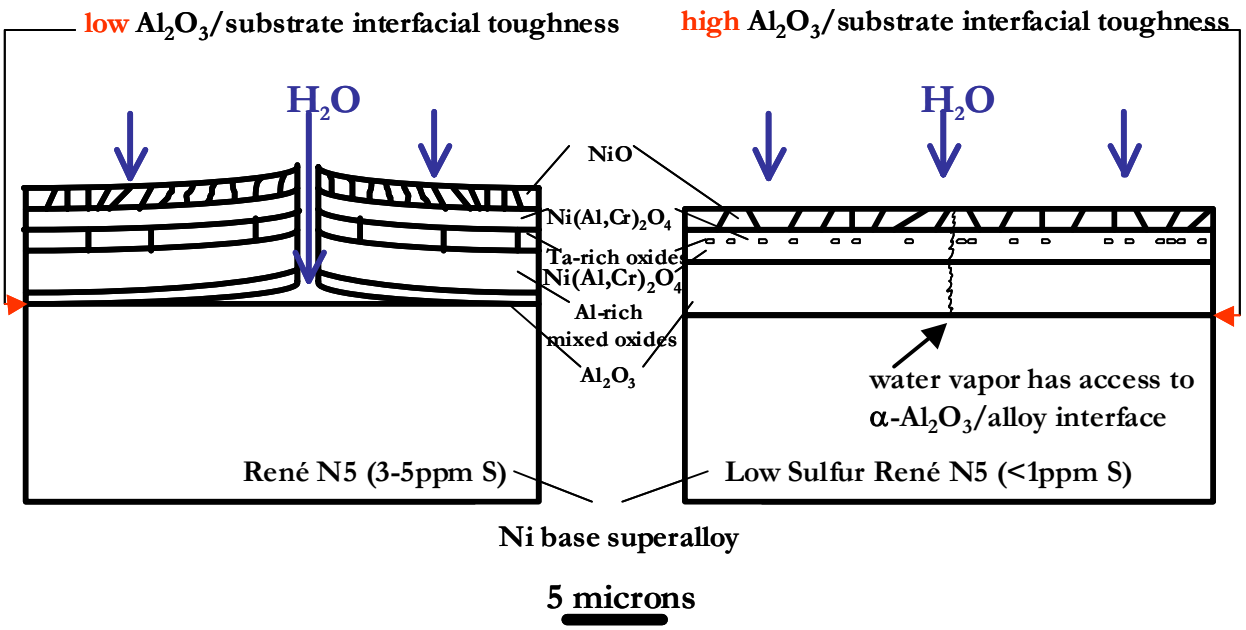

- cracked scale
- thicker scale
- thicker spinel layers

- water vapor has access to α-Al_2O_3/alloy interface
- adherent scale
- thicker alumina scale

Figure 13 Schematic showing scales formed on cyclic exposures (hundreds of cycles) @1100°C in wet air. When sulfur is present (5-8ppm), the ingress of water vapor along the a-Al_2O_3/alloy interface is rapid.

Results that have been obtained with René N5 (regular and low sulfur content) are consistent with data from previous work [3] on other alloy systems (PWA1480, PWA1484, CMSX4). Under water vapor condition tests, the cracking and spalling of the α-Al_2O_3 scales is more pronounced, but this effect becomes less evident as the interfacial toughness becomes greater.

When the alloy sulfur concentration is large and sulfur is present at the oxide/substrate interface, the interfacial toughness is low and water vapor lowers it even more and in this way the oxide spalls easily.

When the sulfur concentration is small, either water vapor has no significant effect or the interfacial toughness is so high that even with the presence of water vapor the α-Al_2O_3/substrate interfacial toughness is still sufficient to inhibit spalling.

As it will be presented in the next subchapter, such results are observed with aluminide coatings as well, where the α-Al_2O_3 scales are substantially more adherent on a platinum modified aluminide coating compared to a simple aluminide coating, even in water vapor conditions.

Increase of mass gain following a quasi-linear rate law is a result of the breakdown of the protective property of the oxide layer. It is assumed that the oxide layer partially spalls off and the metal surface underneath is oxidized forming additional oxide leading to additional mass gain. The oxidation kinetics are quasi-linear as a result of repeated cracking, subsequent oxidation of the free metal surface and healing. When the scale loses contact with the substrate, the adhesion is reduced until the scale spalls off and oxygen arrives at the bare metal giving the start for a rapid oxidation.

As can be seen schematically in Figure 13, when the oxide/alloy interface is weak, water vapor can cause spalling; whereas when this interface is strong, spalling of the α-Al_2O_3 is only sporadic. Smialek and Morscher [77] propose that sulfur and water vapor may interact to promote spalling of α-Al_2O_3 scales. In particular, sulfur at the α-Al_2O_3/ alloy interface causes stretching and weakening of bonds whereby ingress of water vapor proceeds more rapidly with the final result of oxide scale delamination due to formation of weak Al – OH^- bonds. It is proposed that water vapor causes the α-Al_2O_3/alloy interfacial toughness to be decreased, but when the value of the toughness is large – as occurs for α-Al_2O_3 on low sulfur content N5 (and on platinum modified aluminide coatings, as will be shown later on in this work) – the amount of the toughness decrease is not sufficient to cause significant quantities of oxide scales to spall. The mechanism by which water vapor has access to the α-Al_2O_3/alloy interface may be via small cracks that develop in the α-Al_2O_3 during thermal cycling [3]. Kronenberg et al [78] have determined that annealing α-Al_2O_3 in supercritical water between 650°C and 1025°C under pressures in the range 1500 – 2000 MPa introduces interstitial hydrogen defects ($H_i^{\bullet}$) and molecular water clusters. These clusters were found to segregate to surfaces, cracks and grain boundaries. The strength of both α-Al_2O_3 single crystals and polycrystals were reduced by this hydrothermal treatment [79]. The results from Kronenberg et al [78] suggest that molecular water clusters (or OH concentrations of ~ 1700ppm) may diffuse through the α-Al_2O_3 scale via grain boundaries.

The mechanism by which water vapor detrimentally affects the adherence of α-Al_2O_3 scale has been proposed to consist of stress corrosion cracking by which water vapor causes the bonding along the oxide/substrate interface to be weakened. Even though cyclically oxidized René N5 (low S content) and PtAl coatings do not spall as much as René N5 (regular S content)

and straight-aluminides in wet air at 1100°C, in both cases water vapor has access to the oxide/substrate interface. The higher spallation resistance of René N5 low S and PtAl coatings is due to a higher Al_2O_3/substrate interfacial toughness. Water vapor reacts with oxides and glasses (soda-lime glas and sapphire from the study of Weiderhorn[80]) that are subjected to stresses to cause a reduction in strength that increases with time. Acoustic emission measurements[3] show that cracks exist even in very adherent alumina scales. A crack that forms propagates until it is large enough to result in failure. Water vapor has access to the oxide/substrate interface through cracks in the oxide scale and, combined with the stress, can cause spalling of the scale by an interfacial stress corrosion cracking, Figure 14.

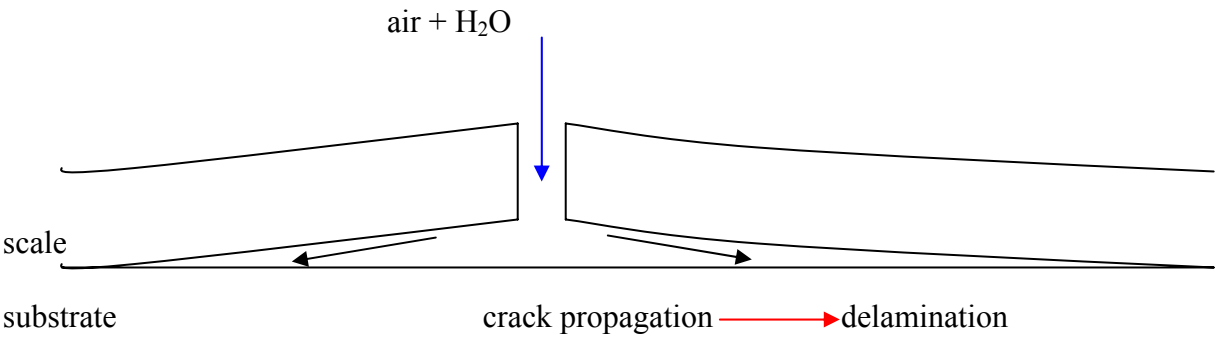

Figure 14 – Schematic for the mechanism of stress corrosion cracking

5.1.1.2 Cracking and Spalling of α-Al_2O_3 Scales on Aluminide Coatings More adherent scales are found for the Pt-modified aluminide coatings, as presented in Figure 15. This plot compares plain nickel aluminides to the platinum-modified version of the aluminide coatings and it clearly shows a significant improvement in terms of the oxidation resistance for PtAl specimens cyclically exposed in air with water vapor next to the plain aluminides' behavior. The data available shows a slow mass gain for the PtAl specimens over a period of about 3000 cycles, Figure 15. This result comes in agreement with results from the oxidation of René N5 superalloys, presented previously in this work, exposed in dry and wet air in showing that the cracking and spalling of the α-Al_2O_3 scales is greater in water vapor conditions, but this effect is less pronounced for higher α-Al_2O_3/substrate interfacial toughness.

Moisture-assisted delamination may be a fast crack propagation phenomenon, where the decrease in the stored compressive strain energy (thermal expansion mismatch) is greater than the increase in surface energy created by spallation.

The concentration of aluminum at the metal surface is known at the beginning of the oxidation process, but the decrease by aluminum consumption upon oxidation must be considered. When aluminum is consumed according to a parabolic rate law, the aluminum consumption by oxidation equals the aluminum supply by diffusion at a certain surface aluminum concentration. The equilibrium is established when this steady state aluminum concentration is established and constant. The aluminum consumption is the highest at the beginning of oxidation and it decreases due to formation of a protective layer. The kinetics of aluminum consumption are not parabolic in the very beginning, but linear. The requirement for a constant surface concentration of aluminum (i.e. aluminum consumption according to a parabolic

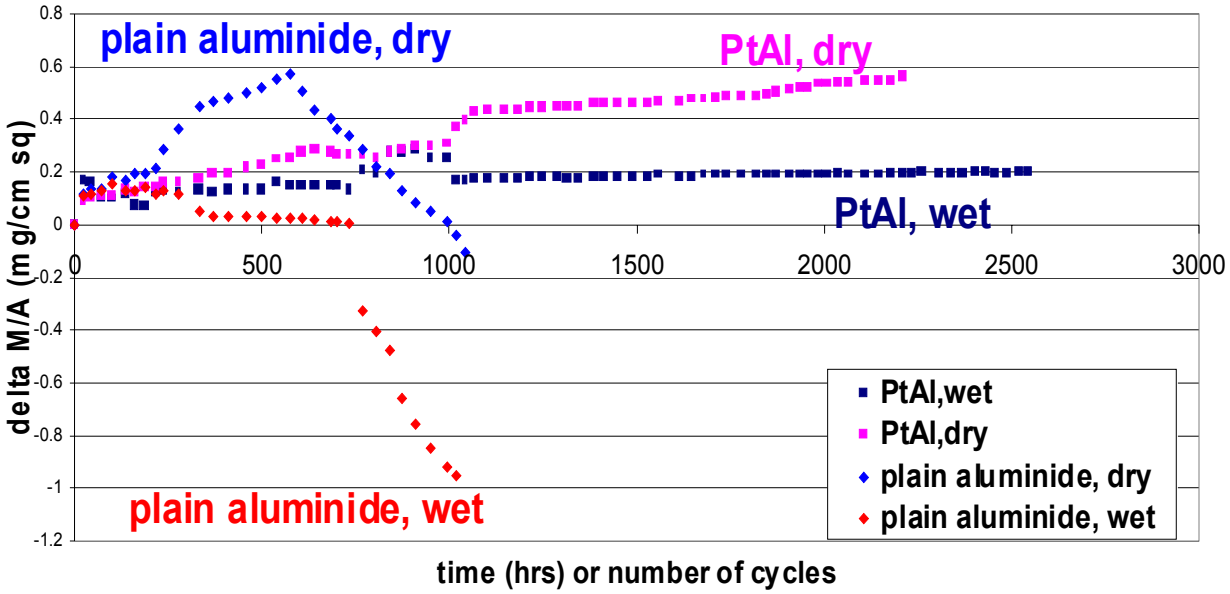

Figure 15 Change in mass vs. time – aluminide coatings cyclically exposed @1100°C, dry and wet (0.1atm) air

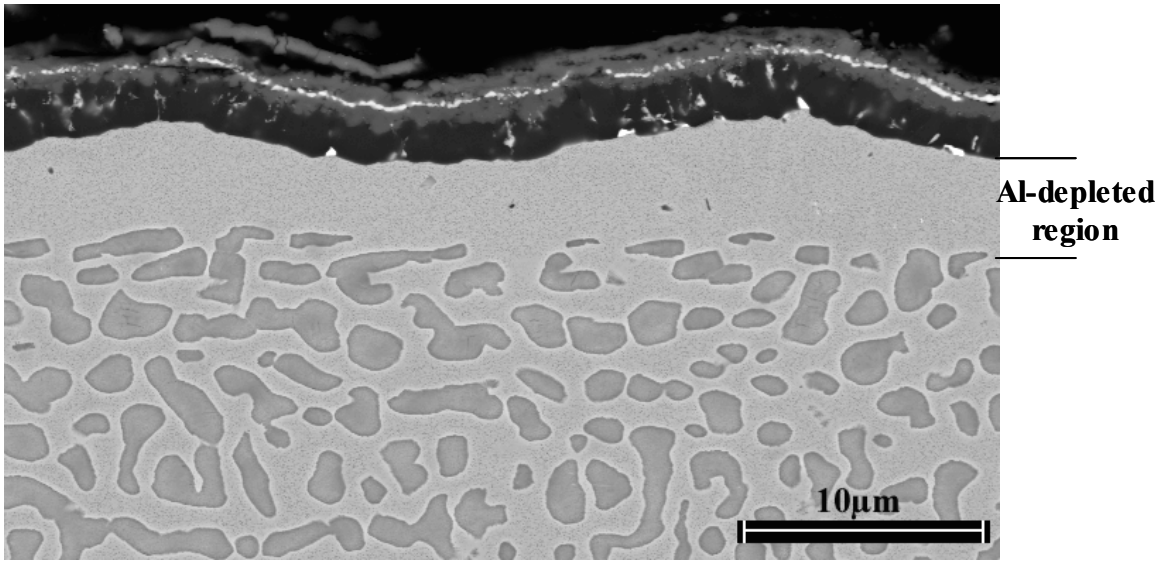

Figure 16 Formation of Al-depleted zone on a cross-section of a specimen of René N5 oxidized for 464 cycles in dry air at 1100°C

rate law) is not fulfilled in the beginning and the surface concentration of aluminum is higher in the beginning. It decreases from the value for the undepleted substrate in the beginning to the equilibrium value after some time of exposure when oxidation kinetics have become parabolic and an aluminum depletion profile with a constant aluminum concentration has been established. An Al-depleted zone develops, Figure 16.

5.1.1.3 Growth Rate of Alumina on Superalloys Weight change versus time measurements for the cyclic oxidation of the superalloy PWA1484 in dry and wet (P_{H2O} = 0.1atm) air at 900°C are presented in Figure 17. The data for PWA1484 in wet air is exhibiting weight losses after about 600 cycles (approximately 450 hours of exposure at temperature), but no indication of weight losses is evident in dry air. The oxide phases formed on the superalloy mostly observed on the dendritic areas were NiO which had a blocky morphology; the interdendritic areas show fine-grain oxide and have a relatively smooth appearance, Figure 18 – using EDAX analysis, strong Ni, Al and O peaks with medium Cr peaks were obtained from this phase.

Disk formations containing oxides of Ni, Ta and Co started to appear as part of the scale in the wet exposed PWA1484; these formations were observed as part of the upper scale in the cross-section images after 2150 cycles of exposure. Deep penetration areas of mixed oxides appeared as the scale formed on the superalloy PWA1484 after the water vapor cyclic exposure at high temperature was completed, Figure 19.

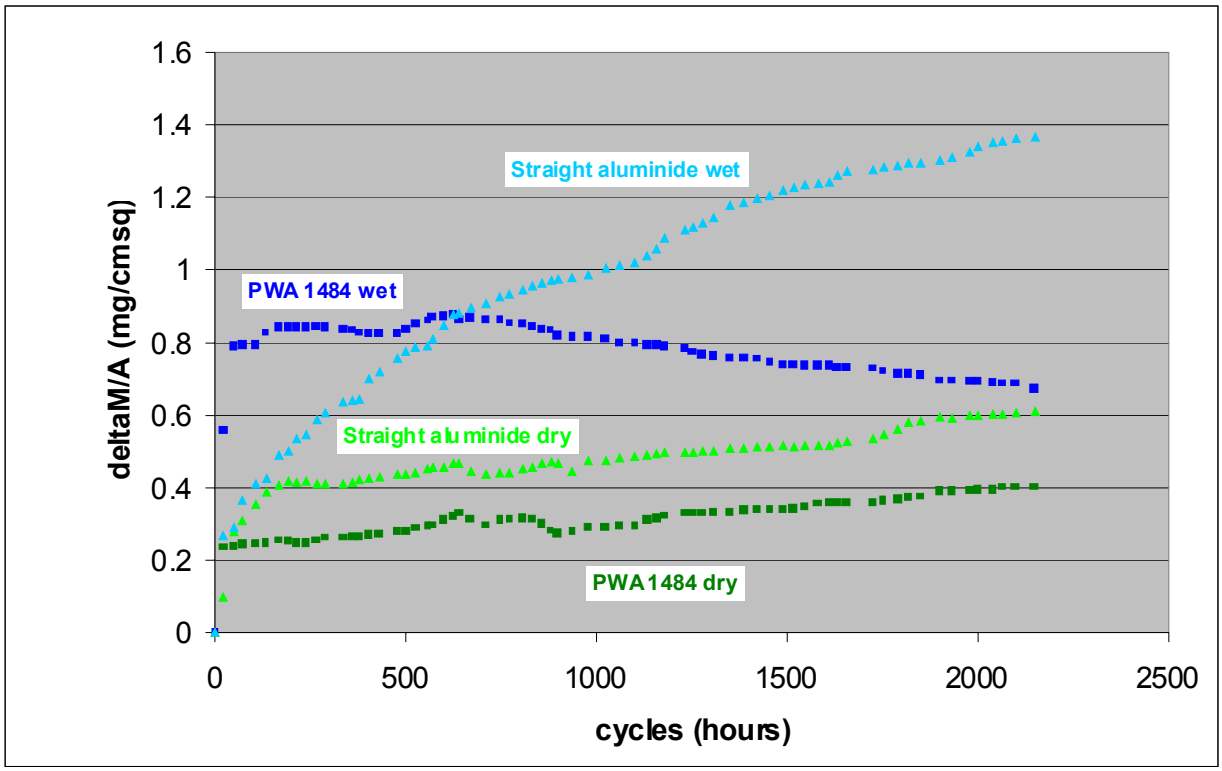

Figure 17 Weight changes versus time measurements for the cyclic oxidation of aluminide coatings on N5 and for PWA 1484 in wet (P_{H2O} = 0.1atm) and dry air at 900°C

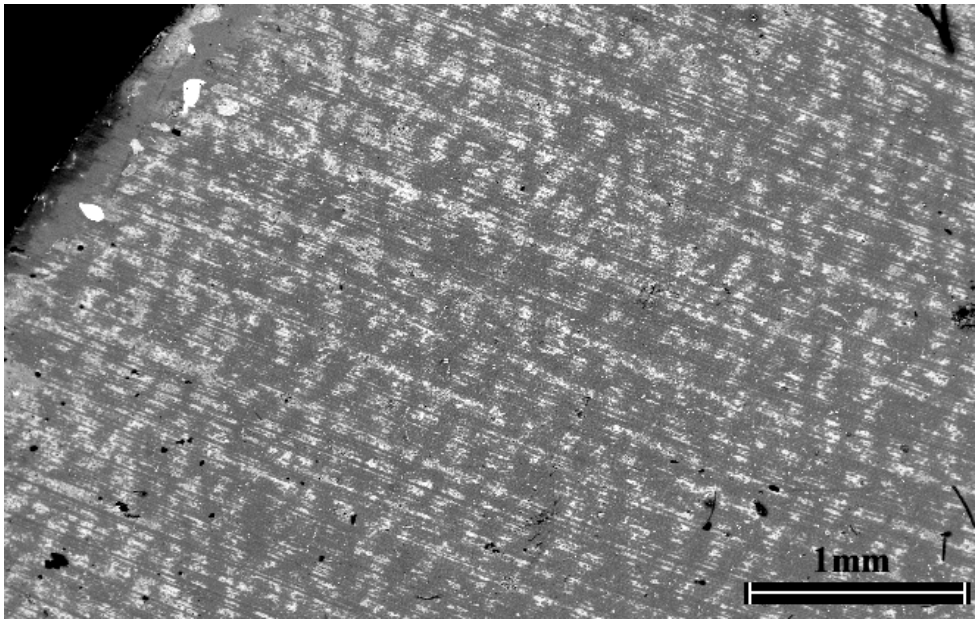

(a)

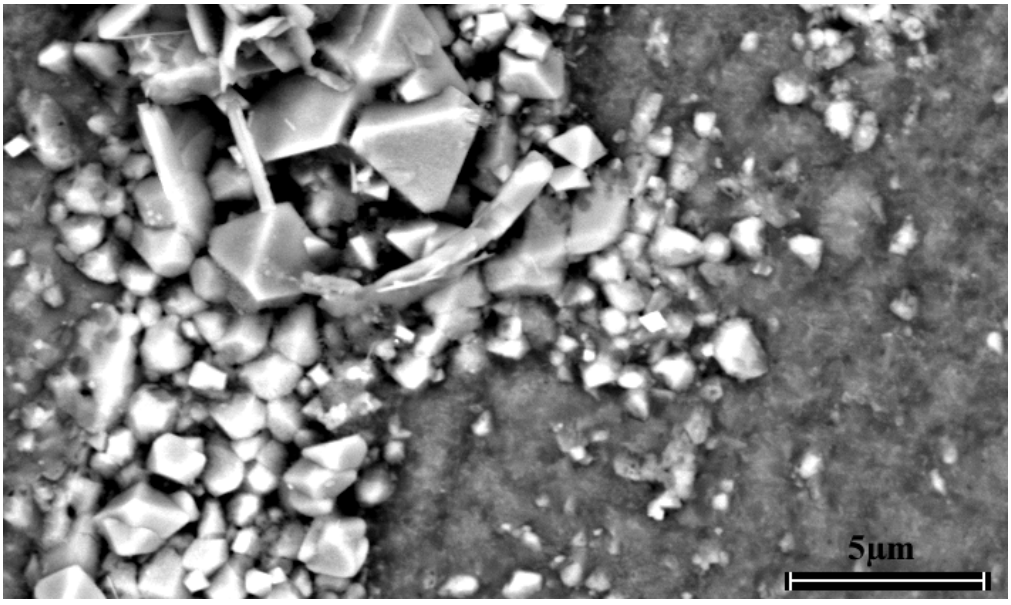

(b)

Figure 18 PWA1484 cyclically exposed for 2150cycles @ 900°C in dry air: (a) low magnification micrograph showing NiO formed on dendritic areas; (b) blocky NiO on dendritic areas and fine-grained oxides on interdendritic areas

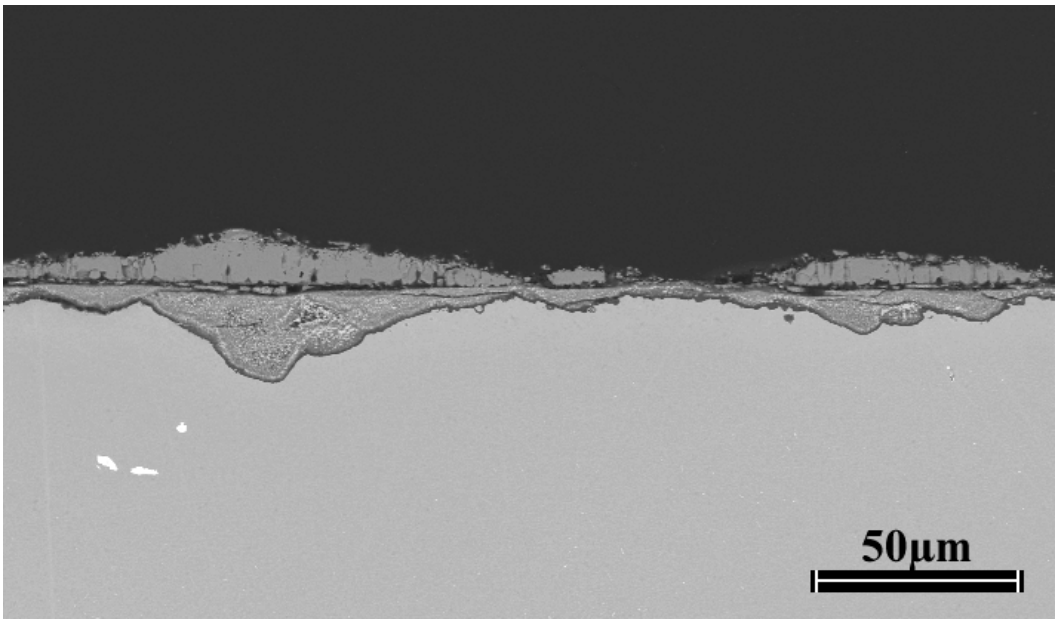

(a)

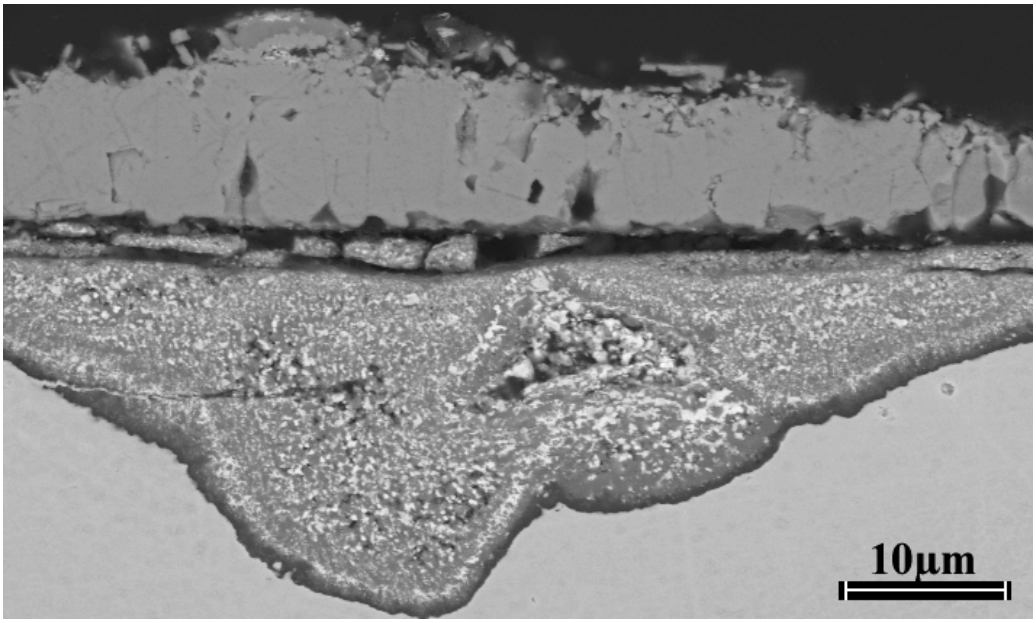

(b)

Figure 19 PWA1484 exposed cyclically for 2150cy@900°C in air with water vapor(0.1atm) - (a) cross-section; (b) higher magnification

In comparison, micrographs showing cross-section areas of the PWA1484 specimen exposed under dry conditions present a much thinner scale, although with a more uniform thickness, multilayered, with α-Al_2O_3 as the base and a spinel phase as the top of the scale. Ta rich oxides could be spotted all along the cross-section examined, situated approximately in the middle of the oxide scale, Figure 20. Such results show that the water vapor is beginning to cause cracking and spalling of the α-Al_2O_3 scale from the PWA1484 specimen. The available data indicates that water vapor is adversely affecting the oxidation of the α-Al_2O_3-formers at 900°C, but the magnitude of this effect is not as large as at higher temperatures.

In the case of superalloy oxidation, the presence of water vapor in the oxidizing atmospheres enhances the cracking and spalling of the oxide and subsequently the α-Al_2O_3 scale reforms with difficulty.

Cyclic oxidation of superalloys in the presence of water vapor at 900°C results in substantial cracking and spalling of the oxide scale and subsequent reoxidation. Large amounts of NiO form together with deep areas of mixed oxides penetration of the substrate and practically no continuity of the alumina scale.

5.1.1.4 Growth Rate of Alumina on Aluminide Coating Oxidation Weight change versus time measurements for the cyclic oxidation of a straight-aluminide coating on René N5 in dry and wet (P_{H2O} = 0.1atm) air at 900°C are presented in Figure 17. Comparing the results for the superalloy to the results for the aluminide coatings, the straight aluminide has larger weight gains in wet air than the one in dry air. This indicates that the α-Al_2O_3 may be cracking on the specimen exposed in air with water vapor. More transient oxides may also be developing.

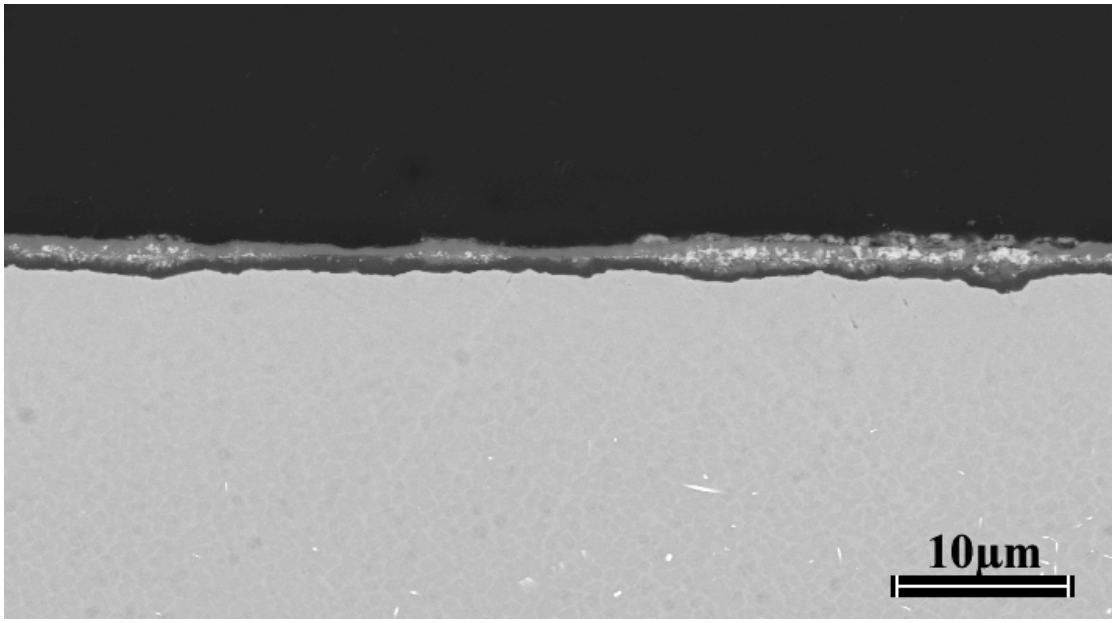

Figure 20 PWA1484 exposed for 2150 cycles @ 900°C in dry air – cross-section showing the scale

In the case of aluminide coating oxidation, alloy depletion is not a factor unless the tests are very long. The data suggests that water vapor is detrimentally affecting the oxidation of these α-alumina formers, with the intensity of the effect not as dramatic as for higher (1100°C) temperatures.

Another important effect of the presence of water vapor for the oxidation of aluminide coatings is the increased growth rate of the alumina scales. The straight-aluminide coatings are presented in Figures 21 and 22. There is a substantial scale thickness difference between the dry-exposed specimen – about 2 – 3µm – and the wet-exposed specimen – approximately 7 – 8µm. The oxide scales are fairly uniform in thickness and adherence in both cases, with the exception of a few areas in the cross-section of the wet exposed specimen where regions of spalled pieces of scale can be observed, regions at which reoxidation must have occurred (Figure 22c).

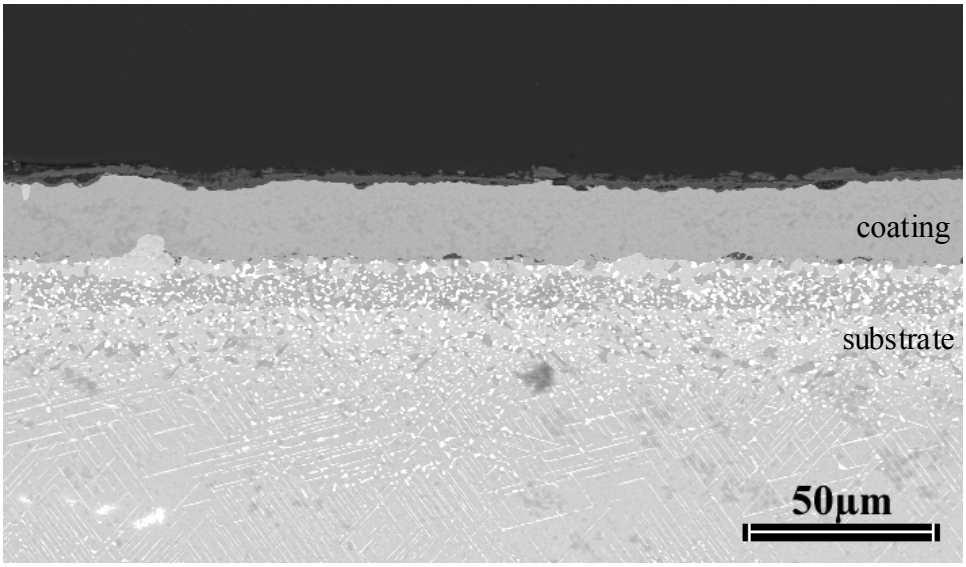

(a)

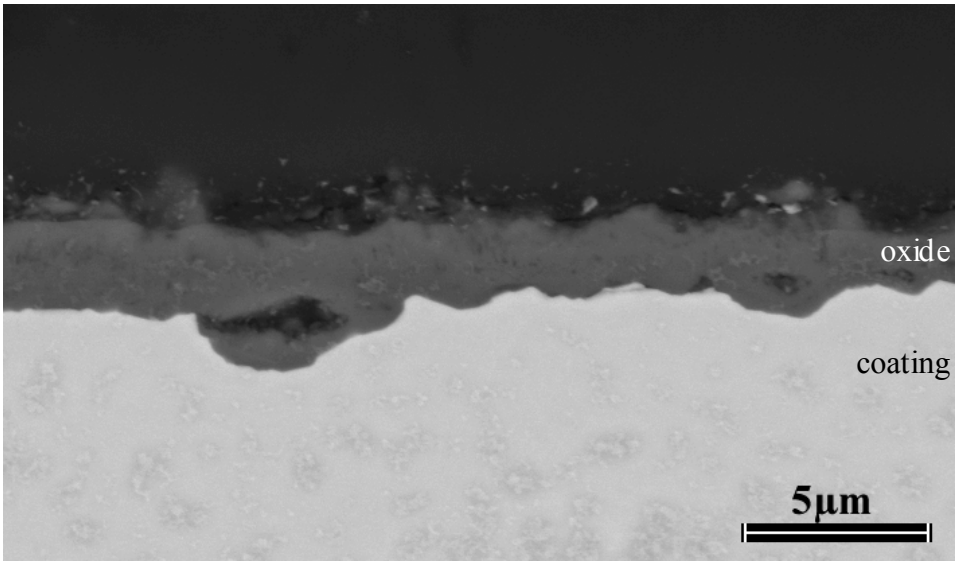

(b)

Figure 21 Aluminide coatings exposed for 2150 cycles @ 900°C in dry air (a) and (b) lower and higher magnifications – cross-sections showing the scale

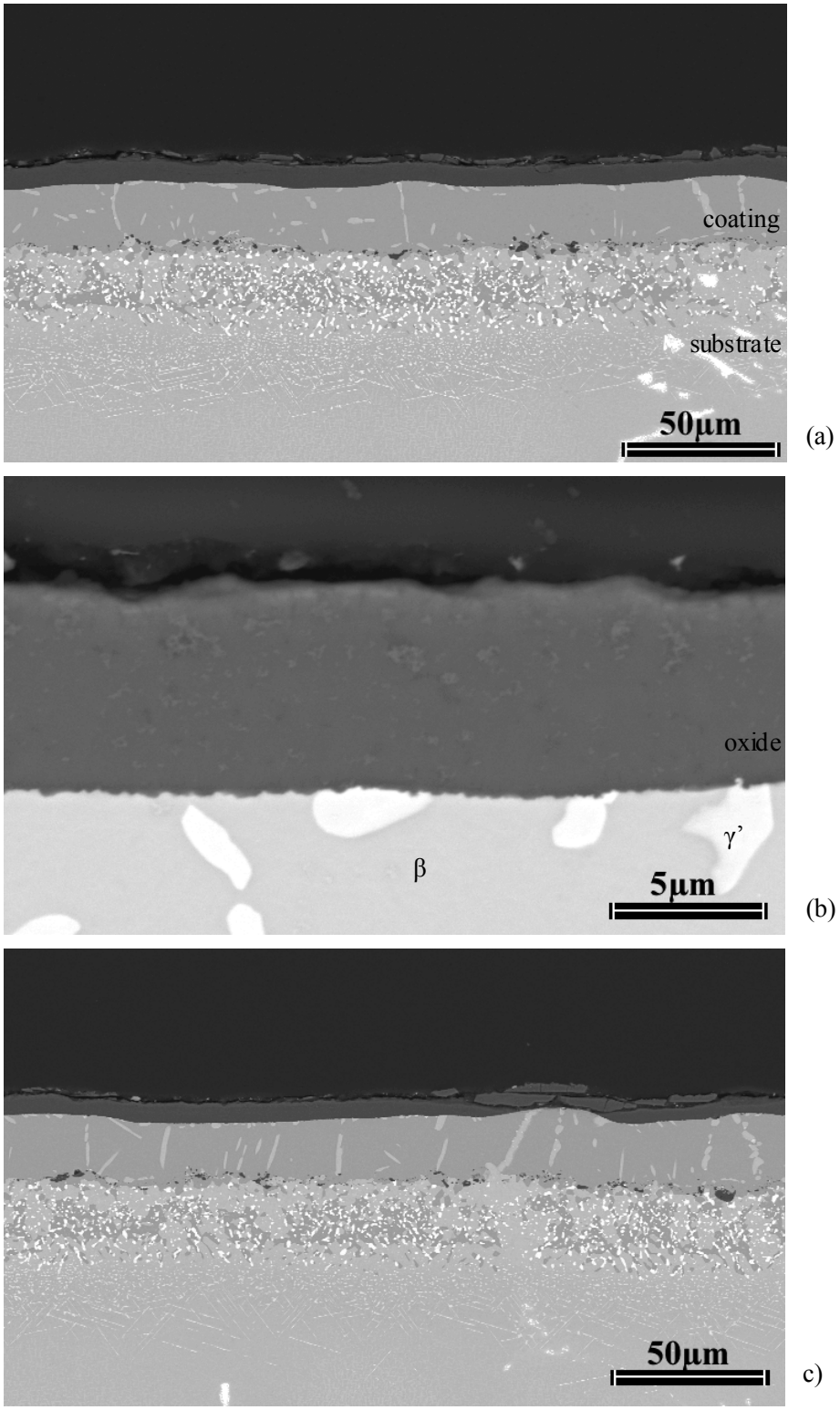

Figure 22 Aluminide coatings cyclically oxidized for 2150 cycles @ 900°C in air with water vapor at 0.1atm; (a) and (b) lower and higher magnifications of cross-sections; c) areas of spalled scales

Also, when observing the nature of the scale/substrate interface, large undulations are noticed for the dry exposed specimen, whereas finer waving is seen at this interface for the wet exposed specimen. This may suggest the possibility of the developing of smaller oxide grains in the thicker scale of the wet exposed sample. Micrographs showing the surface of these specimens, Figure 23, and presenting the morphology of the oxides formed on the two specimens could indicate the difference in oxide grain sizes for the alumina scales.

The metastable alumina formation and transformation from the aluminum hydroxide is given by the following sequence[81]:

$$\gamma\text{-}AlO(OH) \longrightarrow \gamma\text{-}Al_2O_3 \longrightarrow \delta\text{-}Al_2O_3 \longrightarrow \theta\text{-}Al_2O_3 \longrightarrow \alpha\text{-}Al_2O_3 \quad (23)$$

For the oxidation of NiAl in the temperature range 875 – 925°C[81], the values of the parabolic rate constant, k_p, increase with time during oxidation, caused by initial formation of γ-Al_2O_3 which later transforms into the faster growing θ-Al_2O_3. A decrease of k_p is observed in the temperature range 950 – 1050°C with a change of the oxide from θ-Al_2O_3 to the stable α-Al_2O_3. Of course, the latter oxide is the stable slowly-growing oxide that is desired for protection of the alumina-forming alloys.

The data[82] for pure NiAl are shown in the Arrhenius diagram in Figure 24.
At relatively low oxidation temperatures, <1000°C, more or less formation of metastable Al_2O_3 modifications, γ-, δ- and θ-Al_2O_3 is observed on all alumina forming alloys. All these oxides have an FCC closed-packed oxygen lattice with different arrangements of the cations. The diffusivity of Al^{3+} is fairly high and, as a result, these oxides grow relatively fast, often in the

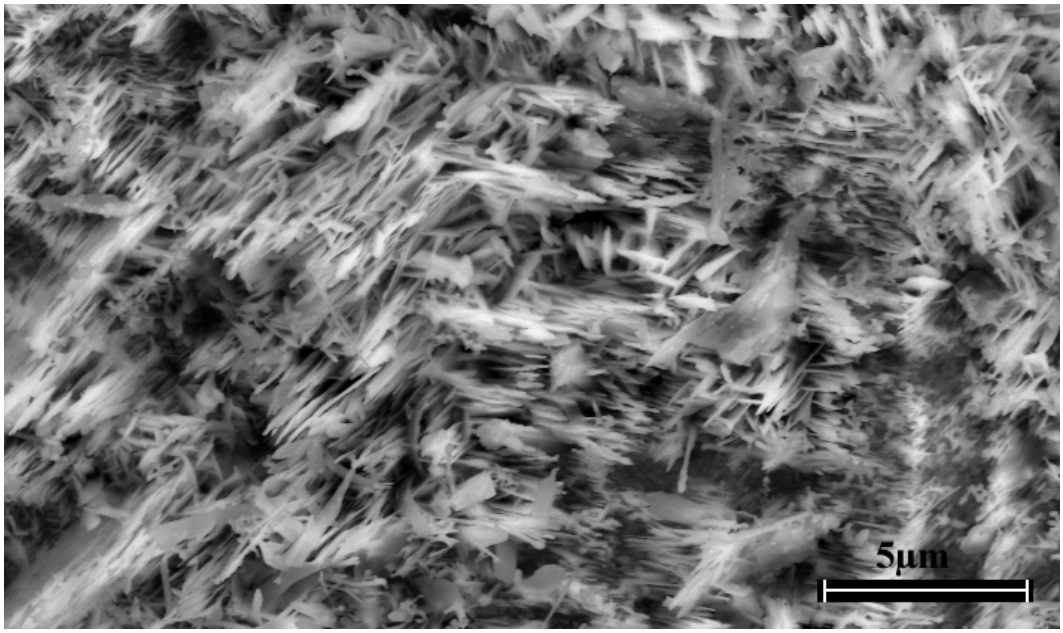

(a)

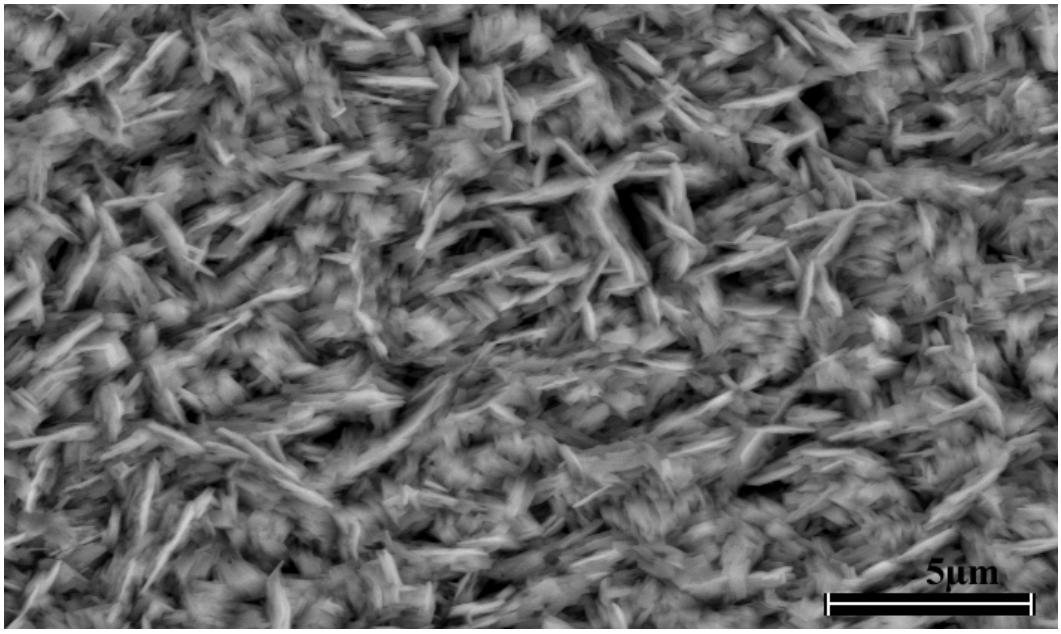

(b)

Figure 23 Straight aluminides oxidized for 2150 cycles at 900˚C in (a) dry air; (b) air with water vapor

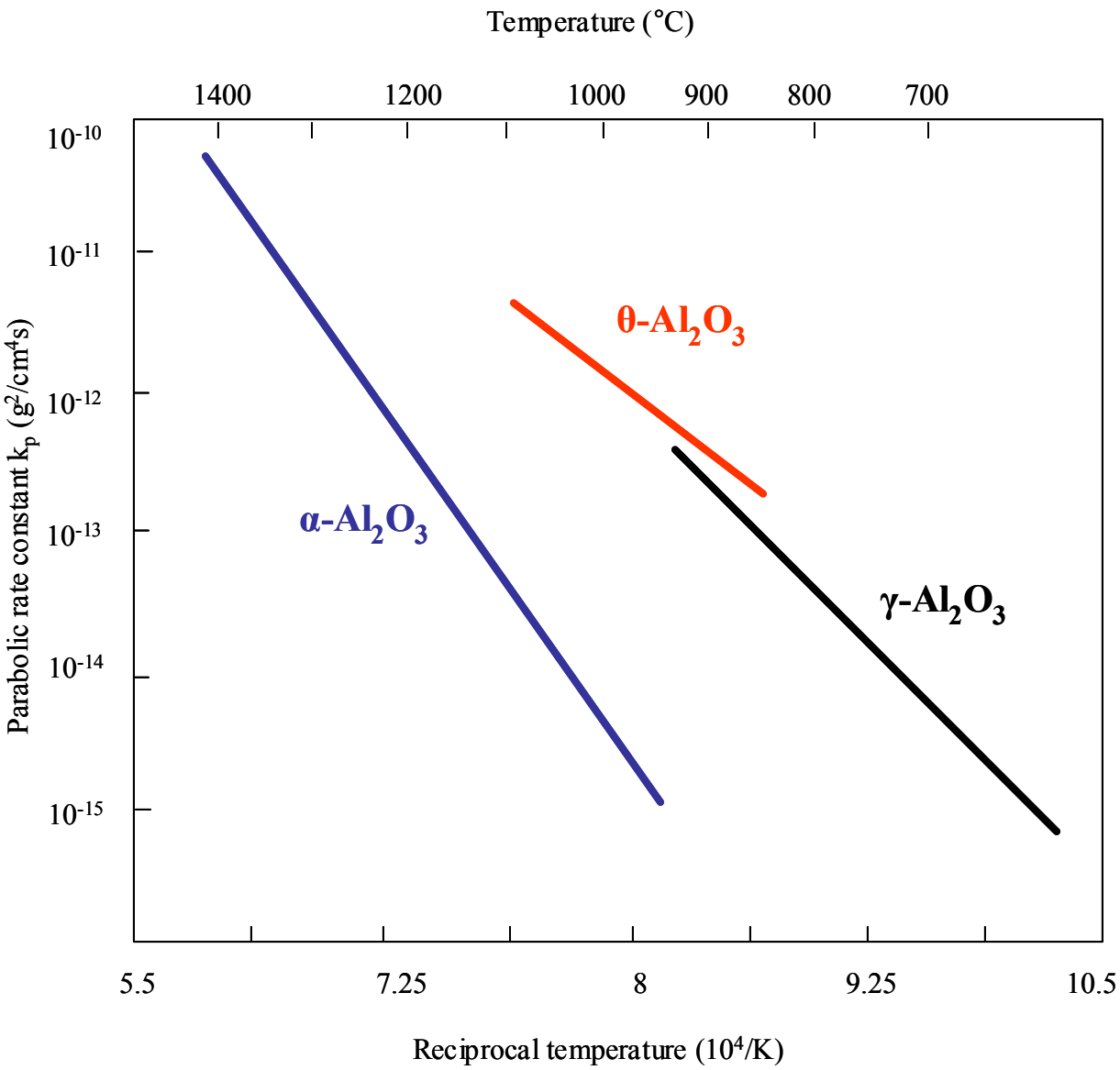

Figure 24 Arrhenius diagram of log k_p versus 1/T for oxidation of pure NiAl

shape of whiskers or blades due to transport along internal channels such as twin boundaries or screw dislocations [83].

X-ray diffraction measurements were performed on specimens of straight-aluminide coatings that were exposed under dry and water vapor conditions, after about 1500 cycles of testing. Peaks of θ-Al_2O_3 were observed for measurements of the scale of the dry exposed specimen, whereas only peaks of α-Al_2O_3 were detected for the scale of the water vapor exposed specimen.

Diffraction peaks for the underlying substrates are found in all cases. This indicates a complete X-ray penetration of the oxide scale, minimizing the possibility of an undetected oxide phase.

Transmission electron microscope studies [84] have shown that the α-Al_2O_3 development on NiAl substrate takes place at the interface between the metal and the oxide and so, when the α-Al_2O_3 is significantly formed, it can easily undergrow the metastable oxides, stop their growth and initiate their transformation. A case of θ-Al_2O_3 to α-Al_2O_3 transition was reported for Pt modified NiAl, where the process was also dependent on orientation [85].

For the straight aluminide coatings exposed in this study, the morphologies of the Al_2O_3 phases are of typical blades and whiskers for the θ-Al_2O_3 and a network of ridges on the oxide layer for the α-Al_2O_3, respectively, Figure 23.

For the temperature range 950 – 1050°C in the study mentioned earlier[84], the parabolic rate constant values decrease for the transformation θ-Al_2O_3 to α-Al_2O_3 in view of the weight change data. For the present study, at the temperature of 900°C, there seems to be an increase in k_p values from θ-Al_2O_3 to α-Al_2O_3 oxides formed on the Ni base superalloy with an aluminide-diffusion coated specimen oxidized in dry air compared to the specimen exposed in air

containing water vapor, respectively, Figures 17, 21b and 22b. It is possible that θ-Al_2O_3, even though it transforms into α-Al_2O_3 earlier, grows faster in wet air conditions.

Fundamental information about the oxidation behavior of materials can be obtained by thermogravimetric analysis – TGA. Specimens of straight-aluminide coatings on René N5 were exposed isothermally in dry air and air containing water vapor at 0.1atm at 900°C for 168 hours. These results showing the normalized data over the unit area are presented in Figure 25. It is apparent that exposing a specimen in wet air results in an increase in the oxidation rate. As seen in the previous cyclic experiments, water vapor is affecting the oxidation of coatings at high temperatures. An examination of the oxide surface on the two specimens indicates that the wet exposed coating shows a more compact alumina scale when compared to the whisker-like surface aspect of the aluminum oxide on the specimen oxidized in dry air, Figures 26 (a and b), exhibiting similar surface morphologies to the ones on specimens of straight-aluminide coatings undergoing cyclic tests, Figure 24.

X-ray diffraction in glancing angle mode revealed the presence of the metastable phase θ-Al_2O_3 on the surface of the specimen exposed isothermally in dry air. No such peaks were found on the pattern of the specimen exposed in air with water vapor; the primary peaks from the oxidation product in this case were those from corundum α-Al_2O_3. Some peaks from the substrate are present, even for the low incidence angle measurements, suggesting that the scales on both dry and wet exposed specimens are rather thin.

Cross-section SEM analysis of the scale after the 900°C isothermal exposure reveals a thin alumina scale, about 1μm thick in most locations along the cross-section, on the specimen oxidized in dry air. A number of voids were observed at the ridges along the scale/substrate interface, Figure 27 – this interface, as well as the gas/oxide interface, shows an undulated, quite

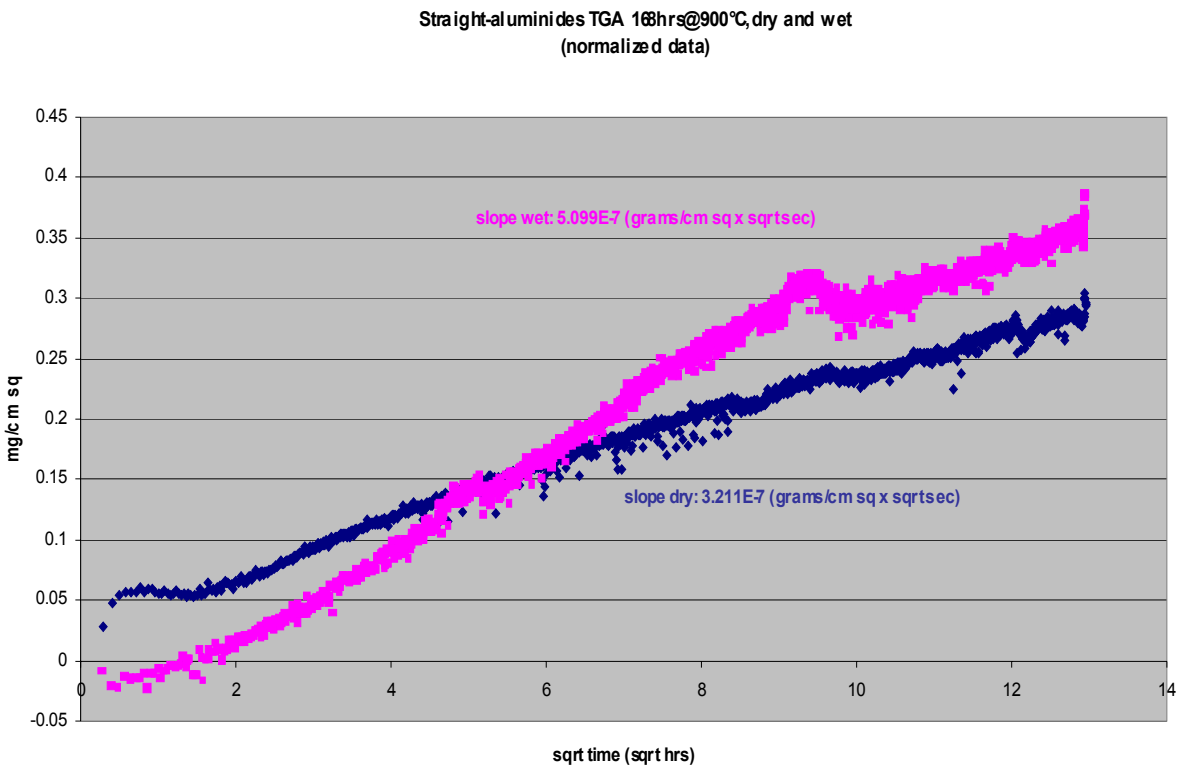

Figure 25 Oxidation kinetics for specimens of straight-aluminide coatings on René N5 exposed isothermally for 168 hours at 900°C in dry air and air with water vapor, respectively

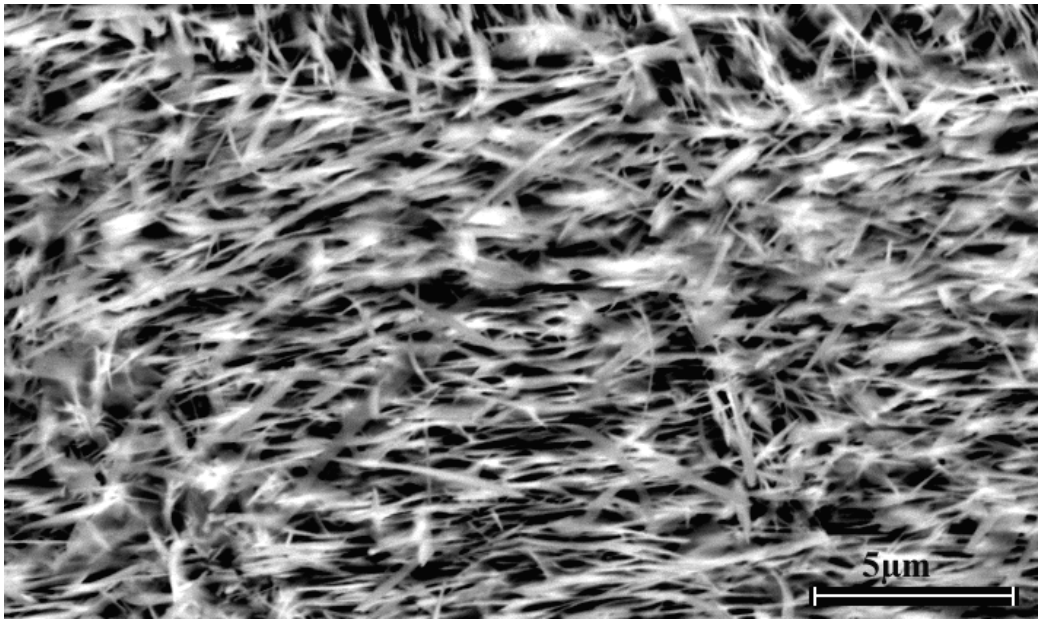

(a)

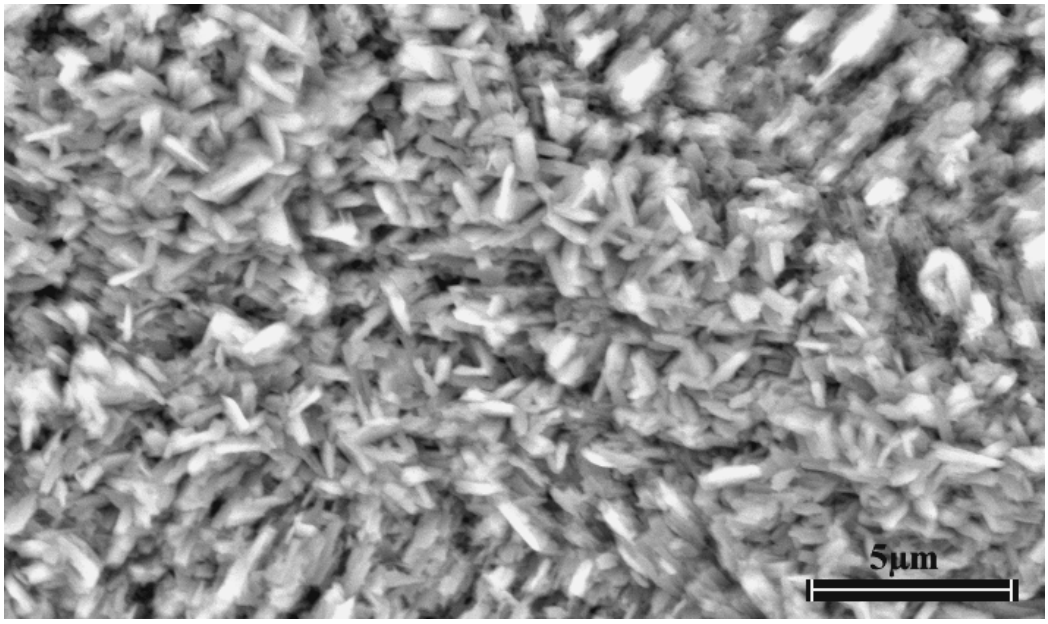

(b)

Figure 26 Straight-aluminide coatings oxidized isothermally for 168 hours @ 900°C in (a) dry air – whisker-like morphology and (b) air with water vapor (0.1atm) – more compact alumina

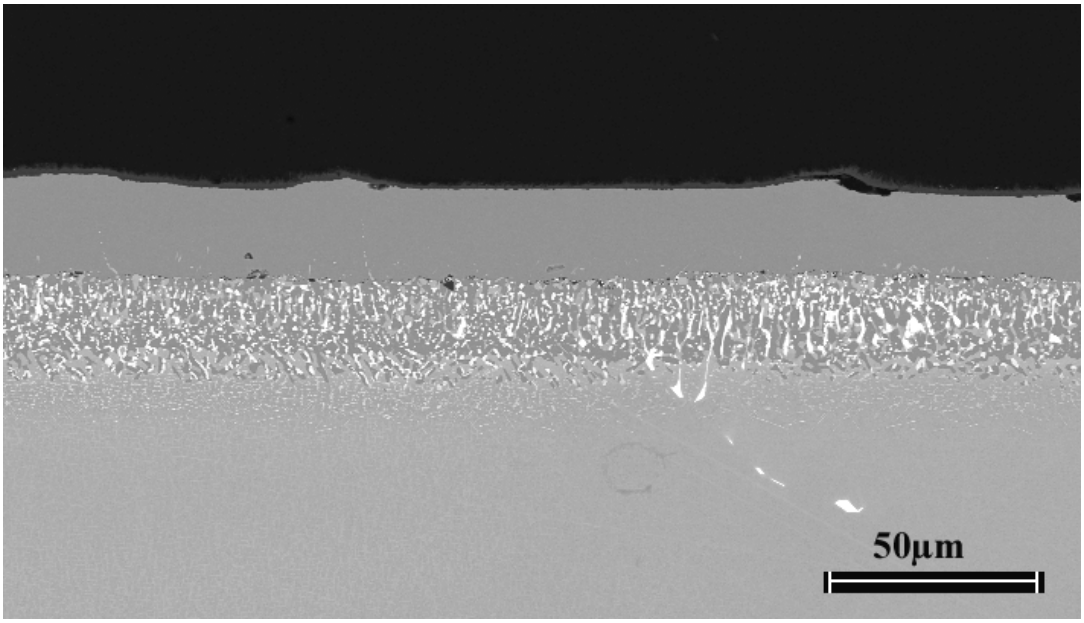

(a)

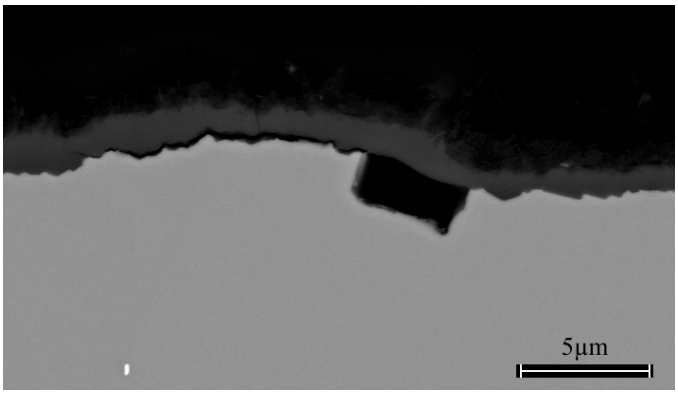

(b)

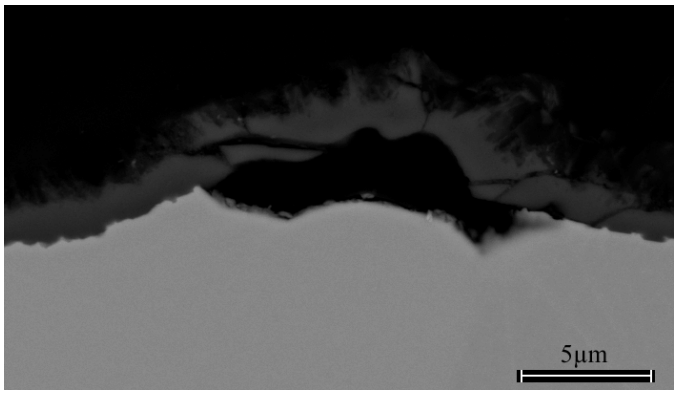

(c)

Figure 27 Cross-section of straight-aluminide coating oxidized isothermally at 900°C in dry air showing voids at scale/substrate interface (a) low magnification; (b), (c) higher magnification

convoluted aspect. The whisker-like oxide – the metastable phase θ-alumina – projecting outwards from the scale surface, Figure 26a and Figure 27(b and c), suggests that the scale grows by outward diffusion of cations, observation that comes in agreement with the oxidation mechanism proposed in previous studies[86, 87]. The voids that form at the metal/oxide interface for the dry exposed specimen, Figure 27, are a consequence of material loss when aluminum diffuses into the metastable oxide layer. Since there is an aluminum depletion taking place at the metal/oxide interface as aluminum is consumed at this interface, a concentration gradient is created which then causes the diffusion of aluminum from the substrate to the metal/scale interface. As a conclusion, voids that appear at the metal/scale interface for the specimen exposed in dry air are related to the type of oxide, namely the metastable θ-alumina.

On the other hand, investigations of the cross-section micrographs for the wet-exposed specimen reveal a much smoother oxide/substrate interface with the observation of a porous region all along the cross-section at about ~ 0.2μm distance, into the scale, from the scale/substrate interface, Figure 28. A restricted region, Figure 29, in the cross-section of this specimen exhibits protrusions of the oxide scale into the metal, suggesting an inward growth of the scale, slowly incorporating islands of substrate and leaving behind the above-mentioned porosity line. An accelerated inward diffusion might be associated with oxygen-containing species from the water vapor phase. The thickness of the scale on the specimen oxidized in wet conditions is slightly larger than the one in dry air, with a range from 1.5 to 2.5μm along the cross-section. No voids were present at ridges and the scale was fairly adherent to the substrate.

Specimens of Pt-modified aluminide coatings on René N5 substrate were isothermally exposed in two atmospheres for 168 hours at 1100°C. The kinetic data for the two specimens, one exposed in dry air and the other one in air with water vapor are shown in Figure 30. Whereas

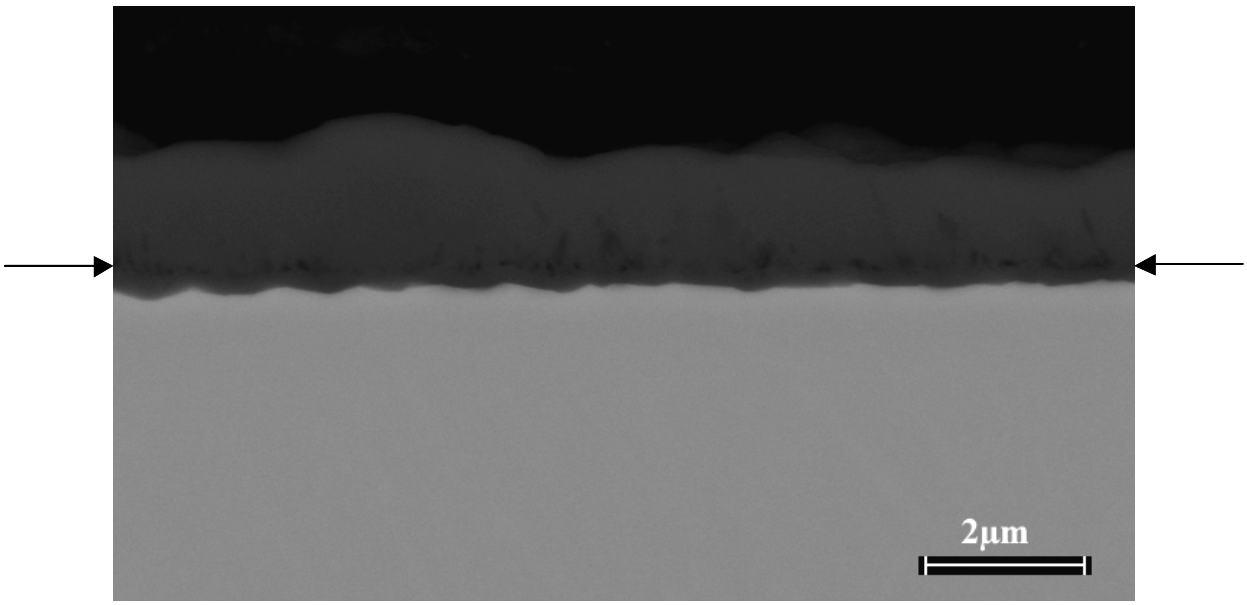

Figure 28 Cross-section of straight-aluminide coating specimen exposed at 900°C isothermally for 168 hours in air with water vapor (0.1atm) showing porosity line in scale. The original surface of the metal is also indicated at arrows. No voids were observed

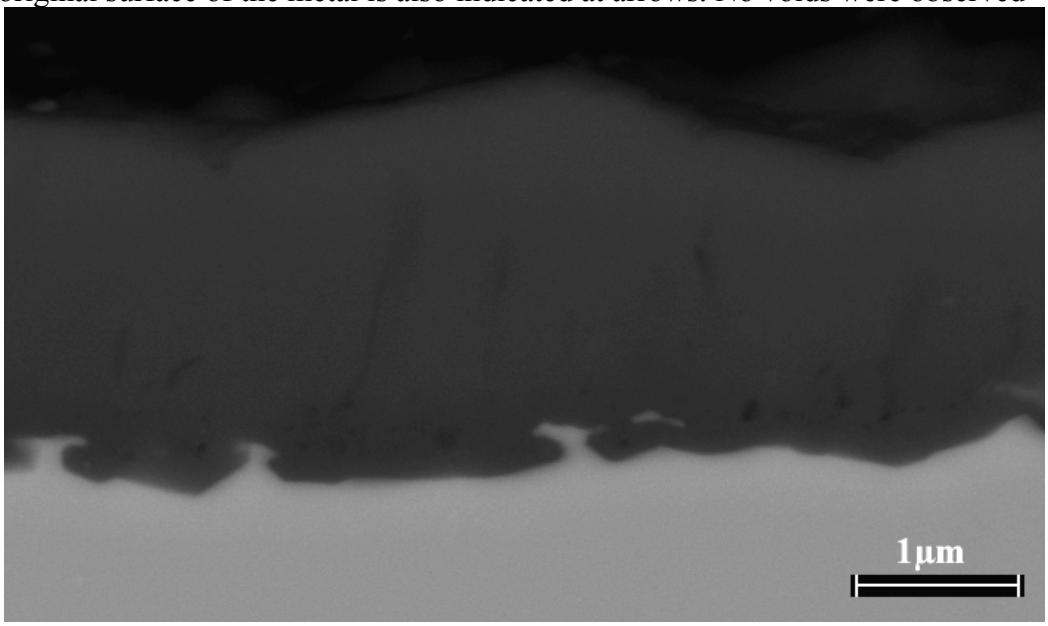

Figure 29 Cross-section of straight-aluminide coating isothermally oxidized for 168 hours at 900°C in air with water vapor – scale protrusions

both specimens gained weight just as the oxidation process started, the sample exposed in wet air exhibits a negative slope - possibly an experimental error - with the completion of the one-week exposure time. The weight losses are very small for the wet exposed specimen – approximately 0.1 mg/cm square, Figure 30. When compared to the oxidation of straight aluminides at 900°C, the Pt-aluminides exposed at 1100°C exhibit much slower oxidation kinetics with mass changes per unit area that are approximately five times smaller for the specimens exposed in wet conditions.

For the above-described specimens, the initial examination was performed with X-ray diffraction in a glancing angle mode. The incidence angle was one degree and the scanning of the samples exhibited a pattern with peaks for beta NiAl, indicating that the entire thickness of the scale was examined.

In both cases, dry air and wet air, the scales were α-Al_2O_3, with strong reflections for alumina. No θ-Al_2O_3 was observed on the dry exposed specimen at 1100°C, whereas θ-Al_2O_3 was the major oxide on the straight aluminide specimen exposed in dry air at 900°C.

Surface images for the Pt-aluminides exposed isothermally for 168 hours at 1100°C in dry and wet air are shown in Figures 31 and 32. A close-up examination of the surface of the two specimens reveals a network-type alumina scale on the specimen oxidized in dry air. The scale was uniform otherwise, with no spalled areas observed on the surface of the scale, Figure 31a. Somewhat resembling a network-like structure, but finer ridge morphology, Figure 31b, the alumina on the specimen oxidized in wet air was more compact. Spinel phase was present at distinct spots on top of the alumina ridges, Figure 32. A small number of areas on the surface of this sample showed delamination of the scale as shown in Figure 32c, leaving behind the PtAl coating with imprints of the alumina grains that used to reside there, Figure 33.

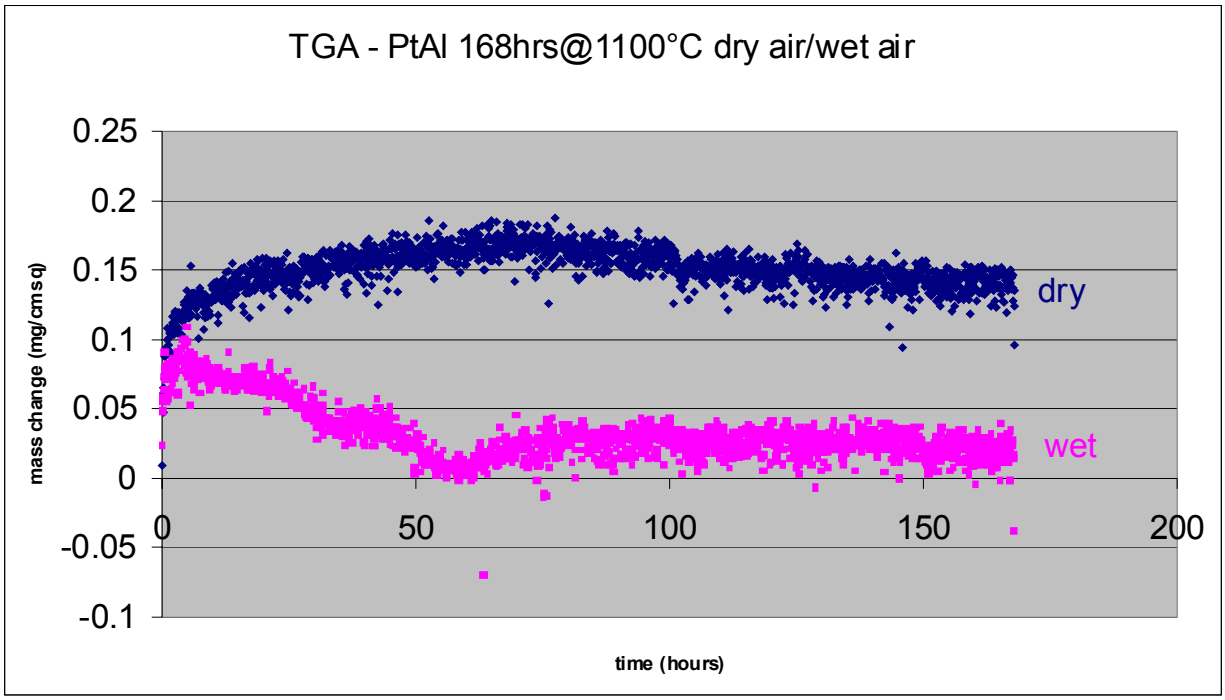

Figure 30 Kinetic data for Pt-Al 168hrs@1100°C - dry air/air with water vapor

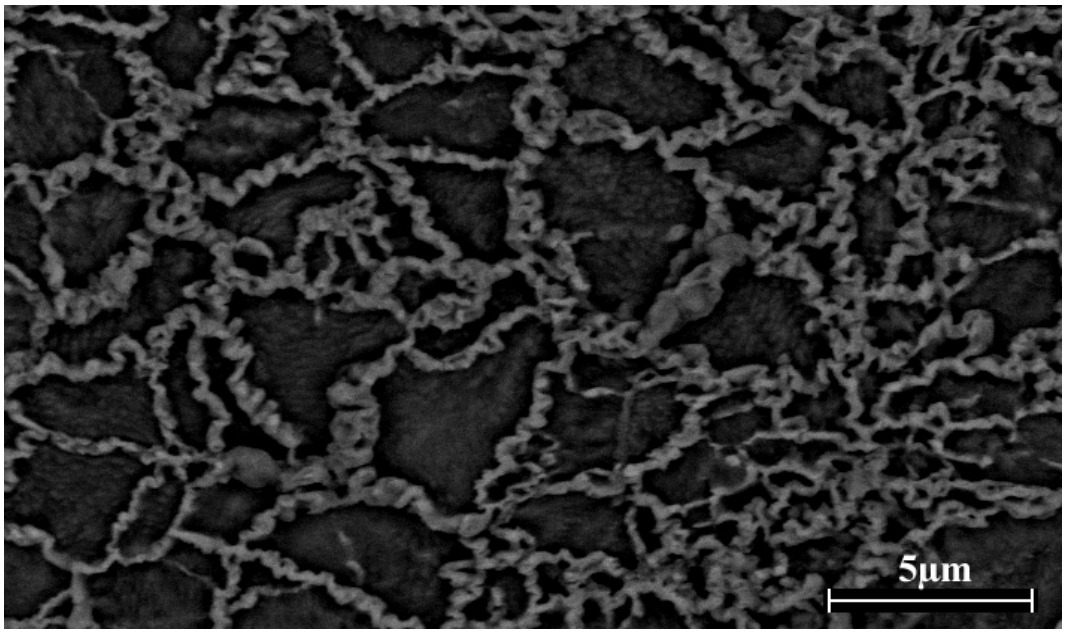

(a)

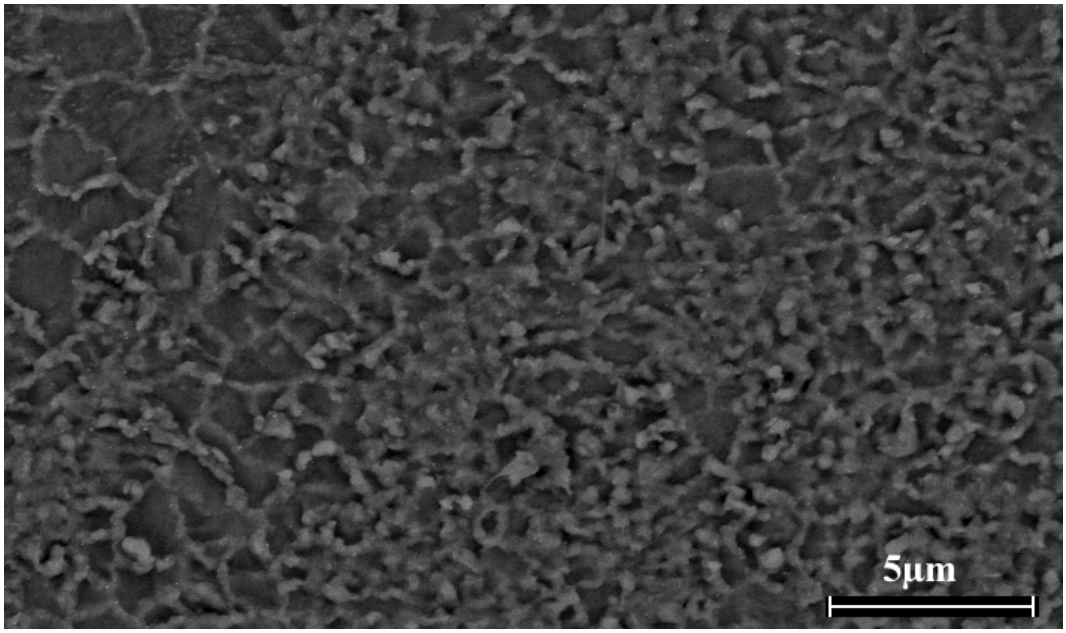

(b)

Figure 31 Surface micrograph of Pt-modified aluminide isothermally oxidized for 168 hours @ 1100˚C in (a) dry air; (b) air with 0.1atm water vapor

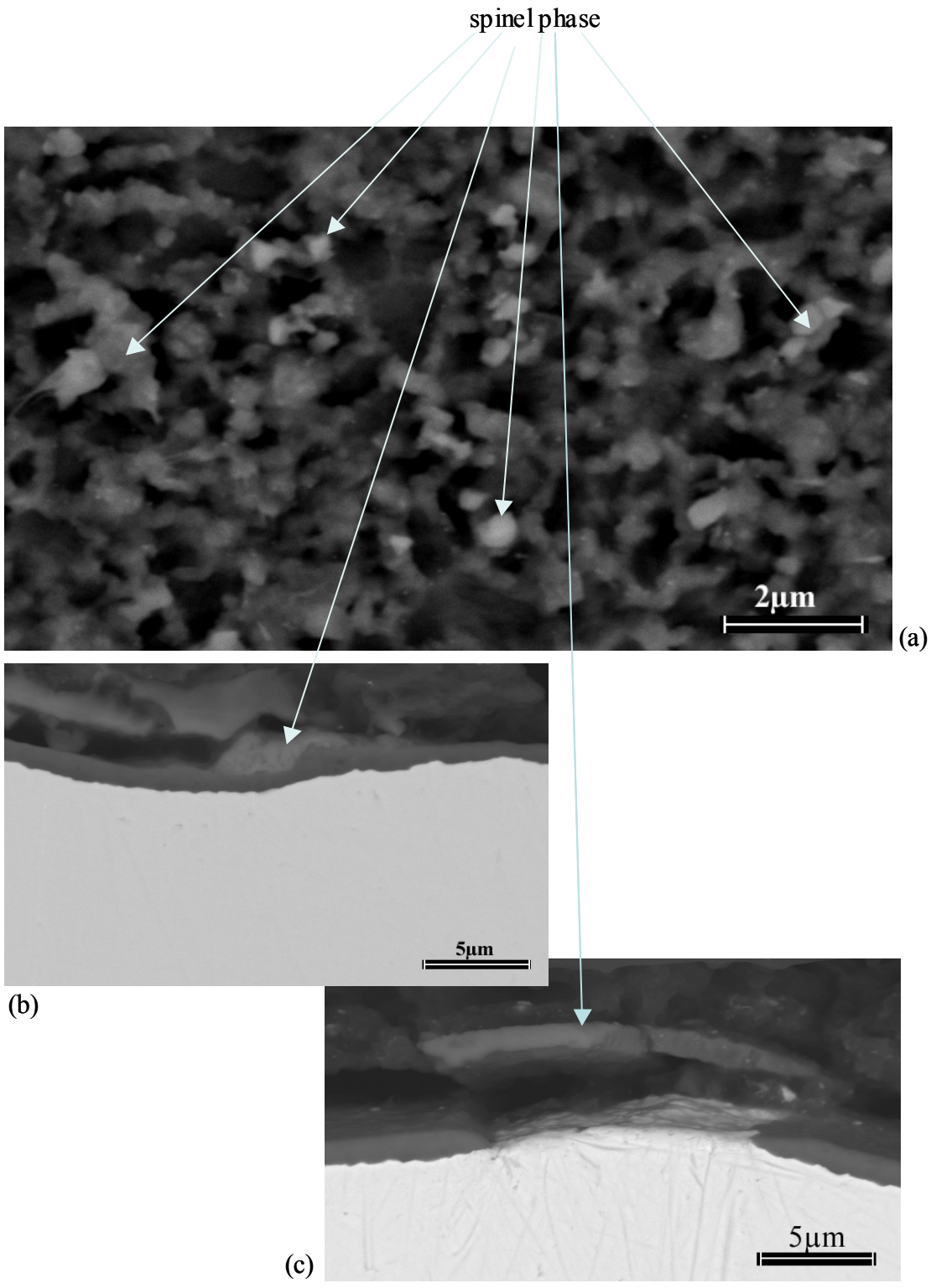

Figure 32 PtAl specimen oxidized in air with water vapor for 168 hours isothermally at 1100°C (a) top view; (b), (c) cross-sectional views. Spinel phase present at arrows.

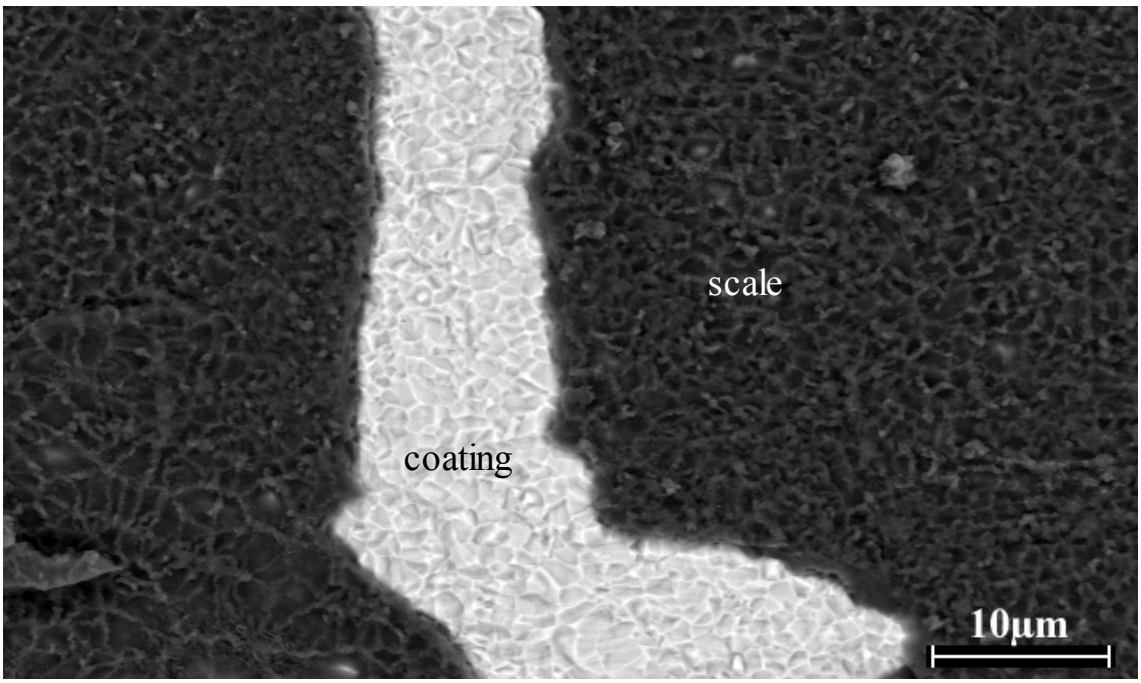

Figure 33 PtAl specimen isothermally exposed at 1100°C for 168 hours in air with water vapor. spalled-off area on surface.

If ridges of oxide, present to a larger extent on the specimen exposed in dry air conditions, Figure 31a, delineate grain boundaries in the oxide, then the comparison between the surface images of the dry and wet exposed specimens shows a smaller size oxide grains for the sample oxidized in wet air, Figure 31.

Cross-section SEM micrographs for the two above-mentioned specimens reveal a thinner scale on the dry specimen, with a less uniform thickness of the scale, Figure 34, ranging from 0.5μm to about 1.0μm. Oxide protrusions at the gas interface were observed at regions where the oxide thickness was larger. Thinner regions of scale were observed with no such protrusions extending from the scale surface plane, Figure 34a (see arrows). The wet specimen exhibited a thicker, more uniform scale of about 1.5μm thickness along the cross-section, Figure 34b. Quantitative EDX analysis revealed Ni and Al peaks on top of the alumina scale at distinct regions for the wet exposed sample. At some of these regions, the scale had spalled, usually at the alumina/coating interface, Figure 32c, suggesting that the water vapor ingress is disturbing the adherence of the scale to the substrate.

Initially, specimens of PtAl were exposed at 1100°C and not at 900°C for more aggressive oxidation conditions at the elevated temperature. Even though the PtAl specimen exposed in water vapor conditions at 1100°C exhibits spalled areas in a few places, the α-Al_2O_3 scale thickness is not as large as that for the straight-aluminide specimen exposed in wet air, but at 900°C. Although there were no experiments done at 900°C for specimens of PtAl coatings, the fact that the alumina scale on PtAl oxidized at 1100°C is not as large as for plain aluminides oxidized at 900°C suggests that the platinum modification to the aluminide coating confers a higher oxidation resistance to the René N5 substrate, even under water vapor atmospheres.

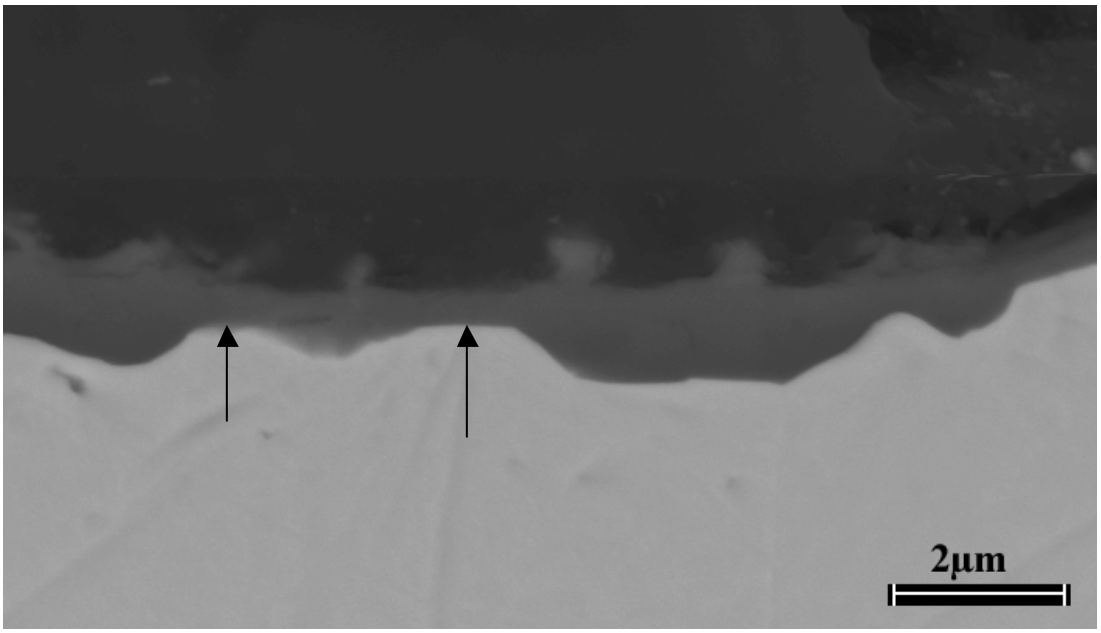

(a)

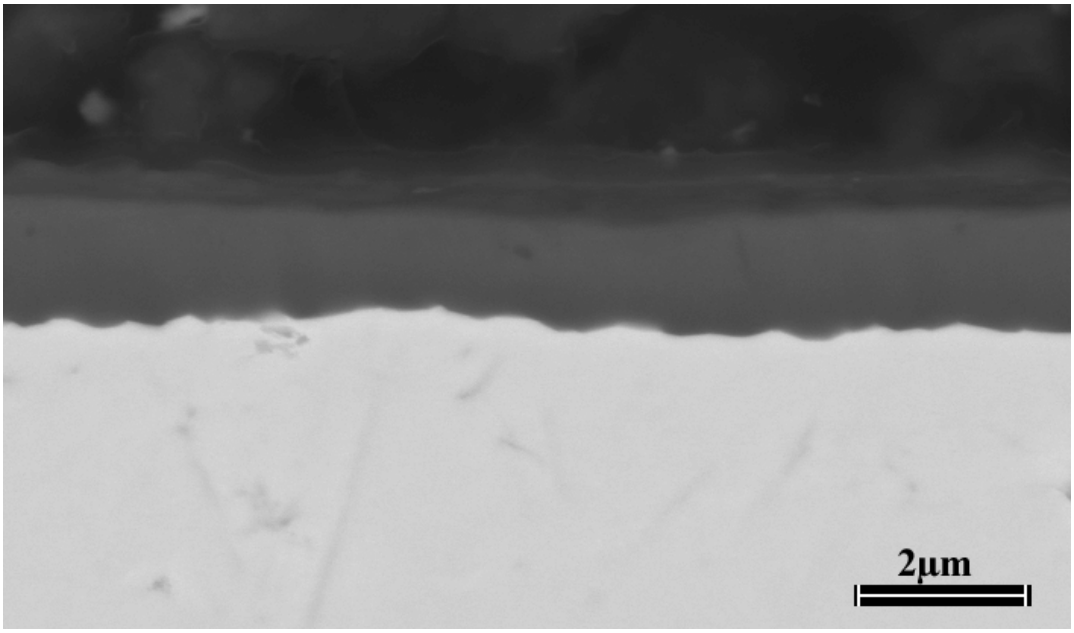

(b)

Figure 34 Cross-section micrographs for PtAl specimens oxidized for 168 hrs@ 1100°C in (a) dry air and (b) air with water vapor. Thinner alumina at arrows in (a)

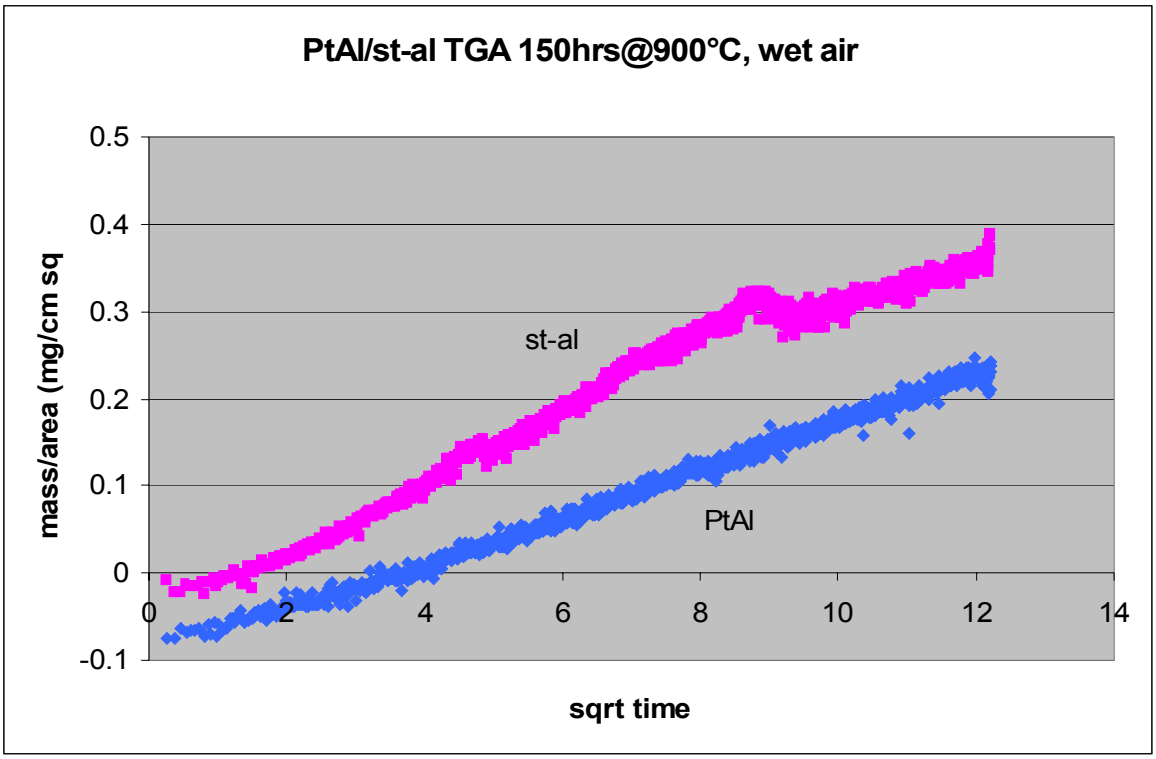

(a)

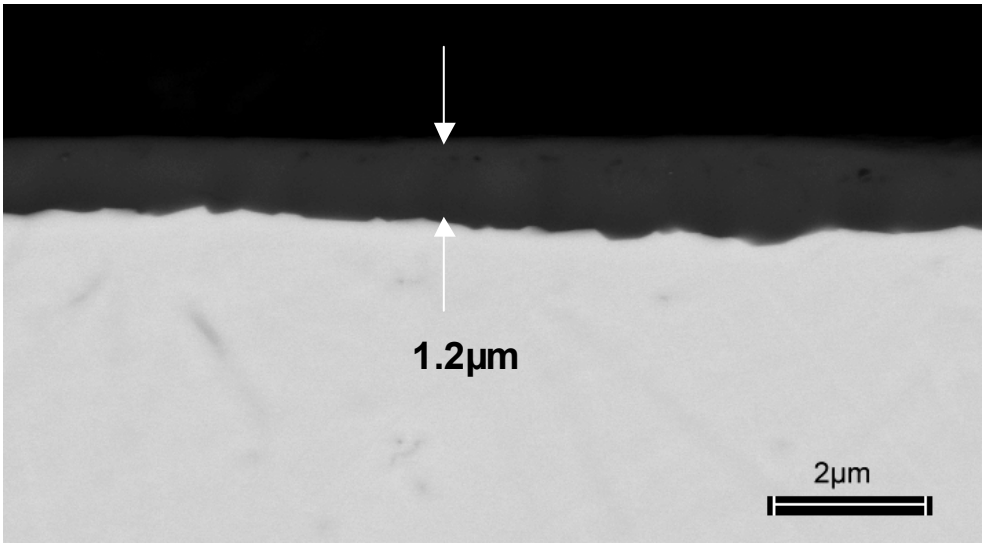

(b)

Figure 35 PtAl isothermally oxidized at 900°C for 150 hours in air with 0.1atm water vapor; (a) oxidation kinetics comparing PtAl with Straight-aluminide; (b) cross-section showing thickness of scale

A PtAl coating specimen was isothermally oxidized in wet air (0.1atm) for 150 hours at 900°C, Figure 35. From the plot presented in Figure 35a, a slower oxidation kinetics can be observed for the aluminide coating with Pt addition when compared to the straight-aluminide coating. Thinner alumina scales have developed at 900°C compared to wet air conditions at 1100°C. X-ray diffraction measurements revealed peaks of α-alumina. A thinner oxide on the specimen of PtAl exposed at 900°C in wet air compared to same conditions but at 1100°C shows a consistent Pt effect on the growth rate of the alumina scale function of temperature.

Finally, it is proposed that smaller grain size of the alumina when this grows in air with water vapor could be accountable for thicker oxides in wet air compared to dry air for straight aluminide coatings, Figures 21b and 22b, and for PtAl coatings, Figures 31 (a and b) and 34b. In this work, etching of the alumina scales was not performed.

5.1.1.5 Summary of Important Effects • The presence of water vapor in the oxidizing gas mixture causes the α-Al_2O_3 scales to crack and spall more profusely than in dry gases (both superalloys and coatings).

Table 2 – Alumina Adherence, cyclic oxidation @ 1100°C

	dry air	**wet air (0.1atm)**	**wet air (0.5atm)**
René N5 regular S	non-adherent	non-adherent	highly non-adherent
René N5 low S	adherent	adherent	adherent
Straight-aluminide	non-adherent	non-adherent	
PtAl	highly adherent	highly adherent	

• The above-mentioned effect becomes less pronounced for very adherent thermally grown oxide scales; in other words, the cracking and spalling under water vapor conditions tests becomes less evident as the interfacial toughness between α-Al_2O_3 and substrate becomes greater (both superalloys and coatings).

• When sulfur is present at the Al_2O_3/alloy interface, water vapor lowers the fracture toughness and spalling of the oxide is increased. When sulfur is not present, the situation changes in the sense that conclusions could be drawn that either the water vapor has not a significant effect or that the interfacial toughness becomes so high that even with water vapor present, the toughness at the interface is still sufficiently high to inhibit spalling.

• Platinum additions to diffusion aluminide coatings on superalloys show an improvement in spallation resistance over the plain aluminides, even in atmosphere where water vapor is present. Also, it appears that the growth of α-Al_2O_3 scales on the PtAl coating specimens is slower compared to straight aluminides. In other words, platinum modification to the aluminide coating confers a higher oxidation resistance to the superalloy substrate, even under water vapor atmospheres.

Table 3 – Alumina Growth Rate (weight change/oxide thickness)

900°C, cyclic (2150 cycles)	**PWA 1484**	dry air wet air	small change in weight accelerated, then consistent weight loss
900°C, cyclic (2150 cycles)	**Straight-aluminide**	dry air wet air	small change in weight consistent weight gain
900°C, TGA (168 hours)	**Straight-aluminide**	dry air wet air	slow (1μm) faster (2μm)
900°, TGA (150h)	**Pt-Al**	wet air	1.2μm
1100°C, TGA (168 hours)	**Pt-Al**	dry air wet air	slow (0.4 – 1.6μm) faster (1.6μm)

• At 900°C, both cyclically and isothermally, α-Al_2O_3 is the detected oxide phase on specimens oxidized in water vapor conditions, whereas the metastable phase θ-Al_2O_3 forms on specimens oxidized in dry air even after hundreds of cycles. Voids present at the metal/oxide interface for specimens exposed in dry air are related to the metastable θ-Al_2O_3 (coatings).

• At 900°C, the growth rate of alumina in water vapor conditions is greater than that in dry air. This may be due to water vapor affecting the growth rate of the metastable phase and/or water vapor causing a smaller grain size oxide to be formed (coatings).

• Metastable oxide transforms to α-Al_2O_3 sooner at higher temperatures. At 1100°C, in dry air and in wet air, the scale that forms on PtAl specimens is α-alumina. At this temperature, the presence of water vapor is causing the α-Al_2O_3 scale to grow faster possibly due to a smaller grain size of the alumina because of an enhanced nucleation of α-Al_2O_3 when grown in wet air. Moreover, spinel is present on top of the alumina scale at certain regions. The presence of spinel can cause delamination of the oxide scale from the substrate. Introducing water vapor in the exposure conditions results in an adverse degradation of the oxidation properties (coatings).

5.1.2 The Effects of Water Vapor on the Selective Oxidation of Al in Alloys

5.1.2.1. Superalloys Oxidation Since other oxides, in addition to α-alumina, seem to be involved in the cracking and spalling of the oxide scale from superalloys such as PWA 1484, CMSX4 and René N5, specimens of these alloys have been exposed to dry air and air containing water vapor (P_{H2O} = 0.1 atm) for short times (1 minute, 10 minutes, 1 hour and 4 hours) at 1100ºC.

Surface and cross-sectional micrographs are presented in Figures 36 to 42. From these images, it is evident that the oxide scales that formed when water vapor was present are thicker even for as short as 10 minutes oxidation time. SEM/EDS cross-section examinations show that the scale structure is more complex in wet air compared to dry air. In the first case, the scale appears to be multilayered, about 1 to 2 microns thick, composed of aluminum, nickel, chromium and tantalum oxides. Aluminum was found with nickel and chromium in the external layers, but only aluminum and nickel were found in the inner part of the scale; tantalum is usually present in the scale as a discrete region as can be seen in Figure 41 and Figure 42 for low sulfur PWA 1484. In the case of PWA 1484 with higher sulfur concentrations, tantalum is randomly distributed in the scale, Figure 37, but it is not clear that this change in the distribution of tantalum in the scale is caused by the sulfur content of the alloy.

The specimens oxidized in dry air are covered by metastable θ-alumina and a small amount of mixed aluminum and nickel oxides. Tantalum-rich oxide is present in distinct regions in the scale. A cross-section of the scale shows a thickness of about 0.3 to 0.5 microns. The scale is rather compact, not really layered, Figures 37a, 39a and 41a.

These results show that the transient oxidation of these superalloys is affected by water vapor and that the initial scales have different structures depending on the presence or absence of

water vapor. Results obtained for low sulfur PWA 1484 (1 – 2ppm) are presented in Figure 41. Substantially more transient oxidation has occurred in air with water vapor. It is apparent that the amount of transient oxidation may increase as the water vapor pressure increases. Results obtained for PWA 1484 (low sulfur content) and CMSX4, Figure 43 and Figure 44, in dry air

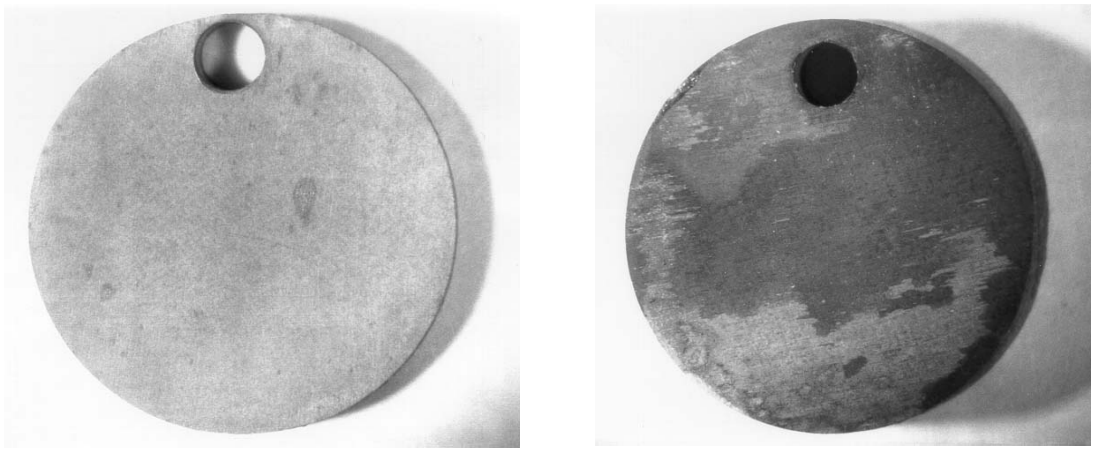

(a) (b)

(c) (d)

Figure 36 PWA 1484 exposed at 1100°C for 1 hour in (a), (c) dry air; (b), (d) air with water vapor at 0.1 atm

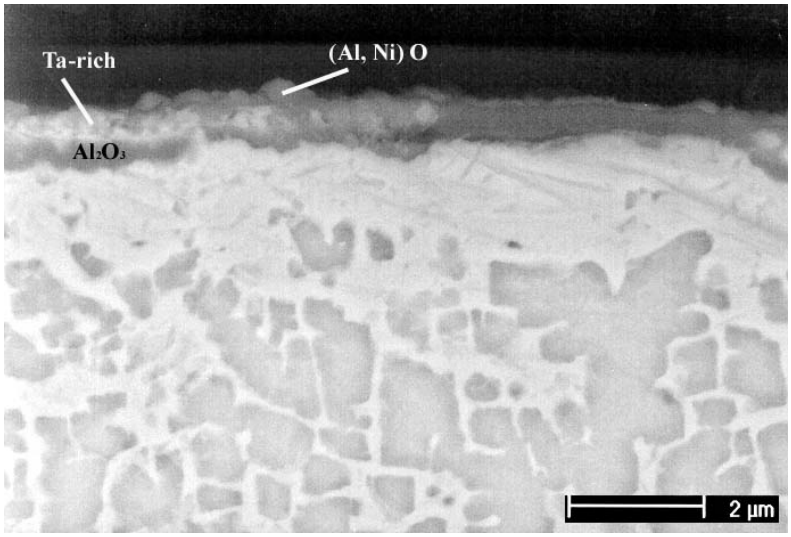

(a)

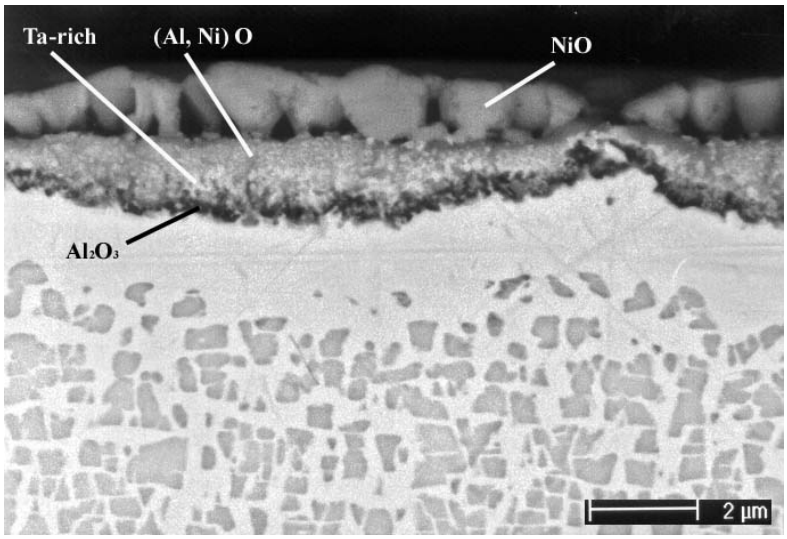

(b)

Figure 37 SEM micrographs showing cross-sectional views of PWA 1484 isothermally oxidized at 1100°C for 10 minutes; (a) in dry air; (b) in air with water vapor at 0.1atm

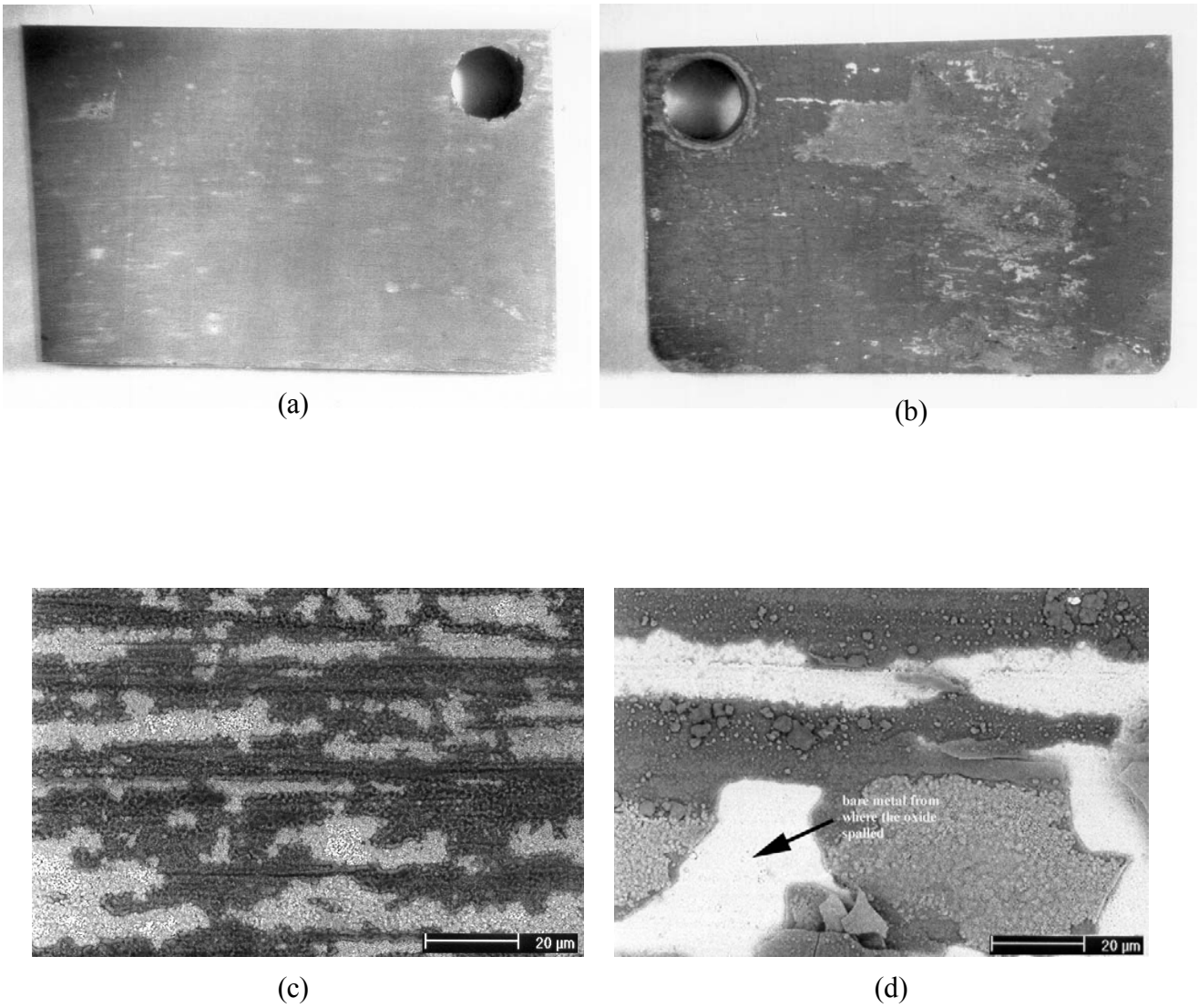

Figure 38 CMSX4 exposed at 1100°C for 1 hour in (a), (c) dry air; (b), (d) in air with water vapor at 0.1atm

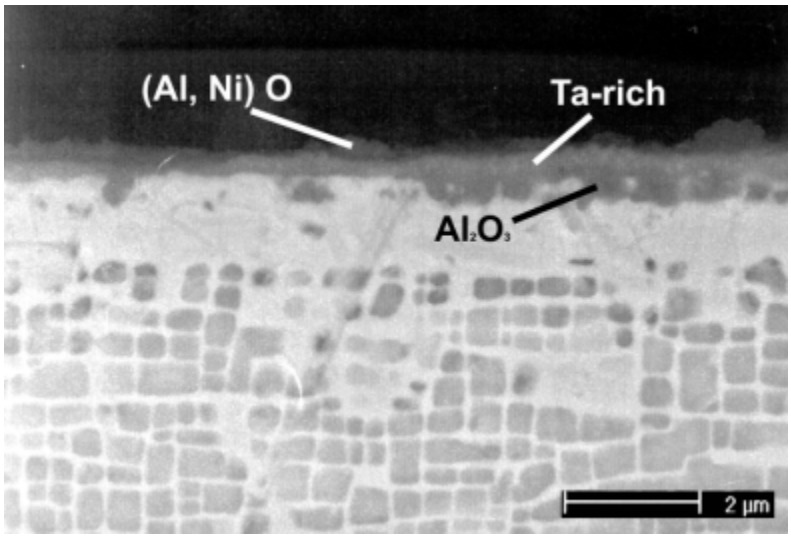

(a)

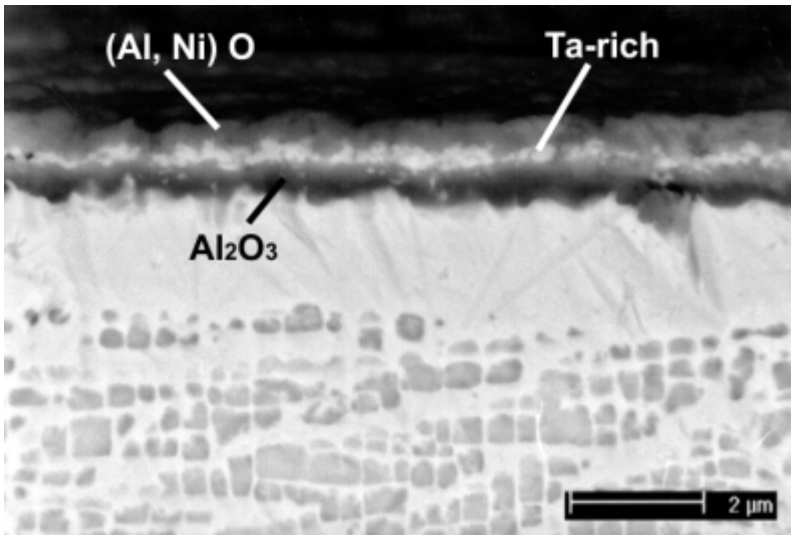

(b)

Figure 39 CMSX4 exposed at 1100°C for 10 minutes (a) in dry air; (b) in air with P_{H_2O} = 0.1atm

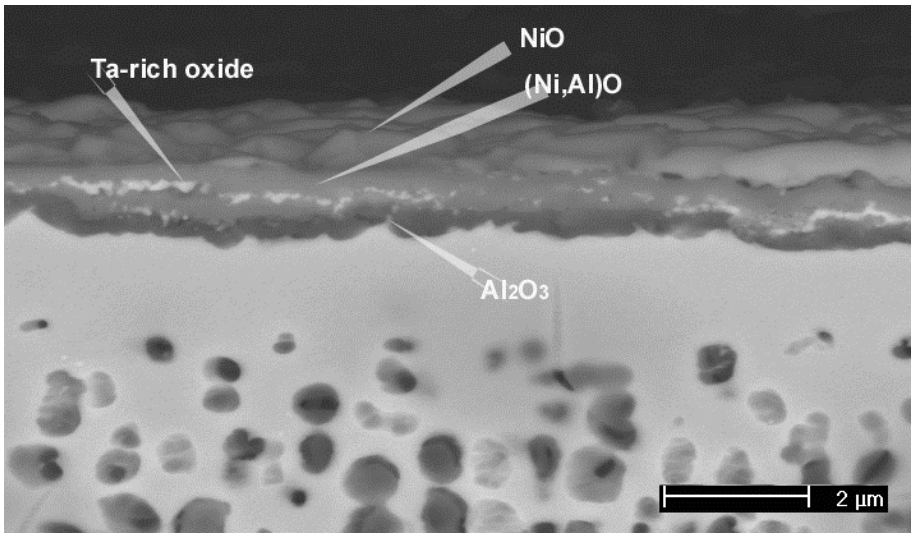

(a)

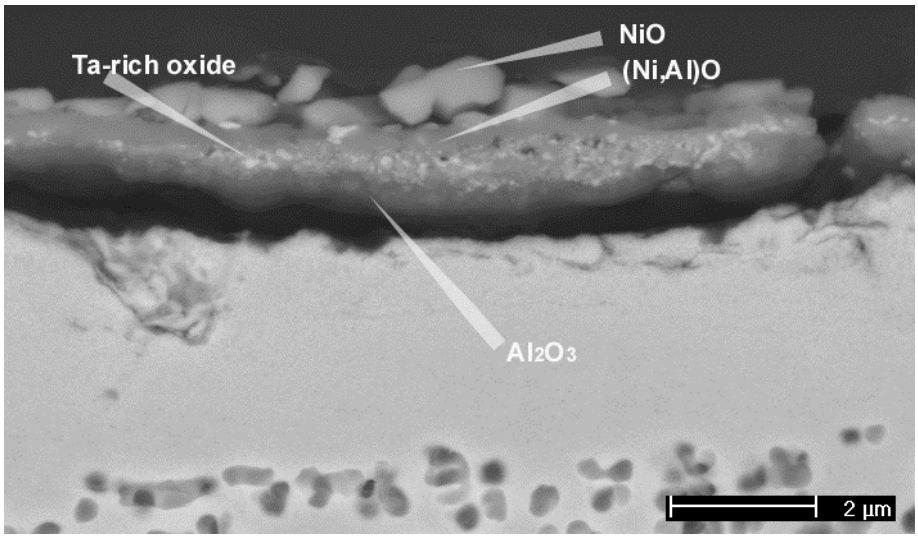

(b)

Figure 40 René N5 oxidized at 1100C for 1 hour in air with water vapor at 0.1atm; (a) N5; (b) René N5 with low sulfur content

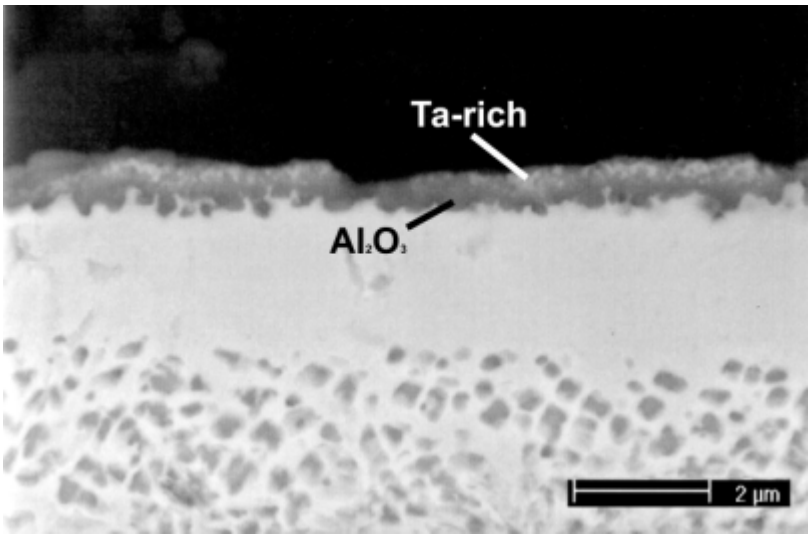

(a)

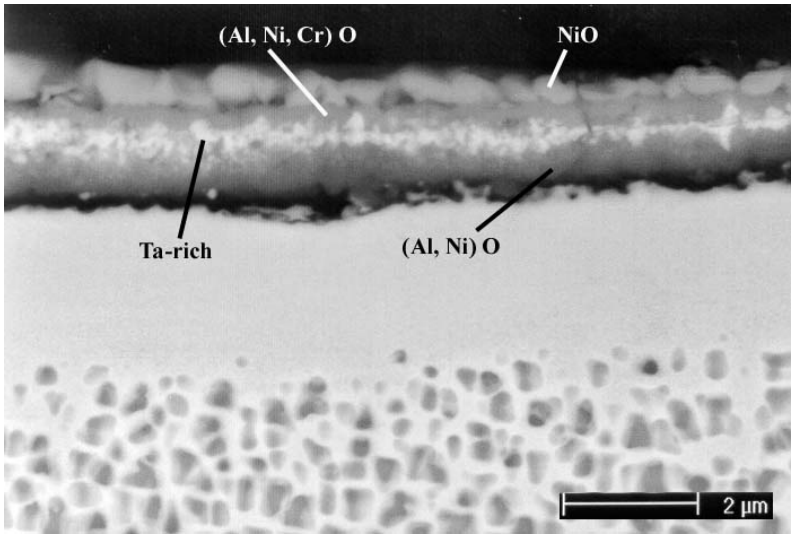

(b)

Figure 41 PWA 1484 with 1 – 2ppm sulfur exposed at 1100°C for 10 minutes (a) in dry air; (b) in air with water vapor at 0.1atm

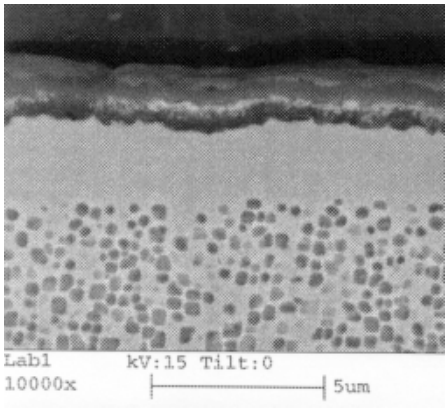

Ni

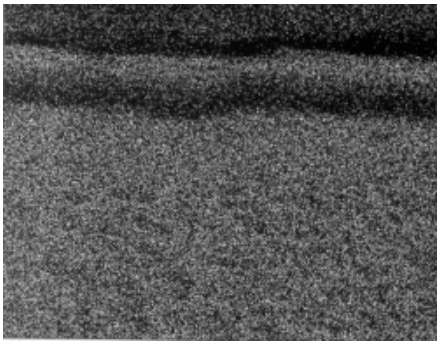

Al

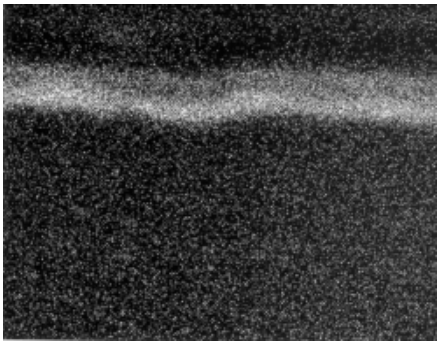

Ta

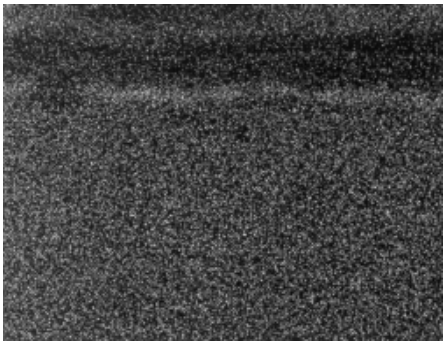

Cr

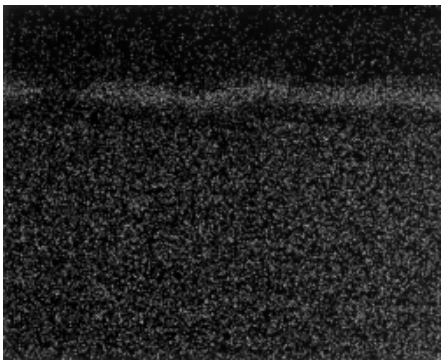

Figure 42 X-ray maps showing elements distribution in the oxide scale formed on PWA 1484 with low sulfur content exposed at 1100°C for 1 hour in water vapor environment

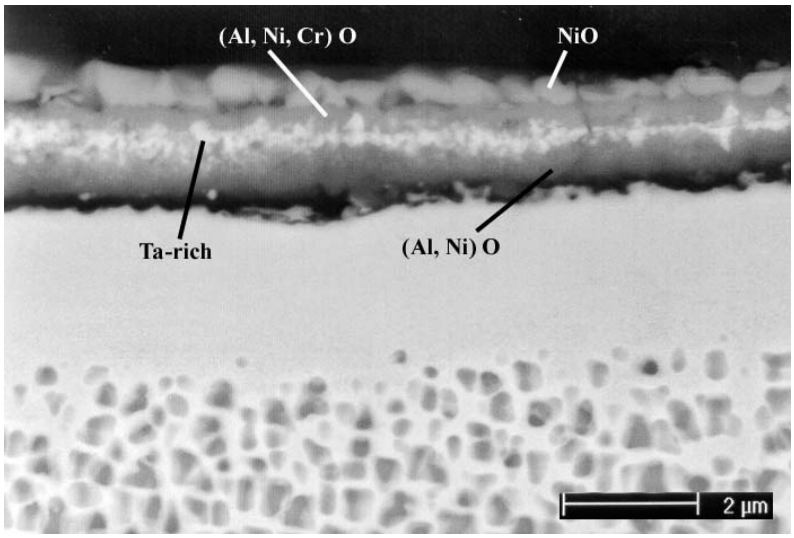

(a)

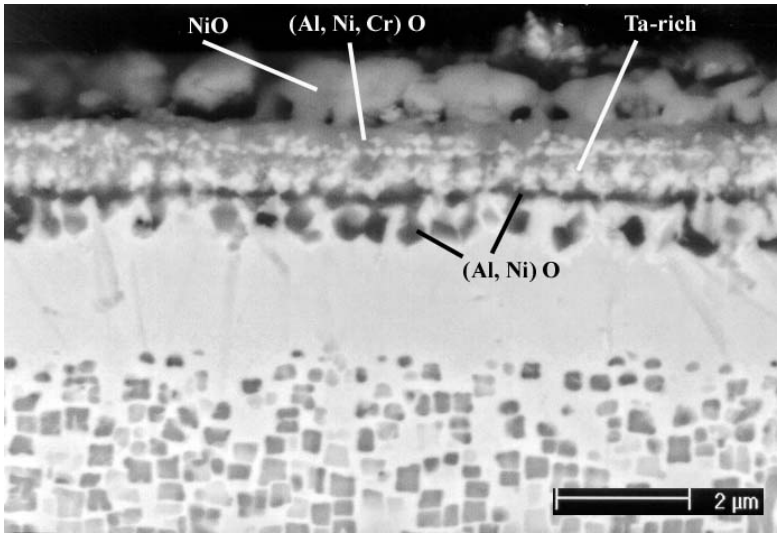

(b)

Figure 43 PWA 1484 (low sulfur) oxidized isothermally at 1100°C for 10 minutes in air with water vapor at (a) 0.1atm; (b) 0.5atm

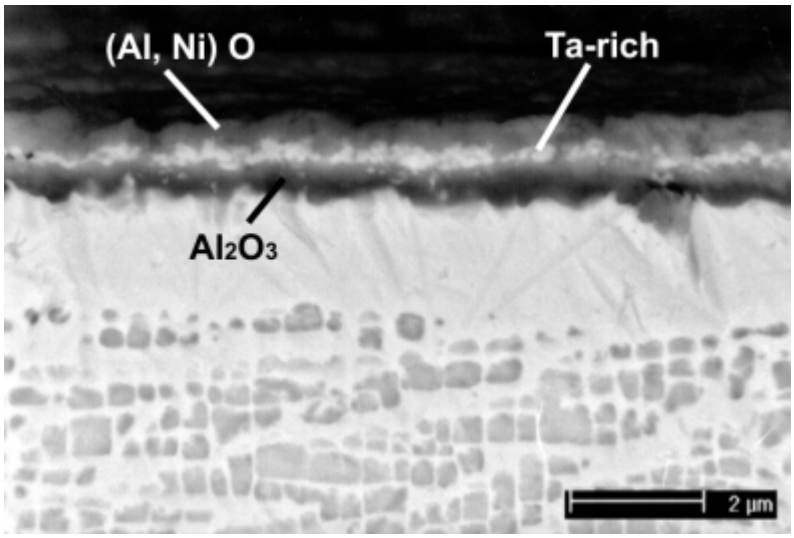

(a)

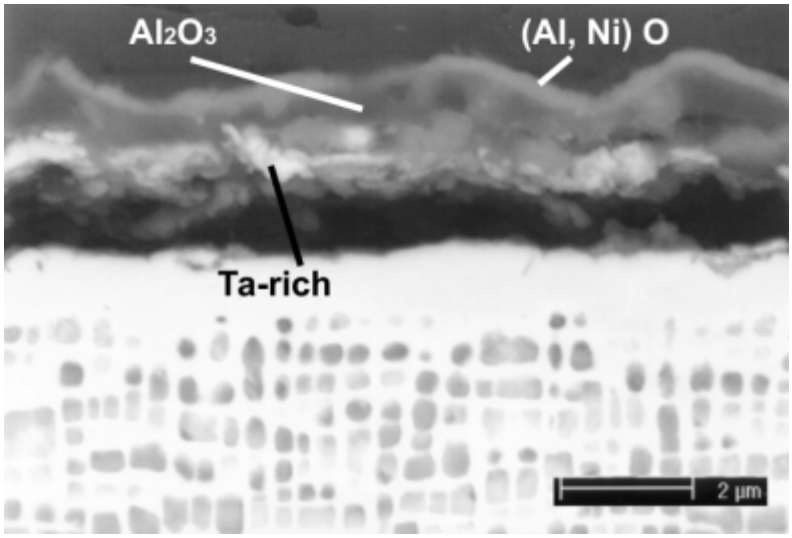

(b)

Figure 44 CMSX4 exposed at 1100°C for 10 minutes in air with water vapor at (a) 0.1atm; (b) 0.5atm

and in air containing two different pressures of water vapor (0.1 and 0.5atm) show that water vapor causes a more extensive transient oxidation stage for the specimen exposed at higher water vapor partial pressure.

The formation of chromia during the transient oxidation period causes the alumina to develop continuity in short periods of time on alloys such as PWA 1484 and CMSX4. Cyclic oxidation tests using specimens of PWA 1480 (containing 10wt% Cr) and PWA 1484/CMSX4 (containing 5wt% Cr) were performed in order to determine whether water vapor is affecting the amount of chromia in the transient scale. These results are presented in Figure 45, indicating similar oxidation kinetics for PWA 1480 and CMSX4. It could be concluded that PWA 1480 does not show better oxidation resistance due to a higher chromium concentration. This conclusion is further supported by the microstructure of 1-hour exposed PWA 1480 at 1100ºC in air with water vapor, Figure 46, where substantial transient oxidation was evident.

From the point of view of the cyclic oxidation kinetics, the effect of water vapor is detectable during the initial (~ 100 cycles) stages of exposure. In this regard, attention is drawn to the first data points (exposure of about 90 1-hour cycles) for specimens of regular and low sulfur content René N5 in Figure 47, where the effect of the water vapor makes a difference between dry and wet atmosphere exposures. During these initial stages of oxidation, the presence of water vapor leads to oxidation of many alloying elements. The scales formed are not expected to be protective due to the presence of nickel and chromium oxides in the scale, Figure 48. Examination of the transient oxide structures that developed during exposures in water vapor, Figures 37, 39, 40 and 41, show that the amount of nickel oxide in the scale is quite large.

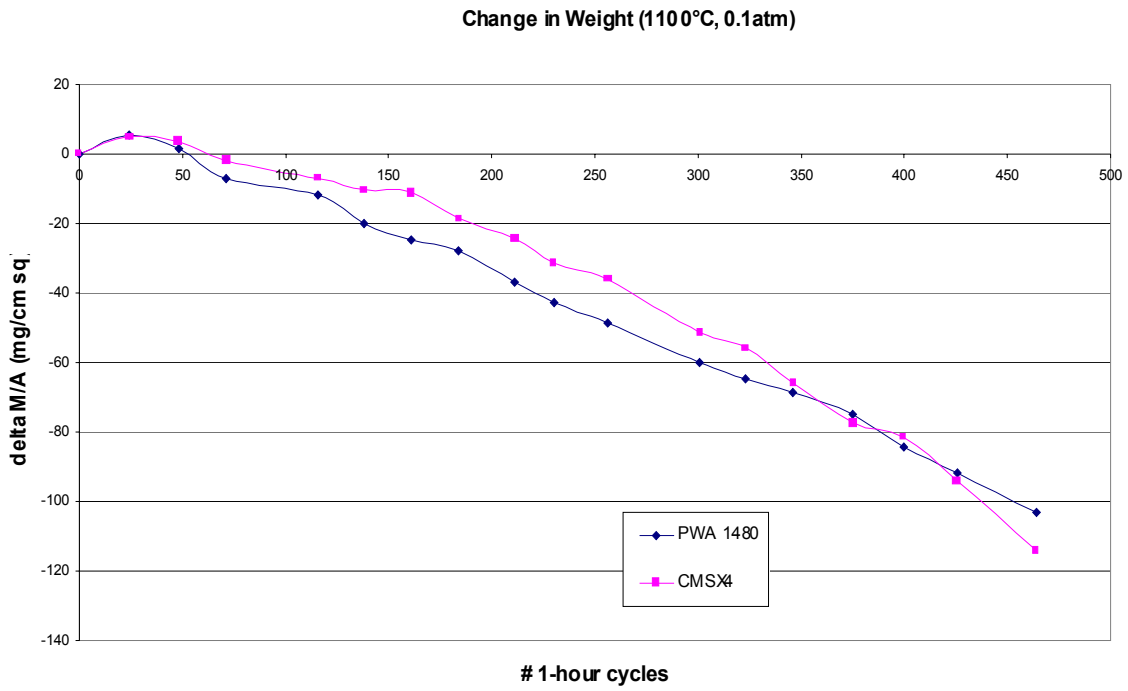

Figure 45 Change in weight vs. time for two superalloys exposed to wet conditions (0.1atm water vapor pressure) at 1100°C

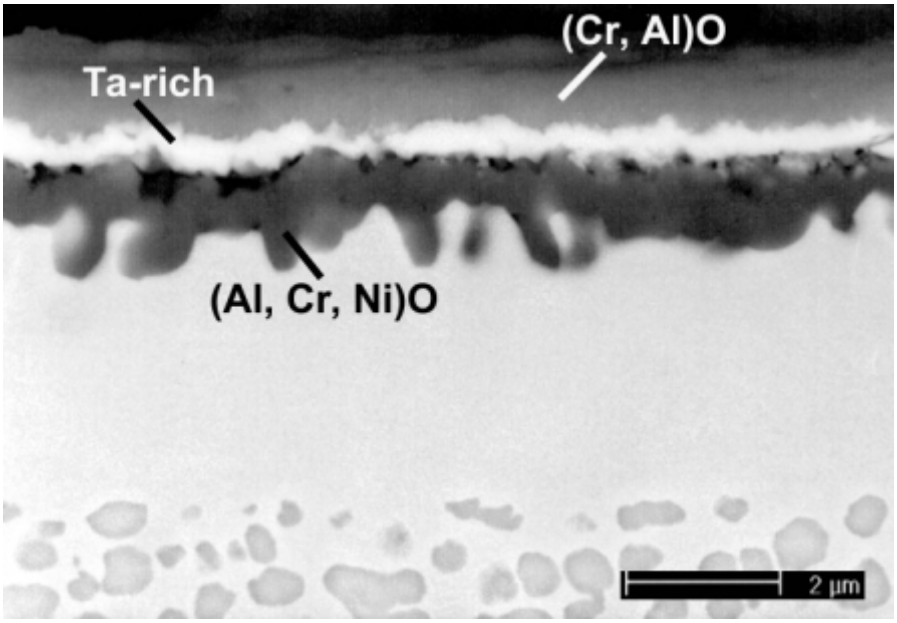

Figure 46 PWA 1480 isothermally oxidized at 1100˚C for 1 hour in air with water vapor at 0.1atm – cross-sectional view

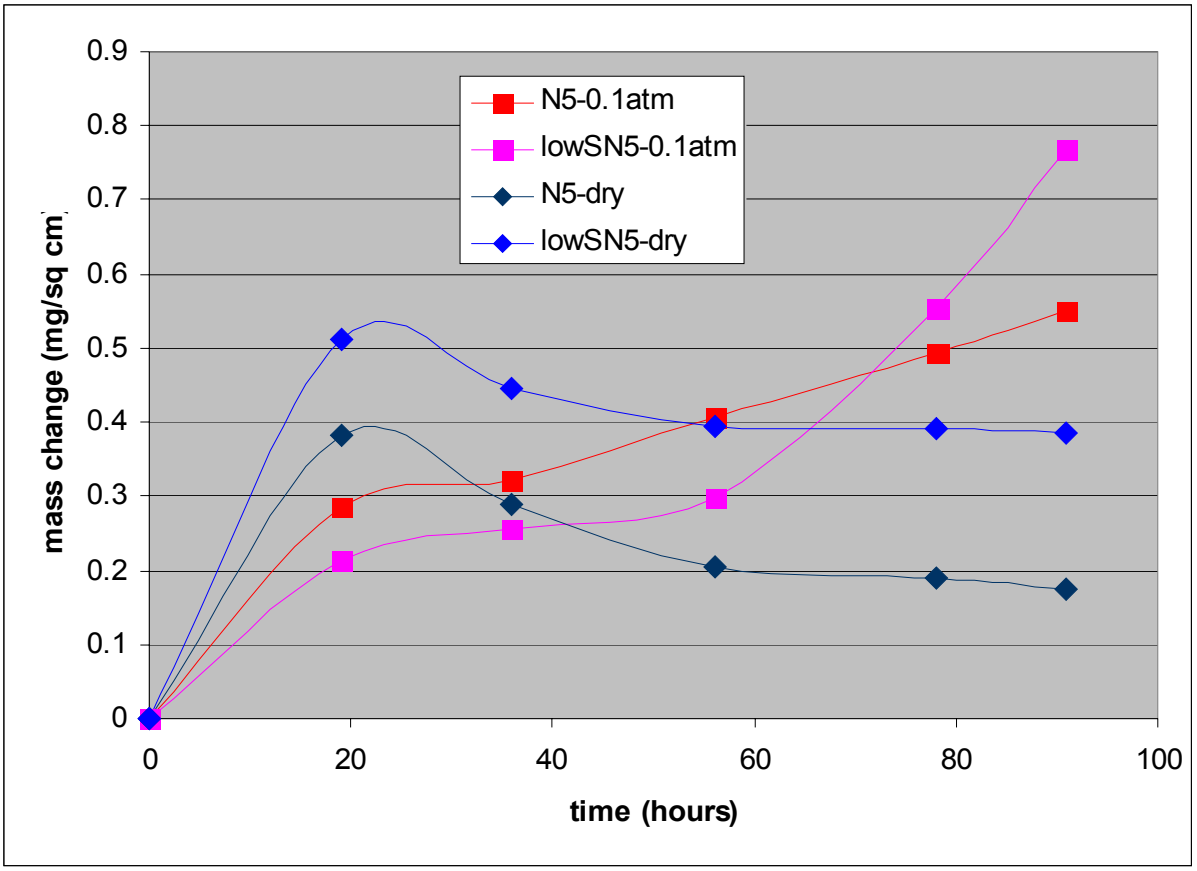

Figure 47 Change in weight versus time for René N5 and low-sulfur René N5 exposed in dry and wet conditions at 1100°C – 91 cycles

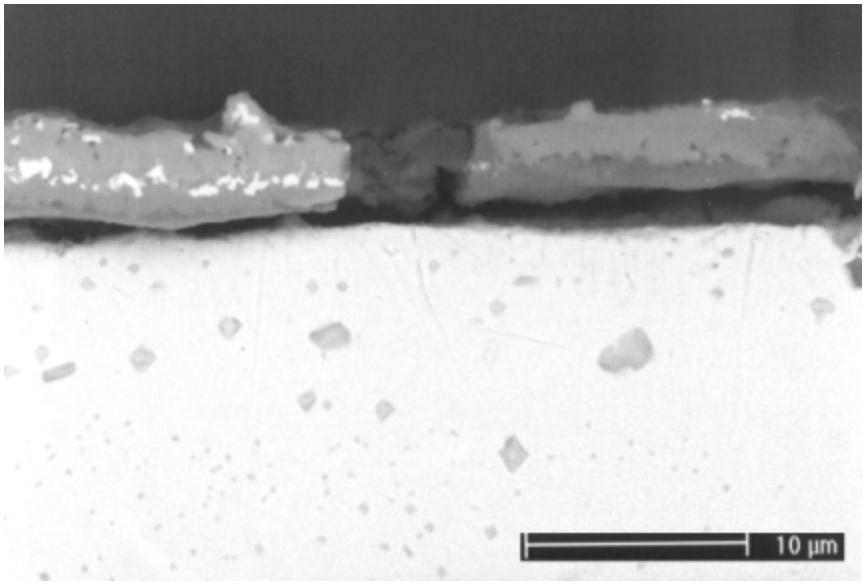

(a)

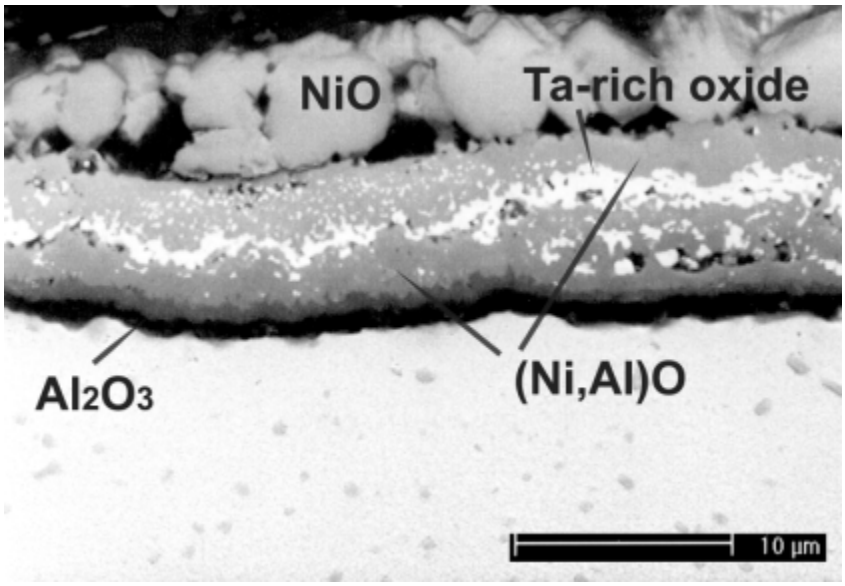

(b)

Figure 48 CMSX4 cyclically exposed at 1100°C for 464 hours in (a) air; (b) air with water vapor at 0.1atm

The growth rate of NiO might affect the amount of transient oxidation that takes place before a continuous scale of alumina is developed. NiO is a p-type oxide [8] with cation vacancies. If hydrogen were incorporated into NiO as an interstitial, the following defect reaction would apply:

$$H_2O(g) = 2H_i^{\bullet} + O_o^{x} + V_{Ni}^{''} \qquad (24)$$

The concentration of nickel vacancies would be increased and this would cause the growth rate of NiO to be increased. The study of Hultquist et al [58] suggests that an increase in metal cations transport in alumina for the high temperature oxidation of a FeCrAlY alloy can be obtained by addition of hydrogen to the metal substrate by electrolysis of water or from the gas phase.

For longer times of cyclic exposure (up to 500 hours) in wet air compared to dry air, the scale is thicker and exhibits a multilayered aspect containing an appreciable, dense and continuous layer of α-Al_2O_3 formed at the alloy surface at some early stage, Figure 48. This layer is maintained while subsequent layers of $NiAl_2O_4$, $Ni(Al, Cr)_2O_4$ and NiO grow in that order on top of the alumina. These results show that nickel may be diffusing through the alumina scale, although it cannot be ruled out the fact that these oxides formed initially as transient oxides.

The growth rate of alumina scales for specimens exposed in water vapor was greater than that in dry air for longer time exposures. Furthermore, the total oxide thickness formed in wet air was twice that for oxidation in dry air, Figure 48.

5.1.2.2. Model Alloy Ni-8wt%Cr-6wt%Al Oxidation The interpretation of the oxidation mechanism of superalloys is quite difficult due not only to the fact that metal and oxygen species diffuse simultaneously, but also that minor and trace alloying elements are incorporated at the same time in the scale and diffusion can occur via bulk grains as well as grain boundaries.

In order to develop nickel base alloys and coating systems with a good and improved oxidation resistance, the influence on oxidation behavior of a selection of elements that would improve the mechanical properties of these alloys (Mo, W, Ta, Al, Ti) and elements that improve oxidation resistance (Y) must be determined. However, nickel base superalloys are a very complex system and before it is possible to examine the influence of all the different elements on the oxidation behavior of Ni base superalloys, it is important to define the oxidation behavior for much simpler, but related, alloy systems such as Ni-Cr-Al alloys.

To further examine the water vapor effect on the initial stages of oxidation, experiments on simpler systems were performed. Such a system was a Ni-Cr-Al model alloy with a sufficiently high level of Al concentration for the system to be an alumina former.

Investigation of the oxidation of Ni-Cr-Al alloys helped in distinguishing the transient period at the beginning of exposure and the subsequent steady-state behavior in dry atmospheres. During the transient period, oxidation of the various alloy constituents takes place, leading to the formation of NiO and $Ni(Cr, Al)_2O_4$ spinel together with Cr_2O_3 and Al_2O_3. For a sufficiently high Al level, a pure Al_2O_3 scale can be expected. For steady-state conditions, different oxides coexist and can be divided in three different types depending on the concentration of Cr and Al in the Ni-Cr-Al alloys, Figure 6. A type III alloy – one that only forms an external layer of Al_2O_3 (after a transient period of oxidation) – was chosen: Ni – 8wt%Cr – 6wt%Al.

A typical as-cast structure of the model alloy Ni-8Cr-6Al substrate before any high temperature exposure is presented in Figure 49 showing the dendritic solidification structure of the alloy. Although the samples were not annealed, the compositional differences in the alloy are not reflected in the surface reactions.

Specimens of Ni – 8wt%Cr – 6wt%Al were exposed for 1 hour at 1100°C to dry air and air with 0.1 atm water vapor conditions. As one can see from the surface micrographs of the exposed specimens, the specimen exposed in dry air formed a continuous scale of α-Al_2O_3, Figure 50a, whereas the specimen exposed to the gas containing water vapor, Figure 50b, exhibited stringers of NiO and α-Al_2O_3. The stringers of nickel oxide appeared to be associated with polishing marks on the specimen's surface. Previous work has shown that selective oxidation of elements can be affected by the surface preparation conditions of specimens [88]. Since the previous specimens had been polished through 600 grit SiC abrasive paper, additional specimens of Ni-8Cr-6Al were exposed after being polished down to 0.05µm α-Al_2O_3 suspension. As shown in Figure 51a, a continuous alumina layer was formed on this specimen upon exposure for one hour in dry air. The specimen exposed for one hour at 1100°C in air with 0.1atm water vapor formed an oxide scale that was rich in NiO, but α-Al_2O_3 appeared to develop at what may have been grain boundaries in the alloy, Figure 51b. The surface of this specimen is shown at higher magnification in Figure 52a, where different oxides are evident. Figure 52b shows a portion of this specimen at a location where the external scale had cracked and spalled. The exposed alloy has different features depending upon the oxide scale that had developed. Scanning electron micrographs showing cross-sections of these specimens are presented in Figure 53a and Figure 53b with the mentioning that Figure 53b depicts the cross-section of Ni-8Cr-6Al after only 1 minute of exposure in air with water vapor at 0.1atm at 1100°C. In dry air,

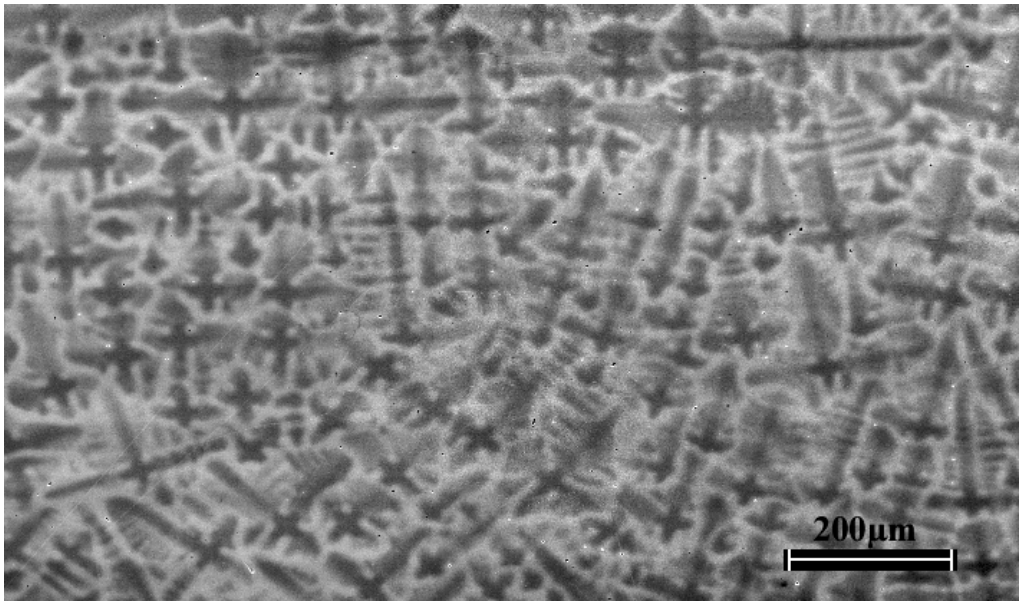

Figure 49 Typical structure of model alloy Ni – 8wt%Cr – 6wt%Al, cast structure

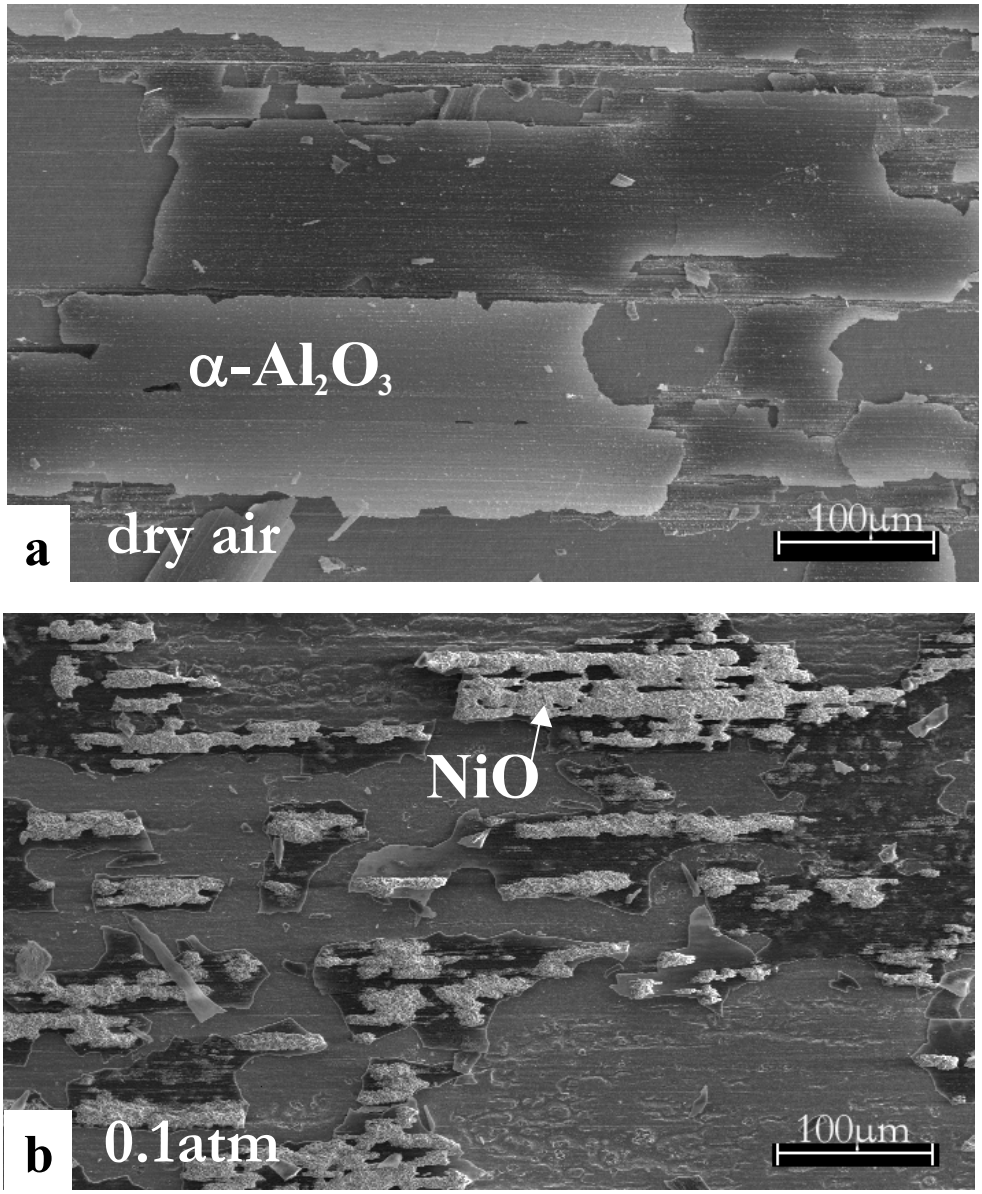

Figure 50 Ni-8Cr-6Al exposed for 1 hour @ 1100°C (surface condition 600grit) (a) dry air; (b) air with water vapor at 0.1atm

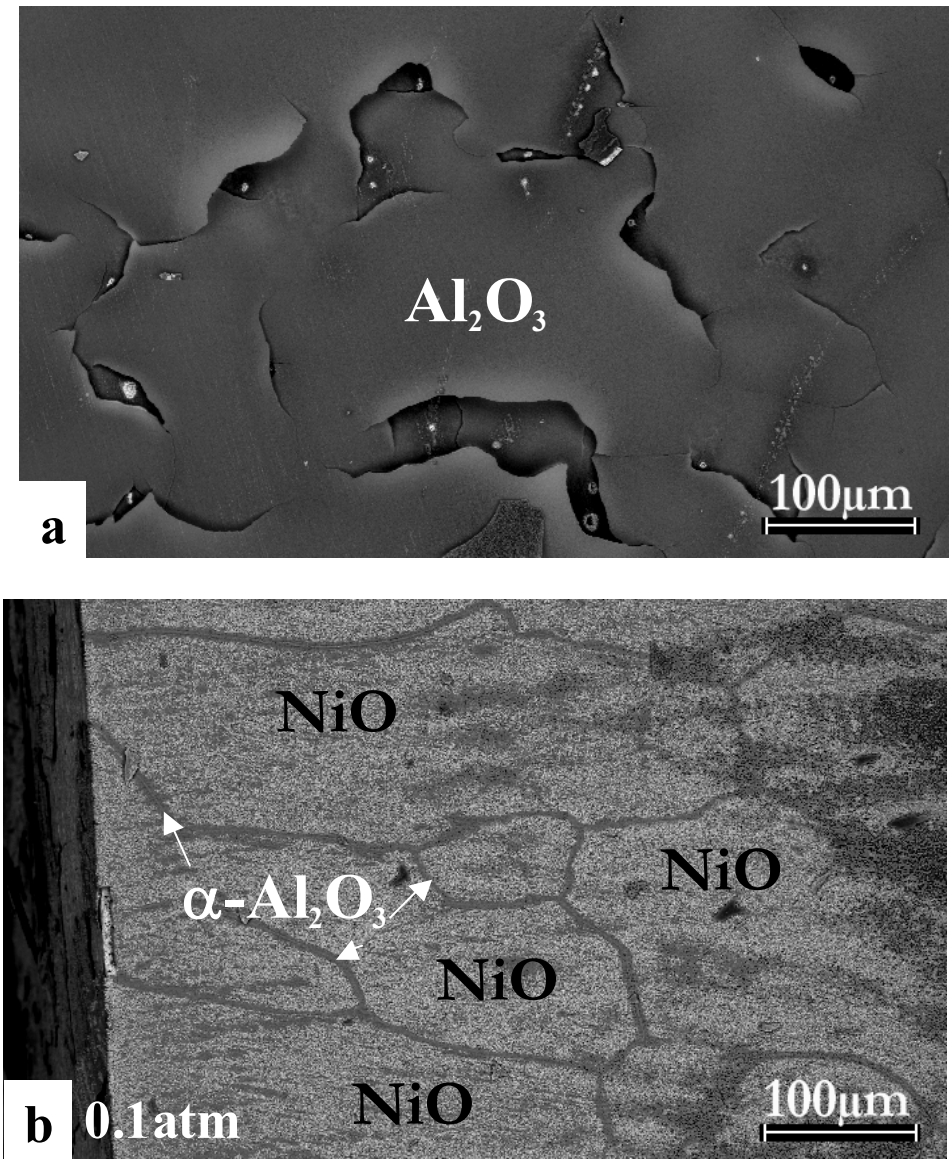

Figure 51 Ni-8Cr-6Al exposed for 1 hour@ 1100°C (initial surface preparation 0.05μm in alumina) (a) in dry air; (b) in air with 0.1atm water vapor

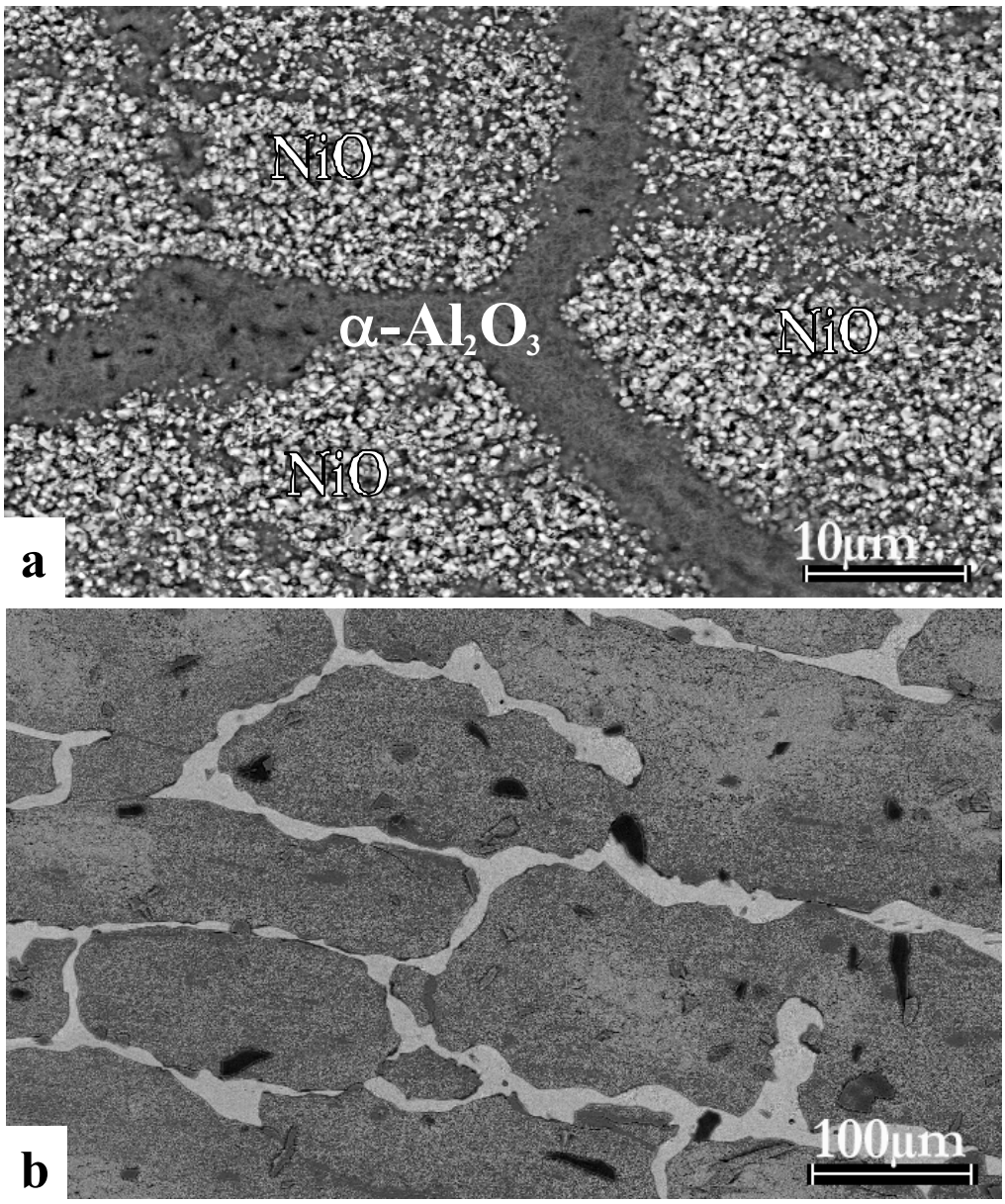

Figure 52 Ni-8Cr-6Al oxidized for 1 hour @ 1100°C in 0.1atm water vapor atmosphere (initial surface preparation 0.05μm in alumina) (a) surface of oxide adjacent to the gas surface; (b) alloy surface after spalling of the oxide scale

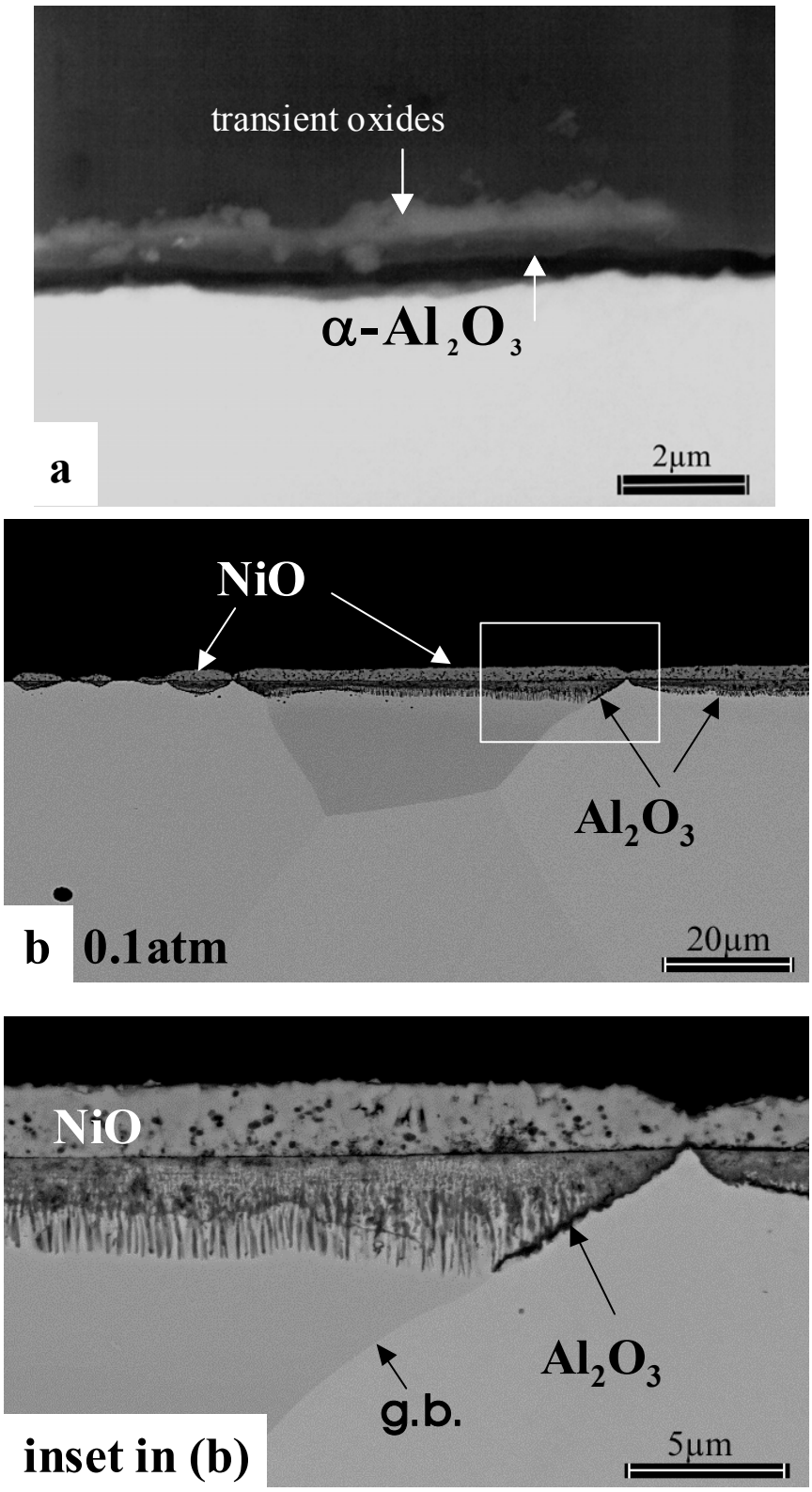

Figure 53 Cross-sections of Ni-8Cr-6Al oxidized @ 1100°C for (a)1 hour in dry air; (b) 1 min in air with water vapor (0.1atm)

the scale is α-Al_2O_3 with some transient oxides formed on top, Figure 53a. The specimen of Ni-8Cr-6Al that was exposed in water vapor has formed NiO in numerous areas, Figure 53b, and the continuous layer of α-Al_2O_3 is only beginning to form in a few areas (arrows in Figure 53b). In fact, the oxide layer over grain boundaries in the alloy contains some transient oxides; nevertheless, a continuous layer of α-Al_2O_3 has developed.

X-ray measurements in glancing angle and fixed incidence mode for the two specimens oxidized for 1 hour at 1100°C in different atmospheres reveal a spinel ($NiAl_2O_4$) phase detected for the wet-exposed specimen, whereas no such peaks are identified for the dry-exposed specimen, Figure 54.

According to observations from Figure 53, alumina develops continuity at grain boundaries in the alloy due to oxygen-containing species meeting the aluminum at these sites (i.e. grain boundaries). The fluxes of oxygen and aluminum are sufficient to form a continuous layer of alumina, Figure 55.

After a certain amount of oxidation time, the outward diffusion of Al is large enough, an optimum composition at the deep front of the internal oxides is reached and alumina starts to form at this front. Away from the sites of grain boundaries, the internal oxidation is still deep in the alloy (i. e. strong inward flux of oxygen-containing species), but there is not enough flux of outwardly diffusing Al to develop continuity of the alumina layer. Alumina does not develop continuity at those regions far away from grain boundaries. There are large amounts of transient oxides formed at these sites, thus inhibiting the selective oxidation of aluminum.

It is proposed that alumina nucleates preferentially at grain boundaries of the alloy and the transport of aluminum from the alloy is more rapid along grain boundaries compared to transport in the bulk grains. It can also be seen that in the zones of internal oxidation, the

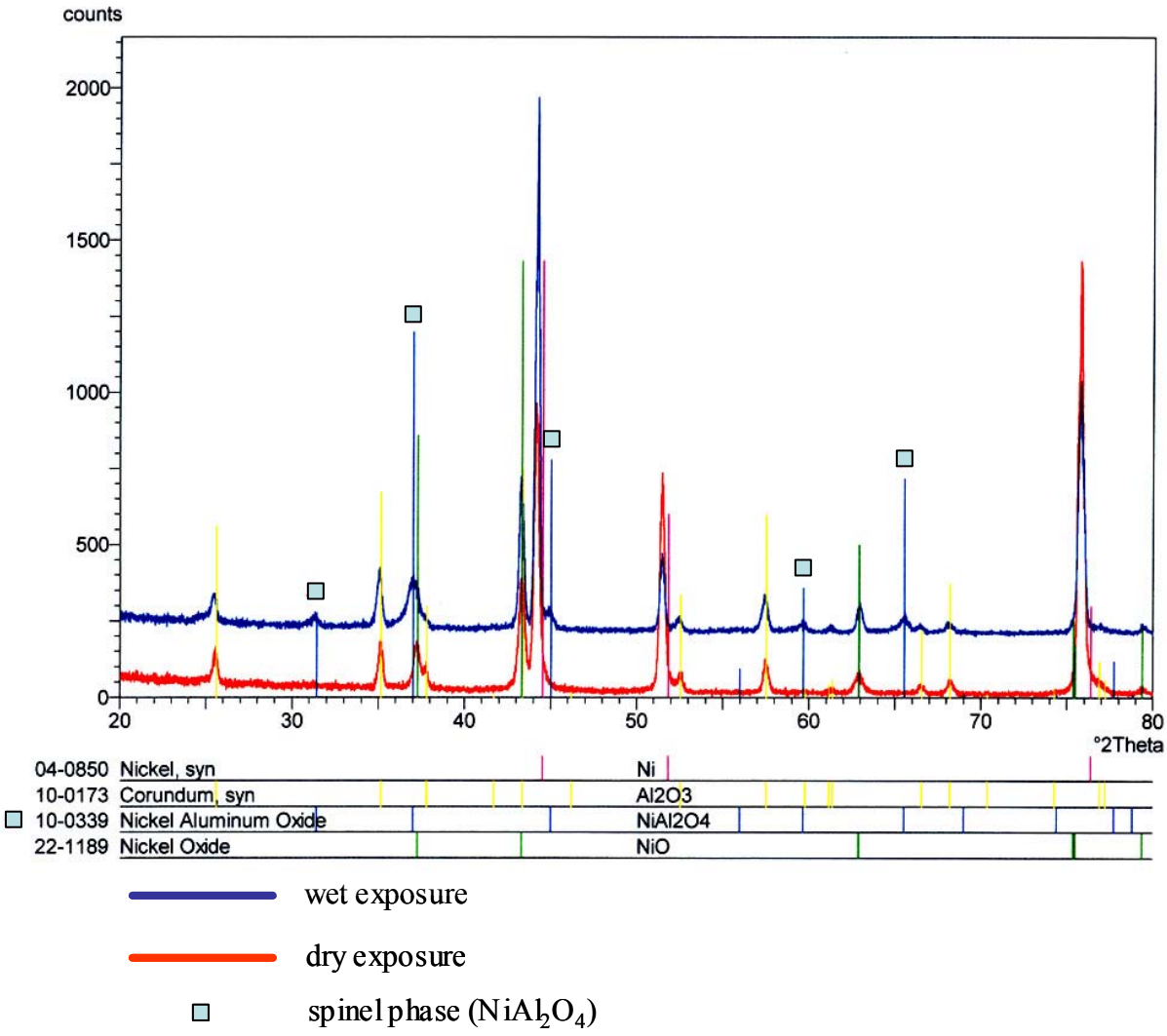

Figure 54 X-ray peaks (spinel/ no spinel) in Ni-8Cr-6Al 1hour@1100°C – oxidation in dry air/air with water vapor at 0.1atm

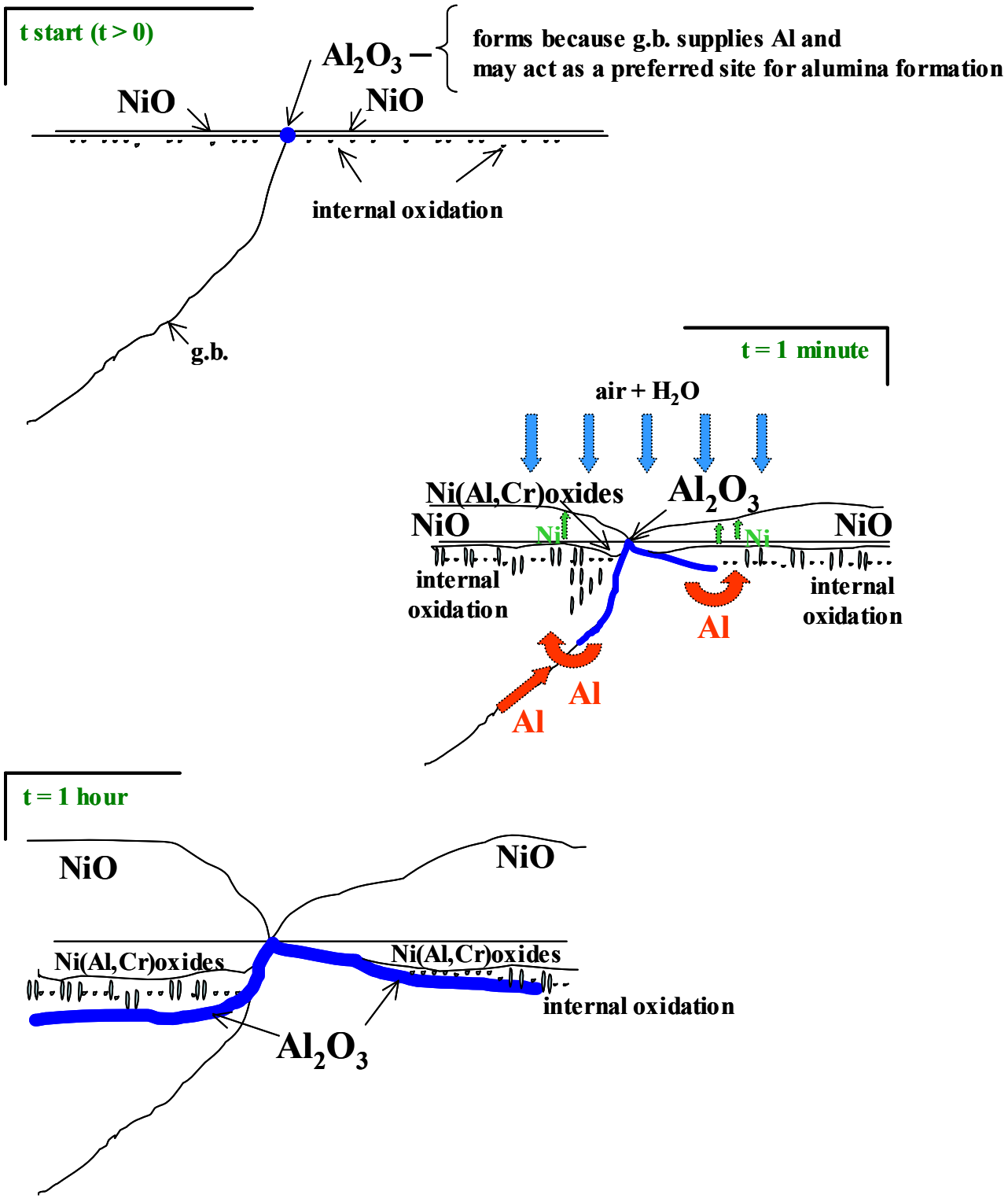

Figure 55 Schematic of three stages of oxidation in air with water vapor for a Ni-8Cr-6Al specimen at 1100°C

continuous alumina forms along the grain boundary in the alloy, Figure 53, and this condition allows aluminum in the alloy to be used to develop continuous alumina at the adjacent zone of internal oxidation where no grain boundary is present, Figure 53.

The process of inward diffusion of oxygen into the Al-depleted zone and α-Al_2O_3 formation, with the necessary Al and O activities reached, leads to internal oxidation and formation of a discontinuous internal α-Al_2O_3 layer, Figure 53 (inset b). For the formation of such a layer, additional Al must diffuse from the substrate. Again, an adjacent region is depleted in aluminum into which oxygen can diffuse. In this manner, a cyclic process is initiated in regions without protective and adherent alumina scale, which causes repeated precipitation of α-Al_2O_3 layers within the substrate. This process is governed by inward diffusion of oxygen and outward diffusion of aluminum. Wide regions of aluminum depletion would suggest that O, rather than Al diffusion, is rate controlling. The inward transport of oxygen is enhanced by diffusion at the oxide/substrate interface.

It appears that the presence of water vapor is resulting in a higher aluminum content for the transition to external oxidation.

Lower temperature exposures for a duration of 4 hours were performed on specimens of Ni-8Cr-6Al at 700°C in dry air, air with 0.1atm water vapor and a gas mixture of argon and water vapor at 0.1atm. The scales on these three specimens are presented comparatively in Figure 56. The specimen exposed in dry air presents in the cross-section a non-uniform scale composed of mixed oxides (Ni, Al and Cr oxides) with alumina starting to develop in a very thin layer at the scale/substrate interface. Examining the cross-section of Ni-8Cr-6Al oxidized in dry air, Figure 56c, it appears that selective oxidation of aluminum is impeded at this lower

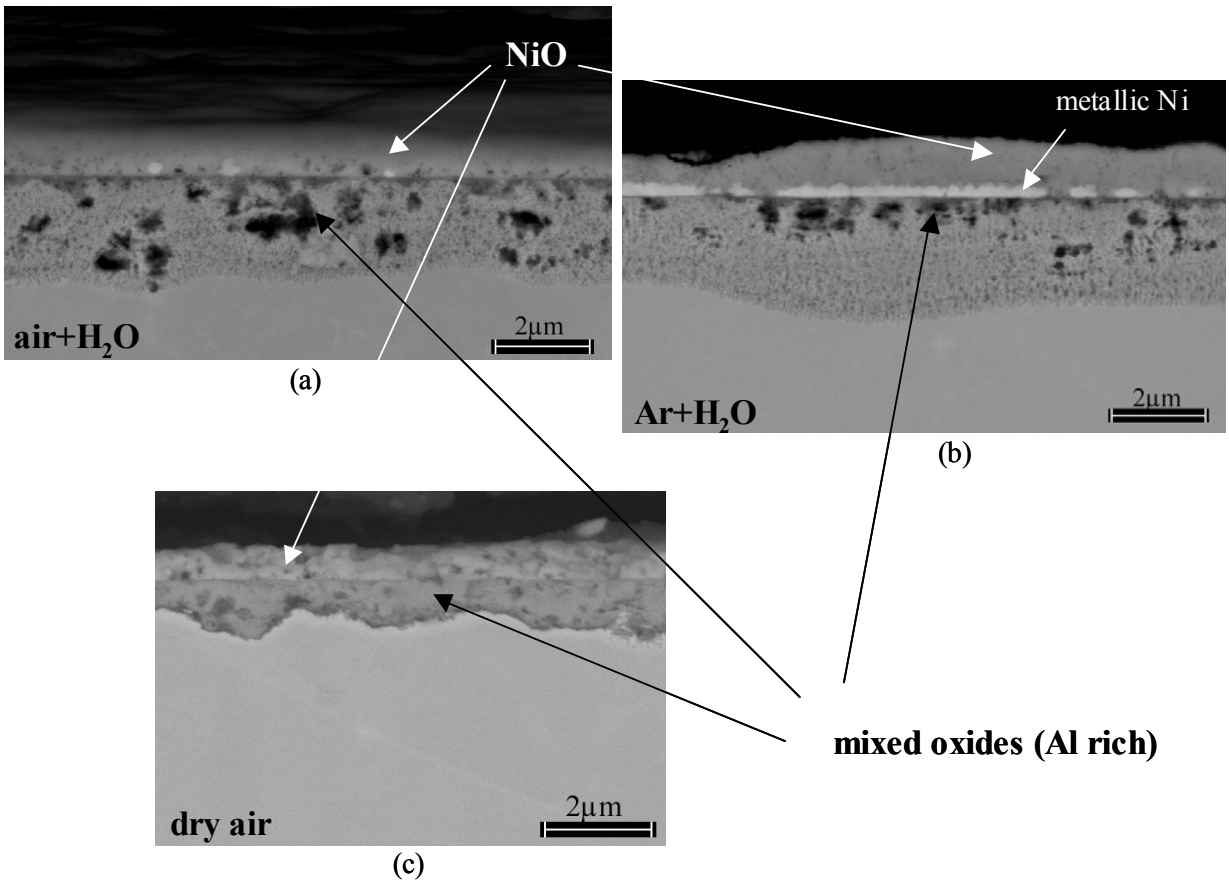

Figure 56 Specimens of Ni-8Cr-6Al exposed for 4 hours at 700°C in: (a) air with 0.1atm water vapor; (b) argon with 0.1atm water vapor and (c) dry air

temperature (700°C). For the specimen exposed in gas containing Ar, the cross-section micrograph shows an approximately 2µm thick NiO layer in which metallic Ni seems to be embedded, possibly 'pushed up' from the substrate. Under this, internal oxides of aluminum can be noticed along with a very fine internal oxidation network of about 2 to 3µm in thickness into the substrate. Some areas of metallic Ni could be observed in the NiO formed on the specimen oxidized in air with water vapor. The internal oxidation zone is comparable in thickness to the one on the Ar-exposed specimen with the note that there is a more pronounced penetration of the aluminum oxides in relation to the fine network of mixed oxides on the above-mentioned specimen. On both these specimens, the networks of internal oxides present a wavy morphology. For the Ar + water vapor exposure, the oxygen pressure is much lower than that in air; nevertheless, the cross-section presented in Figure 56b (Ar + water vapor) is very similar to that in Figure 56a (air + water vapor) with similar amounts of internal oxides and NiO scale. These results suggest a strong effect of the water vapor for the Ar + water vapor oxidizing atmosphere. As can be seen from Figure 56, the specimens exposed in wet gaseous atmospheres, although exhibiting a thicker region of internal oxides – mainly Al-rich oxides – there is no continuity of the alumina along these regions. The fact that there are virtually no locations at which alumina develops continuity leads to the observation that a lower temperature exposure (700°C compared to 1100°C) under water vapor conditions is substantially hampering the selective oxidation of aluminum.

Specimens of Ni8Cr6Al exposed for 5 minutes at 1100°C in different gas- atmospheres show transient oxides and zones of internal oxidation; however, the thicknesses of the transient NiO scales and the zones of internal oxidation were significantly larger for the specimens exposed in wet air, Figure 57b and 57c, compared to dry air, Figure 57a. A large effect of the

water vapor pressure was not observed for these short time exposures since the same amounts of NiO and internal oxidation were present in specimens exposed to air with 0.1 atm and air with 0.5 atm of water vapor, Figures 57b and 57c. The results presented in Figure 57 show that the transient NiO layer is growing more rapidly in wet air. The increased growth of NiO causes the depths of internal zones of oxidation to be greater, which would increase the critical aluminum concentration required for continuous alumina scale formation [89].

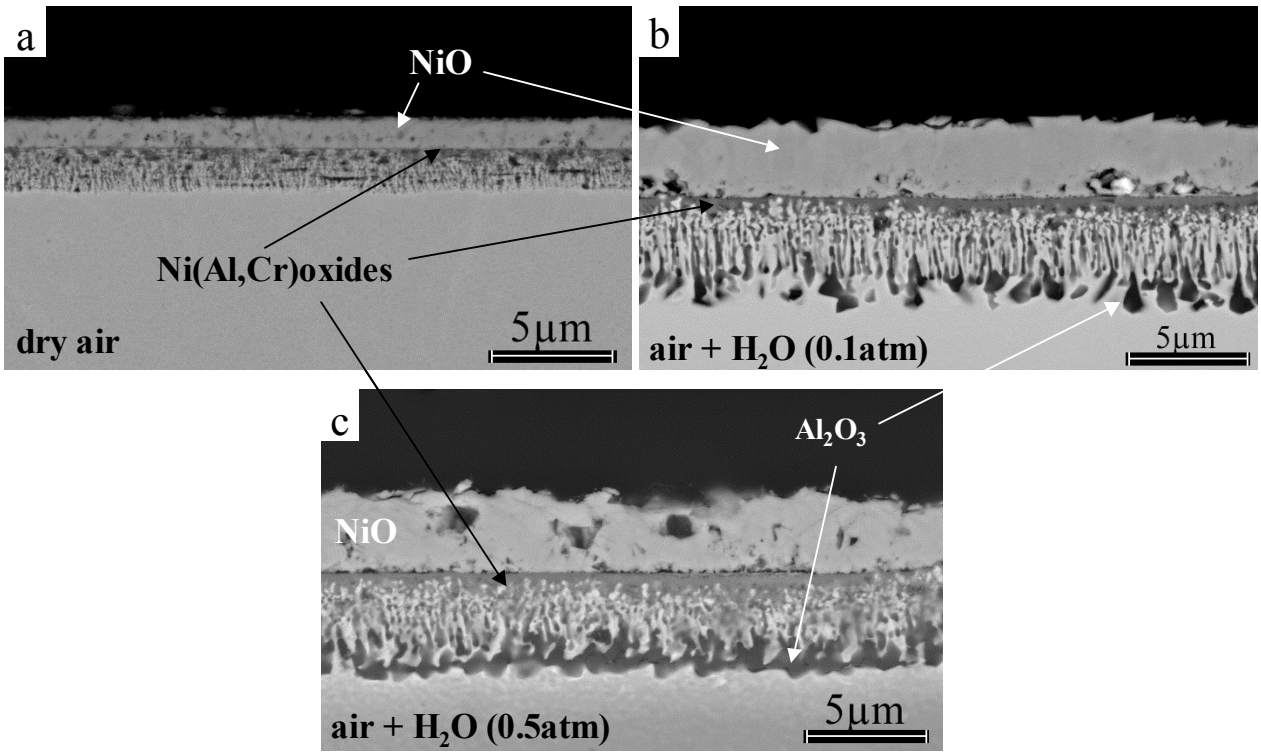

Figure 57 Increased internal oxidation of aluminum associated with accelerated growth of transient Ni and Cr oxides in specimens of Ni-8Cr-6Al oxidized for 5 minutes at 1100°C in (a) dry air; (b) air with water vapor at 0.1atm and (c) air with water vapor at 0.5atm

5.1.2.3 Nickel Oxidation NiO growth on pure Ni was the subject of a detailed study [90] using anion and cation tracers. This study found that the scale growth at T < 800°C was predominantly by outward Ni grain boundary diffusion, while at T > 1000°C, Ni lattice diffusion was prevalent. Also, at high temperatures, inward oxygen short-circuit diffusion became noticeable and could account for the growth of the inner porous layer of the commonly observed duplex scale.

The transport mechanisms in NiO are vacancy mechanisms in which singly charged vacancies ($V_{Ni}^{'}$) predominate [91], whereas doubly charged Ni vacancies ($V_{Ni}^{''}$) are responsible for the cation grain boundary diffusion. Oxygen diffusion occurs via vacancies [92]. The rate of diffusion of oxygen along grain boundaries is much slower than Ni grain boundary-diffusion [93].

Galerie and coworkers [94-96] have performed extensive studies comparing the oxidation rates of a number of pure metals in oxygen and pure, deoxygenated water vapor. They observed that Ti and Cr oxidized faster in water vapor than oxygen atmospheres even though the effective oxygen partial pressure was substantially lower in the water vapor. The results for Ti were explained as the result of smaller hydroxyl ions (r = 0.10 nm) moving over oxide ion vacancies in rutile with a greater mobility than larger oxide ions (r = 0.14 nm), thus increasing the inward growth component of the scale. The results for Cr were also explained as resulting from an increased inward growth component in water vapor except, in this case, it was postulated that the diffusion path for the hydroxyl ions was along chromia grain boundaries. Galerie et al [94] observed that nickel oxidized slower in water vapor as compared to a pure oxygen atmosphere and that the oxidation rate changed from parabolic to linear. This result was explained as being due to the difficulty in forming adsorbed oxygen atoms on the surface of NiO, an oxide that was considered with a 'non-acidic' surface, so that the adsorbed species were mainly OH^-. They argue that the hydroxyl ions cannot enter the scale of p-types oxides. Therefore, the rate-

controlling step becomes the surface reaction to provide oxygen atoms from the adsorbed OH^- to react with the Ni cations arriving at the oxide/gas interface. However, the growth of NiO in atmospheres of air/H_2O mixtures of the present study can be significantly different than oxidation in pure H_2O. The oxygen from the air component in the gas can provide the oxidant to react with the Ni cations at the oxide/gas interface.

To determine as a fact that NiO grows faster in atmospheres that contain water vapor compared to dry air conditions, a number of experiments were performed.

Further investigation in the present work consisted of specimens of pure nickel (99.999+wt%) exposed for one hour at 1100°C in dry air and in air with water vapor. It was determined that the NiO scale thickness formed in air with water vapor was twice that formed in dry air, Figure 58. As mentioned previously, it is possible that hydrogen from the water vapor can enter the NiO scale and can cause the cation vacancy concentration to increase via reaction (24), written before, whereby the transport of nickel through the NiO scale is increased due to the higher cation vacancy concentration.

The oxidation of pure nickel is considered one of the simplest examples of high temperature oxidation of pure metals. However, this ‘simplicity’ is rather ‘complex’ in the sense that many factors such as metal purity level, surface preparation of specimens and grain orientation in the substrate are known to greatly affect the growth kinetics, the external morphology as well as the internal microstructure of the scales that develop upon oxidation.

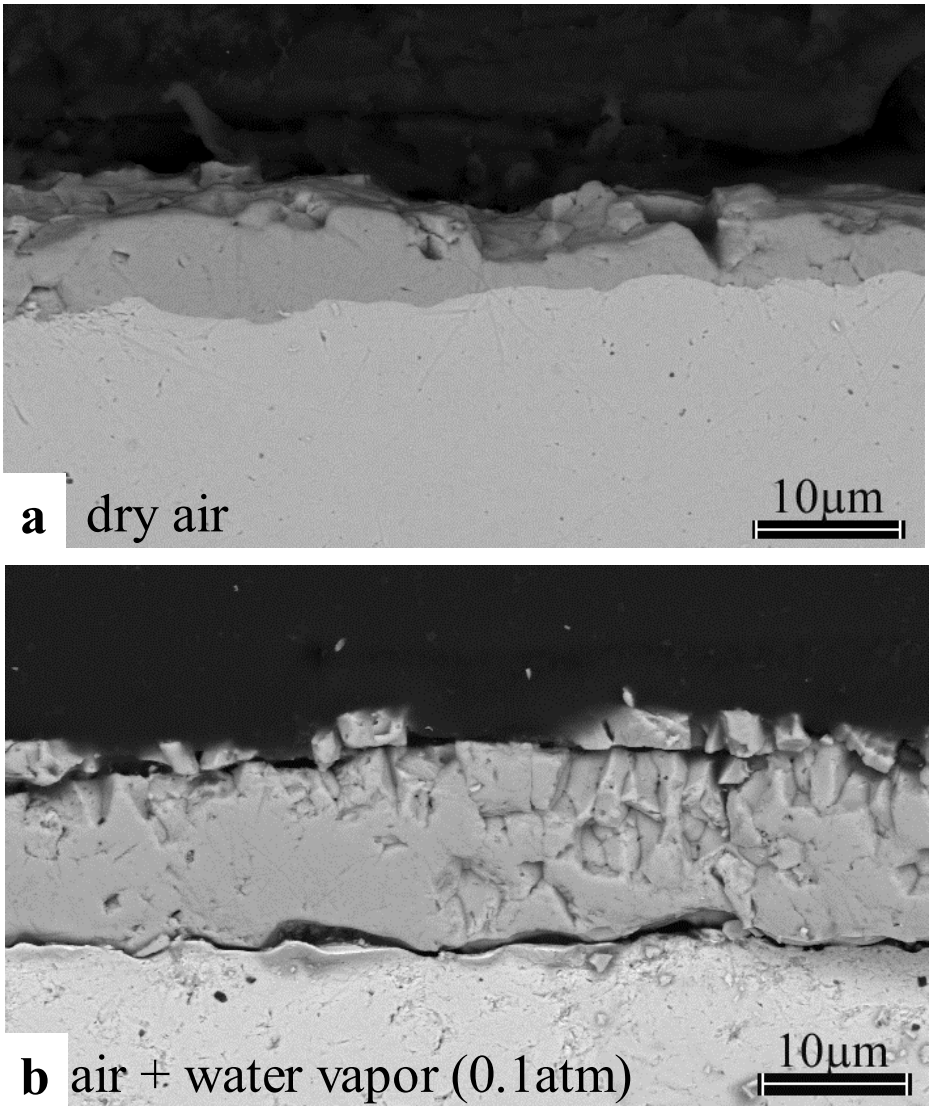

Figure 58 Ni 99.999+% pure, exposed for 1 hour @ 1100°C, in two different atmospheres (SEM cross-sectional images, showing morphology and thickness of NiO scales)

For the present study, for the pure nickel specimen exposed for one hour at 1100°C in dry air, Figure 59, oxide ridges were observed. The thickness of these oxide ridges is approximately 0.5 to 1μm. The growth of such oxide ridges could suggest fast Ni diffusion along NiO grain boundaries.

Comparison of values for the activation energy for nickel volume diffusion through NiO scales from the study of Peraldi et al [97] leads to the assumption that the outward diffusion of cationic species is the main mechanism controlling the NiO scale growth kinetics at temperatures higher than 1000°C. According to their work, at high temperatures (> 1000°C), the internal microstructures of the oxide scales were compact characterized by faceted grains. The growth of the first 5μm of the oxide scale could strongly depend on some transient step (nucleation) and/or interfacial reactions. This hypothesis could explain the large effect of nickel orientation on oxide grains size at these temperatures. Also, they suggested that the grain boundary diffusion of nickel cations could still contribute to NiO growth kinetics at temperatures as high as 1200°C. By comparing oxide scale thickness and oxide grain sizes, it was obvious for their study that the smaller NiO grain size corresponds to a thicker scale.

Comparison of oxide grain sizes for the present study shows that for the specimen exposed in air with water vapor the grains are of a smaller size, somewhat more equiaxed in the inner scale and more columnar on top, creating a network of well established oxide grain boundaries. On the other hand, for the specimen exposed in dry air, the oxide grains are large, extending from the bottom to the top of the scale, Figure 60.

The smaller grain size corresponded with the thicker oxide scale, whereas the larger grain size was observed on the thinner oxide scale, Figure 60 and Figure 61. This observation could be partially explained considering the contribution of nickel grain boundary diffusion. The rate of

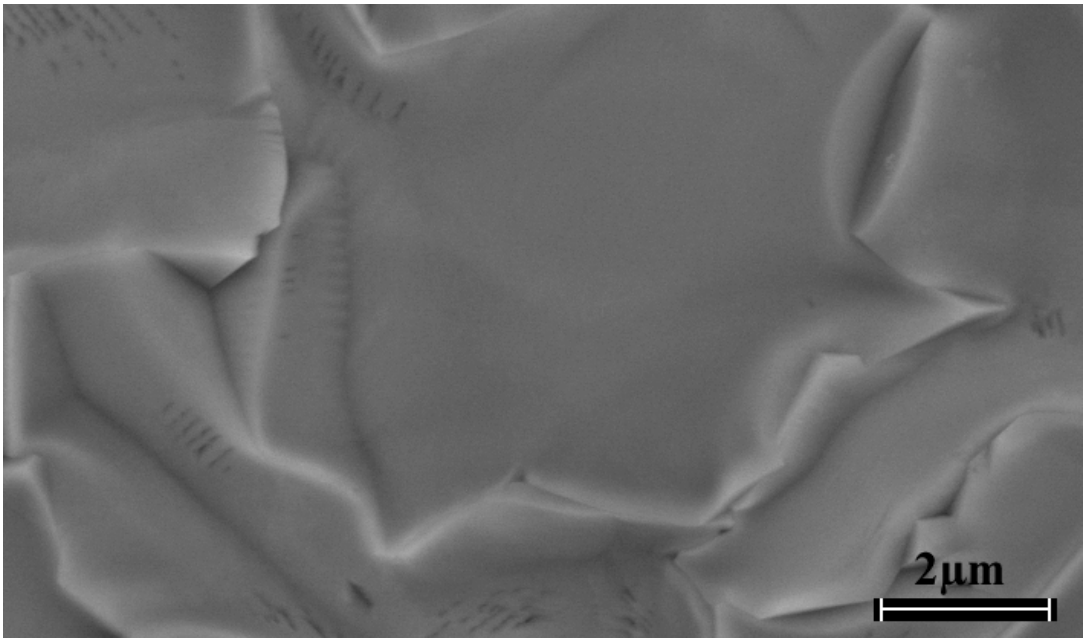

Figure 59 Ni (99.999+wt% purity) oxidized for 1 hour at 1100°C in dry air showing oxide ridges

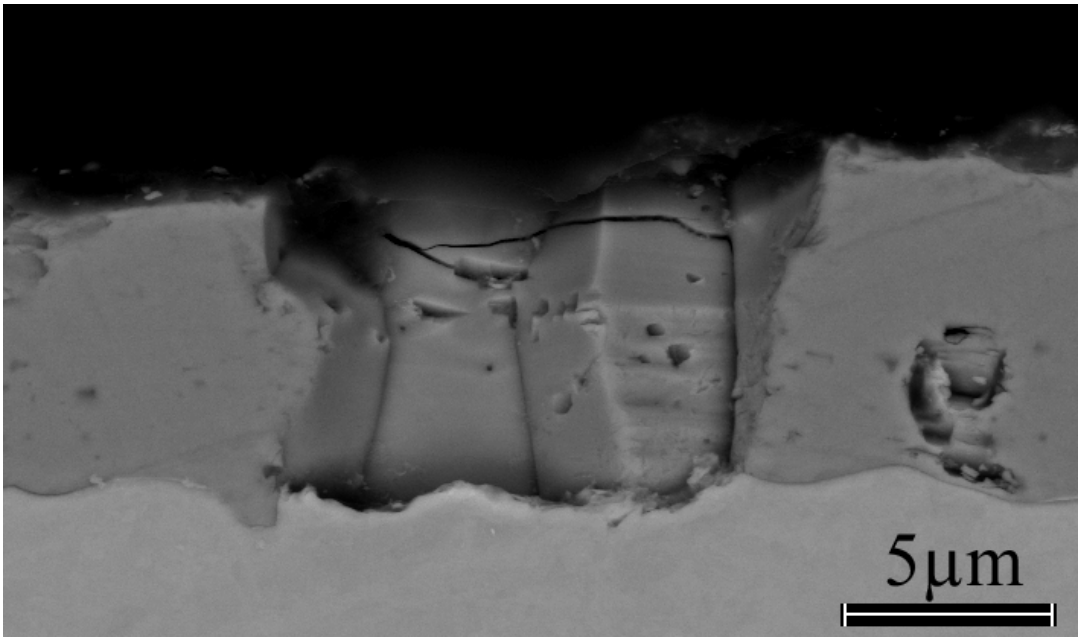

(a)

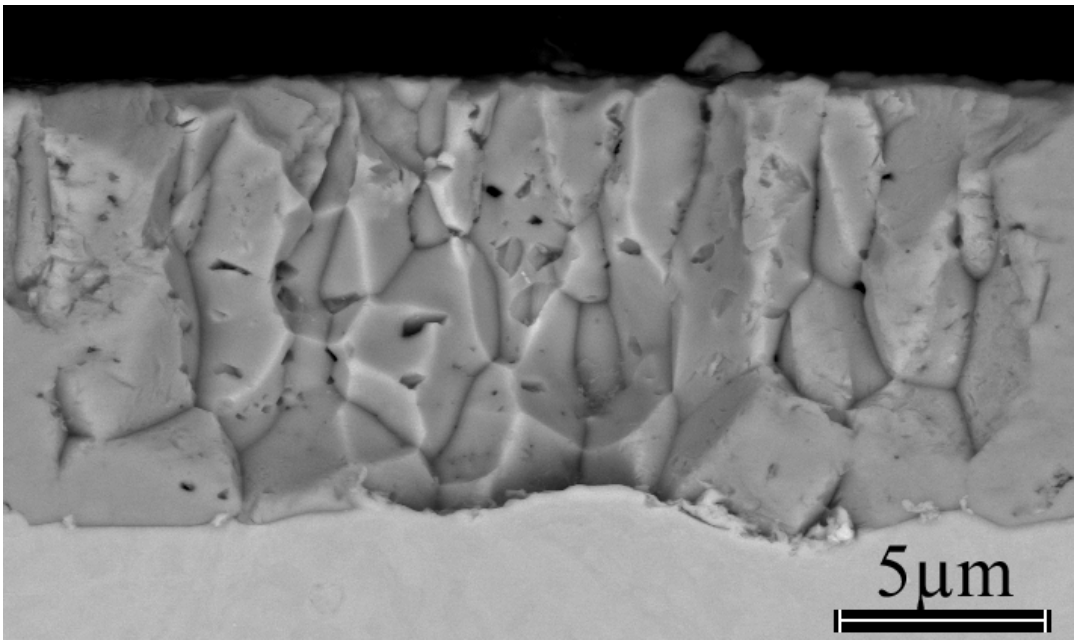

(b)

Figure 60 Ni specimens (99.999+wt%) exposed in dry air (a) and air with water vapor (b) for 1 hour at 1100°C – scales morphology

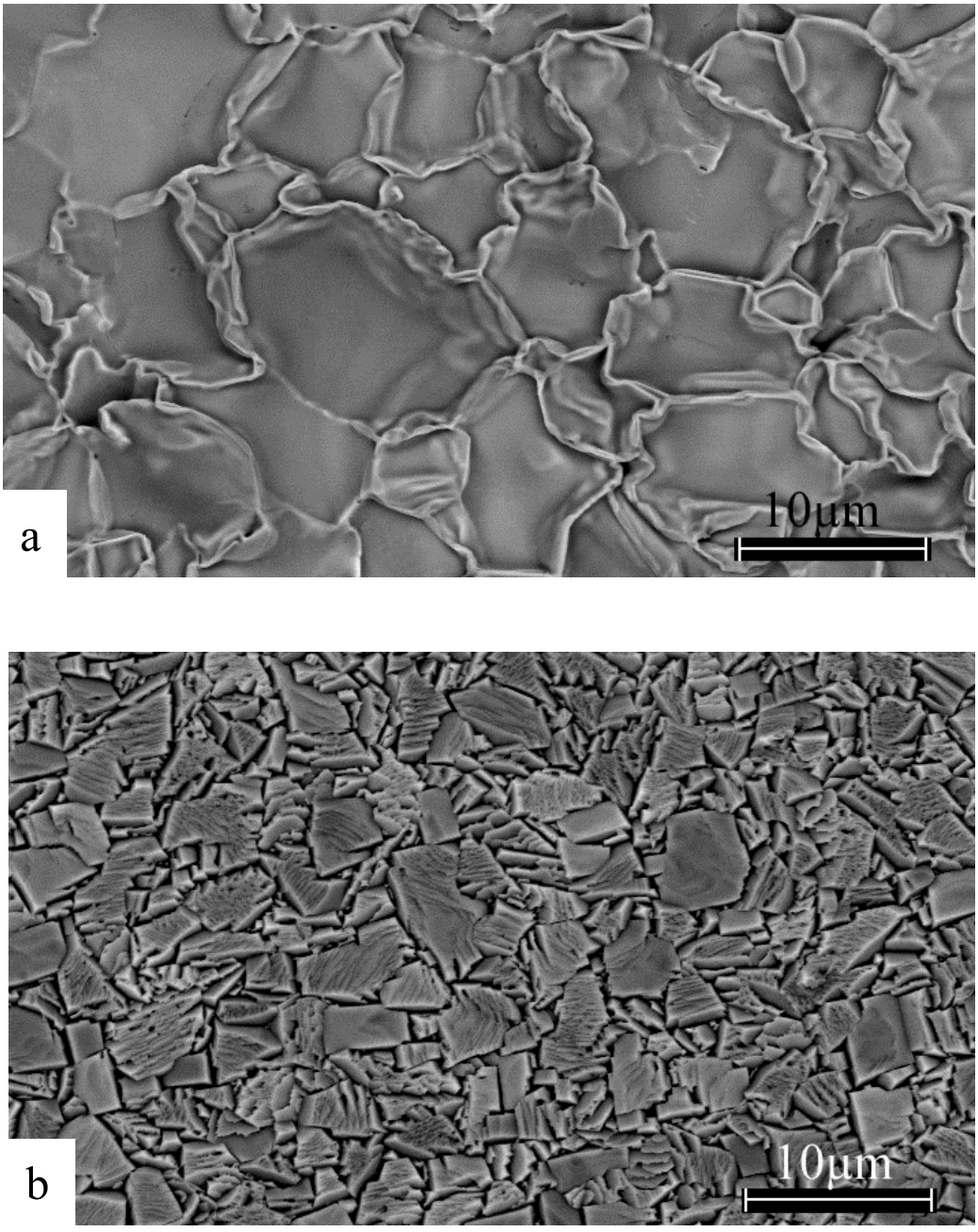

Figure 61 Surfaces of NiO scales formed on pure nickel after oxidation at 1100°C for 1 hour in (a) dry air and (b) air with 0.1atm water vapor

oxygen ingress along the dense grain boundary network in the case of the wet exposed specimen must be high to account for the relatively uniform interface at the scale/metal region. The oxygen transport must be governed by a diffusion-controlled step as long as the oxidation process maintains parabolic kinetics. In view of the grain boundary diffusion mechanism, one should expect rapid oxidation kinetics as long as the oxide grain size is small, since the mechanism involves grain boundary transport. The comparison of NiO scale thickness and oxide grain sizes for the present pure nickel experiments demonstrates that mechanisms other than bulk and grain boundary diffusion may influence the oxidation kinetics, mechanisms not yet clearly elucidated at this point.

Platinum markers were deposited on the surface of the pure Ni specimens prior to high temperature exposures. The markers were deposited in a mesh pattern as shown in Figure 62 by a platinum sputtering process.

As for morphological differences, the pure Ni specimen exposed for 1 hour at 1100°C in dry atmosphere presents larger grains of NiO, a rougher surface with numerous “hills” and “valleys”, Figure 63. For the same specimen, it was observed in cross-section that the Pt markers remained closer to the metal/oxide interface than the oxide/gas interface. The thickness of the NiO layer is about 7 – 9μm, Figure 64.

For the pure Ni specimen exposed for 1 hour at 1100°C in the presence of water vapor, smaller and more angular grains of NiO were noticed, Figure 65b, with a smoother appearance of the oxide surface, Figure 65a.

As an observation, the NiO grains that could be examined exactly on top of the Pt deposit exhibited a modified aspect from the rest of the scale, Figure 66, the oxide having developed with very small grain sizes.

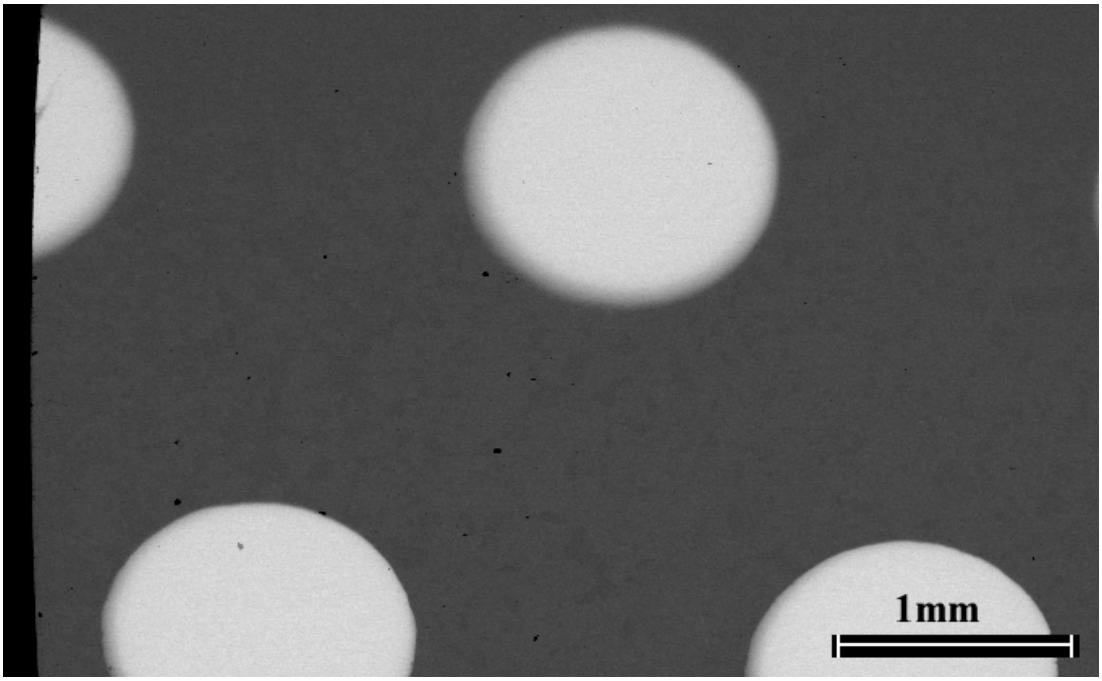

Figure 62 Platinum markers deposited in a mesh pattern on specimens of pure Ni (99.999+wt%)

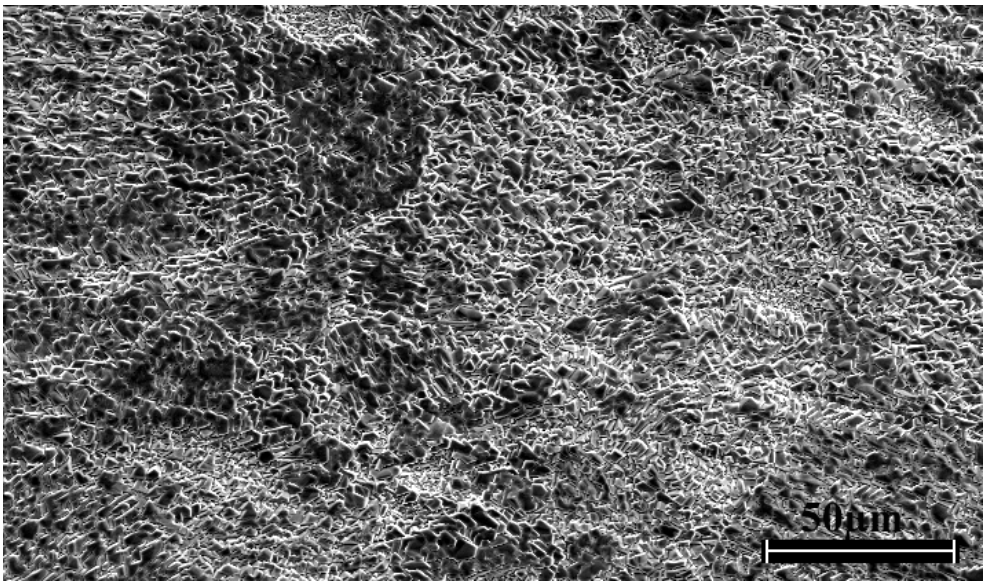

(a)

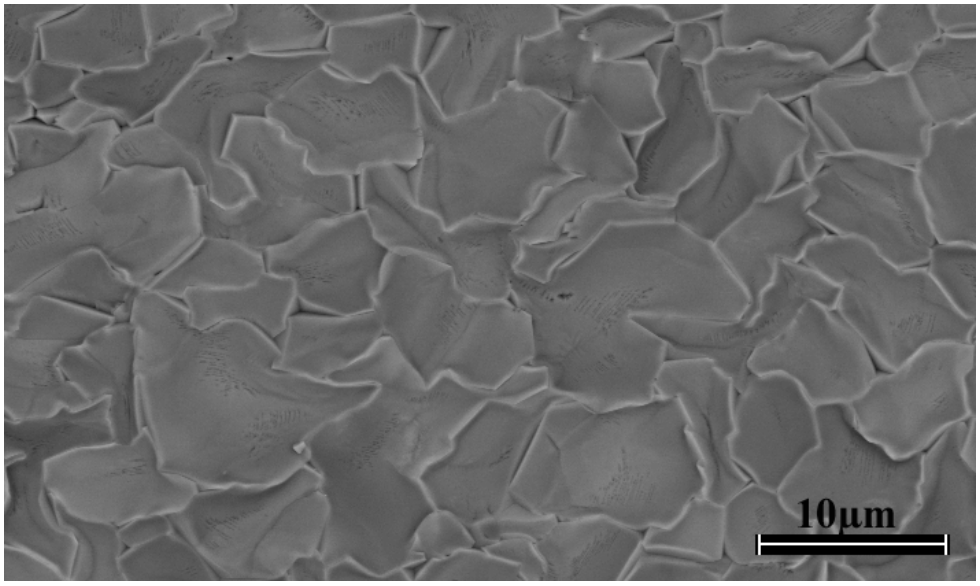

(b)

Figure 63 Specimens of pure Ni (99.999+%) exposed for 1hr@1100°C in dry air (a) SE image showing the relief of the surface; (b) BSE image, higher magnification, showing grains

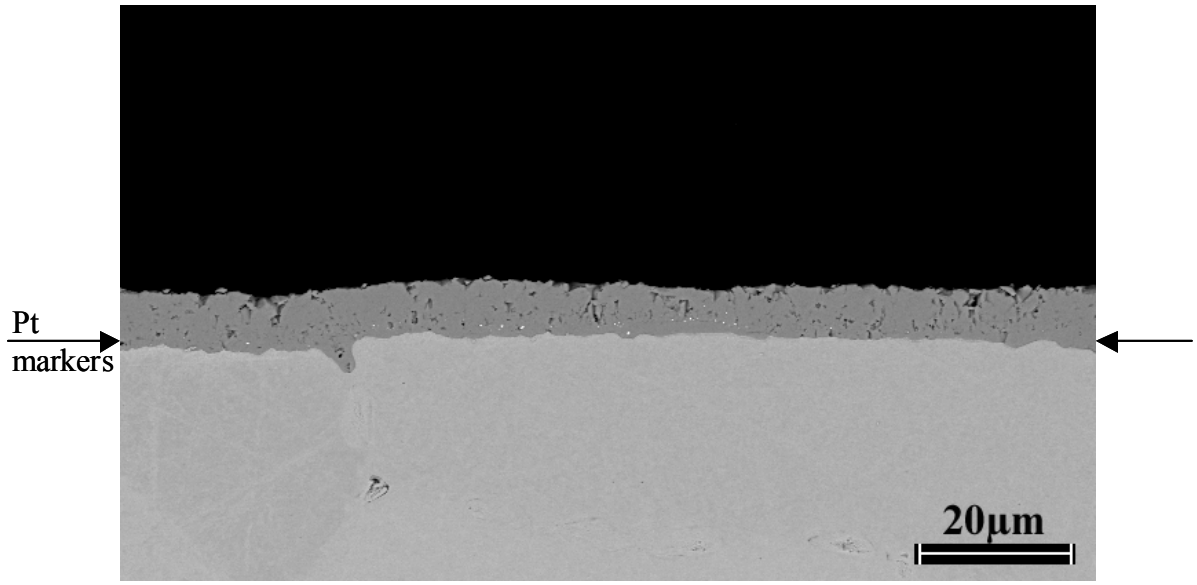

(a)

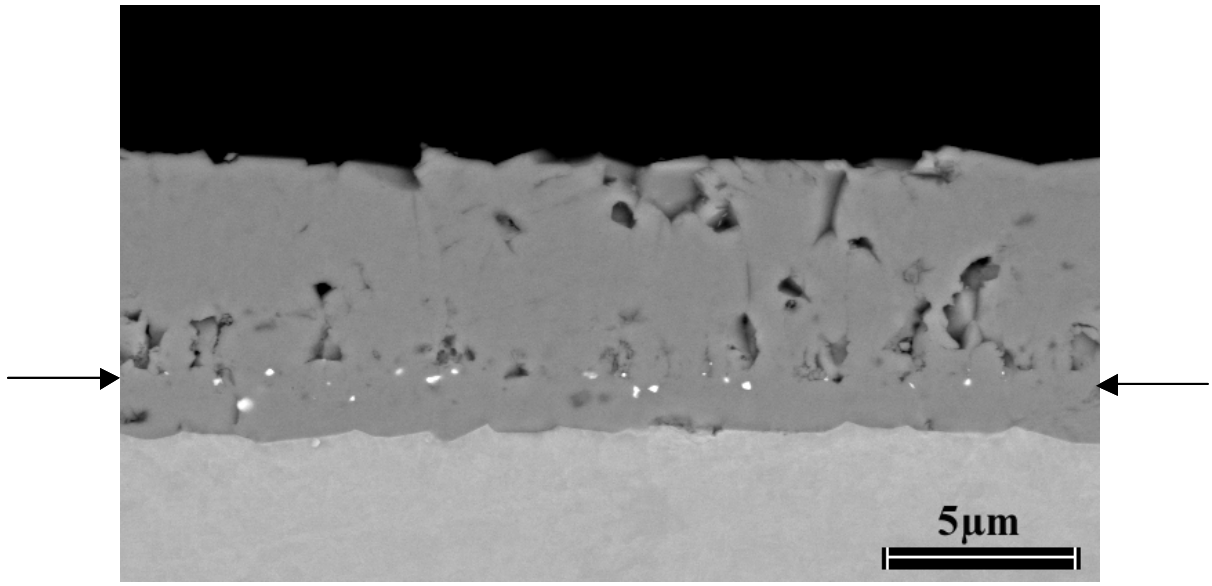

(b)

Figure 64 Cross-sections of Ni specimens showing (a) the Pt markers after exposure of 1hr at 1100°C in dry air (see arrows); (b) higher magnification with bright dots Pt markers

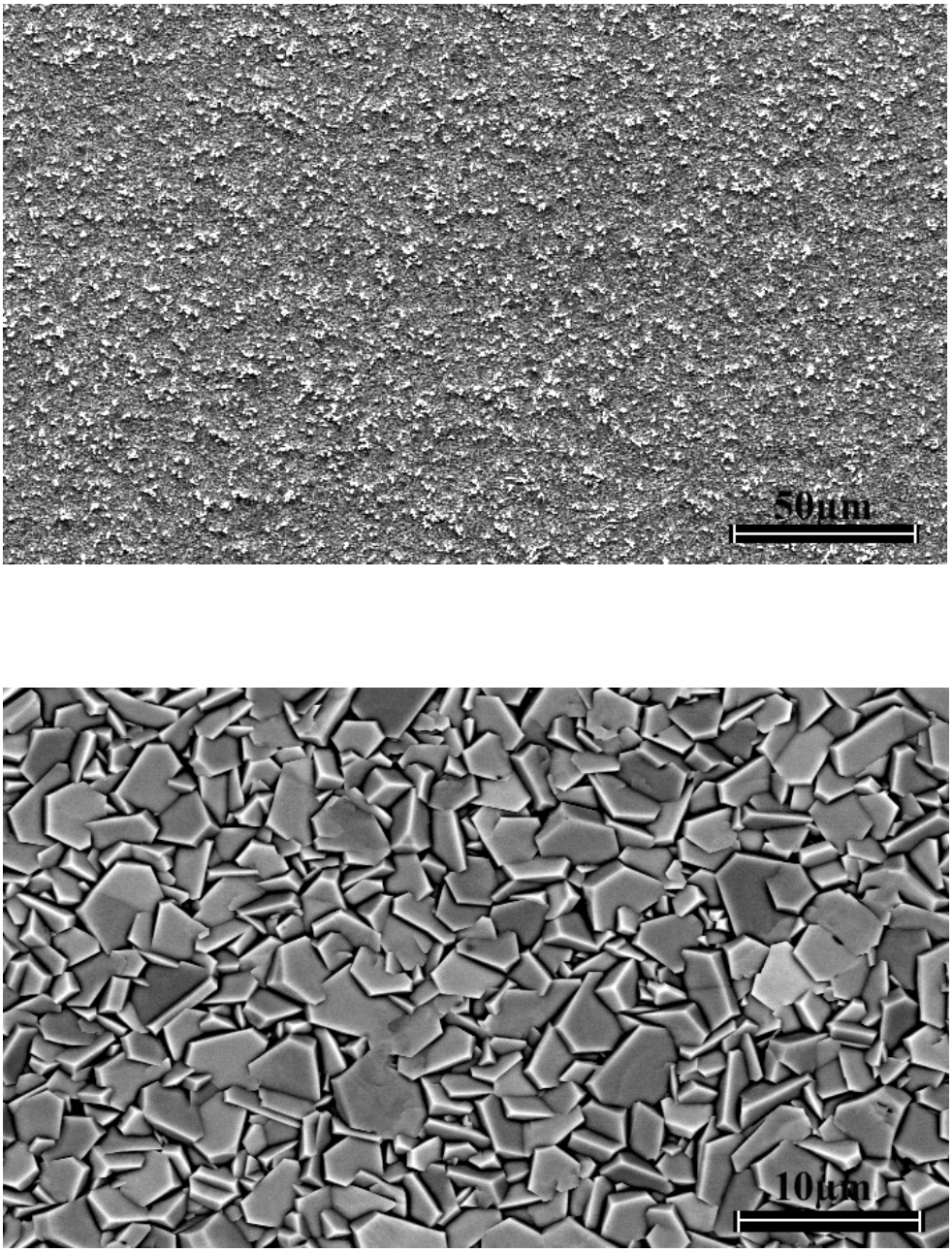

Figure 65 Specimens of pure Ni (99.999+%) exposed for 1hr@1100°C in air with water vapor (0.1atm): (a) SE image showing the relief of the surface; (b) BSE image, higher magnification, showing NiO grains

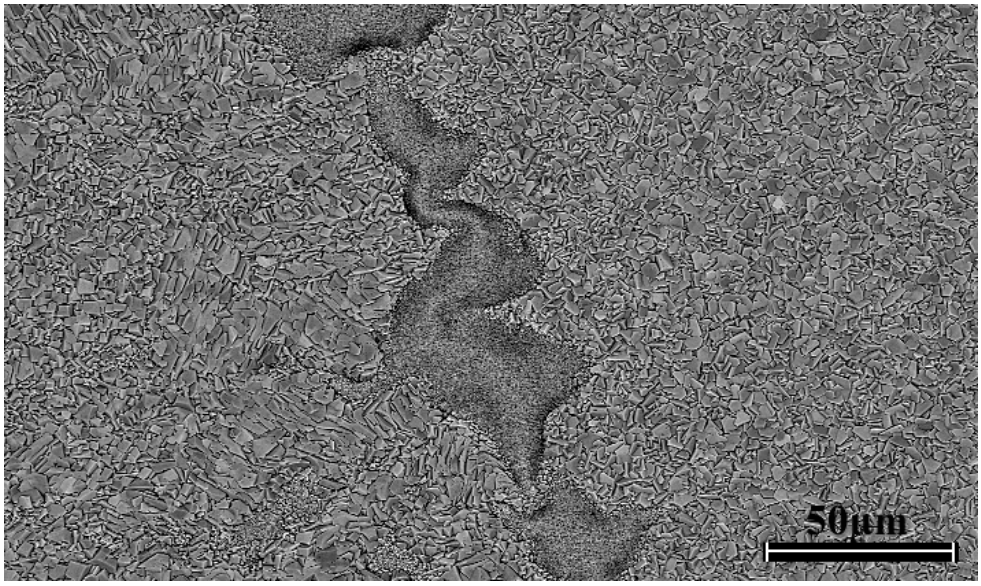

(a)

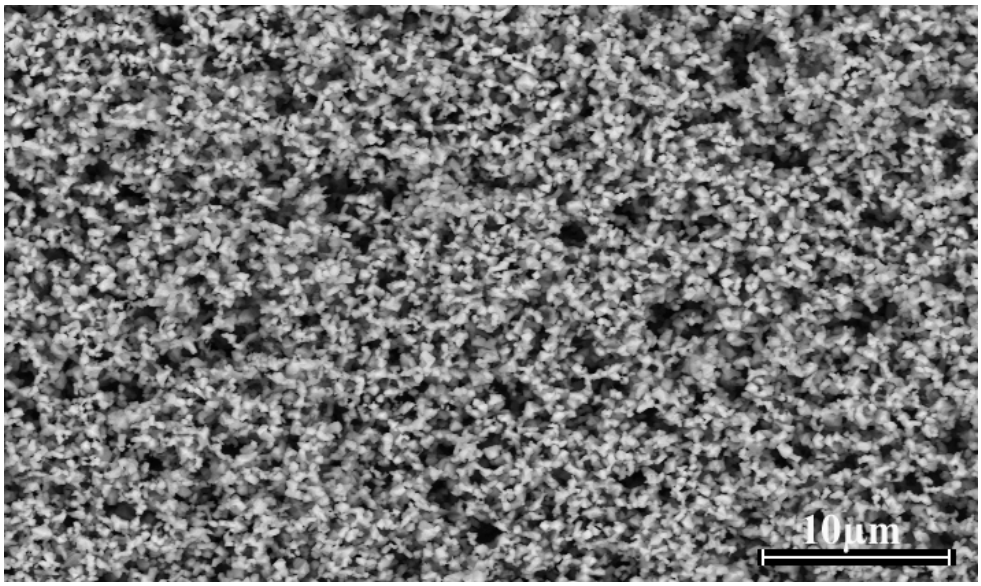

(b)

Figure 66 Pure Ni (99.999+) specimen exposed for 1hr@1100°C in wet air (a)difference in NiO morphology when Pt marker is present on the substrate; (b)higher magnification showing NiO grains on top of Pt

In cross-section, the Pt markers are located about ¾ up in the scale, closer to the oxide/gas interface, Figure 67. Extensive porosity in the bulk of the oxide grains as well as along oxide grain boundaries are shown in Figure 68 for the pure Ni specimen exposed for 1 hour at 1100°C in air with 0.1atm water vapor. The scale formed on the specimen exposed in dry air conditions presented a smaller degree of porosity compared to the oxide that formed in wet air. The more porous region of the scale was observed mostly below the Pt markers, Figure 67. The thickness of the NiO scale is approximately 15 – 17μm or almost twice as thick as the scale formed under dry conditions. Studies in the literature suggested that the NiO 'inner layer' grows via water vapor transport across voids in the scale. For the present study, the observed enhanced oxidation in water vapor conditions seems to be related to an enhanced inward transport of oxygen along the grain boundary network.

Dynamic SIMS analysis in conjunction with $^{16}O_2/^{18}O_2$ oxidation experiments [98] has been used to confirm that both NiO and Cr_2O_3 grow as a result of outward cation diffusion for the high temperature oxidation of Ni and Cr substrates at 900°C, as well as that the diffusing species through the α-Al_2O_3 scale at 1200°C for a FeCrAl alloy are aluminum cations and oxygen anions. For the present study, after cross-section investigation of both pure Ni specimens, one exposed under dry conditions, the other exposed in the presence of water vapor at 1100°C, the following comments may be stated:

For the experiments in this work, it seems that the oxidation process takes place in both cases (dry and wet) at the oxide/gas interface to some extent, but in the presence of water vapor, there is a significantly accelerated inward transport of oxygen. Therefore, a thicker scale has formed on the specimen exposed in air with water vapor, the majority of which was grown below the Pt markers, into the substrate, Figure 67, proving a reaction between nickel and oxygen at the

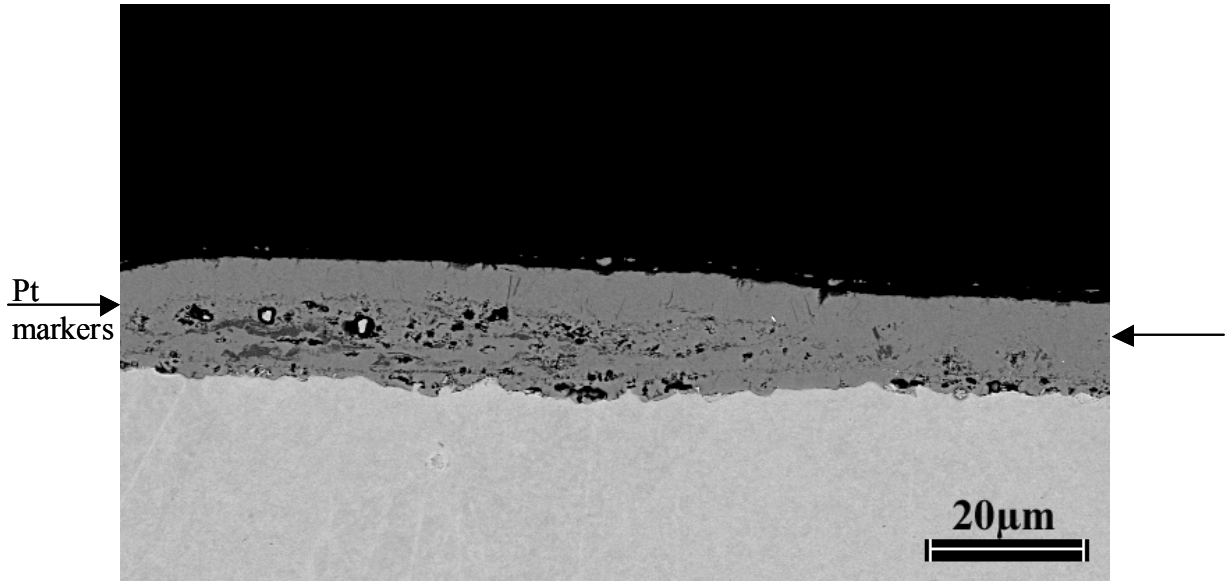

(a)

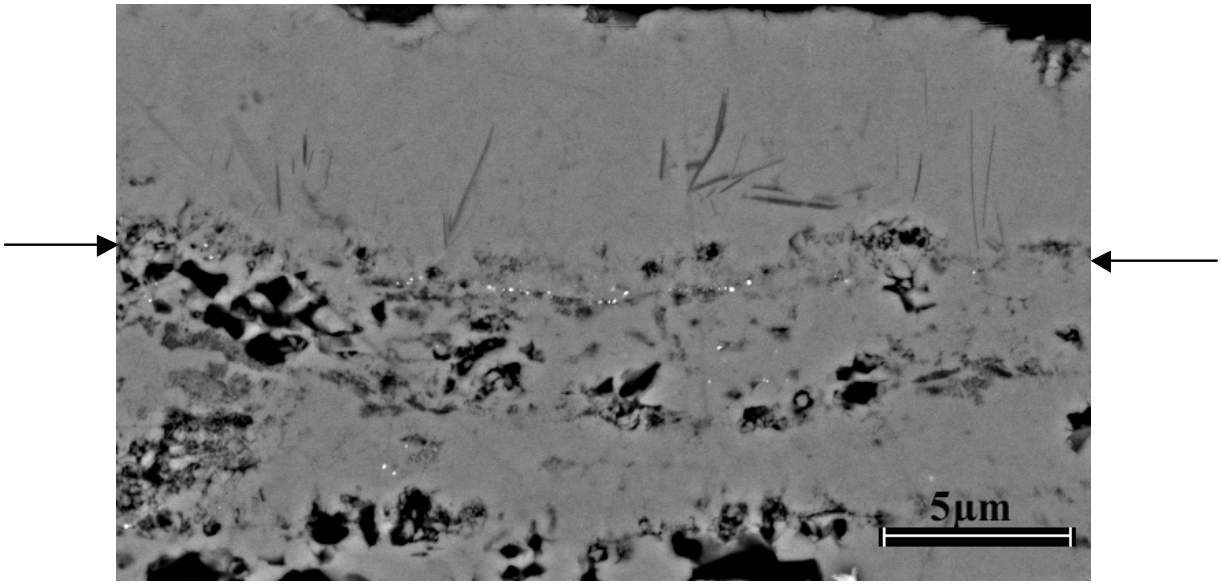

(b)

Figure 67 Cross-sections of Ni specimens exposed for 1hr@1100°C in air with water vapor (a) showing position of Pt markers in the scale (see arrows); (b) higher magnification

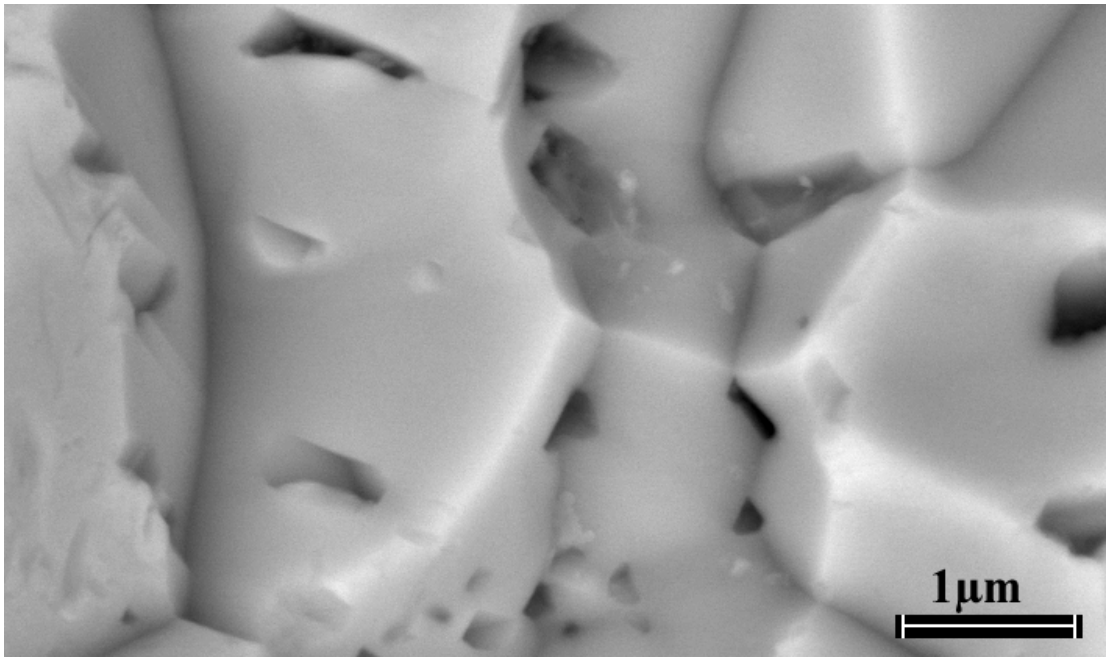

Figure 68 NiO grains on a Ni specimen oxidized for 1 hour at 1100°C in air with water vapor (0.1atm), showing porosity in the grain bulk and along grain boundaries

metal/scale interface. It is apparent that water vapor plays a role in this case: water vapor conditions seem to accelerate the NiO growth rate due to an increased rate of transport of oxygen along the grain boundary network.

At temperatures above 1000°C, the reported growth kinetics of NiO scales is parabolic and interpreted on the basis of Wagner's theory. The oxide scales grown around the temperature ranges of 1000°C to 1300°C are usually faceted. The nickel specimen exposed in wet air at 1100°C in this work exhibits a faceted morphology as seen on the surface aspect of the scale, Figure 61, whereas the dry exposed specimen presents a smoother aspect of the oxide grains as the specimen is examined on the top surface. Studies[99] show that such a faceted morphology results from the outward diffusion of nickel cations and the minimization of surface energy, but for the wet specimen oxidized at 1100°C in this work, it seems to be rather the case of an accelerated oxygen transport as the Pt-marker experiments suggest. The faceted morphology is less developed for oxide scales grown on lower purity nickel substrates [100]. As mentioned previously, high purity nickel specimens (99.999+%) were used in this study.

The important morphological feature of thermally grown NiO cross-sections is the so-called duplex scale structure:

- an outer region consisting of columnar grains
- and an inner region with equiaxed grains.

The inner layer has been suggested to grow by inward transport of oxygen along grain boundaries, ingress by oxygen dissociation across cavities during Ni diffusion, opening of microfissures due to anomalous diffusivity along grain boundaries and in the bulk phase and transport through micropores [99-112].

Nickel oxide is a p-type oxide for which growth is induced by the outward diffusion of cations, a process observed in both cases: dry and wet conditions. However, for the exposure in the water vapor atmosphere, the outward diffusion is overridden by the accelerated inward transport of oxygen-containing species, depicted schematically in Figure 69.

As mentioned previously, one possible role of water vapor in the high temperature oxidation of metals and alloys can be the incorporation of hydrogen in the oxide – and this can change the defect-dependent properties of the oxides resulting in cation and oxygen diffusion. However, the large inward component of the scale growth in water vapor conditions is given by a pronounced inward transport of oxygen-containing species from the water vapor atmosphere along a more dense oxide grain boundary network.

The increased transient oxidation that has been observed for PWA1484 and NiCrAl specimens exposed in gas mixtures containing water vapor must be caused by the increased growth rate of NiO and possibly chromium oxides. It seems that hydrogen may dissolve into NiO and the chromium oxides. The accelerated oxygen transport for water vapor conditions is of major importance; however, hydrogen dissolution in NiO (scale grown above Pt markers in Figure 69) and Cr_2O_3 could be of some significance because it increases the nickel and chromium ions diffusion through the scales resulting in accelerated outward growth rates of NiO and chromium oxides. The observed increased internal oxidation of Al in these alloys could therefore be associated with accelerated growth of transient Ni and Cr oxides which would increase the critical Al content required for continuous alumina scale formation [113].

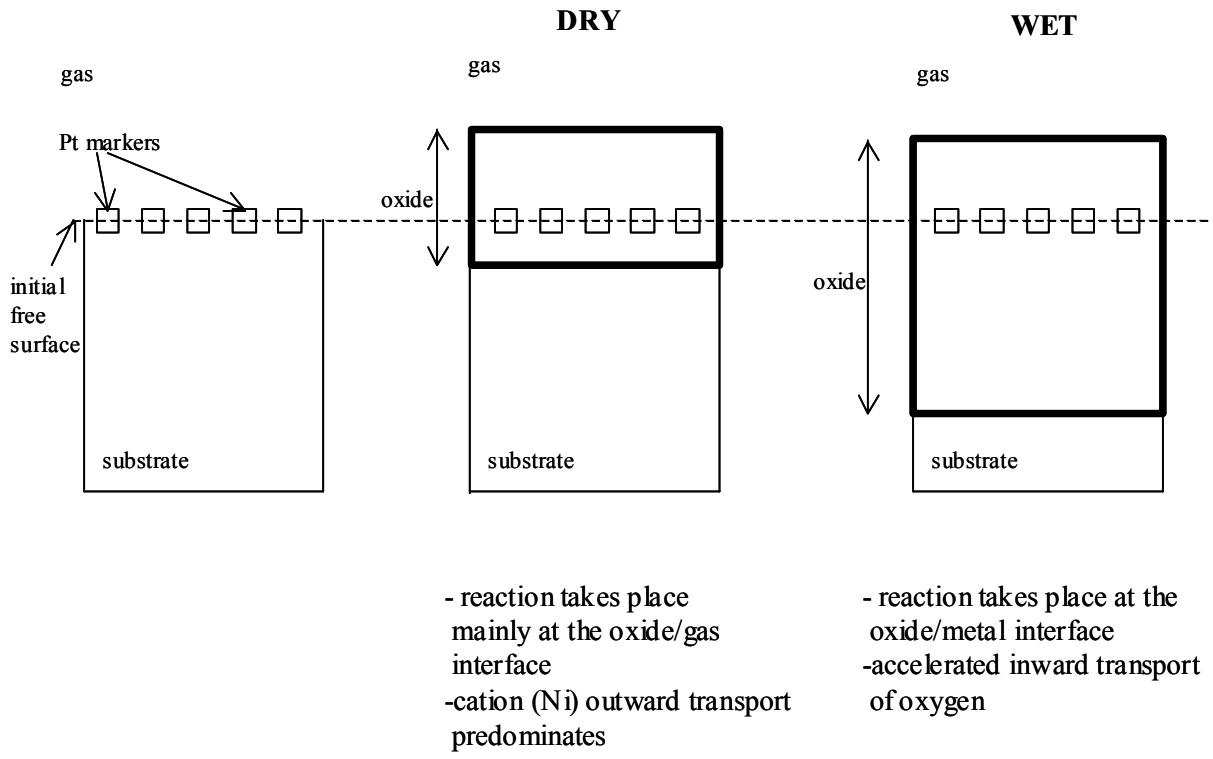

Figure 69 Pure Ni specimens exposed for 1 hour @ 1100°C in dry air / in air containing water vapor at 0.1atm (schematic drawing of position of Pt markers in the scale)

5.1.2.4. Summary of Important Effects

Table 4 - Selective oxidation (oxide type and thickness), 1100°C

	dry air	**dry air**	**wet air (0.1 & 0.5atm)**	**wet air (0.1atm)**
	10 minutes	1 hour	10 minutes	1 hour
PWA1484 reg. S	thin layer, mixed oxides (<1μm)		multilayered scale (2–3μm)	
PWA1484 low S	thin layer, Al-rich oxides (<0.5μm)		mixed oxides (2-3μm - 0.1atm) (4–5μm – 0.5atm)	
René N5 reg. S		thin scale (<1μm)		mixed oxides (2μm)
René N5 low S		thin scale (<1μm)		mixed oxides (2μm)
CMSX4		thin scale, Al-rich oxides (<1μm)	mixed oxides (2μm – 0.1atm) (3-4μm – 0.5atm)	
PWA 1480				mixed oxides+internal oxides (4μm)

• For long times of cyclic exposures of superalloys in an atmosphere containing air with water vapor, when compared to dry air exposures, the scale that forms is thicker and contains an appreciable amount of transient oxides: $NiAl_2O_4$, Ni $(Al, Cr)_2O_4$ and NiO, grown in that order on top of the alumina layer. In conclusion, there is an increase in the transient oxidation in air containing water vapor.

• The growth rate of NiO is found to affect the amount of transient oxides for cyclic exposures of alumina formers. The growth rate of alumina is greater on wet exposed specimens - more complex, thicker scales form, even for short time exposures (i.e. 10 minutes). The oxide thickness for these specimens is twice that of dry exposed ones.

Table 5 – Ni-8Cr-6Al oxidation (type and thickness of scale)

700°C, 4 hours	**dry air**	mixed oxides, thin alumina – 2µm
	air + 0.1atm H_2O	mixed oxides: NiO + internal oxides – 5µm
	Ar + 0.1atm H_2O	mixed oxides: NiO + internal oxides – 5-6µm
1100°C	**dry air**	**5 minutes**: NiO+transient oxides+internal oxides (2µm) **1 hour**: transient oxides+ thin alumina (2µm)
	air + 0.1atm H_2O	**1 minute**: NiO+transient oxides+internal oxides (Al_2O_3 preferentially at substrate grain boundaries)- 6µm **5 minutes**: NiO+transient oxides+internal oxides (8µm) **1hour**: NiO+transient oxides+internal oxides (10µm)
	Ar + 0.1atm H_2O	**5 minutes**: NiO+transient oxides+internal oxides (8µm)

• In water vapor conditions, α-Al_2O_3 preferentially develops continuity at grain boundaries in the substrate as a result of preferential nucleation of the oxide linked with a rapid diffusion of Al along grain boundaries and a strong inward flux of oxygen-containing species from the water vapor.

• Enhanced internal oxides and large amounts of transient oxides form away from the substrate grain boundaries thus inhibiting the selective oxidation of aluminum at these sites. At lower temperatures (700°C), the selective oxidation of alumina is hampered by failure of alumina developing continuity and, at the same time, developing of thick regions of internal oxides, more for specimens oxidized in wet atmospheres, but also for samples exposed in dry air.

Table 6 – Pure Ni oxidation (oxide thickness and grain size), 1hour @ 1100°C

dry air	5 – 6μm, coarse grains
wet air	7 – 10μm, fine grains

• As the results from this study show, scales of NiO grow more rapidly on specimens of pure nickel when water vapor is present in the gas mixture. Enhanced oxidation in water vapor conditions is due to an enhanced inward transport of oxygen along a more dense oxide grain boundary network. Also, an increased concentration of nickel vacancies is probably contributing to the outward growth rate of NiO in atmospheres containing water vapor as well. The accelerated transient oxidation of the superalloys exposed in water vapor conditions is caused by more rapid NiO growth during the transient period in wet exposures.

• As a side note, it was observed experimentally that water vapor has an effect on the microstructure of NiO and on the surface morphology of the oxide layer formed. Smaller size and more faceted NiO grains are associated with exposures in water vapor. Closely related to grain size, a finer network of grain boundaries is present on the specimen expose in air with water vapor.

5.1.3. The Effect of Water Vapor on Spinel Formation in Growing α-Al_2O_3 Scales on Superalloys and Platinum-Modified Aluminide Coatings

5.1.3.1. Platinum-Aluminide Coatings Throughout the present work, platinum additions to aluminide coatings showed a considerable improvement in spallation resistance over the straight-aluminide coatings, even in atmospheres containing water vapor.

The results that have been obtained show that during the growth of α-Al_2O_3 scales on platinum aluminide coatings, a spinel phase ($NiAl_2O_4$) is formed at the α-Al_2O_3/gas interface. Ni and Al strong peaks were identified using energy dispersive analysis in the scanning electron microscope. The amount of spinel that was formed for a given set of exposure conditions increased when water vapor was present in the gas phase. Some results of specimens exposed in dry air are presented in Figure 70 and show a spinel phase on the ridges of α-Al_2O_3 after 525 cycles at 1100°C. Spinel was not observed at such locations during observations performed after earlier exposures. Consequently, this phase is not a result of transient oxidation processes during the formation of a continuous α-Al_2O_3 layer. The surfaces of platinum aluminide coatings on N5 were examined with the SEM after different exposure times at 1100°C in air with water vapor at

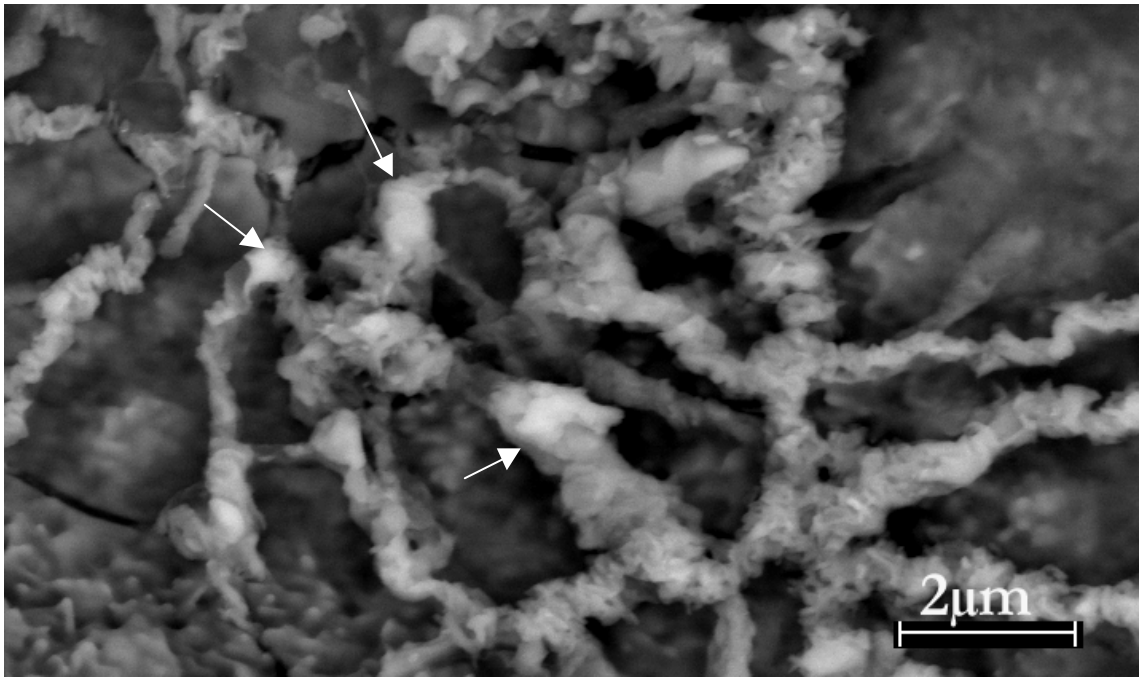

Figure 70 SEM micrograph showing the surface of a PtAl coating oxidized for 525 cycles @ 1100°C in dry air (spinel at arrows)

0.1atm. Cracks that developed in the α-Al_2O_3 scale after 41 cycles were used to examine the same location on the oxide surface, Figure 71, after subsequent exposure times. Inspection of these cracks did not show any oxide formation in them and it is believed that an alumina layer developed on the alloy at the base of these cracks. Spinel was observed over a period of 1194 cycles showing growth at cracks in α-Al_2O_3 and on top of α-Al_2O_3 in the proximity of cracks, Figure 71. Lateral spinel growth along cracks was less in comparison to thickening of the spinel layers over time. Spinel islands were also evident on specimens where no cracking of the alumina scales was apparent and the amount of spinel increased with exposure time, Figure 72. Cross sections of platinum-modified aluminide coatings on René N5 exposed in dry air and in air with water vapor at 1100°C are compared in Figure 73. Some spinel is evident on the specimen exposed in dry air, Figure 73a, but more spinel is present in the scale of the specimen exposed in

air with water vapor, Figure 73b. Moreover, it was observed that the amount of spinel on this specimen increases with exposure time, Figure 73c.

These results strongly suggest that the spinel phase that is formed at the α-Al_2O_3/gas interface results from the outward diffusion of nickel. Inspection of Figure 73c indicates that the spinel layer is relatively uniform in thickness and distribution. Pint et al[114] have found that $NiAl_2O_4$ was formed on an α-Al_2O_3 scale at the gas interface during the oxidation of Ni_3Al. It was proposed that cracks developed in the α-Al_2O_3 during thermal cycling and that, upon subsequent oxidation, NiO was formed in these cracks. Due to the rapid growth of the NiO compared to α-Al_2O_3, it was proposed that the cracks became filled with NiO and the situation permitted NiO to be formed upon the α-Al_2O_3 at the gas interface. Reaction between the NiO and α-Al_2O_3 resulted in $NiAl_2O_4$ formation. It is possible that a similar mechanism caused spinel to be formed on the platinum aluminide coatings in the present studies. However, cracks filled with NiO were not

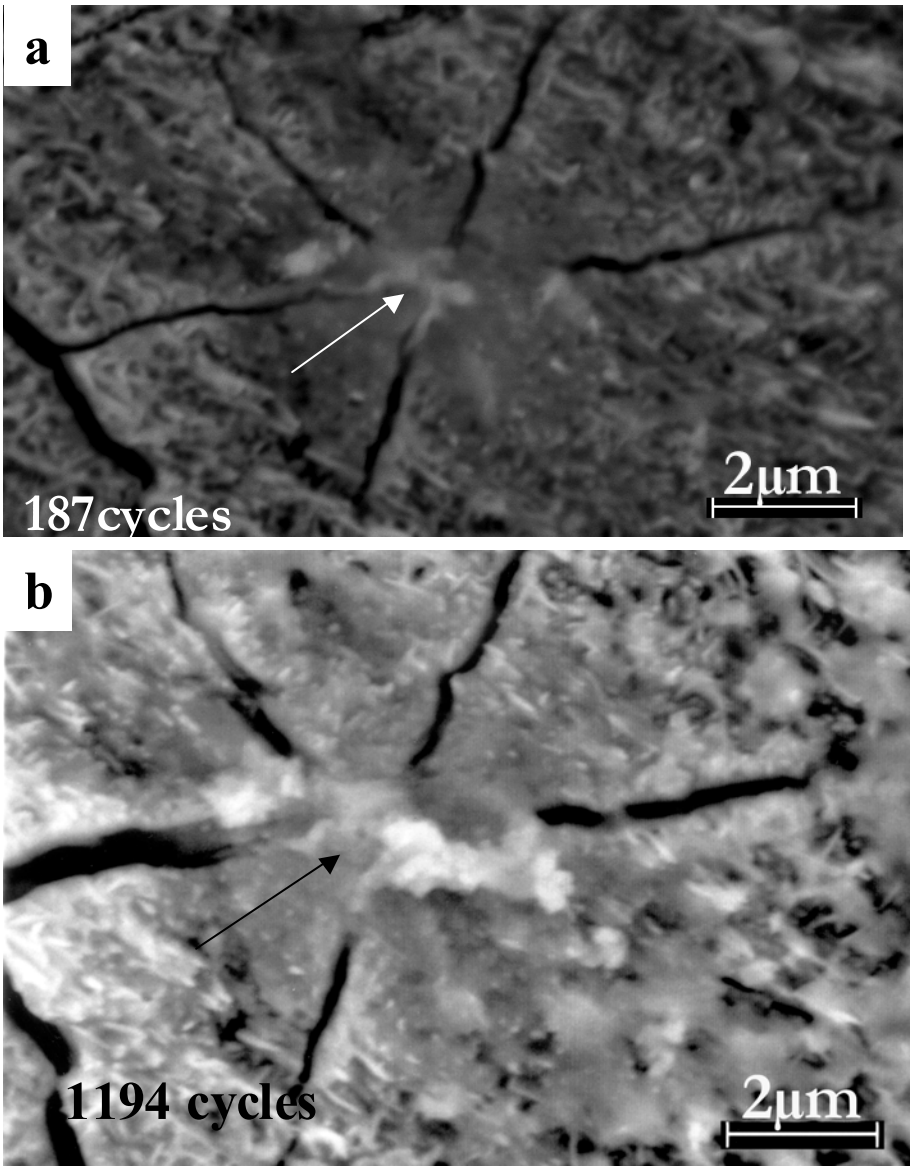

Figure 71 Scanning electron micrographs of the surface of alumina on a platinum aluminide coating after exposure in air with water vapor (0.1atm) at 1100°C for 187 cycles (a) and for 1194 cycles (b). (arrows point to islands of spinel)

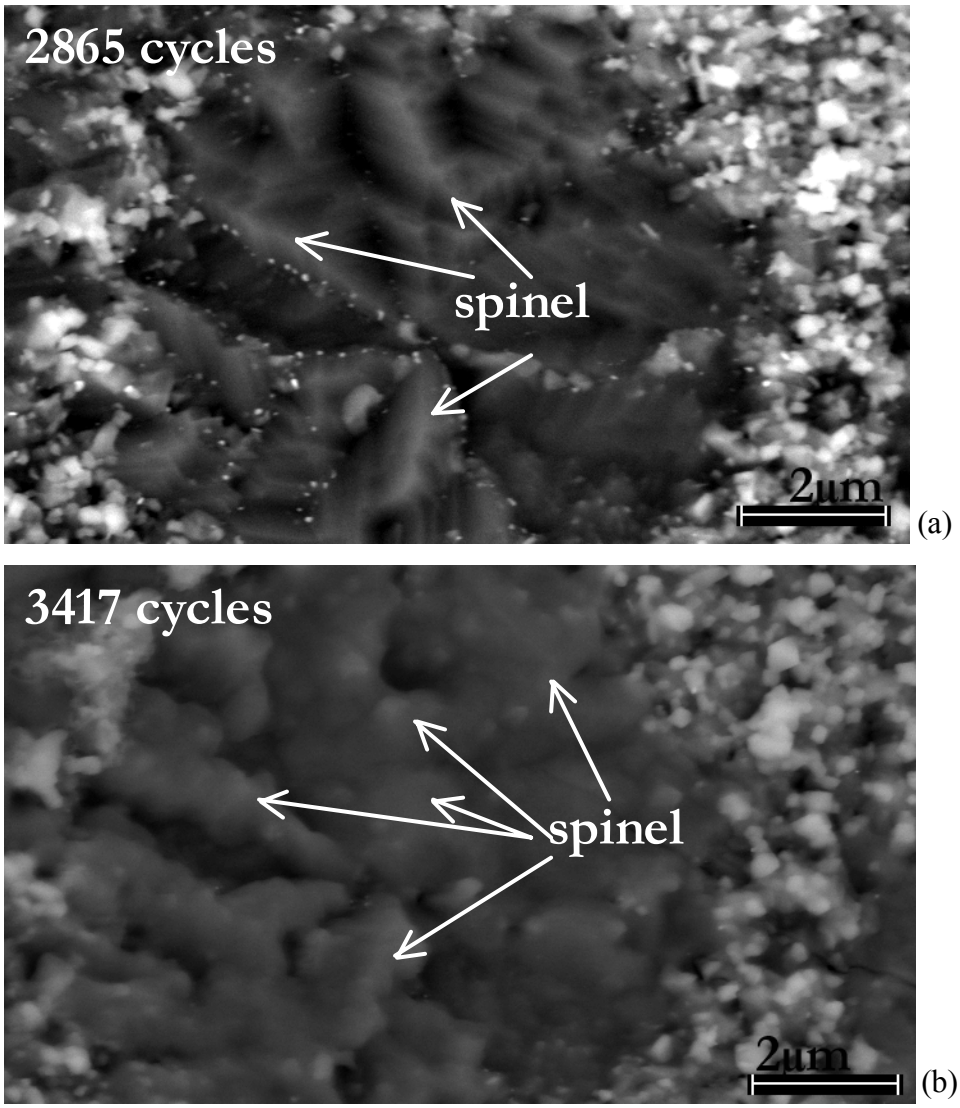

Figure 72 Scanning electron micrographs of the surface of an alumina scale formed on a platinum aluminide coating after 2865 cycles (a) and 3417 cycles (b) of oxidation at 1100˚C in air with 0.1atm of water vapor (arrows point to islands of spinel)

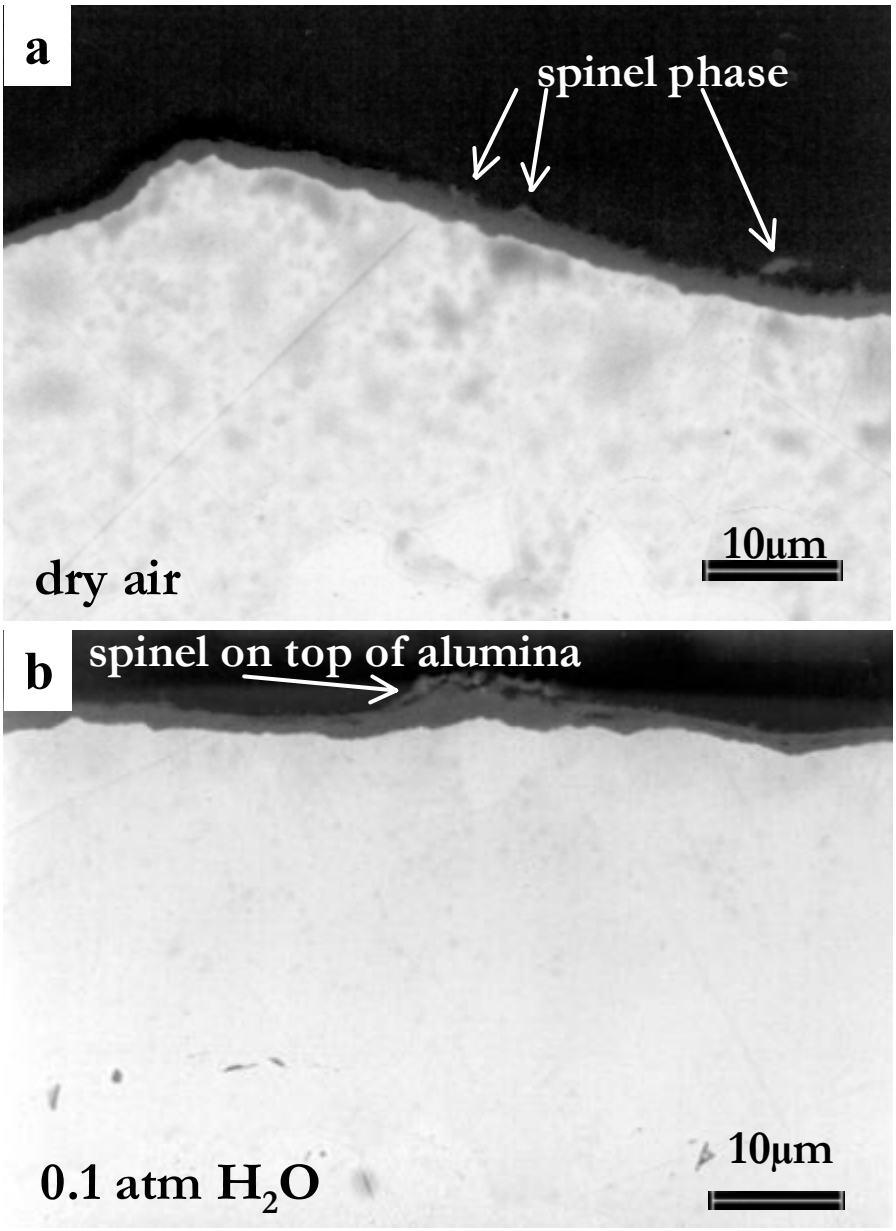

Figure 73 Cross sections of Pt-modified aluminide coatings on René N5

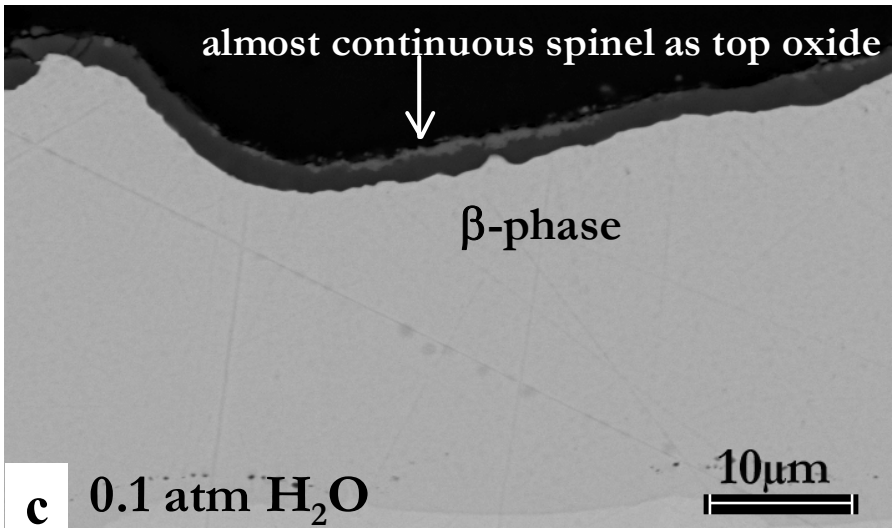

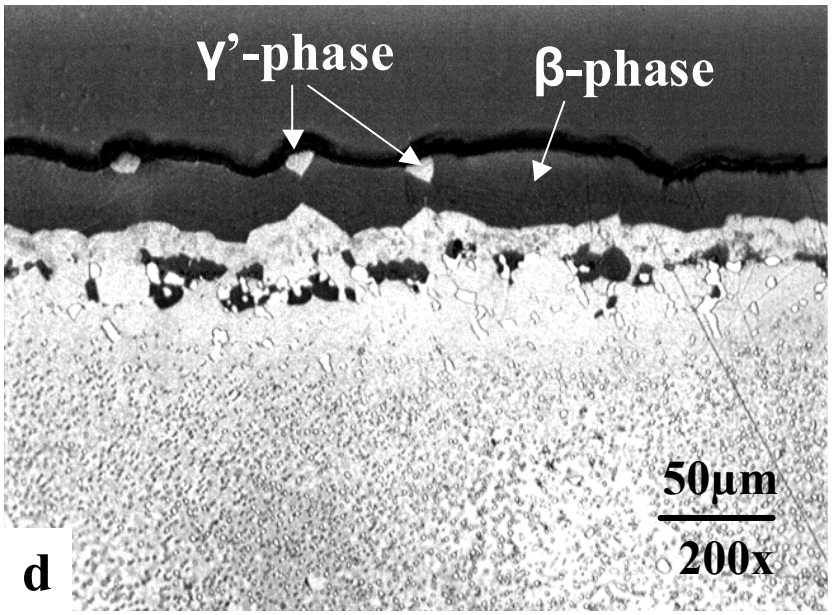

Figure 73 Cross sections of Pt-modified aluminide coatings on René N5 exposed in (a)dry air for 2112 cycles; (b) 0.1atm water vapor pressure for 1194 cycles (c) 0.1atm water vapor pressure for 3417 cycles at 1100°C and (d) the etched coating from (c); The coating is predominantly β-phase NiAl with some γ' at grain boundaries in the coating.

detected in the α-Al_2O_3 scales shown in Figure 73c. Furthermore, the aluminide coating beneath the α-Al_2O_3 was predominantly β-NiAl, Figure 73d, and it would not be expected that NiO would be stable at the bottom of cracks in the α-Al_2O_3. In view of these results, another mechanism is proposed for spinel formation that consists of diffusion of nickel through the α-Al_2O_3 layer to the gas interface.

The Ni-Al-O stability diagram is presented in Figure 74. This diagram has been constructed for a temperature of 1000°C due to the availability of thermodynamic data; at 1100°C, a similar diagram can be expected. In this diagram, the various phases that can be in equilibrium with one another as a function of oxygen pressure and aluminum activity are indicated. $NiAl_2O_4$ is in equilibrium with alloys with aluminum activities between 10^{-17} and 10^{-19}, whereas NiO is the stable oxide phase on alloys with aluminum activities lower than 10^{-19}. In the Ni-Al region, arrows indicate two-phase equilibria and the nickel activities for these equilibria are presented. As one proceeds through the β and γ' phases to the γ phase, the nickel activity increases. In considering the case of spinel formation on a α-Al_2O_3 scale that in turn is on a Ni-Al alloy, spinel may form via the following reaction:

$$Ni + Al_2O_3 + 1/2O_2 = NiAl_2O_4, \qquad (25)$$

which could occur at the α-Al_2O_3/gas interface or at the α-Al_2O_3/alloy interface. In the latter case, the nickel activity at the α-Al_2O_3/alloy interface must be extremely high because the oxygen pressure is so low. For example, if the oxygen activity in the α-Al_2O_3 is 2.5×10^{-6}, a nickel activity of 0.78 is required to form spinel; nickel activities close to unity are necessary as the oxygen pressure is reduced to the three-phase Al_2O_3-$NiAl_2O_4$-alloy equilibrium. On the other

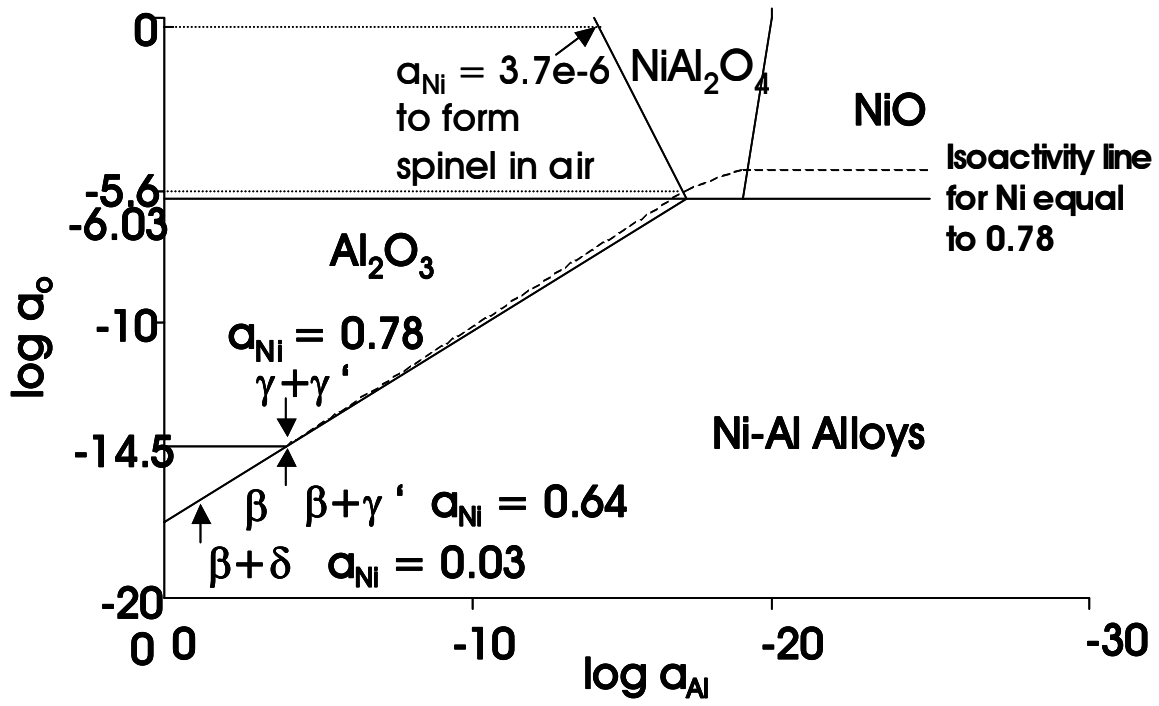

Figure 74 Schematic of Ni-Al-O stability diagram at 1000°C with the activities of nickel indicated for various equilibria

hand, much lower nickel activities are required to form spinel at the α-Al_2O_3/gas interface where the oxygen pressure is high. For example, considering an oxygen activity of that in air, a nickel activity of $3.7x10^{-6}$ is required to form spinel. It is proposed that nickel diffuses through the α-Al_2O_3 to form spinel at the α-Al_2O_3/gas interface. Nickel has been proposed to diffuse through α-Al_2O_3 by Sahin et al [115].

In considering the defect mechanism by which nickel can diffuse through α-Al_2O_3, it is well established that the growth of α-Al_2O_3 scales is controlled by the inward diffusion of oxygen along grain boundaries [116] in the oxide. The equilibrium point defect concentrations in α-Al_2O_3 are extremely small and the defect structure is not definitely known. Schottky defects involving aluminum vacancies, $V_{Al}^{'''}$, and oxygen vacancies, $V_O^{\bullet\bullet}$, have been proposed [117]. It is possible that nickel may diffuse through α-Al_2O_3 via aluminum vacancies. Two possible reaction schemes for formation of spinel are presented in Figure 75, where the Ni^{2+} and Al^{3+} ions would diffuse through the α-Al_2O_3 via aluminum vacancies. In one scheme, the spinel would be formed at the interface between the $NiAl_2O_4$ and Al_2O_3. In the other, the spinel would be formed at the $NiAl_2O_4$/gas interface. In both schemes, the oxygen would diffuse inward via grain boundaries in α-Al_2O_3 and $NiAl_2O_4$. The Ni^{2+} ion is slightly larger than the Al^{3+} ion. For example, the ionic radius for Ni^{2+} is 0.07nm compared to 0.05nm for Al^{3+} and the largest interstice in α-Al_2O_3 is 0.06nm. If the size difference between Ni^{2+} and Al^{3+} prevents Ni^{2+} from diffusing in the bulk crystal, it is still possible that nickel may diffuse along grain boundaries in the α-Al_2O_3 rather than via the bulk lattice. It has been proposed by some investigators that aluminum may diffuse along grain boundaries in α-Al_2O_3 [118].

It is important to note that the activity of NiO in α-Al_2O_3 increases as one proceeds along the α-Al_2O_3 – alloy boundary towards the three phase equilibrium α-Al_2O_3 – $NiAl_2O_4$ – alloy

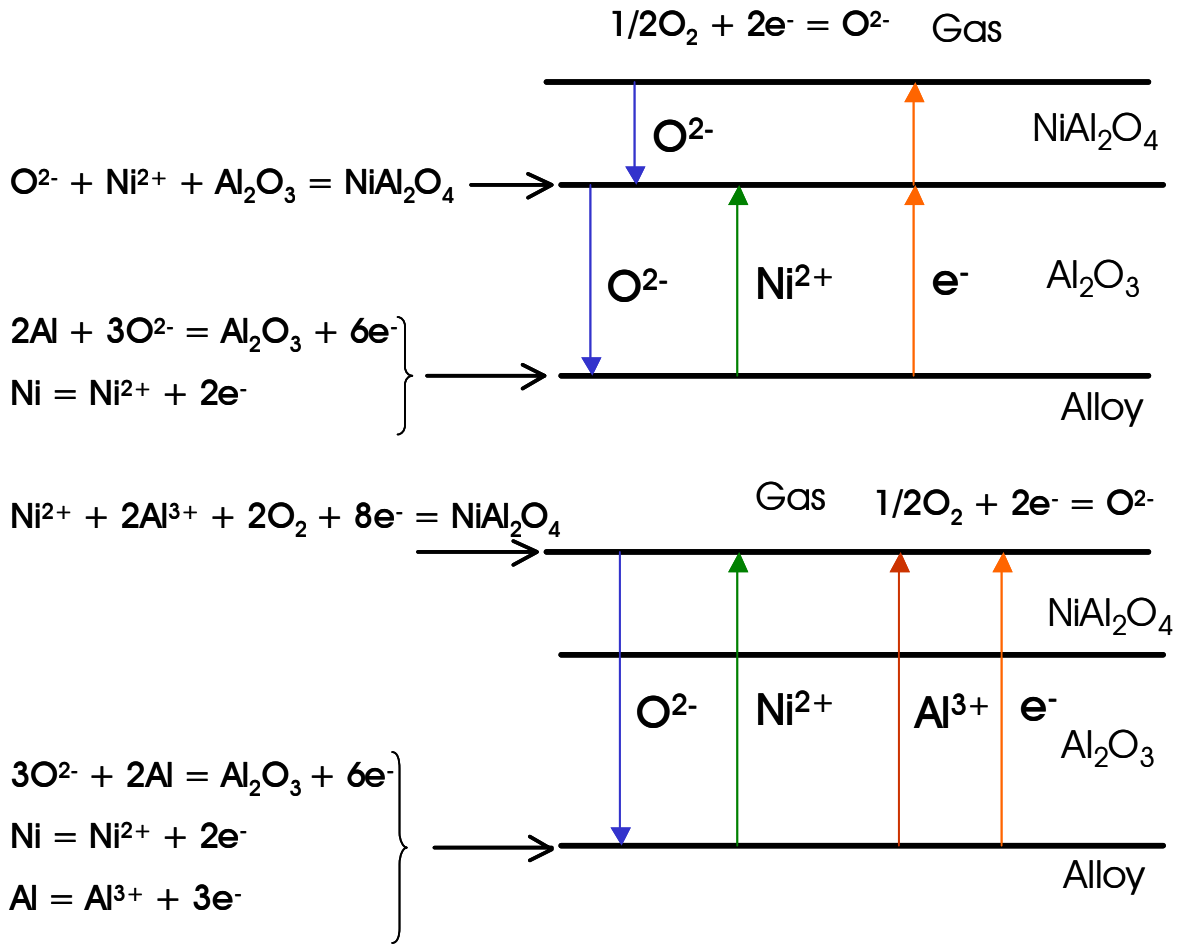

Figure 75 Two possible reaction schemes for the formation of $NiAl_2O_4$ (spinel) on α-Al_2O_3. The Ni^{2+} and Al^{3+} ions would diffuse via aluminum vacancies. The oxygen would diffuse inward via oxide grain boundaries.

shown in Figure 74. For example, at 1000°C, the activity of NiO in α-Al_2O_3 at the α-Al_2O_3 – γ – γ' equilibrium is $4.3x10^{-10}$, whereas the activity of NiO is 0.16 at the α-Al_2O_3 – γ – $NiAl_2O_4$ equilibrium. This suggests that the solubility of NiO in α-Al_2O_3, as well as transport of nickel through α-Al_2O_3, becomes more favorable as the metallic substrate becomes depleted of aluminum or, in other words, as the oxygen reaches levels sufficient to ionize nickel.

Another experiment in this work was performed on specimens of Platinum-modified aluminide (Pt-Al) coatings having René N5 as the substrate. Tapered sections through α-Al_2O_3 scales using procedures developed by Tolpygo and Clarke [118] - described in the "experimental section" and in more detail in the paragraphs that follow - were being employed to study spinel formation on α-Al_2O_3 scales. Alumina scales were formed on platinum aluminide coatings on René N5 substrates by isothermally oxidizing these coatings at 1100°C in wet air (P_{H2O} = 0.1 atm) for 500 hours.

The as-processed aluminide coatings have ridges that develop at grain boundaries in the coating due to the outward diffusion of nickel from the René N5 substrate. In some specimens, the ridges were removed by polishing prior to exposure at 1100°C. In other specimens, the ridges were not removed. The results of tapering through each of these types of specimens are presented in Figures 76 and 77. In the specimen where the ridges were not removed, thin tapered oxide is present over the interiors of grains and over some ridges, arrows in Figure 76a. The specimen where the ridges were removed has a uniform taper through the α-Al_2O_3 scale, Figure 76b.

In Figure 77, micrographs are presented showing the taper for the specimen with ridges at higher magnifications showing the tapered oxide over a grain in the bond coat.

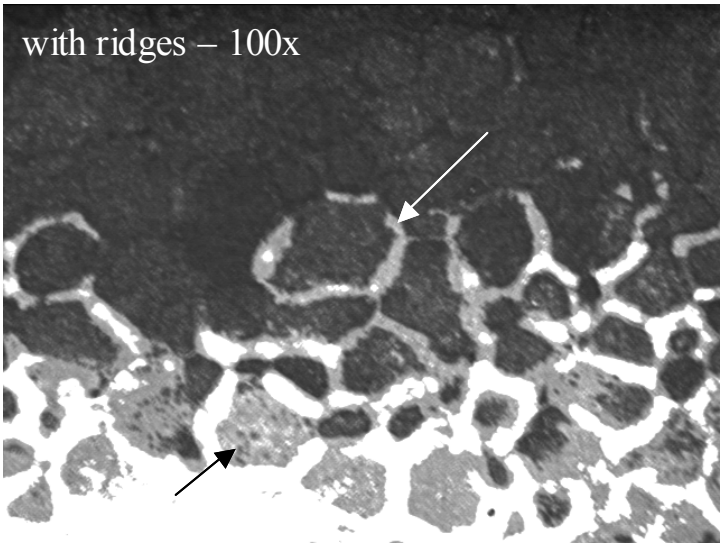

(a)

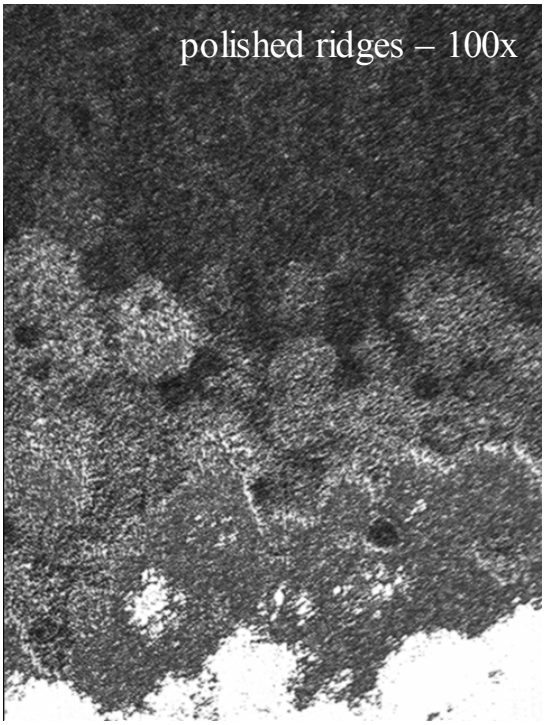

(b)

Figure 76 Optical micrographs showing tapered sections through α-Al_2O_3 scales formed on an aluminide coating after exposure at 1100°C for 500 hours in air with water vapor at 0.1atm. In one specimen, (a), the ridges on the coating were not polished off prior to exposure and in the other specimen, (b), the ridges were removed.

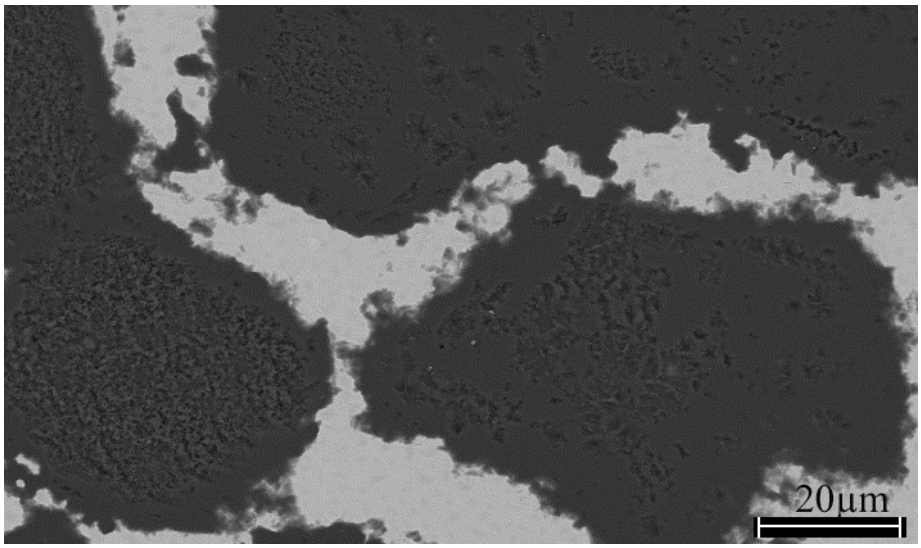

(a)

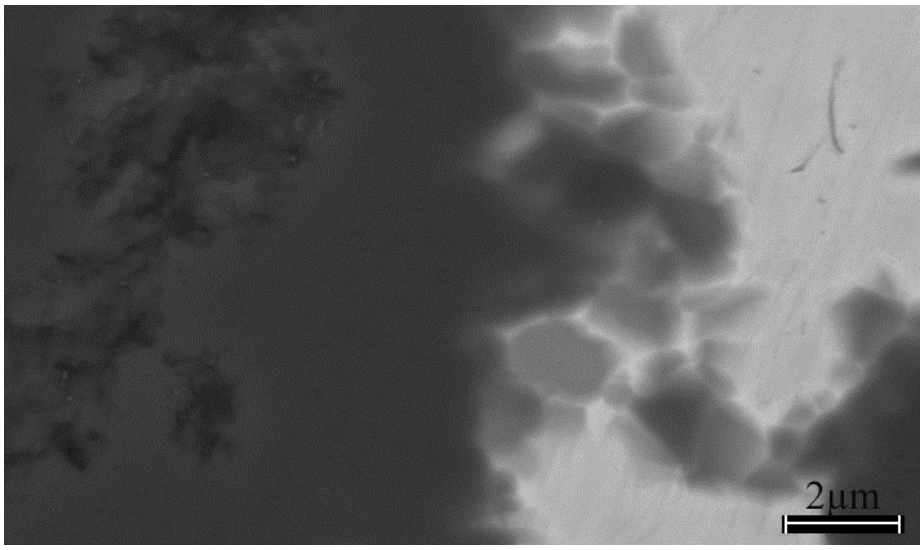

(b)

Figure 77 Scanning electron micrographs showing thin oxide scale over center of grain on the coating with ridges (a) and taper at the edge of the oxide where oxide grains in the scale may be apparent (b) for the two specimens preoxidized at 1100°C for 500 hours in air with water vapor

Figure 77 shows the taper down through this oxide where individual grains in the α-Al_2O_3 scale are present. A schematic drawing of the cross-sectioned taper polishing is presented in Figure 78.

In order to distinguish between the newly formed oxide and the existing oxide, the scale surface was polished between the oxidation stages. The oxidized samples were polished to a 1μm finish using diamond lapping to form tapered sections of the scale. The polishing was performed at a small angle (1° to 2°) to the surface in order to expose approximately 300 - 350μm wide sections of the scale, as shown in Figure 78. The surface of the sample after this taper-polishing operation consisted of three zones:

I - polished metal surface

II - tapered section of the scale

III - 'initial' oxide surface

After taper polishing, the specimens were reoxidized at 1100°C for different times and the scale microstructure was examined by SEM. The attention was drawn to the evolution of the oxide surface in zone (II). The purpose of the reoxidation process was to determine whether Al and Ni outward diffusion play a role in developing/or further growing of the spinel phase on top of the alumina layer. If this were indeed the case, it would be expected that the new oxide would form at the outer/polished surface, leaving behind different features of the top surface as compared to the features before the preoxidation procedure. On the other hand, if this hypothesis is not true, then the new portions of the oxide, after reoxidation, would not emerge at the outer surface, the surface would remain planar, as before reoxidation, even though the oxide thickness would be larger.

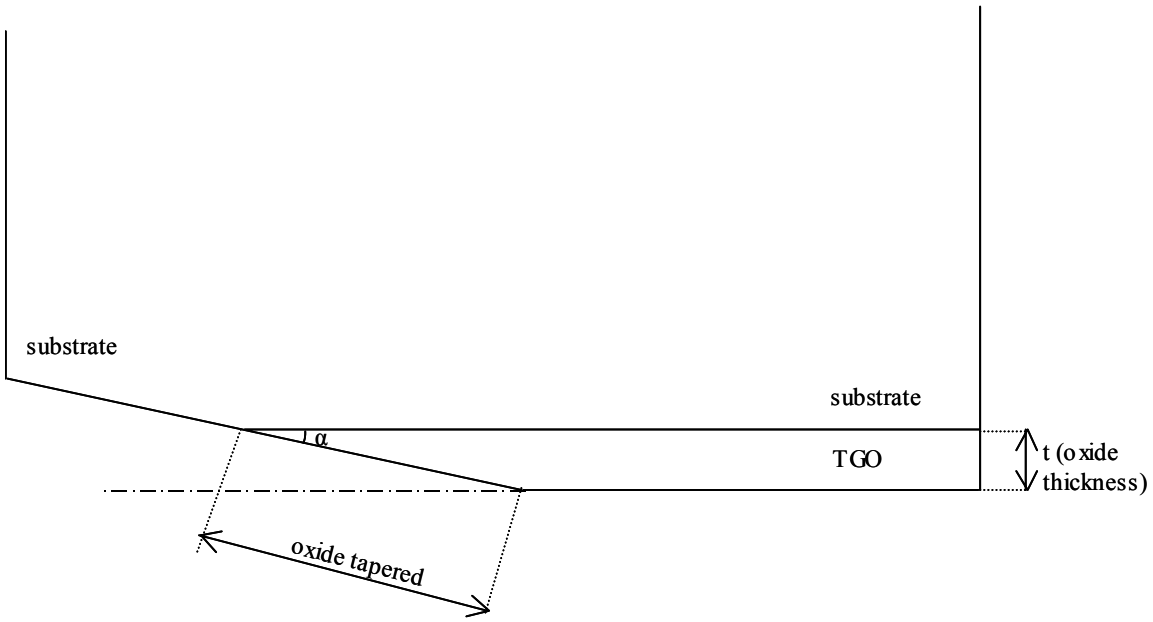

sin α = (oxide thickness)/(oxide tapered)
For example, for α = 1° and t = 5μm, the 'oxide tapered' length is 286μm

Figure 78 Schematic of the cross-sectioned taper polishing

The tapered specimens were exposed at 1100°C in air with water vapor (0.1atm) for two sets of 2 hours each set to observe oxide formation and development upon α-Al_2O_3. Figure 79b presents the micrograph of the same location as in Figure 79a, but after a 2 hours exposure at 1100°C in air with water vapor at 0.1atm. The arrows in Figure 79b point to Ni-rich oxides that formed on top of the α-Al_2O_3 preformed and taper-polished, suggesting that the new spinel phase that is formed at the α-Al_2O_3/gas interface results from the outward diffusion of nickel. The formation of the new portion of the oxide on the polished surface of the scale suggests the outward aluminum and nickel ions diffusion that could take place along existing alumina grain boundaries.

Figure 80 shows the same region on the PtAl coating as in Figure 79, but after another 2-hour oxidation at temperature. Summing up the exposure for this specimen consisted of 500 hours of preoxidation plus two sets of 2 hours each at 1100°C in a gaseous atmosphere containing air with 0.1atm water vapor. Figure 81 presents a higher magnification of the (Ni, Al) oxides formed on top of alumina after the two subsequent exposures of 2 hours each for the samples described above. The regions of spinel observed after 2 hours of oxidation spread more after another 2 hours of exposure, covering a larger area on top of the alumina scale with a thin layer. From the same images, it can be observed that the spinel phase at the left of the micrographs seems to have thickened from 2 hours to 4 hours of oxidation at temperature.

X-ray diffraction measurements for the specimens of PtAl coatings, both with and without ridges, are shown in Figure 82. The symbol “s” accounts for the existing peaks on both patterns – PtAl with ridges and PtAl without ridges specimens – for the spinel phase ($NiAl_2O_4$). These results show that the nodules formed on the tapered section could be spinel or alumina;

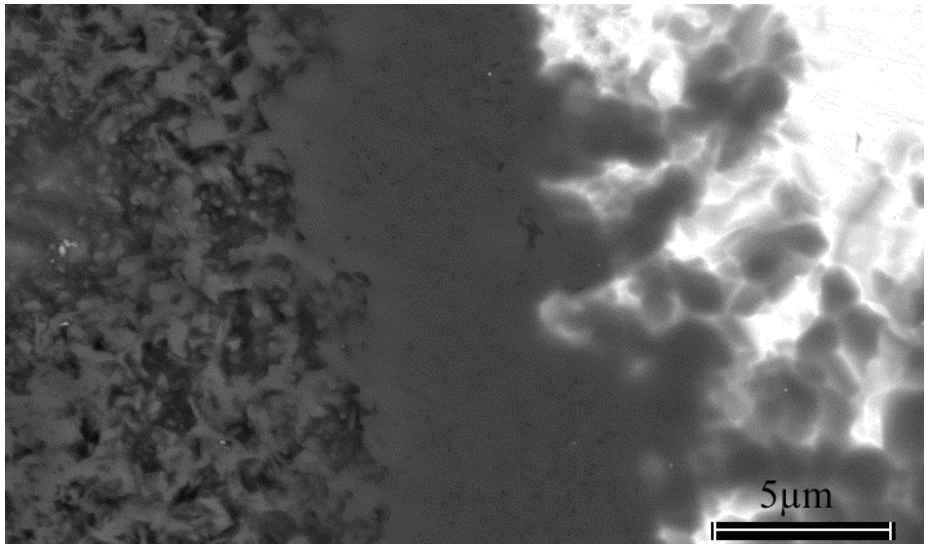

(a)

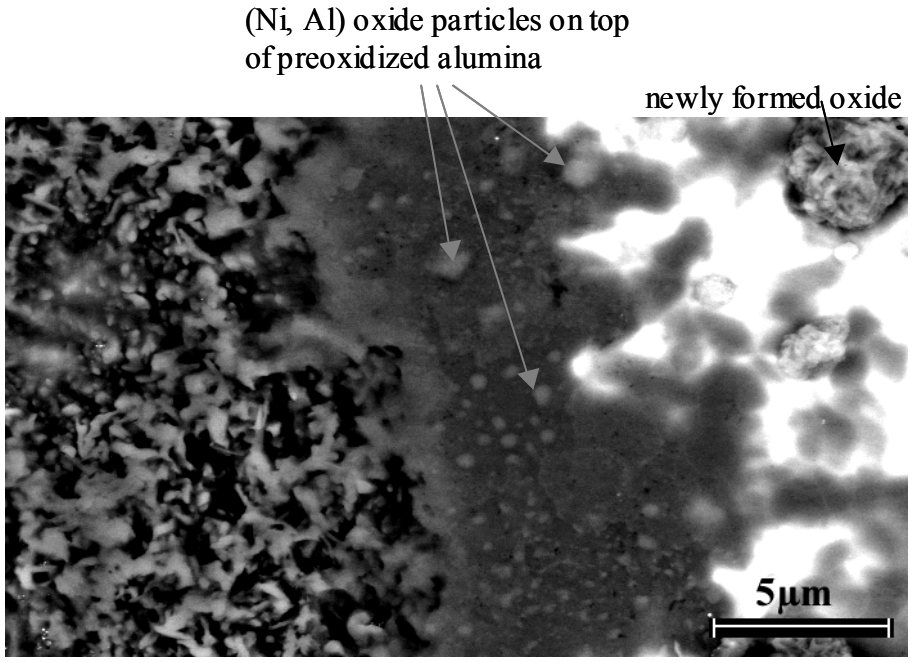

(b)

Figure 79 PtAl on N5, preoxidized for 500 hours at 1100°C in air with 0.1atm water vapor (a) and (b); followed by another 2 hours at 1100°C in air with 0.1atm water vapor (b)

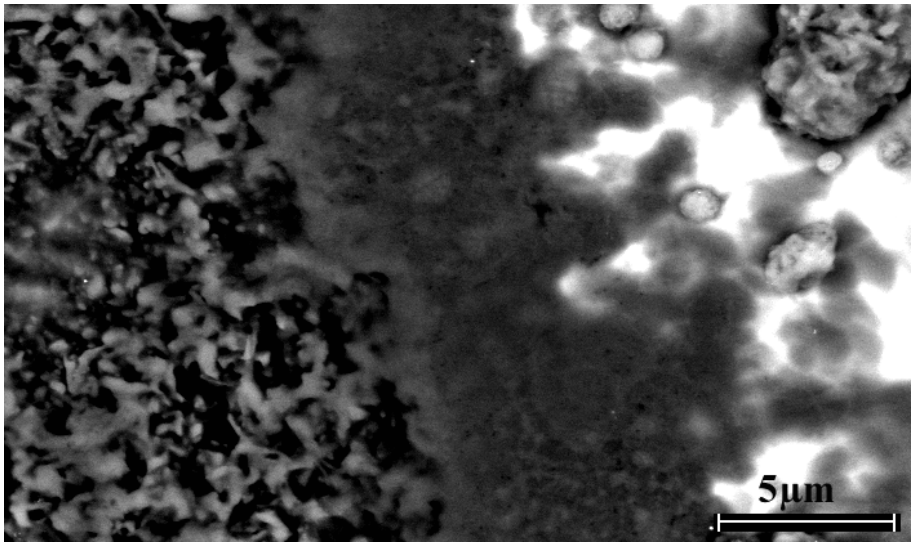

Figure 80 PtAl on N5 preoxidized for 500 hours at 1100°C, followed by two consecutive exposures of 2 hours each at the same temperature in a gaseous atmosphere containing air with 0.1atm water vapor

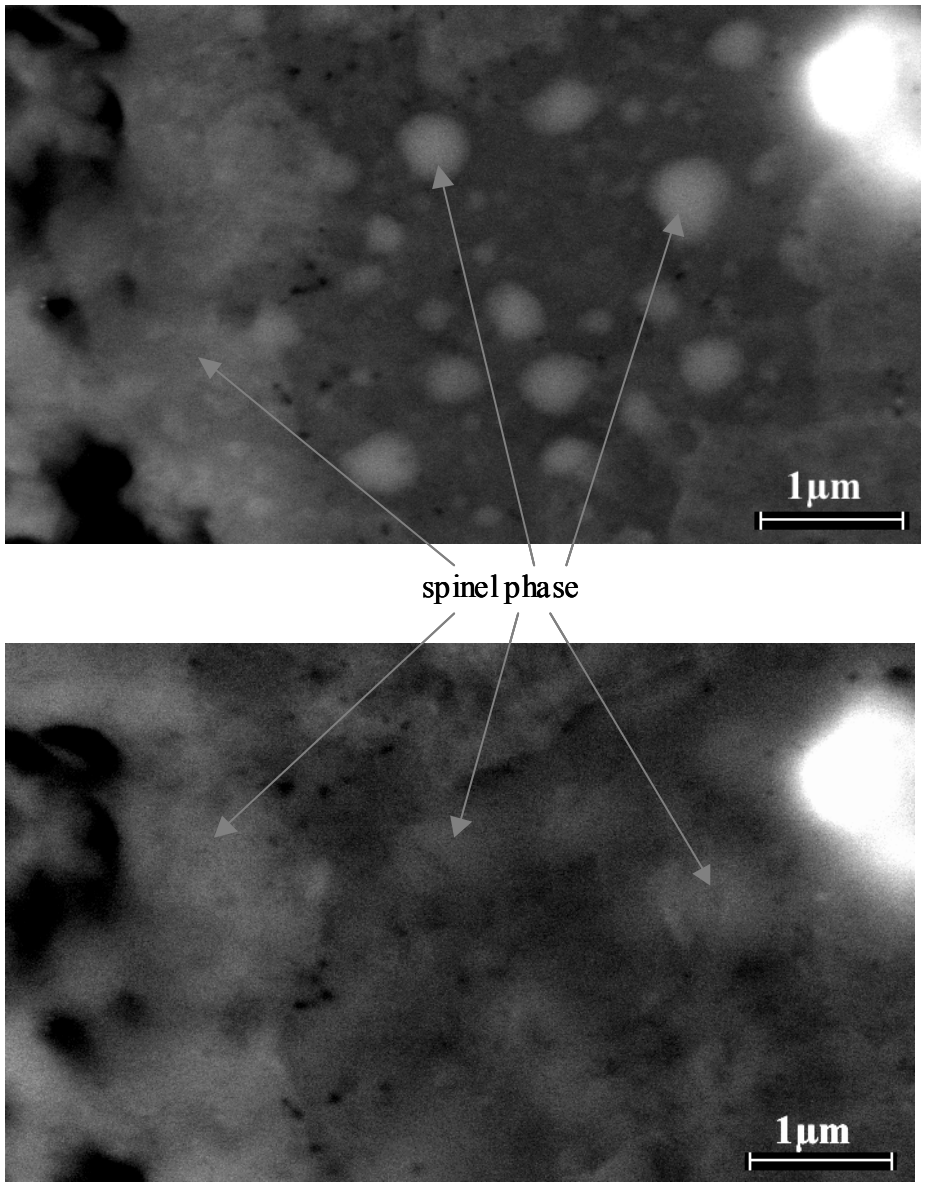

Figure 81 Higher magnification for the samples described in the previous figure, showing the lighter gray coloration as the spinel phase on top of the alumina; (a) after 2 hours of exposure; (b) after 2+2 hours of exposure

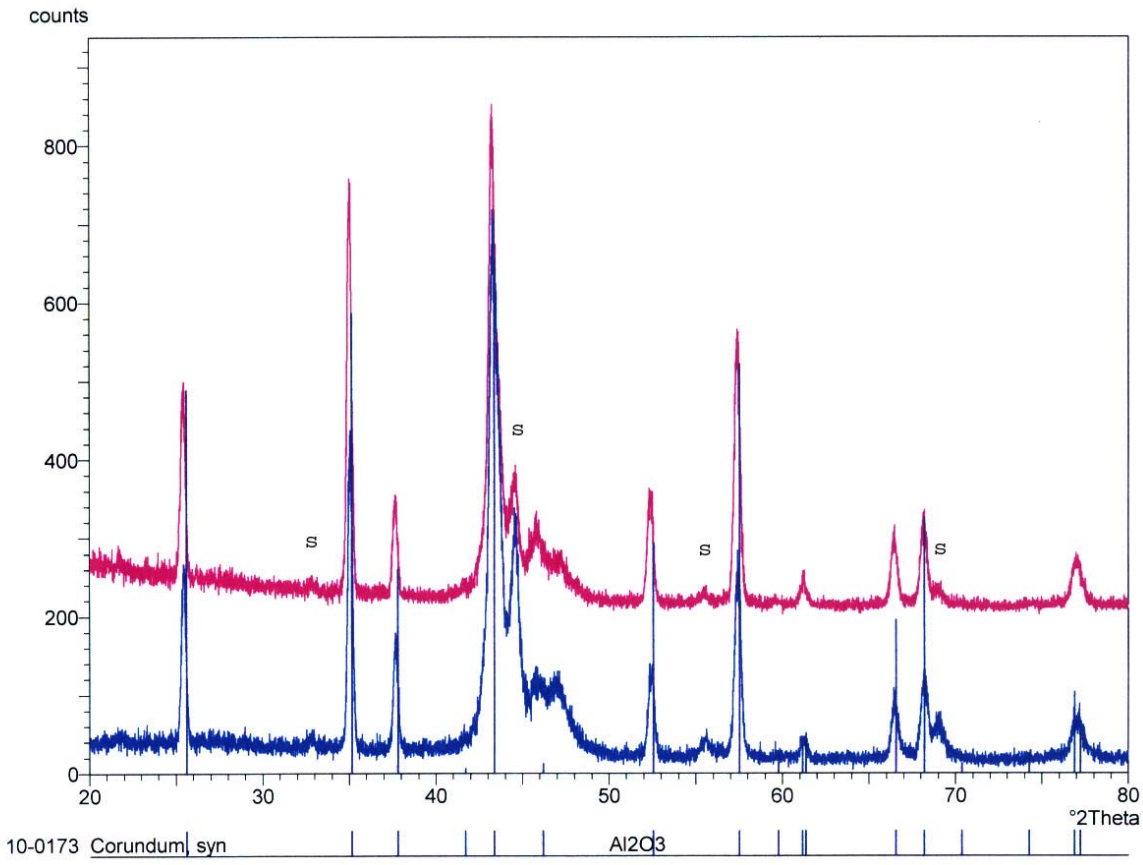

Figure 82 X-ray diffraction pattern for PtAl specimens - with ridges (in red) and without ridges (in blue) – that were oxidized for a total of 504 hours (500 + 2 + 2) @ 1100°C in wet air. The symbol "s" signifies "spinel phase".

however, the spinel phase is more reasonable in view of nickel observed in the nodule areas via EDS analysis.

5.1.3.2. Low Sulfur René N5 A specimen of Ni-base superalloy PWA 1484 with low sulfur content was also preoxidized at 1100°C in air with 0.1atm water vapor partial pressure for 328 hours. Employing the technique described above, the specimen was tapered-polished and subsequently exposed to two sets of 2 hours each at 1100°C in the same wet atmosphere. Micrographs showing the evolution of spinel formation are shown in Figures 83-88. A schematic of the taper-polishing depicting zones of interest on this specimen is presented in Figure 83.

X-ray diffraction measurements for this specimen, taken after a total of 332 hours (328 + 2 + 2) of oxidation at 1100°C in air with water vapor at 0.1atm, show peaks for alumina as well as peaks for the spinel phase to account for all major peaks present in the pattern, Figure 84.

Also, X-ray maps were taken in the scanning electron microscope for the same region on the surface of the sample, at different times: as-tapered, exposure of 2 hours and exposure of another extra 2 hours. From the results shown in Figures 85, 86 and 87, it can be seen that spinel has developed at grain boundaries in the scale of α-Al_2O_3 and that the amount of spinel has increased with exposure time. The fact that spinel first appears over grain boundaries would indicate preferential diffusion of nickel cations along alumina grain boundaries, as has been proposed for aluminum cations [119]. From comparison in Figure 88 concerning how the scale's aspect changes from (328+2) hours to (328+4) hours exposures, it could be noted that the longer exposure leaves the alumina grain boundary network more 'open', in the sense that a larger

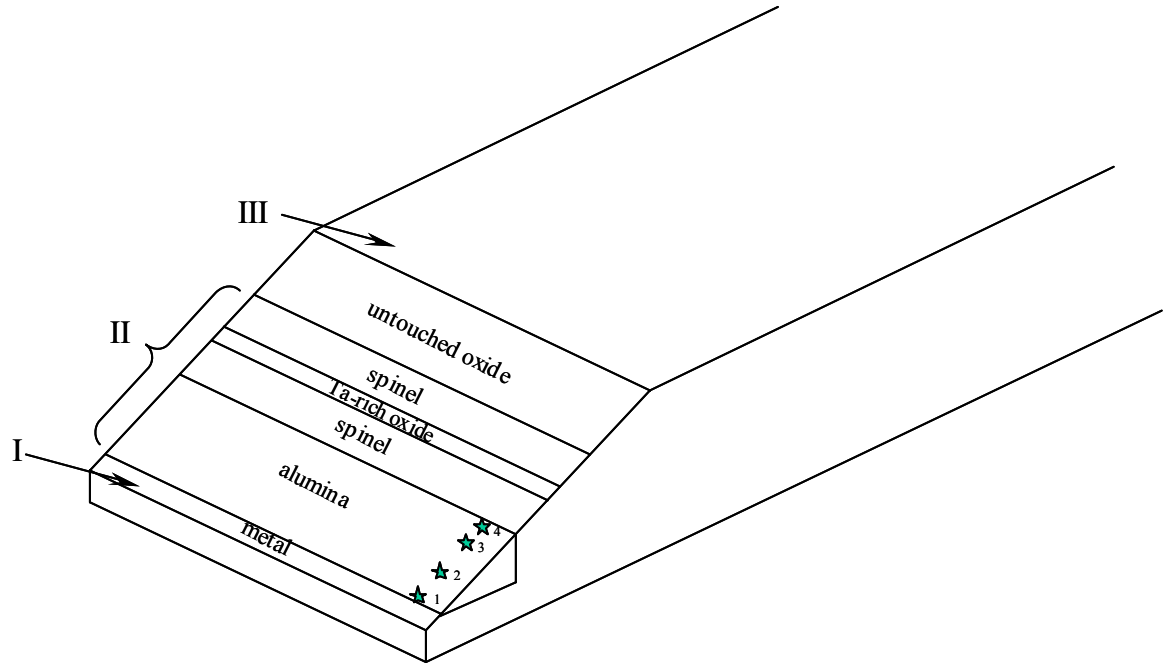

Figure 83 Schematic of the taper-polishing depicting zones of interest: I – metal; II – tapered region of scale; III – untouched initial oxide. The four stars mark the locations of actual micrograph images.

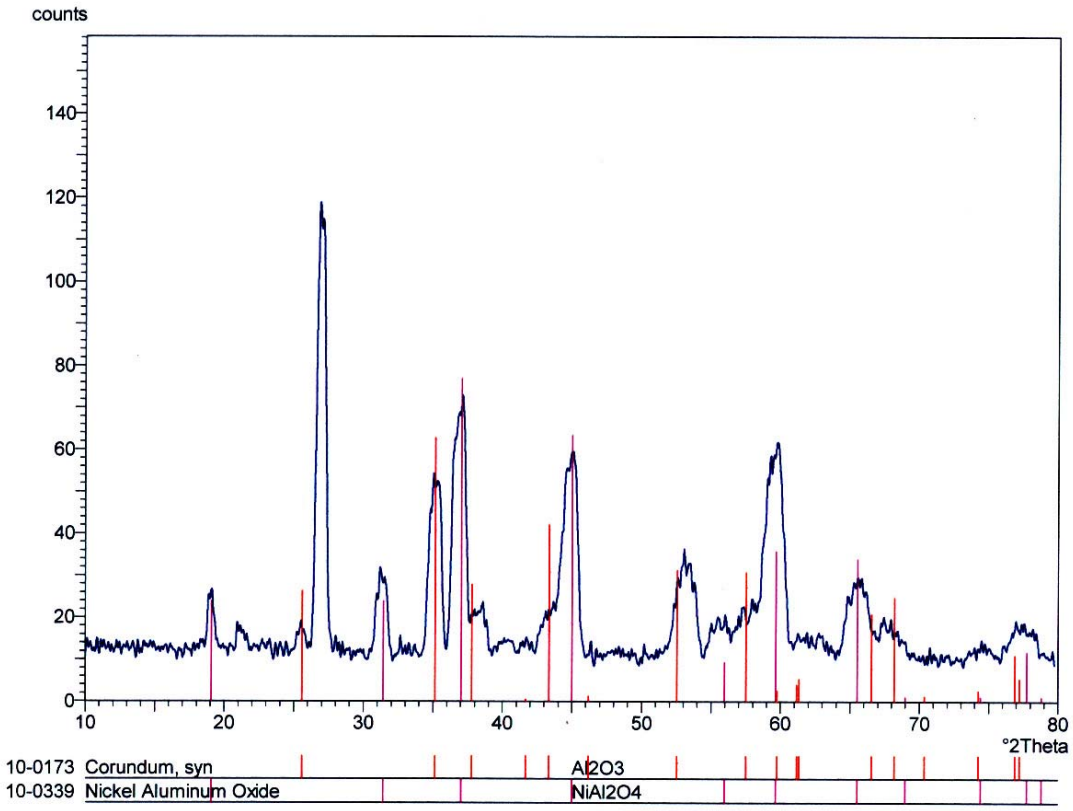

Figure 84 X-ray diffraction pattern for the specimen of lowS N5 oxidized for a total of 332 hours (328 +2 +2) @ 1100°C in air with water vapor at 0.1atm

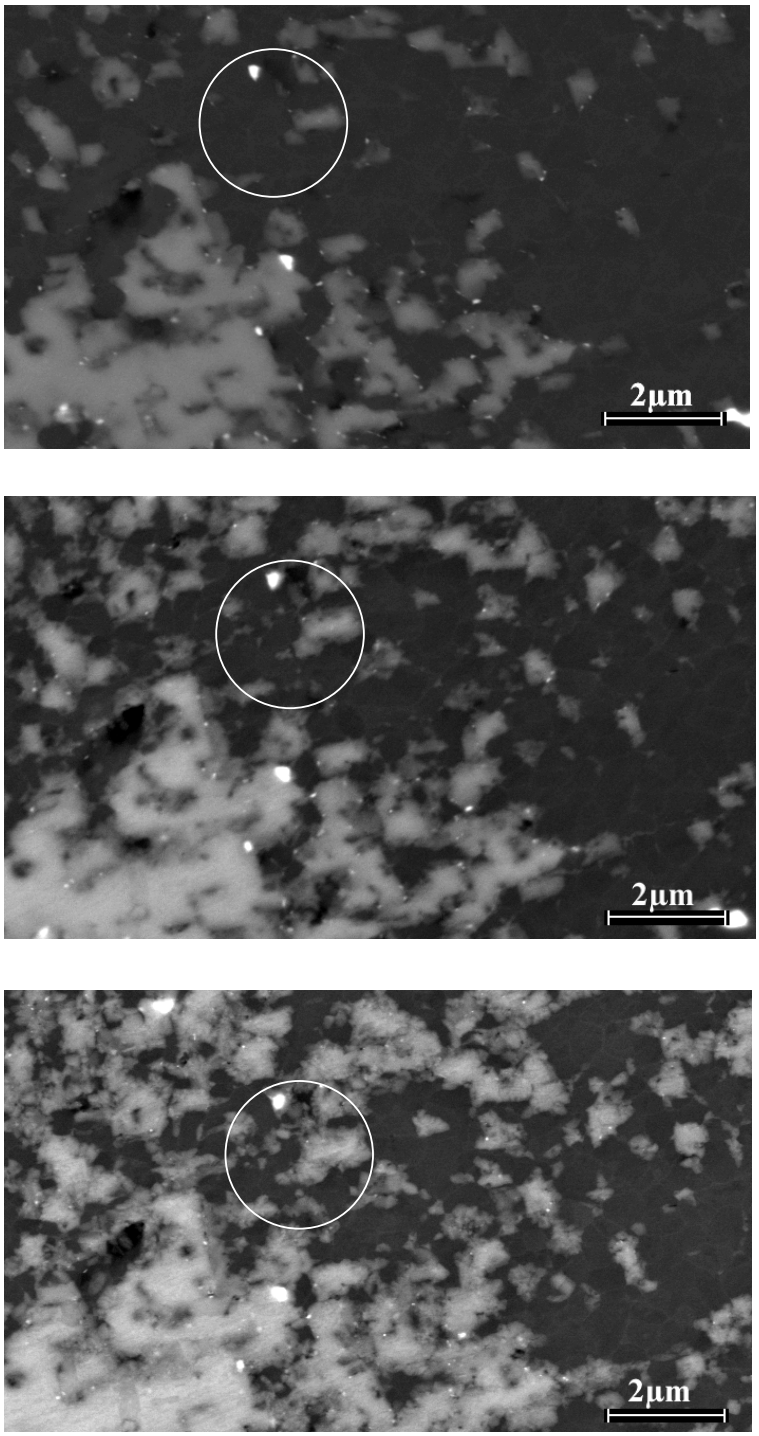

Figure 85 Subsequent exposures of the same specimen (lowS N5) showing the same region over time: (a) 328 hours of preoxidation; (b) 328 + 2 hours; (c) 328 + 2 + 2 hours at 1100°C in air with 0.1atm water vapor. Development and growth (mainly at grain boundaries in alumina) of the spinel phase (lighter coloration). As an example, observe spinel evolution in the circles drawn on micrographs.

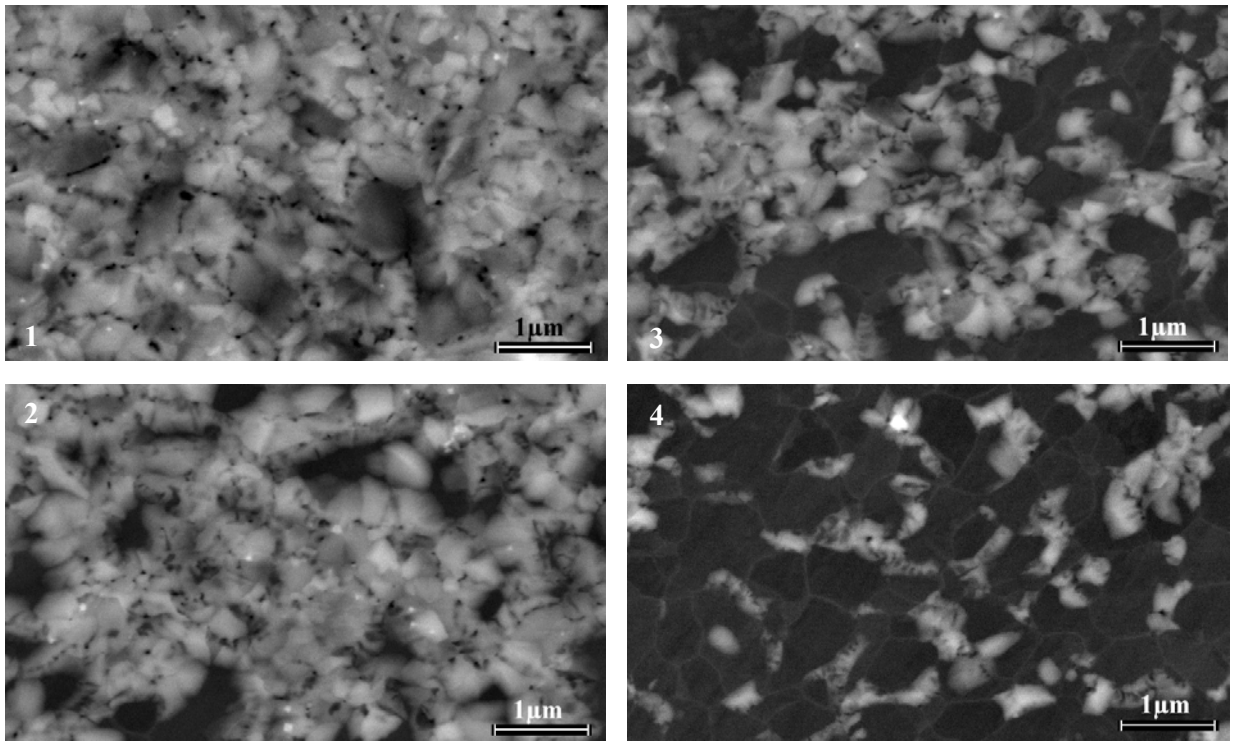

Figure 86 Four regions on the taper-polished sample of lowS N5 exposed for 328 + 2 +2 hours at 1100˚C in air with water vapor. Regions 1, 2, 3 and 4 appear numbered as such on the schematic shown in Figure 83, region 1 being the thinnest alumina and region 4 being the thickest scale.

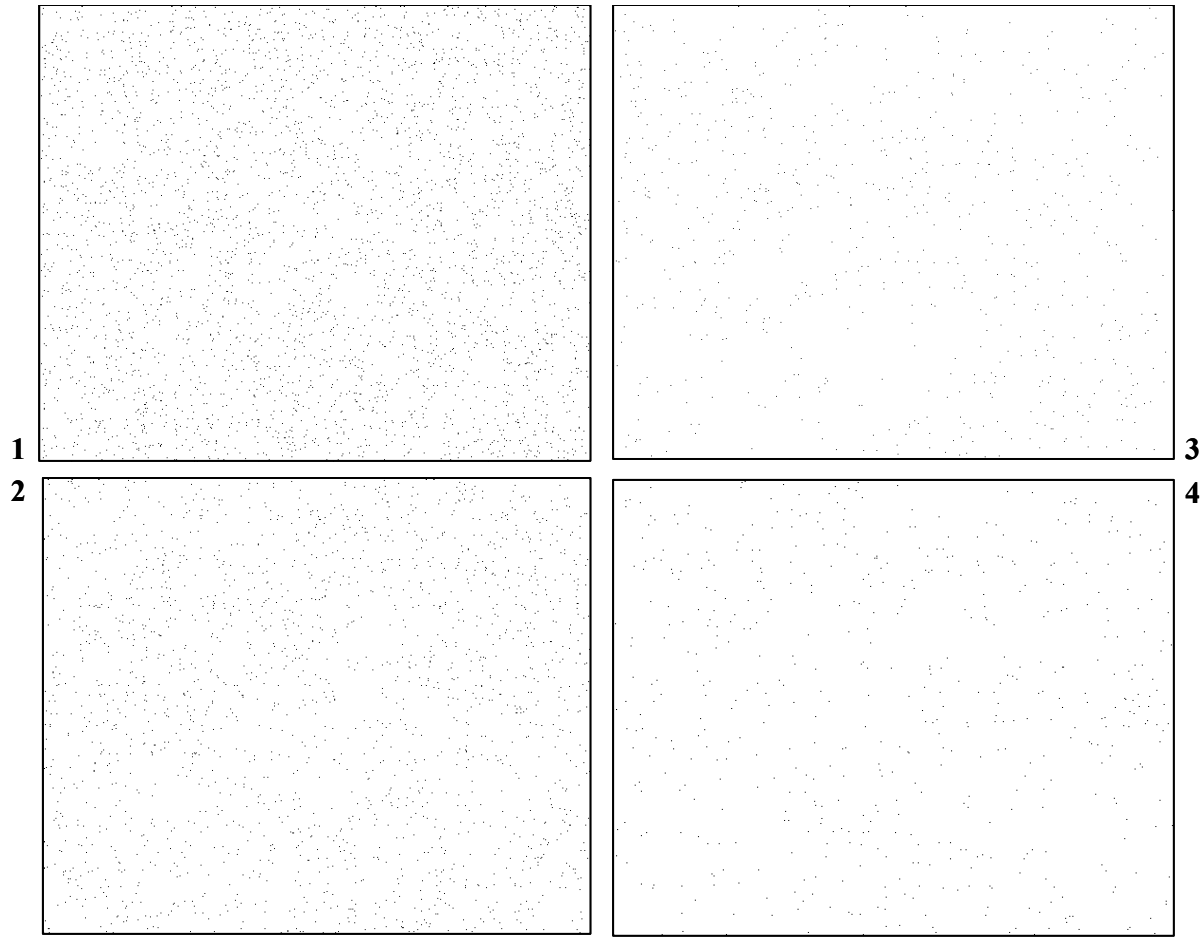

Figure 87 X-ray map on SEM showing the four points of interest (schematically shown in Figure 83) revealing the Ni concentration at these points for the specimen of lowS N5 exposed for 328 + 2 + 2 hours at 1100°C in air with water vapor. The Ni peaks, showing up as bright dots in X-ray mapping, were inverted to dark dots for ease of visualization. From region 1 to region 4, the thickness of specimen increases.

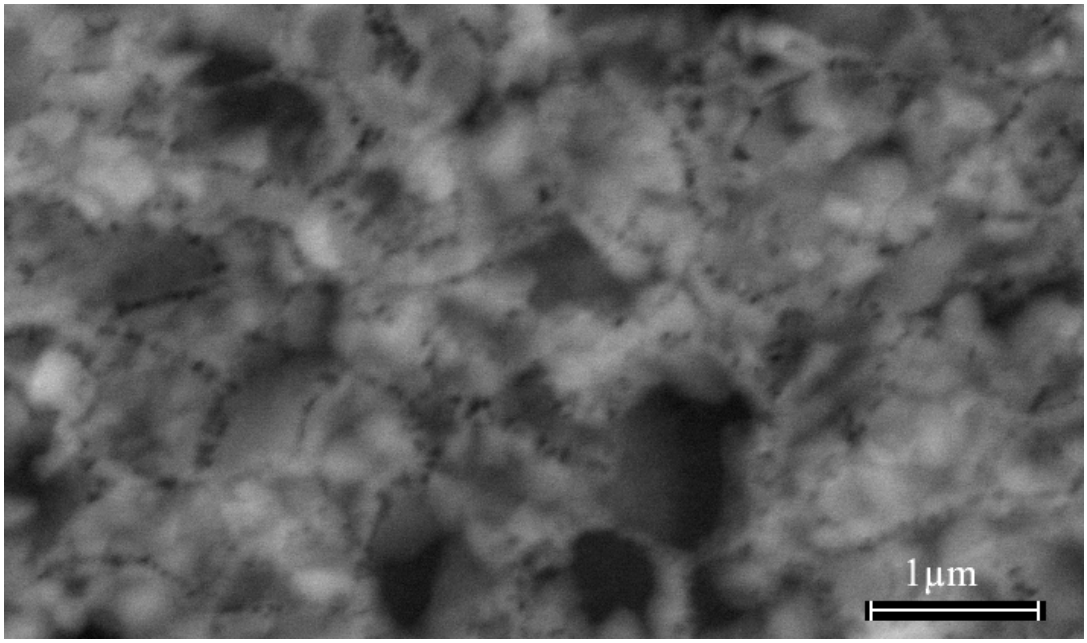

(a)

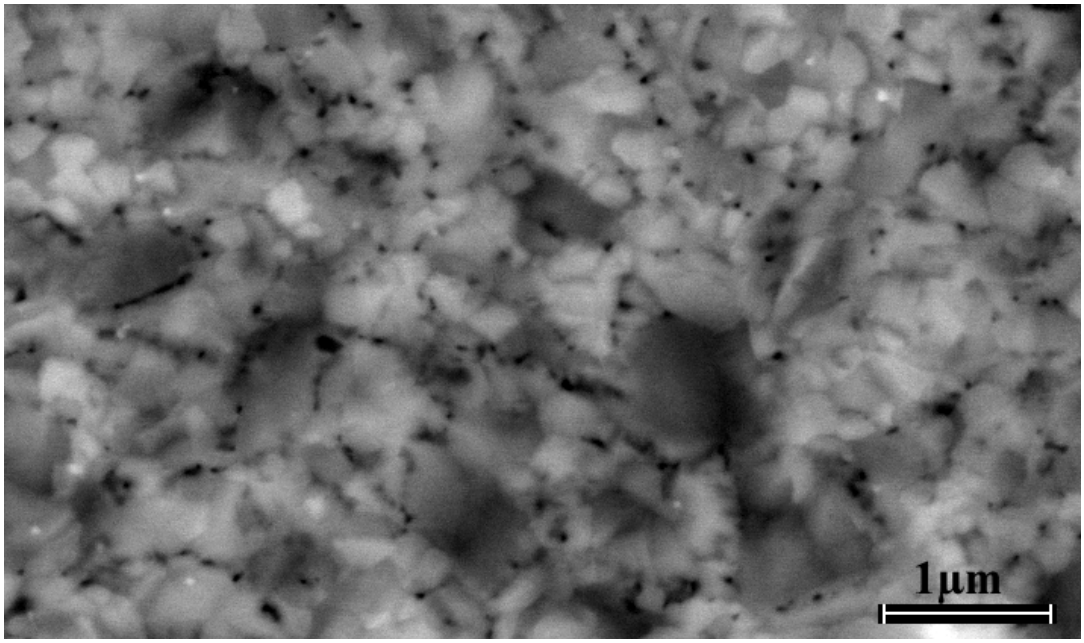

(b)

Figure 88 SEM micrographs showing the same region on the surface of lowS1484 oxidized for (328 + 2) hours (a) and (328 + 4) hours at 1100°C in air with 0.1atm water vapor – larger density of porosity at oxide grain boundaries for the longer exposure.

density of porosity could be observed at those grain boundaries. This suggests that spinel, growing with predilection at these alumina grain boundaries and on top of the alumina scale, can use the network of microchannels, forming at these sites of grain boundaries.

The formation of the new oxide on the polished surface of the scale indicates again the outward aluminum and nickel ions diffusion along existing alumina grain boundaries. Oxygen inward diffusion may still be the major constituent in the transport process – and this process could also occur along oxide grain boundaries, as reported in a number of works [119-121] - leading to the thickening of the oxide scale; however, there are indications that nickel diffusion at alumina grain boundaries significantly contributes to the formation of new spinel phase at the gas/oxide interface.

Comparing the results from the taper-polish oxidized specimens of lowS1484 and PtAl coatings, there seems to be a much larger amount of spinel developed at alumina grain boundaries on the superalloy. This suggests that PtAl specimens, although not 'immune' to spinel formation on top of the alumina scale, show a better behavior in water vapor conditions than the superalloys.

Finally, the experimental results show that spinel formation at the α-Al_2O_3/gas interface becomes enhanced when water vapor is present in the gas mixture. Water vapor does cause α-Al_2O_3 scales to crack and spall more profusely compared to that in dry air and cracks could be responsible for the transport of nickel to the α-Al_2O_3/gas interface. If spinel formation occurs via the outward diffusion of nickel through the α-Al_2O_3 via grain boundary diffusion, water vapor would be expected to accelerate this diffusion process.

When water vapor is present in a gas mixture with air, hydrogen is provided to the gas mixture by the dissociation of H_2O,

$$H_2O = H_2 + 1/2O_2. \quad (26)$$

where, for most of the experimental tests in this study, P_{total} = 1atm and the water vapor partial pressure is P_{H2O} = 0.1atm.

The ratio of the hydrogen pressures in wet (P_{H2O} = 0.1atm) and dry air (dew point -46°C) is given by:

$$P_{H2}\ (wet) / P_{H2}\ (dry) = (P_{H2O}\ (wet) \times P_{O2}^{1/2}\ (dry)) / (P_{H2O}\ (dry) \times P_{O2}^{1/2}\ (wet)). \quad (27)$$

At 1100°C, this ratio is equal to $1x10^3$. In this context, the higher pressure of hydrogen in wet versus dry air could affect the atomic defects in α-Al_2O_3. For example, if hydrogen enters α-Al_2O_3 as an interstitial, then the reaction described by equation (28), written below, would take place and the metal vacancy concentration of α-Al_2O_3 would be increased. The hydrogen may be associated with oxide ions such as $OH_o^{\bullet}$. The outward diffusion of aluminum in α-Al_2O_3 would also be increased but this would not have a significant effect on the growth of the α-Al_2O_3 because the inward diffusion of oxygen is also large.

Along with the possible diffusion of Ni at grain boundaries rather than diffusion through the bulk crystal, an increased cation vacancy concentration in the presence of water vapor can lead to an enhanced distortion of the oxide lattice, in this way permitting more transport of nickel through the oxide.

In dry air, the oxygen-containing species are O^{2-} ions with their ionic radius of r_{O2-} = 0.14nm, whereas in water vapor, the oxygen-containing species are the hydroxyl ions, OH^-, a smaller size ions in comparison with O^{2-}. The radius of OH^- is r_{OH-} = 0.10nm.

Some investigations have also proposed that hydrogen can affect the defect structure of oxides [122]. The interstitial proton defects, $H_i^{\bullet}$, can be present:

$$3H_2 + 3/2O_2 = 6\,H_i^{\bullet} + 2V_{Al}^{'''} + 3O_o^x \qquad (28)$$

In water vapor, the hydroxyl ion OH^- is adsorbed at the surface, namely at the α-Al_2O_3/gas interface and the equation for this effect is written below:

$$OH^- + V_o^{\bullet\bullet} = OH_o^{\bullet} \qquad (29)$$

And, if the hydroxyl ions are considered substitutionally, the equation written below takes place:

$$3H_2 + 3/2O_2 + 3O_o^x = 6OH_o^{\bullet} + 2V_{Al}^{'''}. \qquad (30)$$

The equations (28) and (30) give rise to an enhanced vacancy concentration increase that leads to additional distortion around dislocations present in the oxide lattice. This distortion of the lattice is represented by the extra aluminum vacancies created. This could be a way of nickel diffusing through the alumina by means of extra imperfections of the oxide, possibly more enhanced along the oxide grain boundaries.

5.1.3.3. Summary of Important Effects

Table 7 – Spinel Formation on PtAl, cyclic oxidation @ 1100°C

dry air – 2112 cycles	sporadic regions of spinel
wet air – 1194 cycles	spinel present at more locations
wet air – 3417 cycles	almost continuous layer of spinel on top of alumina scale

• The results presented in this section show that spinel formation at the alumina/gas interface becomes more enhanced in the presence of water vapor for specimens of superalloys and specimens of aluminide coatings on superalloys exposed in oxidizing atmospheres at 1100°C. PtAl specimens exhibit a smaller amount of spinel phase on top of the alumina scale compared to PWA 1484 superalloy specimens. The amount of spinel is found to increase with exposure time.

• Oxygen inward diffusion may still prevail and this process possibly occurs along oxide grain boundaries leading to the thickening of the oxide scale; nevertheless, there are indications that nickel diffusion at alumina grain boundaries contributes considerably to the formation of new spinel phase at the scale/gas interface. Water vapor is found to accelerate this process. Also, an increased cation vacancy concentration in the presence of water vapor can lead to an enhanced distorsion of the oxide lattice, in this way permitting more transport of nickel through the oxide. Data suggest that the solubility of NiO in α-Al_2O_3, as well as transport of Ni through α-Al_2O_3, is increased as aluminum is being depleted from the metallic substrate.

• Spinel formation is due to:

- cracks in the α-Al_2O_3 scales;

- Ni diffusing along oxide grain boundaries and

- a higher H_2 pressure in wet air compared to dry air giving rise to an increased concentration of Al vacancies ($V_{Al}^{'''}$) and Ni diffusing through these vacancies.

5.2 THERMAL BARRIER COATINGS

Additional improvements in oxidation resistance have been realized by protective coatings such as thermal barrier coatings which also form alumina and can prolong the component's life. The duplex system $ZrO_2 – Y_2O_3$ and MCrAlY protects components of industrial gas turbine (e.g. blades and vanes) against high temperature oxidation and high temperature corrosion. This system, called thermal barrier coating (TBC), allows the increase of the gas inlet temperature. Work has been performed to investigate the influence of water vapor on the lives of thermal barrier coatings. During TBC deposition, usually a thin thermally grown oxide (TGO) is formed along the yttria stabilized zirconia (YSZ) and bond coat (BC) interface. The TGO becomes thicker during exposure at high temperatures.

The TBC system studied in this investigation consisted of a single crystal superalloy René N5 coated with a platinum aluminide bond coat and an Electron Beam Physical Vapor Deposition (EBPVD) 8wt% Yttria Stabilized Zirconia (YSZ) Thermal Barrier Coating (TBC). A typical schematic diagram of an as-processed EBPVD YSZ TBC on a single crystal nickel base superalloy with a Pt-modified aluminide bond coat is shown in Figure 89. A thin continuous layer of alumina (TGO) is present along the YSZ/BC interface. No other phases were detected in

the TGO. TBC buttons were subjected to cyclic oxidation in dry air and air with water vapor at high temperatures, namely 1100°C and 1130°C.

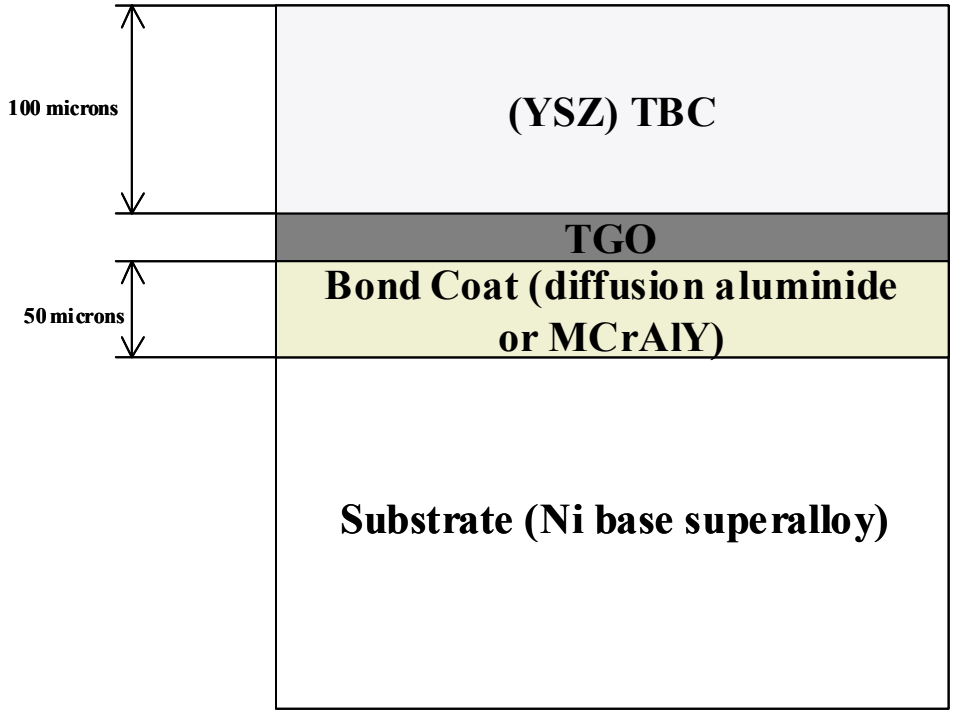

Figure 89 Schematic diagram of an EBPVD YSZ TBC

The EBPVD 8wt% YSZ TBC on the platinum-modified aluminide bond coat, which was exposed in dry air at 1100ºC, failed after 965 cycles. The fractured surface and the underside of the spalled TBC were examined using the SEM, Figure 90, and the TGO/BC interface was found to represent the main percentage of the fracture path area. However, fracture paths along YSZ/TGO interface were observed in some areas; nevertheless, spinel could not be detected on this fracture surface.

Duplicate specimens that were cyclically exposed in water vapor conditions with the partial pressure of water vapor of 0.1atm at 1100ºC failed after 669 hours. Investigation of the

fractured surface showed that spinel ($Ni(Al, Cr)_2O_4$) formation was very pronounced in water vapor conditions. A low magnification photograph of the fracture surface of the sample showing the presence of spinel is presented in Figure 91. From results of these two exposures, in dry air and in air with water vapor, it is evident that the spinel formation is prevalent in the water vapor environment. Since the water vapor exposed TBC specimen has failed earlier than a similar specimen subjected to high temperature dry air exposure, it appears that the spinel development may play a role in this matter. In the case of the wet exposed specimen, the fracture paths were along the oxide phases, a result for which spinel formation could be held responsible. Fracture paths along the TGO/BC interface were limited in area, in contrast to the exposure in dry air, Figure 92; the fracture surface shows that the failure occurs mainly in the oxide phases, rather than at TGO/BC or TBC/TGO interfaces, for the wet exposed specimen.

An indentation test was performed on this specimen and the fracture surface is shown in Figure 91b. The failure seemed to have occurred along the YSZ/TGO interface. Micrographs

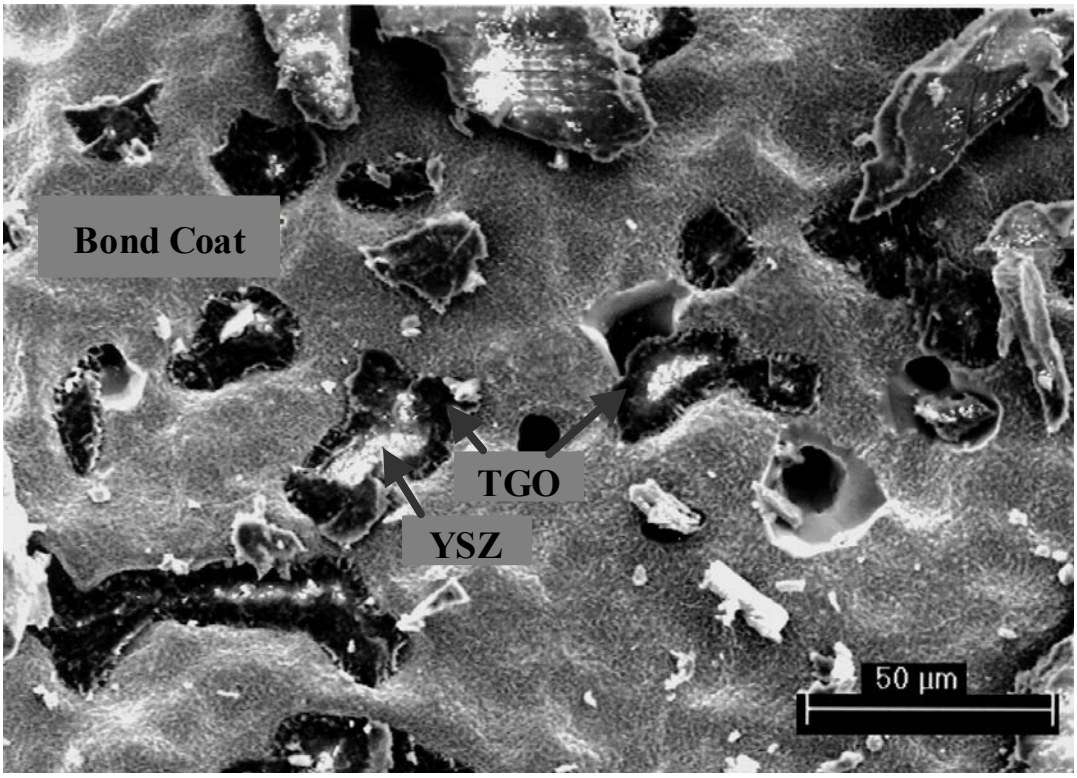

Figure 90 SEM micrograph showing the fracture surface of the EBPVD YSZ TBC cyclically exposed in dry air for 965 hours at 1100°C

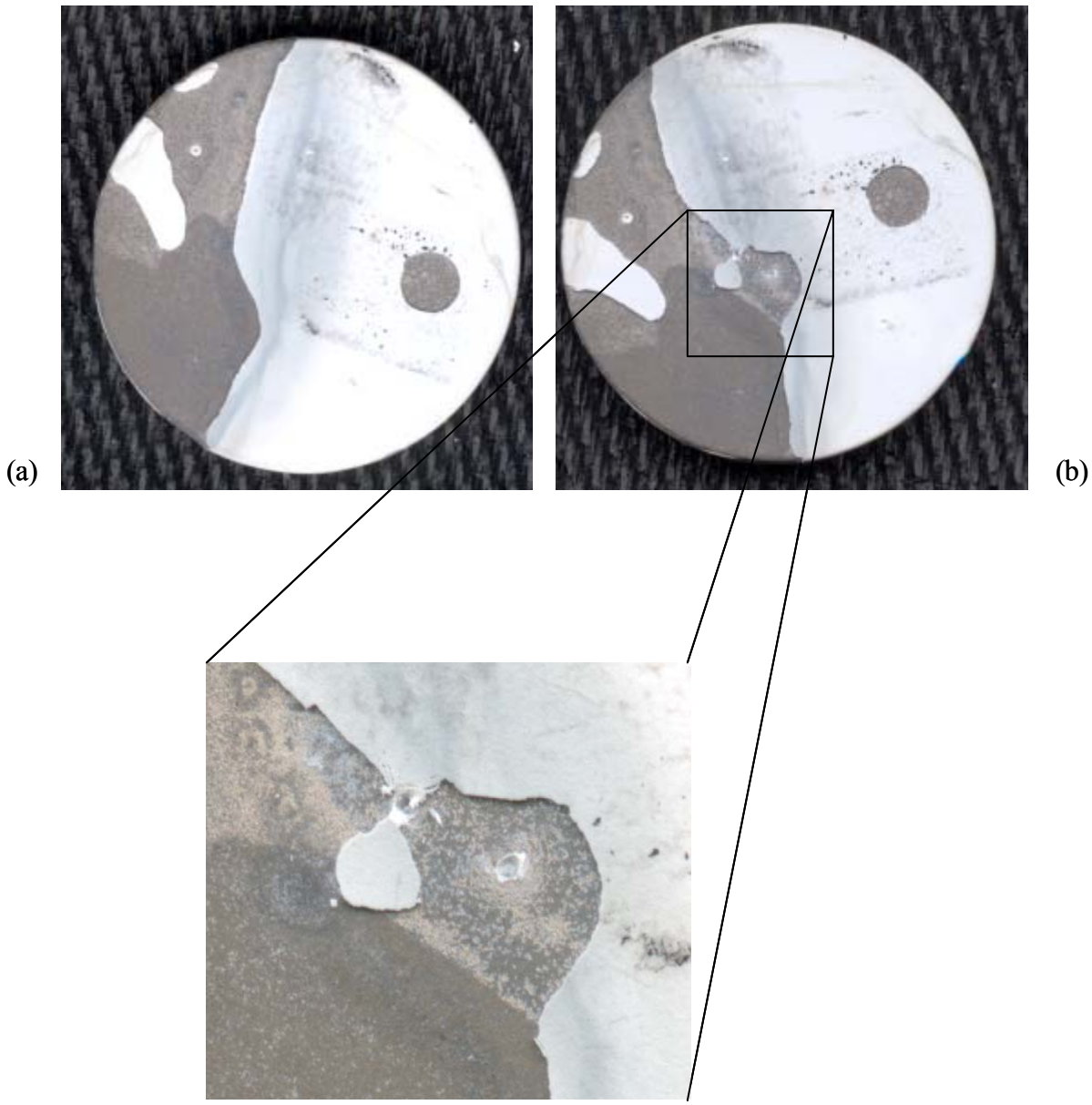

Figure 91 Low magnification photograph of the failed EBPVD YSZ TBC exposed at 1100°C for 669 hours in air with water vapor at 0.1atm (a) as failed; (b) after indentation

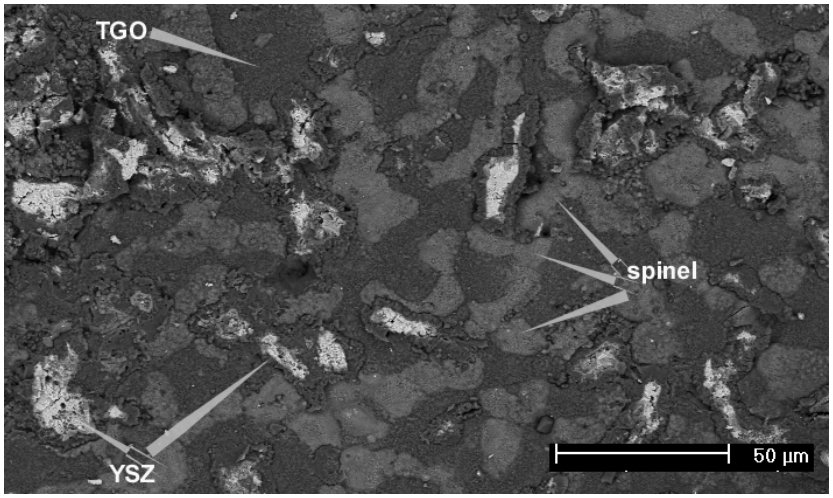

(a)

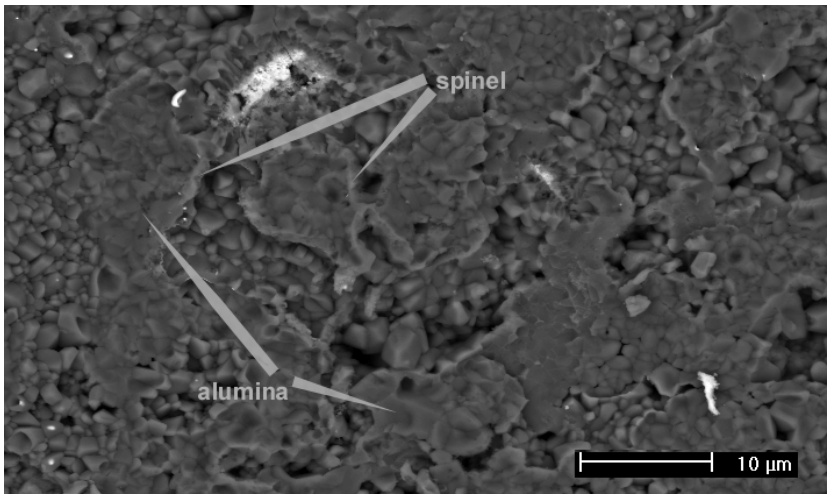

(b)

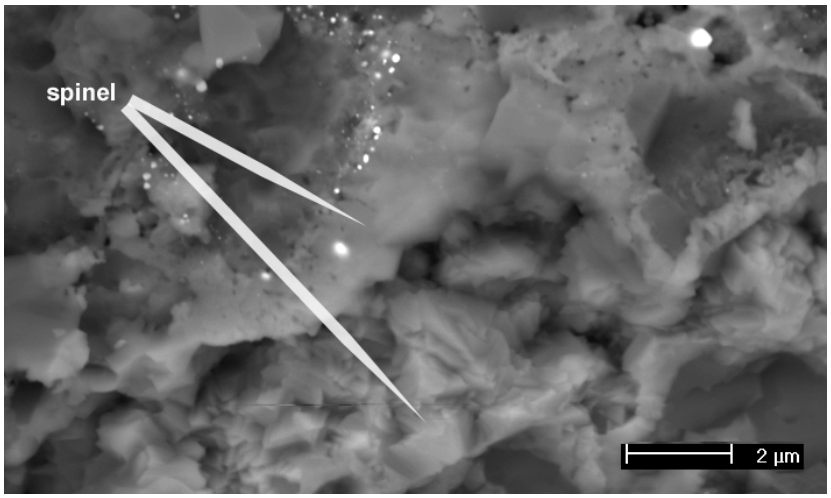

(c)

Figure 92 SEM micros showing fracture surface images of TBC failed after 669 hours of cyclic exposure in water vapor (0.1atm) at 1100°C (a) bond coat surface; (b) underside TBC; (c) higher magnification showing spinel detected on the underside of the spalled TBC

showing the presence of spinel on the fracture surface as well as on the underside of the spalled TBC are presented in Figure 92.

Spinel formed at YSZ/TGO interfaces suggesting that outward diffusion of Ni through alumina must be taking place. As presented in the previous section, the stability diagram for the Ni-Al-O system can be used to explain the thermodynamics of spinel formation at 1000°C, Figure 93a. Reaction paths can be superposed on the schematic stability diagram to determine the sequence of phases, Figure 93b, where the dashed lines correspond to the possible reaction path for nucleation of spinel in air with water vapor. However, the mechanism of nickel diffusion through alumina is not clear. Hydrogen defects could give rise to an increased number of aluminum cation vacancies and this is a possible explanation for the increased transport of Ni in alumina, equation (28). This is also consistent with more rapid alumina growth in water vapor environments. Transport in alumina is complicated due to its small deviation from stoichiometry.

In Figure 94, spinel phase is observed on top of the alumina layer (TGO), at the TGO/TBC interface for the specimen that failed after 669 hours of hot time exposure at 1100°C. Figure 95 shows micrographs of the same specimen with emphasis on different locations along the TGO/TBC interface where detachment of the TBC can be associated with a greater amount of spinel phase present at those locations.

A subsequent experiment exposing cyclically a TBC in water vapor conditions at 1100°C was performed to examine the reproducibility of the above-mentioned results. This specimen failed after 920 hours hot time rather than 669 hours that was observed for the specimens tested in water vapor previously. Examination of fracture paths for this specimen, Figure 96, showed characteristics closer to those for failures that developed during cyclic oxidation in dry air,

(a)

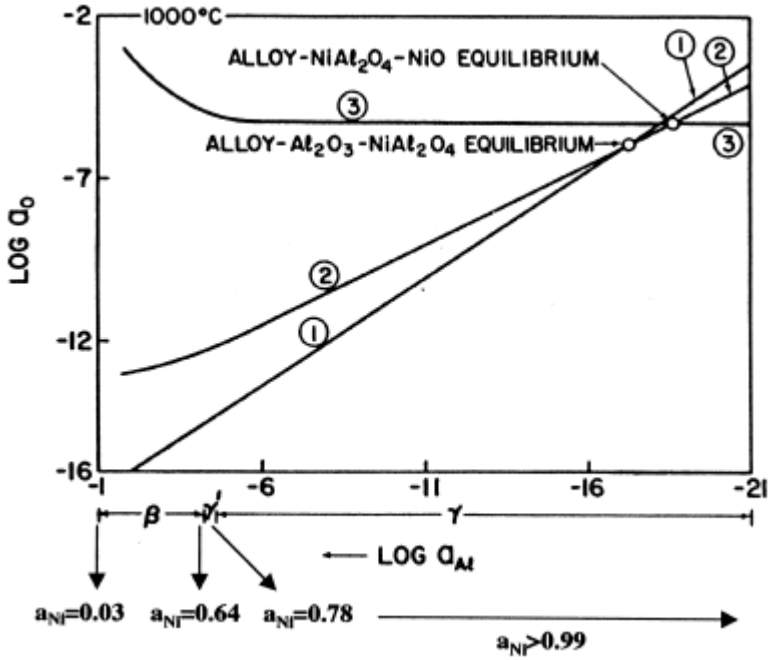

(b)

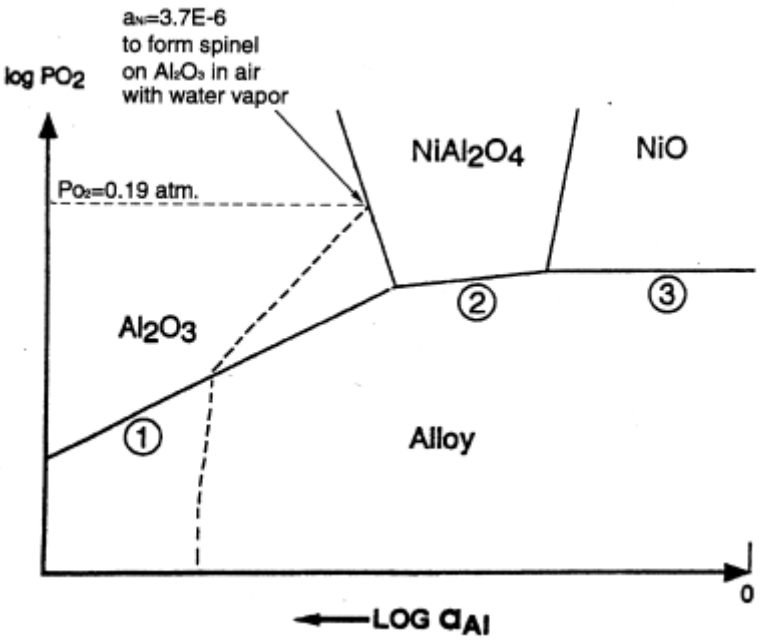

Figure 93 Stability diagram for the Ni-Al-O system (a) thermodynamic diagram at 1000°C; (b) reaction path (dashed line)where spinel begins to nucleate on the TGO in air with water vapor at 0.1atm (*After M.J.Stiger,N.M.Yanar,M.G.Topping,G.H.Meier,F.S.Pettit, Zeit. Metall.12, 1069 (1999))

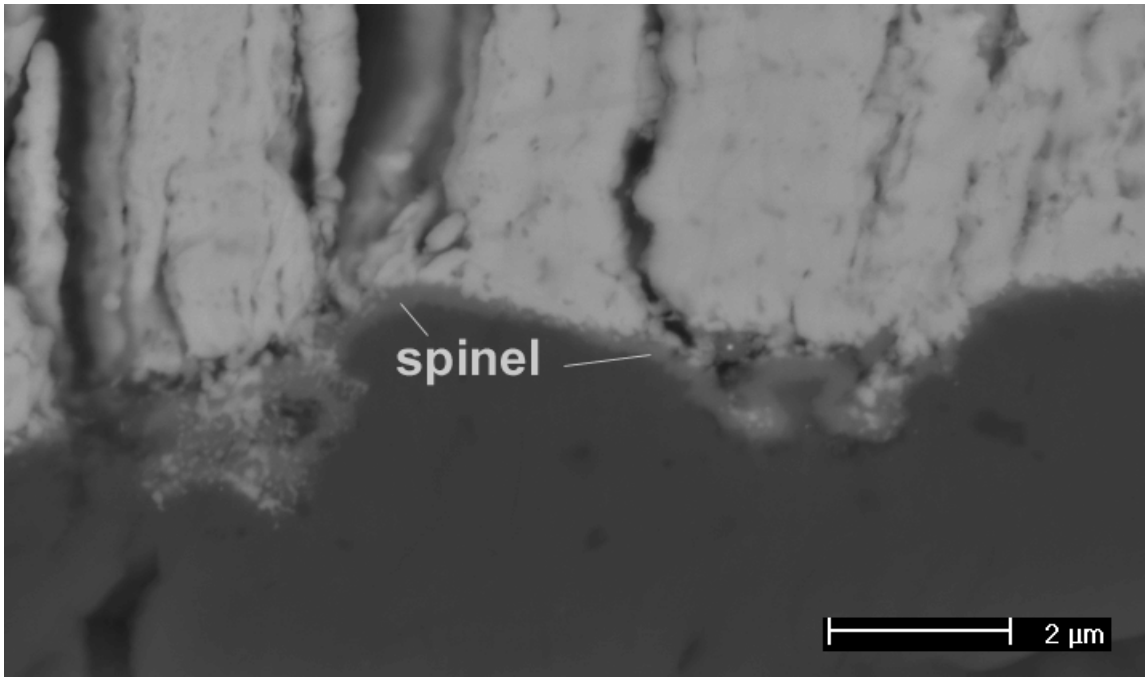

Figure 94 Cross-sectional view of EBPVD YSZ TBC exposed at 1100°C for 669 hours in air with water vapor at 0.1 atm showing spinel phase at the TGO/TBC interface

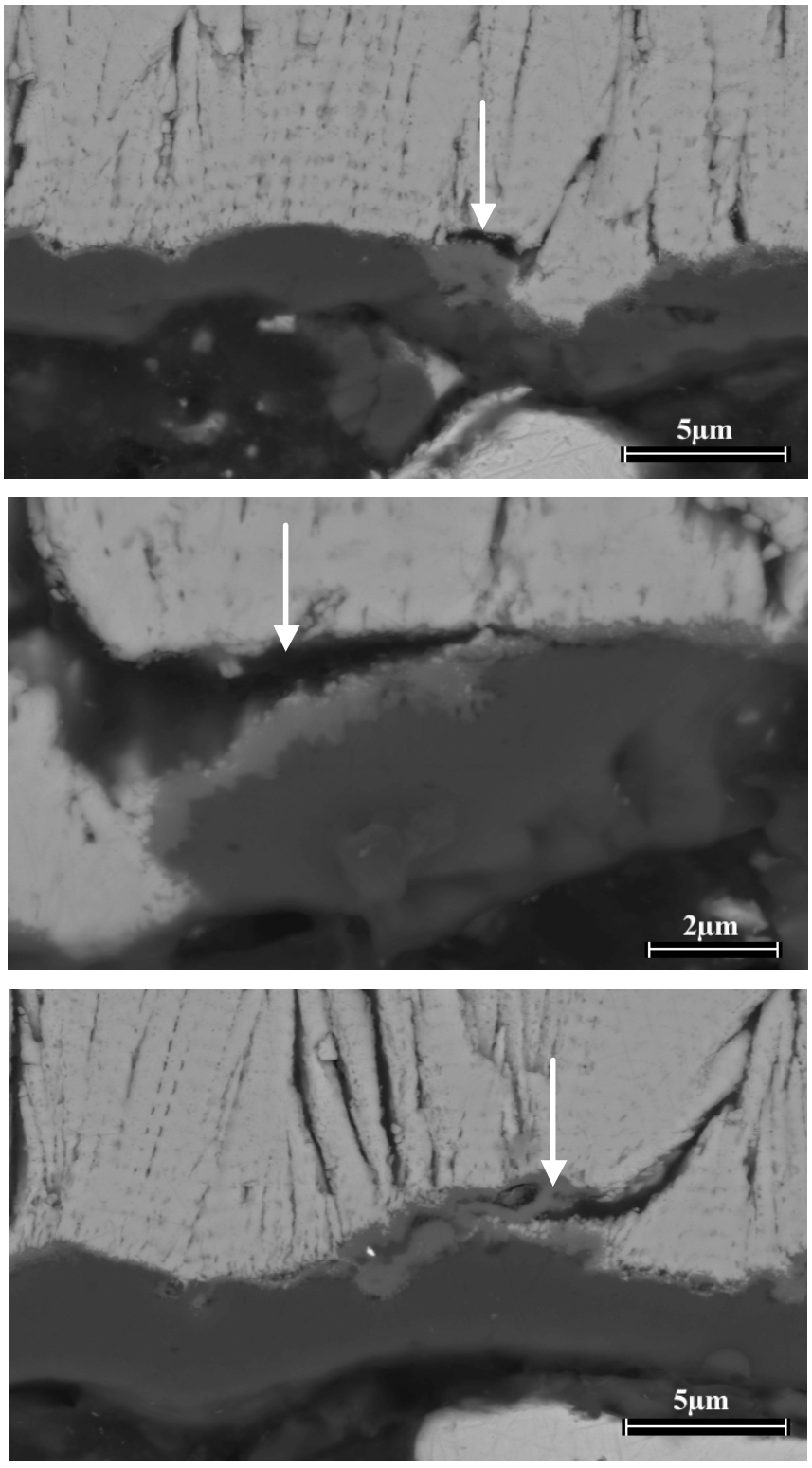

Figure 95 Cross-sectional view of EBPVD YSZ TBC exposed at 1100°C for 669 hours in air with water vapor at 0.1atm showing cracks/defects that developed when spinel was present on top of the TGO (alumina) at the TGO/TBC interface (a), (b) and (c)

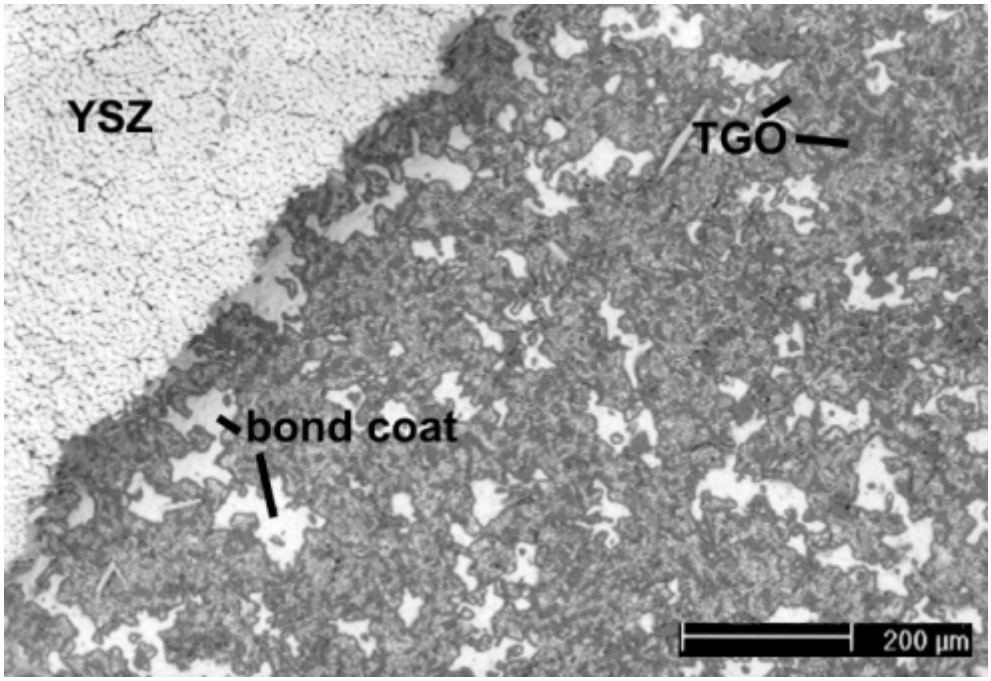

Figure 96 SEM micrograph showing the bond coat surface of the failed TBC exposed at 1100°C in air with 0.1 atm water vapor pressure which failed after 920 hours

Figure 90, rather than those observed at 0.1atm water vapor pressure previously, Figure 92a. No spinel phase was detected on top of the TGO and the fracture path resembled more the one in dry air (i. e. along TGO/BC interface).

After cross-section examination, both bond coats (TBC exposed in water vapor initially and TBC oxidized in water vapor at 0.1atm to account for reproducibility) were found to exhibit about the same amount of depleted aluminum region even though the sample that showed spinel formation failed after 669 hours whereas the other sample lasted for 920 hours. Figure 97 shows a comparison of the two bond coats. It can be observed that the TGO thickness in both cases is about the same, even though one specimen was at 1100°C for about three quarters of the time the other specimen was at temperature. These results suggest that the temperature of exposure for the specimen that failed early could have been higher or some conditions for contamination were present.

Another experiment using the same water vapor conditions, but this time at 1130°C, was performed. The TBC specimen failed after 615 hours. Fracture surface examination revealed a sporadic presence of spinel. The fracture paths were along YSZ/TGO as well as TGO/BC interfaces. Spinel was mainly detected at the edges of the sample on the fracture surface, Figure 98, as well as on the underside of the spalled TBC.

Although the results presented in this part of the work study suggest that enhanced spinel formation is evidently linked to water vapor exposures and that this spinel phase may be held responsible for the TBC failures along the oxide phases, further stages of investigation would have to consist of work on TBC failures directed towards reproducibility of such failures and modeling the mechanism by which water vapor plays a role in these failures.

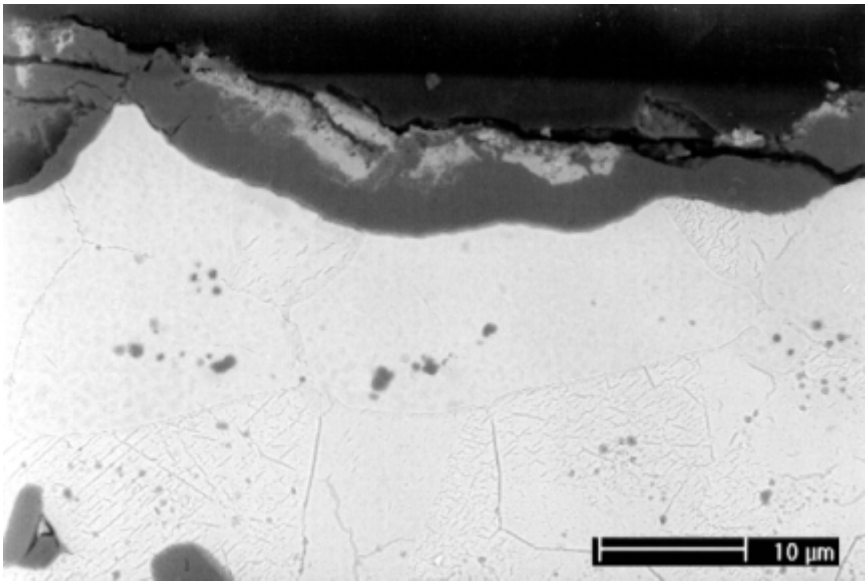

(a)

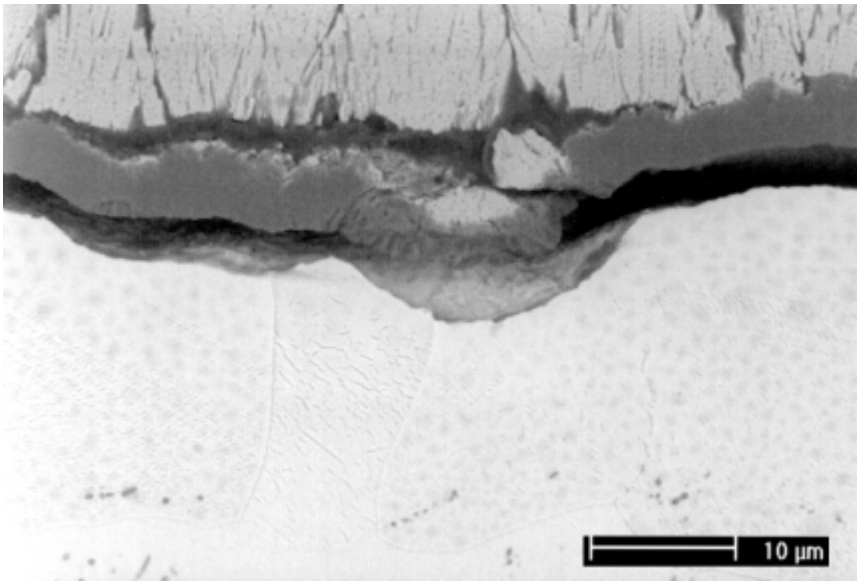

(b)

Figure 97 SEM micrographs showing cross-sectional views of the failed TBC exposed in water vapor at 0.1atm at 1100˚C for (a) 920 hours; (b) 669 hours. Comparison of the oxide (TGO) thickness.

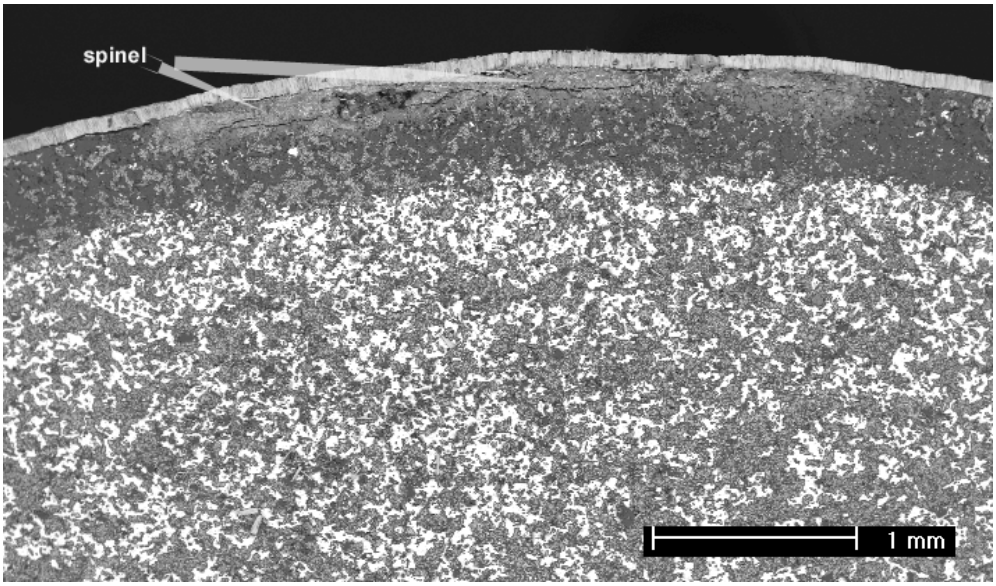

(a)

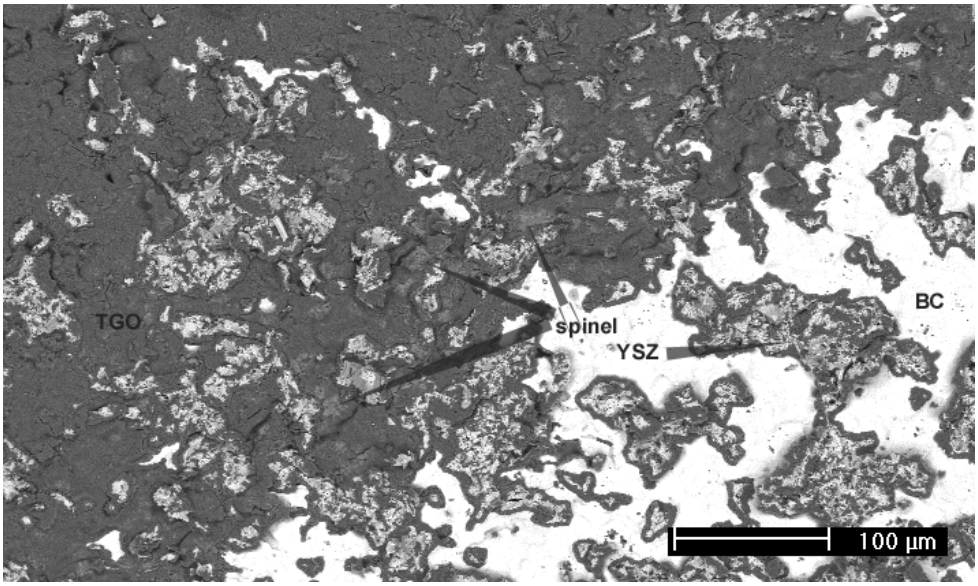

(b)

Figure 98 SEM micrographs showing the fracture surface of the failed TBC cyclically exposed at 1130°C for 615 hours in water vapor conditions (0.1atm) (a) low mag, showing edge of specimen; (b) higher mag showing fracture surfaces along YSZ/TGO and TGO/BC interfaces

5.3 OTHER EFFECTS OF WATER VAPOR OBSERVED IN THIS STUDY

5.3.1 Effect of Water Vapor Pressure

The results obtained from oxidation in the presence of water vapor at different partial pressures show that there was no difference in the cyclic oxidation of alloys in water vapor at 0.05atm and 0.1atm. Figure 99 shows the change in weight versus time for PWA 1484 and CMSX4, respectively, exposed in air with water vapor at the two mentioned partial pressures. The weight losses for CMSX4 in both cases are much larger than those obtained for PWA 1484. These results show that there is not a significant difference in cyclic oxidation behavior. A higher water vapor pressure (0.5atm) must be used to conclusively determine if cyclic oxidation is dependent on the water vapor pressure. The specimens that were exposed at 0.5atm water vapor pressure in air at 1100ºC are René N5 and René N5 with a low content of sulfur. It appears that the amount of degradation of the cyclically exposed René N5 increases as the pressure of the water vapor in the gas increases, Figure 10. As mentioned earlier in subchapter 5.1.1, an external scale containing NiO with virtually no continuous α-Al_2O_3 is evident on the René N5 specimen exposed for 802 cycles at 1100°C in a gas mixture with 0.5atm of water vapor, Figure 11, scanning electron micrographs showing cross-sectional views of the exposed specimens being consistent with the previous results, Figure 12.

Specimens of superalloys PWA 1484 with low sulfur content and CMSX4 exposed for 10 minutes at 1100°C in air with water vapor at different partial pressures (0.1atm and 0.5atm),

presented in cross-section in Figures 43 and 44, exhibit a more extensive transient oxidation stage for the increased water vapor pressure.

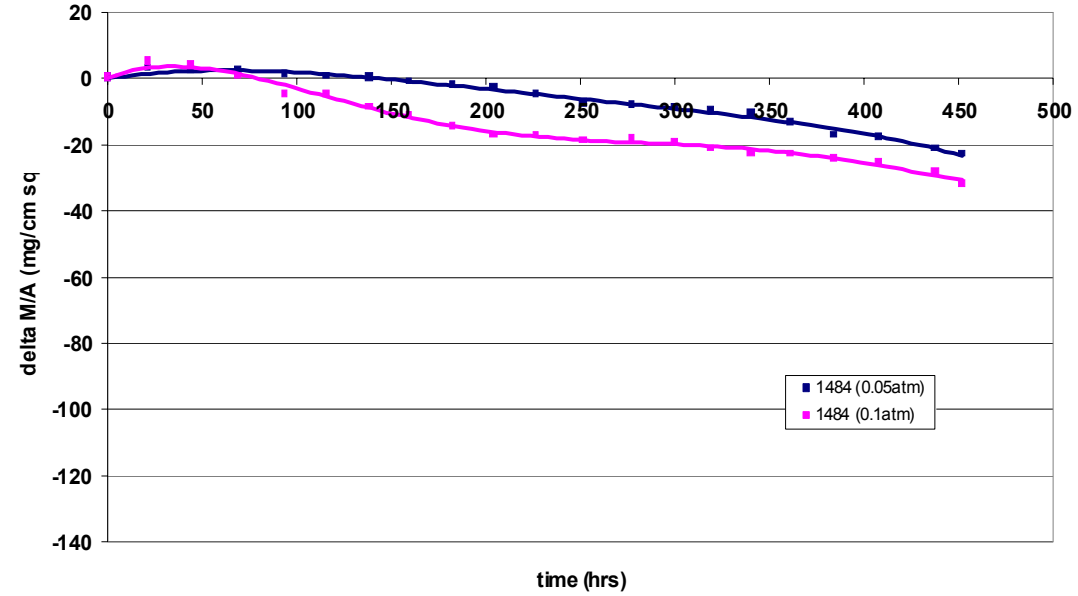

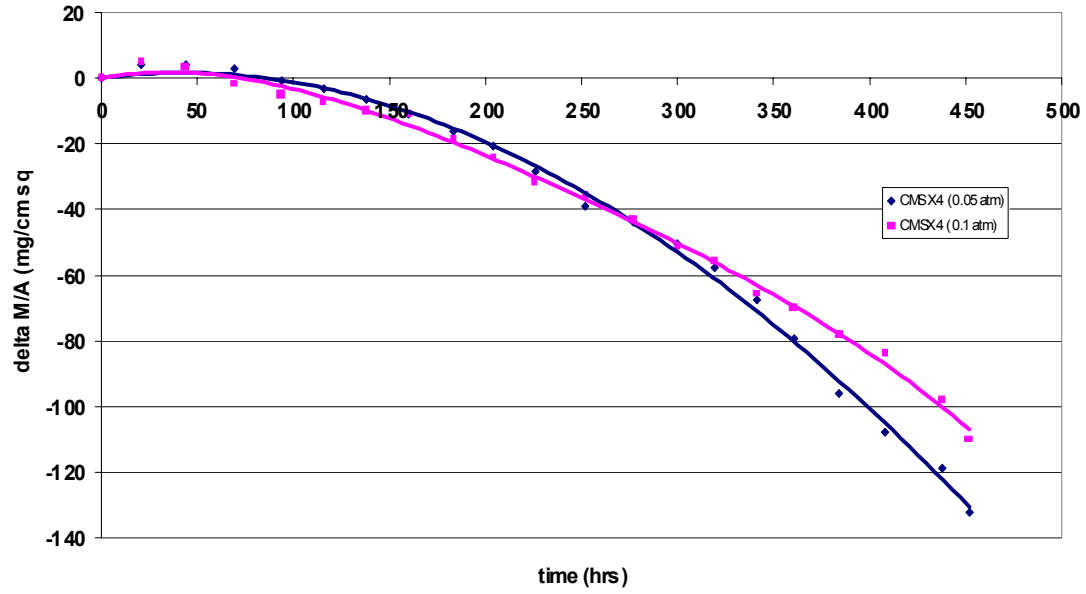

Figure 99 Weight change versus time data for the cyclic oxidation of (a) PWA1484 and (b) CMSX4 in air with water vapor partial pressures of 0.1atm and 0.05atm at 1100°C

On the other hand, specimens of Ni-8Cr-6Al with fine polished (up to 0.05μm Al_2O_3 suspension) surfaces were exposed for 5 minutes at 1100°C in air with water vapor at 0.1atm and 0.5atm partial pressures, respectively. The cross-section of the higher pressure exposed specimen presents a thick - rather porous NiO layer - with oxide thickness along the cross-section up to 5μm, under which a large penetration of internal oxides – Al_2O_3 along with Ni and Cr oxides – of about 5 to 7μm has developed, Figure 57c. For the specimen oxidized in air with 0.1atm water vapor, a similarly thick NiO scale formed, but this layer of NiO does not contain the observed porosity of the NiO scale on the 0.5atm specimen. The amount of the mixed oxides and internal oxides underneath NiO are comparable for both specimens exposed at 0.1atm and 0.5atm.

From the results presented here, it can be said that early time exposures of model alloy Ni8Cr6Al in wet atmospheres do not show a large effect of the water vapor pressure for these short time oxidations since the same amounts of NiO and comparable internal oxidation were present in specimens exposed to air with 0.1atm and air with 0.5atm of water vapor, Figures 57b and 57c. Nevertheless, for similar exposure conditions as for Ni8Cr6Al specimens, Ni base superalloy specimens show an increased transient and internal oxidation process for a higher water vapor pressure (i.e. 0.5atm). It is possible that this difference in the oxidation behavior is due to a larger involvement of the alloying elements (i.e. Ta, W, etc) for the case of more complex systems such as Ni base superalloys.

5.3.2 Effect of Specimen Thickness

The residual stresses in the alumina scale on Ni base superalloys were measured at room temperature after cyclic oxidation tests. The alumina scale developed under a transient oxide layer at the interface with the René N5 substrate at 1100°C, Figure 100.

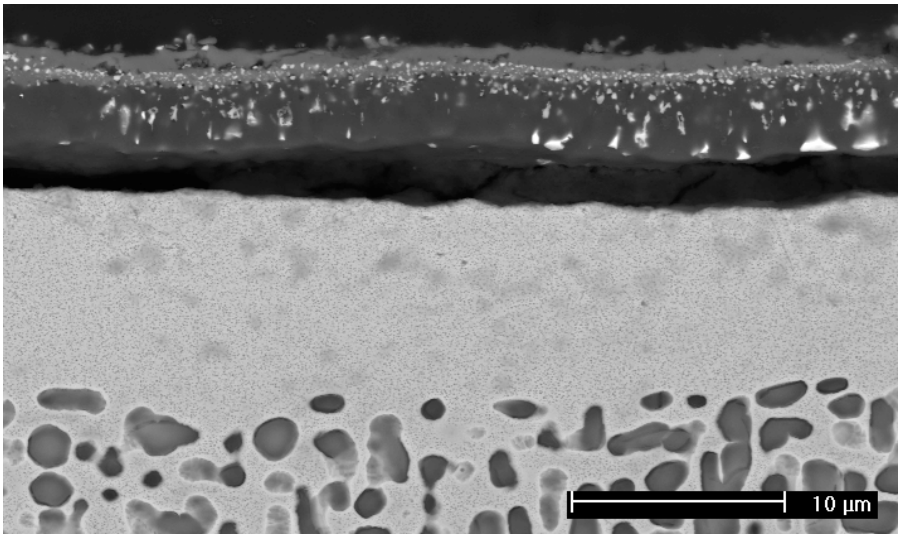

(a)

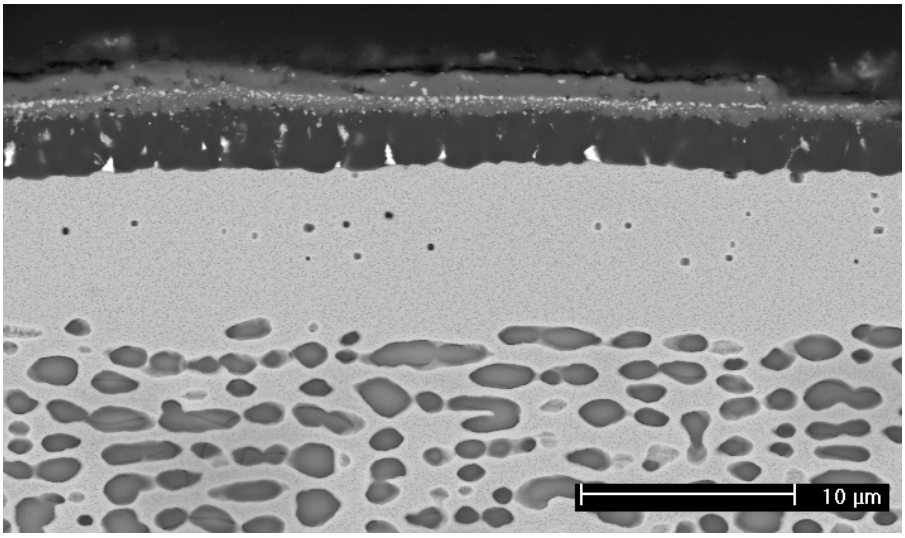

(b)

Figure 100 PWA 1484 cyclically oxidized in dry air for 650 hours at 1100°C (a) thick specimen (thickness 2 mm); (b) thin specimen (thickness 0.4 mm)

The thickness of specimens can affect the magnitude of the residual stresses that develop during growth of scales and cooling from the exposure temperature. Coupons of PWA 1484 and PWA 1484 with low sulfur content with thicknesses of 0.4 mm and 2 mm were cyclically oxidized at 1100ºC in dry and wet air to compare their oxidation behavior. Weight change versus time measurements were monitored. Results from these experiments are presented in Figures 100 and 101. PWA 1484 specimens with low sulfur content, exposed in dry air, Figure 100, exhibit an alumina scale contaminated with tantalum and the same thickness of the oxide scale, as well as comparable Al depletion zones, were found for both specimen thicknesses.

On the other hand, specimens of different thickness of PWA 1484 with regular sulfur content, oxidized in a water vapor atmosphere, show much cleaner alumina scales but different thicknesses of the transient oxides, alumina and Al-depleted zones. The degree of the enhanced oxidation may not be of significance for specimens of large enough thicknesses, but it seems to be important for thin specimens. The thinner specimen shows a greater amount of transient oxides on top of the alumina scale, Figures 101, a and b. Also, the 0.4mm specimen (the thin specimen) displays almost twice the thickness of the aluminum depletion region compared to the 2mm specimen (the thick specimen).

The results of the change in weight measurements for four superalloys, PWA1484, PWA1484-low sulfur content, CMSX4 and PWA1487, each with two samples exposed in the test – a thick (2mm) and a thin (0.4mm) specimen – are presented in Figure 102. For all four substrates, the thinner specimen exhibits less weight losses as compared with their thicker counterpart, suggesting that the stored elastic energy is less for all thin specimens in this case.

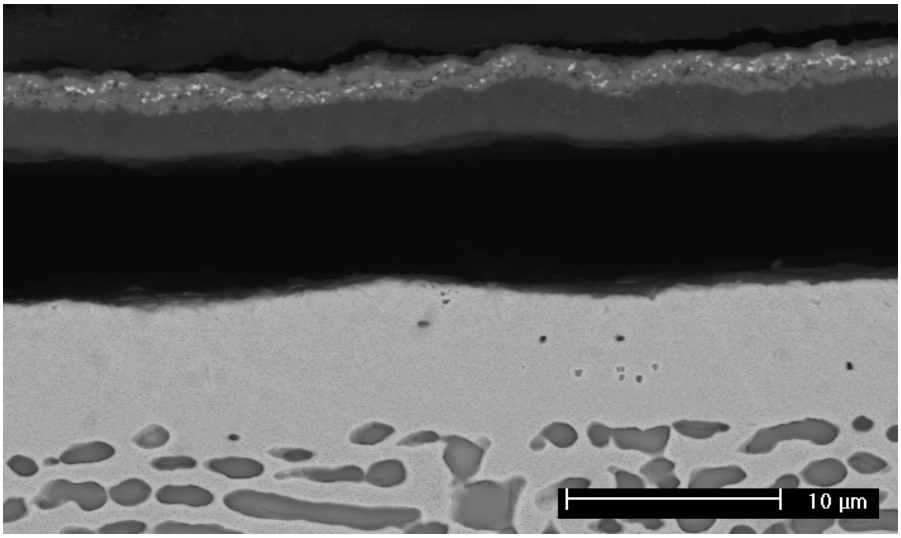

(a)

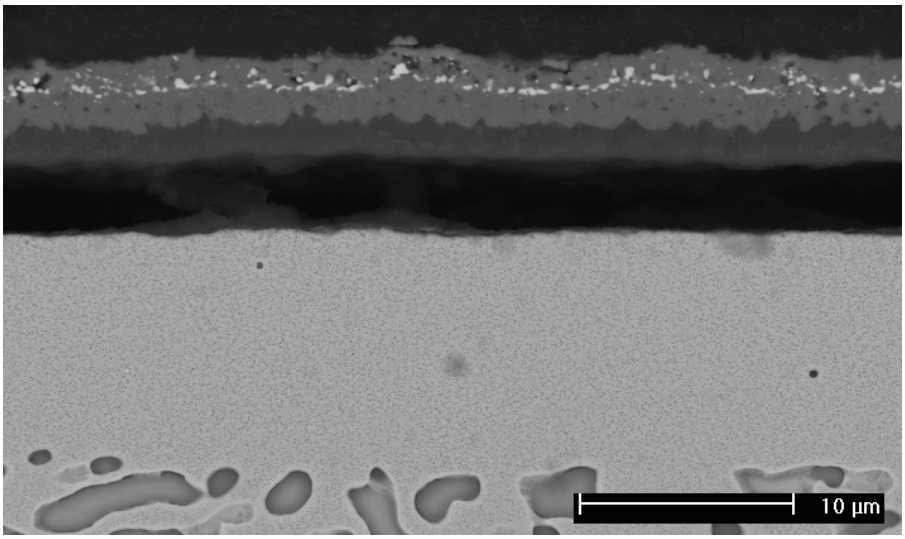

(b)

Figure 101 PWA 1484 (low sulfur content) cyclically exposed at 1100C for 664 hours in air with water vapor at 0.1atm (a) thick specimen (2 mm); (b) thin specimen (0.4 mm)

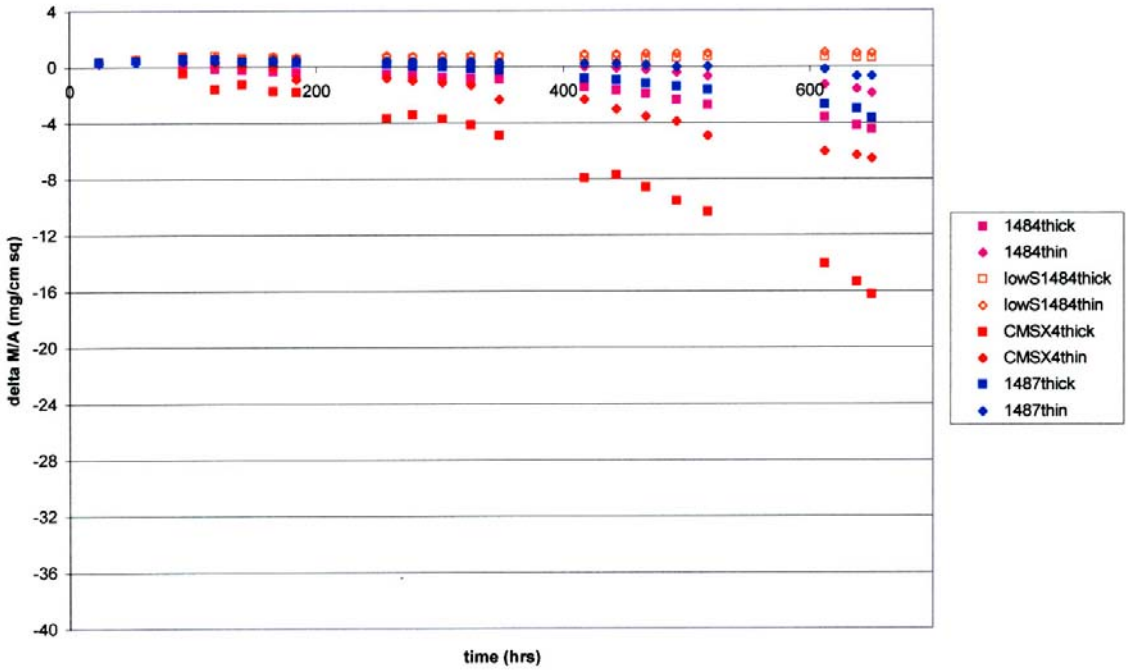

Figure 102 Change in weight measurements for four different substrates oxidized at 1100°C for 650 cycles, in air. Each substrate was tested for two different thicknesses of specimens: thick (2mm) and thin (0.4mm).

Residual stresses in an oxide and substrate can result from the growth of the oxide scale, from thermal cycling and from the geometry of the specimen. These stresses can be relaxed by spalling of the oxide scale or by creep of the oxide and/or the substrate. Using the "sin ψ^2" technique described in the experimental section, results from the residual stress in alumina scales formed on specimens of PWA1484 (low sulfur content) oxidized in air with water vapor at 0.1atm are shown in Figure 103. From the results provided in this part of the study, it appears that the experimental residual stresses increase with increasing substrate thickness, Figure 103c. A magnitude of a compressive -3.83GPa was found for the thin (0.4mm) specimen of low sulfur content 1484 and a -4.29GPa was found for the thick (2mm) specimen of the same substrate. The experimentally obtained stress values can be compared to the thermally generated stress that can be calculated using the complete equation that includes both the oxide and the metal thickness[8]:

$$\sigma_{ox} = E_{ox}\Delta T(\alpha_{ox} - \alpha_m)/[1 + 2(E_{ox}/E_m * t_{ox}/t_m)] \quad (31)$$

where E = elastic modulus, α = coefficient of thermal expansion, t = thickness and subscripts "ox" and "m" refer to the oxide and the alloy substrate. With these parameters, the values of the residual stress after cooling to room temperature from 1100°C are equal to -4.425GPa for the thin substrate and -4.481GPa for the thick specimen.

All stresses including growth and thermal stresses obey the condition of the mechanical equilibrium given by a force balance across the interface with the measured thickness of scale and substrate from which the average stress in the substrate, which would be of opposite sign, can be calculated. In the absence of any external forces, the average stress in the substrate for the two specimen thicknesses is given by[123]:

$$\sigma_m \, t_m + 2 \, \sigma_{ox} \, t_{ox} = 0 \qquad (32)$$

from which:

$$\sigma_m = - \, \sigma_{ox} \, (2 \, t_{ox} / \, t_m) \qquad (33)$$

using the same notations as above. In general, the stresses in the substrate are small and tensile since the scale is thinner than the substrate. From equation (33), values of σ_m = 34.47MPa for the thin sample and 9.44MPa for the thick superalloy specimen are calculated. The room temperature stress in the metal is rather small. In the present experimental conditions, the tensile stress is not sufficient to produce plastic deformation of the substrate after cooling.

If the calculated values of the residual stresses given by equation (31) are compared to the experimental ones for both substrate thicknesses, it is observed that the calculated residual stresses are larger than the experimental ones. This indicates that relaxation occurs during cooling and it depends on the thickness of the alumina and the thickness of the substrate or their ratio $t_m/2 \, t_{ox}$. The smaller this ratio, the more significant is the stress relaxation.

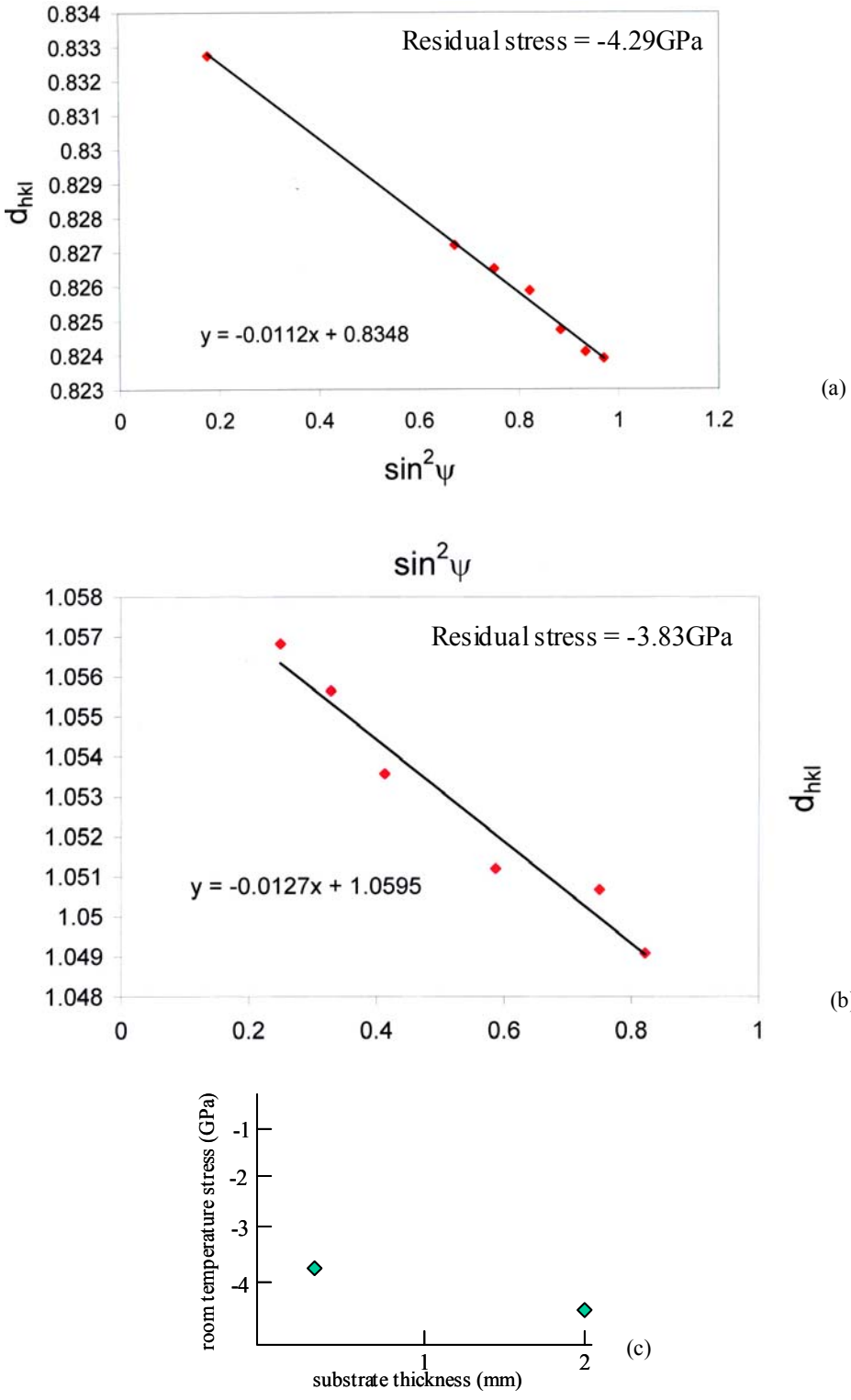

Figure 103 'd vs. $\sin^2\psi$' plots, giving the values for the residual stress for the (a) thick and the (b) thin specimen, respectively. The specimens substrates are lowS1484 exposed for 328 hours at 1100°C in air with 0.1atm water vapor

6.0 CONCLUSIONS

The high-temperature oxidation of alumina forming alloys and coatings has been found to be affected by water vapor in certain ways. The development of continuous and adherent alumina scales is inhibited in water vapor environments. The water vapor adversely affects the adherence of α-Al_2O_3 scales to alloy substrates causing the α-Al_2O_3/substrate interfacial toughness to be decreased. Spalling and cracking in wet condition exposures is less evident for thermally grown oxide scales with very good adherence to the substrate. Very adherent oxide scales have a high interfacial toughness between the α-Al_2O_3 and the substrate.

At 1100°C, the growth rate of α-Al_2O_3 is increased in water vapor conditions. This is believed to be caused by the development of a smaller grain size in the α-Al_2O_3 in the presence of water vapor. At 900°C, the growth rate of alumina scales in water vapor is greater than in dry air. This may happen because of water vapor affecting the growth rate of the metastable (θ-Al_2O_3) phase and/or water vapor causing a smaller grain size oxide to develop.

At higher temperatures (i.e. 1100°C), beside the faster growing α-Al_2O_3 scales, a spinel phase, $NiAl_2O_4$, develops on top of the alumina scale in certain regions. The faster growing alumina scales in water vapor condition tests is caused by the accelerated inward diffusion process which is associated with diffusion of the oxygen-containing species from the water vapor atmosphere.

From all the results in this work, it can be concluded that Pt modification for the aluminide coatings on superalloy brings an improvement in terms of spallation resistance and

oxidation behavior over the plain aluminides and, of course, over the superalloy substrates even in atmospheres where water vapor is present in the oxidizing gas. Platinum-modified aluminide coatings exposed in wet conditions at 1100°C exhibit not as thick an alumina scale as the straight-aluminide coating specimens oxidized in the same wet conditions, but at 900°C.

The transient oxidation process is affected by the presence of water vapor for the high temperature oxidation of superalloys and coatings. This happens because NiO grows more rapidly during the transient period in water vapor conditions. Results have been obtained that indicate oxygen-containing species from the water vapor phase diffuse into the alloy more rapidly when water vapor is in the gas environment. This condition affects the selective oxidation process. α-Al_2O_3 preferentially develops continuity at grain boundaries in the metallic substrate as a result of enhanced inward diffusion of oxygen-containing species from the water vapor phase together with rapid transport of aluminum from the alloy along grain boundaries. Enhanced internal oxidation and accelerated transient oxidation take place away from the grain boundaries in the substrate thus inhibiting the selective oxidation of aluminum at these locations.

At lower temperatures (i.e. 700°C), the selective oxidation of aluminum is inhibited due to alumina failing to develop continuity and forming of internal oxides for water vapor exposures more so than for dry exposures.

From the results presented in this study, there are indications that nickel diffusion at alumina grain boundaries significantly contributes to the formation of new spinel phase at the oxide/gas interface and water vapor is found to enhance this process. This can happen because of cracks in α-Al_2O_3 scales and Ni diffusing along cracks and/or grain boundaries in α-Al_2O_3 while water vapor causes a finer grained α-Al_2O_3 to be formed. Also, there is a higher H_2 pressure in

wet environments compared to dry air, so that more $V_{Al}^{'''}$ are formed and Ni diffuses along these vacancies.

Water vapor has been found to influence the failures of thermal barrier coatings probably by enhanced spinel formation at the TGO/TBC interface, but the exact conditions for which water vapor causes these TBC failures still remain to be defined.

Results from experiments using three different water vapor partial pressures in the oxidizing gaseous mixtures suggest that early time exposures in wet atmospheres do not show a significant effect of the water vapor pressure for these short time oxidation processes. Nevertheless, results from the oxidation of superalloys suggest a more extensive transient oxidation period for the higher water vapor partial pressure (i.e. 0.5atm). The results also show that there is not a large difference in cyclic oxidation behavior for water vapor partial pressures of 0.05atm and 0.1atm in the case of a high interfacial toughness between the oxide and the substrate, as it is for the low sulfur content N5 specimens. On the other hand, for a low interfacial toughness – i.e. the case for regular sulfur content N5 – the amount of cracked and spalled oxides increases as the water vapor pressure increases.

From experimental data in this work, it can be concluded that the high temperature oxidation of superalloys in air with water vapor conditions is accompanied by generation of fairly high compressive stress in the alumina scale.

7.0 FUTURE WORK

Work that has been done thus far in this research includes a number of interesting results such as an increased severity of cracking and spalling of α-alumina scales in water vapor for alloys that spall somewhat in dry air, more transient oxidation in gas mixtures containing water vapor and detection of spinel at the thermally grown oxide and TBC interface with specific exposure conditions in water vapor atmospheres. Some of these results need further detailed examination. Also, there are a number of test variables that must be further investigated to be able to more clearly define water vapor effects on the high temperature oxidation of alloys.

Additional experiments could be necessary since some effects of water vapor pressure were observed for the oxidation of superalloys.

Work has been done on two aluminide coatings on René N5: one aluminide coating without additions of Pt and one Pt-modified aluminide coating. It has been verified that platinum addition in aluminide diffusion coatings improves the adherence of α-alumina. It is very important to establish how much the amount of Pt would improve the cyclic oxidation of aluminide coatings in gas mixtures with water vapor. Experiments using modified aluminide coating specimens with different thicknesses of Pt deposition should be performed to clarify this aspect of the issue.

- Effects of additional variables

Some variables that are expected to influence the cyclic oxidation behavior of superalloys in water vapor environments should be investigated. The variables to be examined in order of the priority of study are: temperature, cooling rate, cold zone temperature and cold zone holding time.

Some alloys and coated systems that were not profoundly affected by water vapor at 1100°C should be oxidized at 1200°C in wet and dry air; also, longer time exposures (1500 – 2000 one-hour cycles) for one superalloy and one aluminide system at 900°C - 1000°C are necessary in order to determine if spalling would occur.

Based on availability of experimental procedures to vary the cooling rate, the cold zone temperature and the cold zone holding time, experiments should be performed at 1100°C in wet and dry conditions.

In the current experiments, the cooling rate of the specimens has been 240°C/minute. Half and double this rate could be used in dry air and air with water vapor experiments. Cold zone temperatures of 25°C rather than 100°C should be applied to experiments in wet and dry air. Furthermore, cyclic oxidation experiments with two-hour cold zone holding time (rather than 15 minutes) should be performed.

It may be possible to reduce the effects of the water vapor on the α-alumina growth rates by high temperature pretreatments of specimens. Preoxidation treatments could be performed in dry air at 1100°C to obtain an oxide with fairly coarse grain size.

- TBC investigations

The exact conditions in which water vapor causes TBC failures have to be defined. The mechanism by which water vapor affects these failures is critical to TBC use and must be

understood. Additional experiments with regard to reproducibility of previous results should be designed. An experiment in which a $NiSO_4$ intentional contamination should be tried on a TBC specimen to assess for observations made about the ‘blue-streak’ TBC specimens exposed earlier in this work.

Further SEM and TEM (as required) investigations are needed when the development of the oxides scales and interfaces require careful examination.

BIBLIOGRAPHY

1. P. Kofstad, High temperature corrosion, Elsevier Applied Science, London/New York 1988

2. R. L. McCarron and J. W. Schulz, Effect of water vapor on the oxidation behavior of some heat resistant alloys, Proc. of Symposium on High Temperature Gas-Metal Reactions in Mixed Environments, AIME, New York, 1973, p.360

3. R. Janakiraman, G. H. Meier and F. S. Pettit, Met. & Mat. Trans. A, 30A, 2905 (1999)

4. A. Rahmel and J. Tobolski, Corros. Sci., 5, 33 (1965)

5. E. A. Irene, J. Electrochem. Soc., 121, 1613 (1974)

6. I. Kvernes, M. Oliveira and P. Kofstad, Corros. Sci., 17, 237 (1977)

7. Superalloys II, Sims, Stoloff and Hagel ed., p.295

8. N. Birks, G. H. Meier, Introduction to high temperature oxidation of metals, Edward Arnold Ltd. (Publishers), 1983

9. P. Kofstad, High Temperature Corrosion, Elsevier Applied Science, London, 1988

10. H. Rickert, J. Chem. Phys. 23, 335 (1989)

11. M.T. Tinker, L.W. Hobbs, in: G.C. Bailey (Ed.), Proceedings for the 39th Annual Meeting of Electron Microscopy Soc. For America, Claitor's Publishing Div., Baton Rouge, 1981, p. 86

12. C. Wagner, Z. Phys. Chem., B21, 25 (1933)

13. J. S. Schackeford, Introduction to Material Science for Engineers, Prentice Hall International, London, 1996

14. B. Fedelich, Comp. Mat. Sci., 16, 248 (1999)

15. J. Bressers, D. J. Arrell, K. Ostolaza, J. L. Valles, Mat. Sci. Eng., A220, 147 (1996)

16. G. E. Fuchs, Mat. Sci. Eng., A300, 52 (2001)

17. H. M. Tawancy and N. M. Abbas, Surf. Coat. Technol., 49, 1 (1991)

18. H. M. Tawancy and N. M. Abbas, Surf. Coat. Technol., 54/55, 1 (1992)

19. H. M. Tawancy, N. Sridhar, B. S. Tawabini, N. M. Abbas, T. N. Rhys-Jones, J. Mater. Sci., 27, 6463 (1992)

20. K. L. Lin and C. M. Hwang, Surf. Coat. Technol., 56, 81 (1992)

21. J. H. Sun, H. C. Jang, E. Chang, Surf. Coat. Technol., 64, 195 (1994)

22. M. Gobel, A. Rahmel, M. Schütze, M. Schorr, W. T. Wu, Mater. High Temp., 12, 301 (1994)

23. G. R. Krishna, D. K. Das, V. Singh, S. V. Joshi, Mat. Sci. Eng., A251, 40 (1998)

24. J. R. Nicholls, K. J. Lawson, D. S. Rickerby, P. Morrel, Advanced Processing of TBCs for reduced thermal conductivity, Agard Rep. p.823, 1998

25. J. R. Nicholls, Smart multilayered coating with controlled thermal conductivities using plasma assisted deposition, CIP Conf. 1999

26. D. B. Marshall, A. G. Evans, J. Appl. Phys. 56, 2632 (1984)

27. E. Dorre, H. Hubner, Alumina, Springer Verlag, 1984

28. M. Gell, K. Vaidyanathan, B. Barber, J. Cheng, E. Jordan, Met. & Mat. Trans. A, 30A, 427 (1999)

29. H. A. Wang, F. A. Kroger, J. Amer. Cer. Soc. 63, 613 (1980)

30. J. L. Smialek, Metall. Trans. A, 9, 309 (1978)

31. E. J. Felter, F. S. Pettit, Oxid. Met. 10, 189 (1976)

32. C. Bandini, F. Laurella, Surf. Coat. Technol. 135, 291 (2001)

33. V. K. Tolpygo, D. R. Clarke, Oxid. Met. 49, 187 (1998)

34. J. L. Smialek, JOM – January, 22 (2000)

35. H. J. Grabke, Phys. Chem. 69, 48 (1965)

36. A. Gala, H. J. Grabke, Arch. Eisenhuttenwes. 43, 463 (1972)

37. H. J. Grabke, K. J. Best, A. Gala, Werkst. Korros. 21, 911 (1970)

38. T. Akermark, G. Hultquist, Oxid Met., 47, 117 (1997)

39. E. A. Gulbransen, T. P. Copan, Nature 186, 959 (1960)

40. S.J. Roosendaal, J.P.R. Bakker, A.M. Vredenberg, F.H.P.M. Habraken, Surface Science 494, 197 (2001)

41. S. Jianian, Z. Longjian, L. Tiefan, Oxid. Met. 48, 347 (1997)

42. K. Fritscher, Y. T. Lee, JOM 34 No. ¾, 295 (1989)

43. R. T. Foley, J. Electrochem. Soc., 278 (1962)

44. S. Jianian, Z. Longjiang, L. Tiefan, JOM 48, No. ¾, 347 (1996)

45. S. Taniguchi, N. Hongawara, T. Shibata, Mat. Sci. Eng. A307, 107 (2001)

46. J. V. Cathcart, R. A. Perkins, J. B. Bates, L. C. Manley, J. Appl. Phys. 50, 4110 (1979)

47. O. W. Johnson, S. H. Paek, J. W. DeFord, J. Appl. Phys. 46, 1026 (1975)

48. S. K. Roy, R. L. Coble, J. Am. Ceram. Soc. 50, 435 (1967)

49. P. Kofstad, Nonstochiometry, Diffusion and electrical conductivity in binary metal oxides, Robert E. Krieger, Malaban, Fl, 1983

50. A. Zeller, F. Dettenwanger, M. Schütze, Intermetallics 10, 59 (2002)

51. S. Henry, J. Mougin, Y. Wouters, J-P. Petit, A. Galerie, Materials at High Temp., 17, 231 (2000)

52. F. Passier, Y. Wouters, A. Galerie, M.Caillet, Oxid. Of Met. Vol 55, No.1/2, 153 (2001)

53. F.A. Kroger, H.J. Vink, Solid State Physics, Vol. 3, F. Seitz and D. Turnbull eds. (Academic Press, New York, 1956), p. 307

54. T. Norby, Defect chemistry of solids, 101 (1989)

55. T. Norby, P. Kofstad, High Temperatures. High Pressures. 20, 345 (1988)

56. C. T. Fujii, R. A. Meussner, J. Electrochem. Soc. 111, 1215 (1964)

57. N. Fukatsu, N. Kurita, H. Shiga, Y. Murai, T. Ohashi, Solid State Ionics 152-153, 809 (2002)

58. G. Hulquist, B. Tveten, E. Hörnlund, M. Limbäck, R. Haugsrud, Oxid. Met., 56, 313 (2001)

59. Y. W. Kim, G. R. Belton, Met. Trans. 5 (8), 1811 (1974)

60. G. C. Fryburg, R. A. Miller, F. J. Kohl, C. A. Stearns, J. Electrochem. Soc. 124, 1738 (1977)

61. A. Hashimoto, Geochim. Cosmochim. Acta 56, 511 (1992)

62. E. L. Brady, J. Phys. Chem. 57, 706 (1953)

63. N. S. Jacobson, J. Am. Ceram. Soc. 76 (1), 3 (1993)

64. I. Gurrappa , S. Weinbruch , D. Naumenko , W.J. Quadakkers , Materials and Corrosion, 51, Issue 4, 224 (2000)

65. H. Bouaouine, F. Armanet, C. Coddet, International Congress on Metallic Corrosion, Toronto 1989, p.379

66. C. W. Tuck, M. Odgers, K. Sachs, Corros. Sci. 9, 271 (1969)

67. H. Buscail, S. Heinze, P. Dufour, J. R. Larpin, JOM 47, 445 (1997)

68. P. A. Thiel, T. E. Madey, Surf. Sci. Rep. 7, 211 (1987)

69. D. M. Kotchick, R. E. Tressler, J. Mat. Sci. 10, 608 (1975)

70. R. J. Charles, R. R. Shaw, GE Rep. 62, 1962

71. S. M. Wiederhorn, Int. J. Fract. Mech. 4, 171 (1968)

72. M. Gell, Met. & Mat. Trans. A, 30A, 427 (1999)

73. J. Harris, Acta Metall., 26, 1033 (1978)

74. F.H. Stott, G.H. Wood, Mater. Sci. Engng., 87, 267 (1987)

75. J.E. McDonald, J.G. Eberhard, Metall. Trans., 233, 512 (1965)

76. H.J. Grabke, D. Wiemer, H. Viefhaus, Appl. Surf. Sci., 47, 243 (1991)

77. J.L. Smialek, G.N. Morscher, Mat. Sci. and Eng. A, 332, 11 (2002)

78. A.K. Kronenberg, J. Castaing, T.E. Mitchell, S.H. Kirby, Acta Mater., 48, 1481 (2000)

79. J. Castaing, A.K. Kronenberg, S.H. Kirby, T.E. Mitchell, Acta Mater., 48, 1495 (2000)

80. S.M. Weiderhorn, J. Am. Ceram. Soc., 50, 407 (1967)

81. P.T. Moseley, K.R. Hyde, B.A. Bellany, G. Tappin, Corros. Sci., 24, 547 (1984)

82. M.W. Brumm, H.J. Grabke, Corr. Sci., 33, 1677 (1992)

83. H.J. Grabke, Intermetallics, 7, 1153 (1999)

84. E. Schumann, J.C. Yang, M.J. Graham, M. Rühle, Mat. Corr., 47, 631 (1996)

85. J.P. Roux, H.J. Grabke, Appl. Surface Sci., 68, 49 (1993)

86. J. Doychack, J.L. Smialek, T.E. Mitchell, Metall. Trans. 20, 499 (1989)

87. R. Prescott, M.J. Graham, Oxid. Met., 38, 233, (1992)

88. C.S. Giggins, F.S. Pettit, TMS-AIME, 245, 2509 (1969)

89. F. Gesmundo and F. Viani, Oxid. Met. 25, 260 (1986)

90. A. Atkinson, R.I. Taylor, P.D. Goode, Oxid. Met., 13, 519 (1979)

91. A. Atkinson, R.I. Taylor, Phil. Mag. A43, 979 (1981)

92. J.C. Cano-Cabrera, J. Castaing, J. Phys. Lett., 42, 119 (1980)

93. A. Atkinson, F.C.W. Pummery, I. Monty, G. Simkovich and V.S. Stubican (Eds), Transport in Non-Stoichiometric Compounds, Plenum, NY, 1985

94. A. Galerie, Y. Wouters, M. Caillet, Mater. Sci. Forum, 369-372, 271 (2001)

95. S. Henry, J. Mougin, Y. Wouters, J.-P. Petit, A. Galerie, Materials at High Temperatures, 17, 231 (2000)

96. S. Henry, A. Galerie, L. Antoni, Mater. Sci. Forum, 369-372, 353 (2001)

97. R. Peraldi, D. Monceau, B. Pieraggi, Oxid. Met., 58, 275 (2002)

98. M.J. Graham, R.J. Hussey, Corr. Sci., 44, 319 (2002)

99. G.M. Raynaud, R.A Rapp, Oxid. Met., 18, 89 (1984)

100. G.M. Raynaud, L. Brossard, International Congress Metal Corrosion, 1, 27 (1984)

101. A. Brückman, R. Emmerich, S. Mrowec, Oxid. Met., 5, 137 (1972)

102. P. Maak, Werkstoffe Korros., 12, 273 (1961)

103. A. Brückman, Corros. Sci., 7, 51 (1967)

104. A. Atkinson, D.W. Smart, J. Electrochem. Soc., 135, 2886 (1988)

105. A.G. Robertson, D. Manning, Mater. Sci. Technol., 4, 1064 (1988)

106. D.P. Moon, Oxid. Met., 31, 71 (1989)

107. D.P. Moon, I.R. Harris, P.R. Chalker, D. Mountfort, Mater. Sci. Technol., 4, 1101 (1988)

108. S. Mrowec, Corros. Sci., 7, 563 (1967)

109. P. Kofstad, Oxid. Met., 24, 265 (1985)

110. G.J. Yurek, H.S. Schmaltzried, Ber. Bunsenges, Phys. Chem., 79, 255 (1975)

111. A. Evans, D. Radjev, D.L. Douglass, Oxid. Met., 4, 51 (1972)

112. G.B. Gibbs, R. Hales, Corros. Sci., 17, 487 (1977)

113. F. Gesmundo, F. Viani, Oxid. Met., 25, 269 (1986)

114. B.A. Pint, A.J. Garratt-Reed, L.W. Hobbs, Oxid. Of Metals, 56, 119 (2001)

115. O. Sahin, S. Nourbakhsh, W.H. Rhee, H. Margolin, Met. Trans. A, 23A, 3151 (1992)

116. A.E. Paladino, W.D. Kingery, J. Chem. Phys., 37, 957 (1965)

117. F.A. Kroger, "Defects and Transport in SiO_2, Al_2O_3 and Cr_2O_3", p.89-100, High Temperature Corrosion, Editor R.A. Rapp, NACE-6, National Association of Corrosion Engineers, Houston, Texas (1981)

118. V.K.Tolpygo, D.R.Clarke, "Evidence of Outward Aluminum Grain Boundary Diffusion in Y and Zr – Doped Alumina Scales", Kofstad Symposium, October 1999, The Electrochemical Society, Pennington, NJ

119. B.A. Pint, J.R. Martin, L.W. Hobbs, Oxid. Met. 39, 167 (1993)

120. C. Mennicke, E. Schumann, M. Rühle, R.J. Hussey, G.I. Sproule, M.J. Graham, Oxid. Met. 49, 455 (1998)

121. K. Messaoudi, A.M. Huntz, B. Lesage, Mater. Sci. Eng., A247, 248 (1998)

122. P. Kofstad, Oxid. Met., 44, No. ½, 3 (1995)

123. J.C. Noyan, Adv. In X-ray Anal., 35, 461 (1992)